2024

On Design Load Prediction and Extreme Response Modelling of Floating Offshore Renewable Energy Structures

Tosdevin, Tom

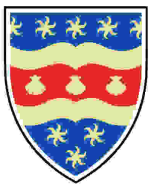

UNIVERSITY OF
PLYMOUTH

On Design Load Prediction and Extreme Response Modelling of Floating Offshore Renewable Energy Structures

by

Tom Tosdevin

A thesis submitted to the University of Plymouth
in partial fulfilment for the degree of

DOCTOR OF PHILOSOPHY

School of Engineering Computing and Mathematics

June 2023

Acknowledgements

FIRST AND FORMOST I would like to thank my supervisory team for all their guidance and encouragement. Dave for the weekly meetings and always being available to talk, Martyn for encouraging me to apply for the PhD / postdoc positions I didn't feel qualified for, and Deborah for all the valuable feedback. I would also like to thank the COAST laboratory staff without whose patience and expertise the physical experiments would have been a lot less fun and a lot more stressful.

Finally I'd like to thank my Mum for being such a great role model and imparting her work ethic; Dad for the proof reading and teaching me how to use a semicolon properly; (<- is this right? I'm not sure this is right... never mind) my in-laws for all the food/shelter/childcare; and last but not least my wife Sarah and our children Elyas and Annie for providing both the motivation for, and a welcome distraction from, the research.

Authors declaration

AT NO TIME during the registration for the degree of Doctor of Philosophy has the author been registered for any other University award without prior agreement of the Doctoral College Quality Sub-Committee. Work submitted for this research degree at the University of Plymouth has not formed part of any other degree either at the University of Plymouth or at another establishment. Relevant scientific seminars and conferences were regularly attended at which work was often presented.

Word count for the main body of this thesis: **51,912**

Signed:

Date: 29/06/2023

Posters and conference presentations:

Tosdevin,T. & Hann,M. & Simmonds, D. & Greaves, D. Poster presentation: *On the calibration of a WEC-Sim model for heaving point absorbers* INORE 2019, Nocera Umbra Italy.

Tosdevin, T. & Hann, M. & Simmonds, D. & Greaves, D. Conference paper and poster presentation: *On the calibration of a WEC-Sim model for heaving point absorbers* EWTEC 2019, Naples Italy.

Tosdevin, T. & Simmonds, D. & Hann, M. & Greaves, D. Conference presentation: *On the Application of a Design Loads Generator Methodology in the Determination of the Design Loads of a Point Absorber Wave Energy Convertor* Primare 2020, Online.

Tosdevin, T. & Jin, S. & Simmonds, D. & Hann, M. & Greaves, D. Poster: *Extreme Responses of a Raft Type Wave Energy Converter* Supergen annual assembly 2021, Plymouth UK.

Tosdevin, T. & Jin, S. & Simmonds, D. & Hann, M. & Greaves, D. Conference paper and presentation: *Extreme responses of a hinged raft type WEC* EWTEC 2021, Plymouth UK.

Tosdevin, T. & Jin, S. & Simmonds, D. & Hann, M. & Greaves, D. Conference presentation: *Extreme responses of a parked semi-submersible floating wind turbine* Primare 2022, Falmouth UK.

Jin, S. & Tosdevin, T. & Hann, M. & Greaves, D. Conference paper: *Experimental study on short design waves for extreme response of a floating hinged raft wave energy converter* IWWWFB 2022, Sicily Italy and online.

Tosdevin, T. & Simmonds, D. & Hann, M. & Greaves, D. Poster presentation: *Short design waves for semi-sub FOWTs experiencing viscous drift* Supergen early career researcher event / anual assembly 2022, Queen's College, Oxford.

Tosdevin, T. & Jin, S. & Simmonds, D. & Hann, M. & Greaves, D. Presentation: *On the use of short design waves for characteristic load prediction in physical model testing* RenewableUK 2022, Glasgow UK.

Tosdevin, T. & Jin, S. & Simmonds, D. & Hann, M. & Greaves, D. Conference paper and presentation: *On the use of short design waves for characteristic load prediction* RENEW 2022, Lisbon, Portugal.

Abstract

Tom Tosdevin

On Design Load Prediction and Extreme Response Modelling of Floating Offshore Renewable Energy Structures

FLOATING offshore renewable energy (FORE) is a marginal industry and as such cost reductions are essential in order for it to become competitive with other forms of electricity generation. Design practices for evaluating the extreme responses of FORE devices are still under consideration by standards authorities, thus methods that enable potential speeding up of the design and development phases, particularly physical model testing are needed. Probabilistic design approaches have proved effective in bringing down costs in the aerospace and automobile industries and so provide a potential route to viability by allowing partial safety factors to be reduced. However, the scarcity of real world data and early development stage of the sector mean that the suitably large data sets needed to evaluate extreme responses and uncertainties have to be generated numerically. This poses a challenge when there is a trade-off between fidelity and run time. This thesis seeks to understand the extent to which fast mid-fidelity models such as WEC-Sim (a potential flow, Cummins equation based model) can model the extreme responses of FORE devices compared with physical experiments and where and how short design waves can be used in speeding up the prediction of design loads.

A WEC-Sim numerical model was found to perform reasonably accurately in evaluating extreme mooring responses of a generic point absorber wave energy convertor (WEC), with a median error relative to physical experiments of around 10%. It was then used to develop a methodology for using short design waves during physical model tests, conducted in the COAST lab at the University of Plymouth, and evaluated for a hinged raft type WEC and semi-sub floating offshore wind turbine (FOWT). The approach used constrained focused waves scaled to an inflated target percentile amplitude or response in place of the one to three hour irregular wave time series commonly used in the prediction of design loads. Recommendations were given on the suitability of the method in different sea conditions; for different response types; and on how to calibrate the waves in physical experiments. Constrained NewWave (CNW) and conditional random response wave (CRRW) profiles were compared and found to perform well in different situations, with the CNWs being a better choice when modelling snatch loads in steep sea states for a hinged raft type WEC. It was found that a single, frequency specific phase correction calculated from a focused wave could be used to calibrate the constrained focused waves, greatly speeding up the calibration time. Difficulties in the calibration of the short design waves in steeper sea states make the developed method increasingly difficult to apply close to the wave breaking limit.

Physical experiments on a semi-sub FOWT were conducted and the results compared with a WEC-Sim model for the responses of pitch, nacelle acceleration and mooring load. It was found that an additional drag term had to be added to the numerical

model to improve the accuracy of the low frequency surge motions and mooring loads. Furthermore, it was found that the wave theory used to generate the wave surface elevation input to the edited numerical model had a significant impact on the surge response, resulting in a difference of over 30%. A constrained wave group was proposed as an alternative short design wave when studying the moorings of Semi-subs. This thesis has developed a short design wave method to improve the efficiency of the design process of FORE devices, provides several case studies on the methods applicability and has assessed the extend to which mid-fidelity numerical models are able to model extremes.

Contents

List of Figures

List of Tables

Abreviations

BEM	Boundary Element Method
BF	Benjamin Feir
BM	Back Mooring
BSS	Brier Skill Score
CALM	Catenary Anchor Leg Mooring
CCDF	Complimentary Cumulative Distribution Function
CDF	Cumulative Distribution Function
CFD	Computational Fluid Dynamics
CI	Confidence Interval
CNW	Constrained NewWave
CRRW	Conditional Random Response Wave
DLC	Design Load Case
DLG	Design Loads generator
DoF	Degrees Of Freedom
EMEC	European Marine Energy Centre
EVD	Extreme Value Distribution
FK	Froude Krylov
FM	Front Mooring
FNPF	Fully Nonlinear Potential Flow
FORE	Floating Offshore Renewable Energy
FOWT	Floating Offshore Wind Turbine
GEV	Generalised Extreme Value
GPD	Generalised Pareto Distribution
IEA	International Energy Agency
IEC	International Electrotechnical Commission
IFORM	Inverse First Order Method
LCOE	Levelised Cost of Energy
MC	Monte Carlo
MLER	Most Likely Extreme Response
MLRW	Most Likely Response Wave
MPM	Most Probable Maximum
MSE	Mean Square Error
NREL	National Renewable Energy Laboratories
OWSC	Oscillating Wave Surge Convertor
PCA	Principal Component Analysis
PCC	Power Conversion Chain
PDF	Probability Density Function
POT	Peak Over Threshold
PTO	Power Take Off
QTF	Quadratic Transfer Function

RAO	Response Amplitude Operator
RMSE	Root Mean Square Error
ROSCO	Reference Open Source Controller
SALM	Single Anchor Leg Mooring
SNL	Sandia National Laboratories SPH
Smooth Particle Hydrodynamics	
TEV	Target Extreme Value
TLP	Tension Leg Platform
VCG	Vertical Centre of Gravity
WDRT	WEC Design Response Toolbox
WEC	Wave Energy Converter
XCG	X Centre of Gravity

Nomenclature

β	Beta term
ε	Bandwidth parameter
ε	Shape parameter
ε_j	Phase term
η	Wave surface elevation $[m]$
γ	Peak shape parameter
λ	Wave length $[m]$
μ	Dynamic viscosity
μ	Location parameter
ω	Angular frequency $[rad/s]$
Φ	Standard normal cumulative distribution function
ρ	Water density $[kg/m^3]$
σ	Scale parameter
A_∞	Infinite frequency added mass $[kg]$
A_d	Characteristic area $[m^2]$
a_j	Spectral amplitude $[m]$
B	Radiation damping $[kg/s]$
b_j	Response spectral amplitude
BSS	Brier skill score
C_d	Quadratic drag coefficient $[-]$
c_p	Phase velocity $[m/s]$
C_v	Linear drag coefficient $[-]$
F_B	Buoyancy force $[N]$
F_m	Moorings force $[N]$
F_v	Viscous force $[N]$
F_{exc}	Excitation force $[N]$

F_{ME}	Morrison elements force $[N]$
F_{PTO}	PTO force $[N]$
F_{rad}	Radiation force $[N]$
g	Acceleration due to gravity $[m/s^2]$
h	Water depth $[m]$
H_s	Significant wave height $[m]$
k	Wave number $[m^-1]$
KC	Keulegan-Carpenter number
L	Characteristic length $[m]$
m	Number of samples of the Gaussian process
m_n	Spectral moment of the nth degree
MSE	Mean square error
n	Number of peaks in given exposure time
p_3	Nonexcedance load percentile
$r(t)$	Autocorrelation function
RAO	Response amplitude operator $[-]$
Re	Reynolds number
S	Wave spectral density $[m^2/Hz]$
S_p	Significant steepness
S_r	Response spectral density $[units^2/Hz]$
T_e	Energy period $[s]$
T_p	Peak period $[s]$
TEV	Target extreme value
U	Mean wind speed $[m/s]$
z_k	Derived process $[m]$

Chapter 1

Introduction

Chapter summary

The introduction aims to provide a broad overview of the design process for floating offshore renewable energy devices and extreme response modelling. Challenges in improving the efficiency of the design process are identified and used to form the basis of the thesis aims and objectives.

1.1 Introduction

1.1.1 Motivation

Renewable energy devices are being deployed at an accelerating rate globally, some of which are capable of making sizeable contributions to the energy mix. Offshore wind in particular is transforming the UK's energy strategy with a goal of 50 GW of capacity installed by 2030, up to 5 GW of which is targeted to be from floating offshore wind turbines Floating Offshore Wind Turbines (FOWTs) (Department for Business (2022)). Fixed offshore wind is limited in its deployment outside of the shallow waters of the North sea due to a roughly 60m water depth limit (Pacheco et al. (2017)). Consequently floating platforms are thought to be a key future technology with the first large scale commercial deployment scheduled for South Korea in 2024 (engie (2022)). Whilst wave and tidal stream energy devices are more limited in their potential to contribute, they are none the less capable of contributing to the mix in the UK at perhaps 15% (Carbon Trust (2012)) and 11% (Coles et al. (2021)) of present day electricity demand each respectively. Although MacKay (2008) points out that the range of long term

estimates, based on the available resource and the physics, suggest the exact numbers and whether they will ever be economically achievable are highly uncertain.

Presently the cost of floating wind, tidal stream and wave energy devices are still relatively high and so all require subsides to compete with fixed offshore wind and gas generation (Greaves et al. (2023)). As floating offshore renewable energy (FORE) industries are marginal, much design innovation will be needed to bring down costs and make them competitive. This is not an issue for the oil and gas industry which can afford to over engineer by adopting large, but still cost effective safety factors. As such, the design process itself is an active area of research. FORE technologies will have to withstand harsh, energetic wave environments and so accurate extreme response modelling and reliability assessments are of key importance. The term 'extreme' is defined in this thesis as a value of interest for a particular sea state which lies above the 1st percentile of the cumulative distribution function (CDF) of the extreme value distribution (EVD).

There are still many floating wind platform concepts in development with different methods of stabilisation (Leimeister et al. (2018)). The four main platform types are semi-submersibles, spars, tension leg platforms (TLPs) and barges. These and their method of stabilisation —ballast, buoyancy, mooring —and commonly used mooring type are illustrated in Fig.1.1.

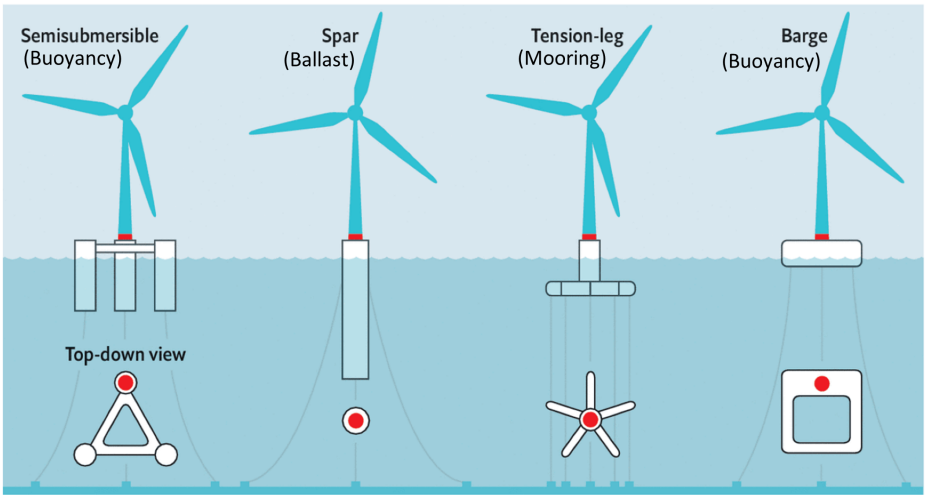

Figure 1.1: FOWT device types. Adapted from Mei and Xiong (2021).

There are a large number of wave energy converter (WEC) concepts with eight overall types according to the European Marine Energy Centre (EMEC) (EMEC (2022)). Fig.1.2 displays three of the most common. Point absorbers extract energy primarily by heave hloscillations with the waves. Oscillating wave surge convertors (OWSC), have their principle axis parallel to an incoming wave crest and 'terminate' the wave. Attenuators are oriented parallel to the direction of wave propagation and extract energy by the relative motion of their segments. The two most relevant to this thesis are the point absorber and attenuator, as examples of such devices are studied by way of physical experiments in later chapters.

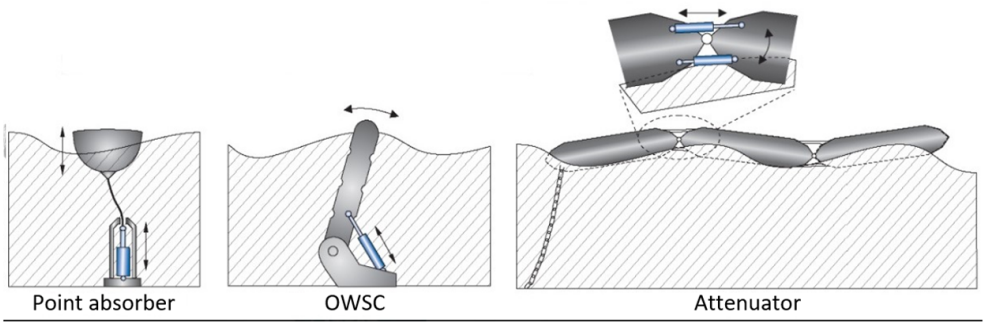

Figure 1.2: WEC device types. Adapted from Hansen et al. (2013).

Mooring configurations for WECs may differ significantly from the tension leg and cate-

nary configurations illustrated in Fig.1.1. In a review of mathematical modeling approaches for WEC moorings, Davidson and Ringwood (2017) identify several varieties shown in Fig.1.3, these may involve masses and floats, as is the case with lazy-S systems or buoys and hawsers as for catenary anchor leg systems (CALM) and single anchor leg moorings (SALM).

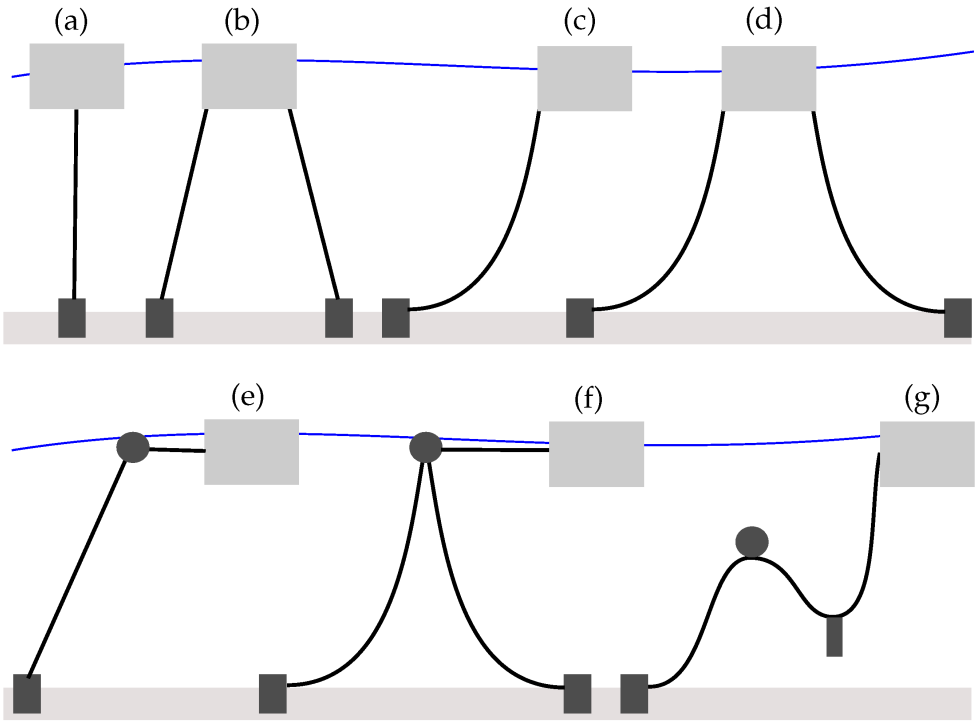

Figure 1.3: Mooring line configurations: (a) Taut; (b) Taut spread; (c) Catenary (d) Multi-catenary; (e) SALM; (f) CALM; and (g) Lazy-S. Taken from Davidson and Ringwood (2017).

Clark and DuPont (2018) suggested in a review paper on probabilistic design for ORE that as a consequence of the large number of platform types, device types and operating principles, research interests may diverge. This is due to components which may be specific to a particular concept. Therefore common features should be the focus of future research efforts in order to maximise impact. Following that advice, this thesis will have a particular focus on the design process itself and to a lesser extent, on moorings which are relevant across all floating ORE devices.

1.1.2 Design

The purpose of the design process is to create a device which is able to produce electricity at the lowest possible price, often measured by the levelized cost of energy (LCOE) (Ambühl et al. (2014)). The LCOE takes into account all the costs, such as manufacturing and maintenance, and revenues, such as sale of electricity, associated with a device over it's lifetime. Survivability and reliability are therefore as important as the power capture. The traditional design process seeks to calculate a 'characteristic load' which is set so that there is a specific annual probability of failure, typically 2% for unmanned ORE (DNV (2018)). The 'design load' the device is designed to withstand is then calculated by multiplying the characteristic value by a partial safety factor. Ultimate limit states are assessed to make sure the device withstands the largest loading events likely to occur over the deployment lifetime, fatigue limit states are assessed to check that the device withstands repeated cyclic loading.

Probabilistic design approaches, where uncertainties in the design inputs are propagated to the ultimate and fatigue load calculations, have had success in bringing down costs in the automotive and aerospace industries where extensive data is available (Johannesson et al. (2016)). Offshore renewables, however, lack this level of data and what little does exist is commercially sensitive and so generally not accessible. Therefore, data must be created synthetically using numerical models which must run fast enough to perform the thousands of sea state evaluations necessary. The number of model runs required of the full probabilistic method is many times greater than the traditional design approach outlined in various design standards and so, surrogate modelling, where a fast running, statistical approximation of the numerical model is developed, is also considered necessary (Eskilsson et al. (2022)).

The promise of probabilistic methods is that the partial safety factors applied in the traditional design approach may be relaxed and so reduced materials and therefore cost may be achieved in the manufacture of devices. The traditional approach outlined in design standards is a mismatch of deterministic and probabilistic methods where the

uncertainties in the environmental conditions and response within particular sea states are the only uncertainties considered. The characteristic loads determined are then multiplied by partial safety factors to compensate for unaccounted for uncertainties and modelling simplifications (DNV (2018)). This process has the advantage of being relatively straightforward to apply and the safety factors can be tuned to empirical data so that the desired probabilities of failure can be achieved. It may however lead to over or under design of devices in the early design stages when empirical data from physical deployments is unavailable. Such a situation was found to occur for in deck loading of oil and gas platforms as outlined in Gibson (2020c) partly as a consequence of under predicting crest height statistics due to the limitations of the applied wave theory. The over design of a device on the other hand may have severe implications for the economic viability of a concept.

An additional and equally serious problem for designers reliant on numerical modelling is the uncertainty in the validity of their numerical models. High fidelity models run too slowly to be capable of running the irregular wave simulations needed in the evaluation of characteristic values recommended in the design standards. Conversely, fast mid-fidelity models may be unable to accurately simulate the physics responsible for the extreme motions of FORE devices in storm conditions. Presently, mid-fidelity models, which may only take account of nonlinear effects in a limited way, commonly used for WECs such as WEC-Sim, are regularly used for the modelling of extreme conditions, (e.g.Van Rij et al. (2019b), Li et al. (2018), Van Rij et al. (2019a)). However, the ability of such, largely linear, models to accurately model extremes is still highly questionable (van Rij et al. (2019)). In order to model extreme loads faster and more accurately therefore, either a method has to be found to reduce simulation times with high fidelity models, or the accuracy of mid-fidelity models has to be assessed and improved.

Short design waves have the potential to reduce simulation times relative to irregular waves, where 1-3 hour time series are typical. Single and constrained focused waves are commonly used in offshore engineering applications to speed up the modelling of

extreme conditions (Tromans et al. (1991), Taylor et al. (1997)). Focused waves produce a single wave profile predicted to lead to an extreme device response, constrained focused waves constrain the single wave profile into a short 5-10 minute random irregular background. They are potentially short enough to be implemented in high fidelity models and reduce costs during physical tank testing. However, it has been reported that they do not always produce responses as large as those during irregular waves when modelling FORE devices e.g. Hann et al. (2018).

1.1.3 Aims and structure

Thus, the main aims of this thesis will be to:

1) Analyse to what extent fast mid-fidelity models such as WEC-Sim can model the extreme responses of FORE devices compared with physical experiments.

2) Determine whether focused and constrained focused waves can be applied during the design process for FORE devices and provide guidance on their use and range of applicability.

Several objectives are outlined here in service of these aims:

1) Review the literature to understand existing design methods and standards and how they are implemented in industry and academia.

2) Review the literature to understand how short design waves are used in extreme response modelling.

3) Assess the ability of a readily accessible, widely used potential flow model - WEC-Sim - to quickly reproduce extreme responses by comparison with physical experiments.

4) Analyse the sea states and wave profiles leading to extreme responses of interest for 3 different FORE devices.

5) Assess the suitability of short design wave sequences for characteristic load prediction from both numerical and physical model investigations and give recommendations

on their use.

Chapter 2 addresses objectives 1 and 2 and starts with a discussion of extreme response modelling which leads into a review of the relevant design approaches and numerical methods they employ. A discussion of short design waves and the ways in which they are used in the literature is then undertaken. The design standards recommended by various organisations are summarised. Numerical models are briefly compared in terms of their suitability for the task and one selected.

Chapter 3 investigates whether WEC-Sim is able to model the extreme responses of a taught moored point absorber WEC. The model is then used to analyse short design wave methods for predicting an extreme value distribution. A method for characteristic load prediction using constrained focused waves is inferred from the results.

Chapter 4 applies the constrained focused wave approach for characteristic load prediction experimentally to a lazy S moored hinged raft type WEC and utilises the contour method to identify the design sea. A fast method of calibrating the constrained focused waves during physical experiments is investigated. Both an extreme and benign sea state are analysed in detail. Snatch loads are studied and complications due to wave breaking are discussed.

Chapter 5 tests the approach experimentally on a semi-sub FOWT. It is found that, whilst the characteristic loads can be predicted in some situations using the short design waves, viscous effects complicate the analysis. A constrained wave group based on a specified number of peaks is introduced to better model extremes of semi-subs in steep sea states. Numerical models of the FOWT are discussed in chapter 6 and are found to underpredict low frequency device motions. An additional drag term is introduced to improve the results.

In the last chapter the findings of the case studies are summarised in relation to the stated thesis aims and future work is outlined.

Chapter 2

Review of design methods and extreme response modelling

Chapter summary

This chapter presents a review of the relevant literature and numerical methods relating to response modelling, characteristic load prediction and short design waves.

2.1 Response modelling

To evaluate the design loads of a device it's responses in extreme conditions must be modelled, either numerically, or physically by scale model experiments in a wave tank. Extreme conditions are defined as those sea states with a high return period, typically fifty years for unmanned floating ORE applications. The exposure time of interest is typically one hour for FOWT and three hours for WECs. This difference is due to the fact that wave conditions are considered statistically stationary over a one to six hour period as opposed to ten minutes for wind (IEC (2019)). The one hour exposure used for FOWTs therefore is a compromise between the wind and wave conditions.

2.1.1 Wave theory

Linear (Airy) wave (Airy (1845)) and wave maker theory is most commonly applied in both the mid-fidelity numerical models commonly used for FORE devices and during physical wave tank testing (Lawson et al. (2014b), NREL and SNL (2021)). This means that the surface elevation (η) is treated as a summation of cosine components dependent on the sea spectral density $S(\omega)$ (Kim (2012)).

$$\eta(t) = \sum_{j=1}^{N} a_j \cos(k_j x - \omega_j t + \phi_j) \tag{2.1}$$

Where ϕ_j is the random phase in radians, k is wave number, ω_j is the angular frequency in radians and x the horizontal position in metres, taken as distance from the wave paddles in physical testing. The spectral amplitude is:

$$a_j = \sqrt{2S(\omega_j) \triangle \omega_j} \tag{2.2}$$

Sea states are most commonly modelled using a JONSWAP spectrum defined with significant wave height (H_s) in metres, peak period (T_p) in seconds and the peakedness parameter, gamma (γ) (DNV (2014)).

In reality, linear wave theory is only strictly accurate for low steepness sea states, steepness is given here using $S_p = 0.5 \times H_s \times k_p$ where k_p is the wave number of the peak period (T_p) of the sea state. Non-linear wave development in steep seas causes higher crests and shallower troughs and the use of unidirectional waves causes larger crests than observed for directionally spread seas (Latheef and Swan (2013)). Error waves, caused by the discrepancy between linear wave theory and reality, are also generated. This is a particular problem when testing in shallow water (Mortimer (2022)), where shallow water is commonly defined at depths which are 1/20th the wave length ($\lambda/h > 20$), deep water where the wave length is twice the water depth or more ($\lambda/h < 2$), and intermediate as being between the deep and shallow cases. In deep water interaction with the sea floor is not 'felt', in shallow water the sea floor has a very large influence on the waves (Journe and Massie (2001)). Waves propagate at different speeds in different water depth conditions according to the phase velocity (c_p) which can be calculated from the wave length according to the dispersion relation.

$$c_p = \sqrt{\frac{g \tanh kh}{k}} \tag{2.3}$$

where the wave number k is defined as

$$k = \frac{2\pi}{\lambda} \tag{2.4}$$

where the wave length λ is

$$\lambda = \frac{g}{\pi} T^2 \tanh\left(2\pi \frac{h}{\lambda}\right) \tag{2.5}$$

Breaking is also influenced by water depth (Journe and Massie (2001)).

2.1.2 Numerical modelling

Computationally expensive, high fidelity approaches to modelling extreme responses are increasing in popularity such as computational fluid dynamics (CFD) and smooth particle hydrodynamics (SPH). Whilst these methods incorporate more of the physics and so are likely to predict responses closest to those of physical experiments, they are not presently capable of running the hundreds of hours of simulations necessary to participate in full probabilistic design approaches. Similarly, they are currently too slow running to be used in the traditional 'deterministic design' approaches involving running many irregular waves (Van Rij et al. (2019a)). Running six, five to ten minute constrained focused waves for several sea states is also impractical. Single focused wave runs however, are workable. Research into domain decomposition, propagating extreme waves using fully non-linear potential flow (FNPF) models before switching to higher fidelity methods in a small region around a device (e.g. Davidson and Costello (2020)), make the use of several constrained focused waves a more viable option.

The remainder of this subsection reviews numerical modelling software commonly used in the modelling of FORE devices.

2.1.3 NEMOH

At the other end of the fidelity scale, frequency domain models are able to quickly predict device motions (Van Rij et al. (2019a)). Frequency domain boundary element methods (BEM) are commonly used to calculate the coefficients required to determine

the resistive forces due to the radiated wave, excitation forces and buoyancy forces which can then be used to predict response amplitude operators (RAOs) which can in turn be used to predict motions via transfer functions. NEMOH (Babarit (2014)) is one such code which is open source and based on linear potential flow. It therefore relies on a number of simplifying assumptions, the most important of which being;

- Inviscid fluid - Viscous effects such as flow separation and turbulence are neglected.
- Incompressible and irrotational flow - constant density and no net rotation.
- Small amplitude motions - amplitudes are small relative to the wave length of the incident wave.
- Linear wave theory - wave surface elevation and kinematics follow Airy wave theory.

Due to these simplifying assumptions, low fidelity models, characterised here as frequency and time domain models which are purely linear, are unable to accurately capture device responses in extreme conditions when and if these are violated.

2.1.4 WEC-Sim

WEC-Sim is a mid-fidelity, Cummins equation and potential flow based open source model, written in matlab and simulink, developed by the National Renewable Energy Laboratory (NREL) and Sandia National Laboratories (NREL and SNL (2022b)). In order to use BEM solvers to model devices in the time domain the Cummins equation, equation 2.6, is used which can be defined and solved numerically with a set of ordinary differential equations (Cummins et al. (1962)). The hydrodynamic forces acting on a body are due to the sum of the incident, diffracted and radiated waves.

$$m\ddot{X} = F_{exc}(t) + F_{rad}(t) + F_{PTO}(t) + F_v(t) + F_{ME}(t) + F_B(t) + F_m(t) \tag{2.6}$$

where $\ddot{X}$ is the acceleration vector of the device (m/s^2), m is the mass matrix (kg), $F_{exc}(t)$ is the wave excitation force, $F_{rad}(t)$ is the force vector as a result of the radiated wave, $F_{PTO}(t)$ is the force due to the PTO, $F_v(t)$ is the damping force vector, $F_{ME}(t)$ is the Morison element force vector, $F_B(t)$ is the buoyancy force, and $F_m(t)$ is the force vector due to the moorings. $F_{exc}(t)$, $F_{rad}(t)$ and $F_B(t)$ are calculated from the hydrodynamic coefficients given by NEMOH. The resistive forces acting on the device due to the radiated wave $F_{rad}(t)$, calculated for the body oscillating in still water, are dependent on the added mass (proportional to the device acceleration) and damping (proportional to the device velocity) matrices $A(\omega)$ and $B(\omega)$ (NREL and SNL (2022b)). All these force terms can be given in Newtons.

$$F_{rad}(t) = -A_\infty \ddot{X} - \int_0^t K_r(t-\tau)\dot{X}d\tau \tag{2.7}$$

where K_r is the radiation impulse response function which captures the fluid memory and A_∞ the added mass at infinite frequency.

$$K_r(t) = \frac{2}{\pi}\int_\infty^0 B(\omega)\cos(\omega t)d\omega \tag{2.8}$$

The excitation force is that felt by the fixed body in small amplitude waves, composed of the Froude-Krylov force due to the pressure of the undisturbed wave and diffraction forces due to the diffracted wave.

The viscous quadratic drag forces are not accounted for in potential flow based models and so are implemented with the Morison equation

$$F_v = -C_v\dot{X} - \frac{C_d\rho A_d}{2}\dot{X}|\dot{X}| \tag{2.9}$$

where C_v is the linear drag coefficient, C_d the quadratic drag coefficient, ρ is the water density (kg/m^3), A_d the characteristic area and $\dot{X}$ the device velocity in a particular degree of freedom. The drag terms are defined for each of the six degrees of freedom

individually. The values of C_d must usually be defined by experiments or with the use of high fidelity, non potential flow based numerical models. As C_d is dependent on the flow around a device the coefficients may need changing based on the sea state studied. The flow regime can be inferred with the use of the Keulegan-Carpenter (KC) and Reynolds (Re) dimensionless numbers, defined here for sinusoidal motion. The beta term β is often also reported to provide information on the evolution of the flow (Journee and Massie (2001)).

$$Re = \frac{2\pi A \rho L}{T\mu} \tag{2.10}$$

$$KC = 2\pi \frac{A}{L} \tag{2.11}$$

$$\beta = \frac{Re}{KC} \tag{2.12}$$

where A is the motion amplitude, μ the dynamic viscosity, T the period and L the characteristic length which for a sphere would be taken as its diameter.

Fast, mid fidelity, potential flow models are typically based on small amplitude waves and motions (NREL and SNL (2022b)). The physics complicating the modelling of the extreme responses not traditionally included in linear potential flow based models can be divided into several categories:

1. Non-linear motions in steep waves due to variable wetness of the hull are particularly relevant to WECs (Merigaud et al. (2012)).

2. Drift forces caused by 2nd order hydrodynamic pressure due to the 1st order wave (mean drift force) and interaction between 1st order motion and the 1st order wave. These effects have been observed to be important for WECs (Fonseca et al. (2008)) and FOWTs (Mahfouz et al. (2020)).

3. Forces due to viscous flow separation - this can lead to vortex induced motions in currents and has been observed for spar type FOWTs (Jie et al. (2020)).

4. Slap and slam impulse loads - impact pressure effects caused by breaking and steep waves are recognised as potentially important to WECs (Katsidoniotaki (2021)) and offshore wind (Pierella et al. (2021)).

5. Ringing and springing - third order wave forces can set off high structural natural frequency responses of the tendons of tension leg platforms (Bachynski and Moan (2014)) and fixed wind monopiles (Suja-Thauvin et al. (2018)).

6. Non-linearity of the wave kinematics are particularly important to fixed offshore wind where the Morison equation is used to determine loading. Efforts have been made to make sure the kinematics are accurately captured using non-linear potential flow based models (Pierella et al. (2021)). It is also likely important for viscous drag dominated effects where the relative velocity between a floating device and the wave will have a significant influence on its motion.

7. External forces such as from moorings and the PTO. E.g. Snatch and snap loading, where a mooring becomes taut, or suddenly goes slack and then retensions (Sirigu et al. (2020)), or control strategies for the PTO of a wave energy convertor in operating conditions (Giorgi (2018)).

The numerical model WEC-Sim is constantly being improved and updated in an attempt to capture these effects and benefits from being extremely flexible and easy to edit. Points 1 and 2 have been addressed by the inclusion of the non-linear hydrostatic and Froude-Krylov forces which relate to the buoyancy and wave excitation (Lawson et al. (2014a)). These are implemented by WEC-Sim with the aid of a mesh to calculate the wetted volume of the device at each time step which greatly increases the simulation time but allows the excitation force in steep waves and the drift response to be modelled. Wheeler stretching (Wheeler (1970)) is used where the particle velocities are capped at the still water values for wetted panels above this level.

$$z^* = \frac{h(h+z)}{(h+\eta)} - h \tag{2.13}$$

where h is the water depth and η the instantaneous water level. The equation shifts z linearly so that z^* is in the range 0 (still water level) to h.

Slamming can be accounted for in the WEC-Sim models as described in (Cruz Atcheson Consulting Engineers (2018)) and implemented in (Atcheson et al. (2019)). However this edited model has not been made publicly available. Ringing and springing has not been addressed in WEC-Sim or OpenFAST but there exist methods to do so (e.g. Bachynski and Moan (2014)). In regard to Point 6, WEC-Sim uses linear kinematics with the Wheeler stretching method applied, which avoids the over prediction from linear theory, and instead results in an under prediction of particle velocities above the mean still water level. Modelling of highly non-linear mooring effects, such as snatch loading by dynamic mooring codes, is an ongoing area of study (Palm et al. (2016)).

2.1.5 OpenFAST

OpenFAST (NREL (2021)) is an aero-hydro-servo-elastic model for wind turbine modelling. The main difference between how the hydrodynamics are dealt with in WEC-Sim and OpenFAST is the treatment of the drift forces, which in OpenFAST are captured using quadratic transfer functions (QTFs), rather than calculating the non-linear Froude-Krylov and hydrostatic stiffness terms (NREL and SNL (2021)). This allows OpenFAST to run much faster than WEC-Sim, but requires a second order BEM solver, such as WAMIT (Wamit (2024)) or AQWA (ANSYS (2024)).

2.1.6 Moordyn

Moordyn (Hall (2015)) is the dynamic mooring model used by both WEC-Sim and OpenFAST. Dynamic models take account of the drag and added mass on the mooring line. It is an open source lumped mass model for the time domain (Sirnivas et al. (2016)), where lines are treated as a series of masses connected by massless springs. A system of equations of motion are solved at the location of each mass.

OrcaFlex (Ltd (2024)) is the industry standard model and currently has the advantage over Moordyn that it uses the wave kinematics in its drag calculations where as Moordyn V1 assumes still water. According to the WEC-Sim development roadmap, this limitation of Moordyn is due to be updated by Moordyn V2 in the third quarter of 2023 (NREL and SNL (2022a)).

2.2 Reliability methods

Once a response model is chosen, the next step in the design process is to estimate the largest load / response a device is likely to experience over its deployment life. There exist many different ways to do this and what follows is a review of the most common in the FORE literature which draws heavily on the WEC design response toolbox (WDRT) and accompanying publications. The WDRT is a python toolbox created by Sandia National Laboratories and NREL to evaluate design loads of WECs Coe et al. (2016a).

The most accurate and direct method of determining the lifetime extreme value distribution of the responses is to run Monte Carlo simulations for the device and response in question (Kim (2012)). E.g. for a device with a one year lifetime, one years worth of simulations would be run and the largest response recorded, this would then be repeated with a different sample of annually representative sea states a large number of times and the data used to produce the empirical CDF. However, in practice this is currently unworkable using anything other than low fidelity frequency domain models, as it would otherwise take far too long and require excessive computing resources.

2.2.1 Short term extreme value distributions from time series

As direct Monte Carlo simulation is ruled out, extreme response distributions for a selection of representative sea states for a location of study are most often estimated from relatively small data sets and then combined to predict the design load (Coe et al. (2018)). An extreme response or extreme value distribution (EVD) is defined as the distribution of the maxima occurring in a chosen exposure time, so the 'true' EVD for the pitch response in a one hour sea state could be determined by running a very large

number of one hour simulations and recording the largest pitch response occurring during each one hour run (Kim (2012)). These distributions for individual sea states in an x hour exposure time are termed 'short term' distributions, the prediction of which require distribution fitting and extrapolation. This is an ongoing subject of study and debate as fitting response distributions based on limited data can lead to significant uncertainties in the tails of a distribution (Michelen and Coe (2015), Doherty et al. (2011), Saeed Far and Abd. Wahab (2016)). The general procedure as explained in detail in Michelen and Coe (2015), involves simulating the sea state in question by irregular waves (either numerically or physically) and recording the global peak responses between zero up-crossings. A distribution can then be fitted to these peaks, the best distribution to fit however is not a certainty and goodness of fit plots (quantile plot, probability plot, return period, probability density function (PDF)) are commonly used to compare and select the appropriate distribution. A peak over threshold method can be employed where only the peaks over a certain threshold are used to fit a generalized Pareto distribution. However, this method can produce wide ranging results depending on the chosen threshold, the selection of which is itself an area of study and debate (Saeed Far and Abd. Wahab (2016)). Michelen and Coe (2015) use a linear frequency domain model to study the convergence of four different methods of determining short term extremes, all peaks Weibull, Weibull tail fit, peak over threshold (POT) and block maxima. These methods are presented below as implemented in Michelen and Coe (2015) for a case study on the extreme force on the power conversion chain (PCC) of a point absorber WEC using a frequency domain model.

The POT method involves the selection of a threshold, the data below which is excluded from the analysis. A generalized Pareto distribution (GPD) is then fitted to the data above the threshold (exponential or Pareto distribution, the tail equivalent of the generalised extreme value (GEV) distribution).

$$F_p(x-u) = 1 - \left(1 + \frac{\varepsilon(x-u)}{\sigma^*}\right)^{-\frac{1}{\varepsilon}} \tag{2.14}$$

where ε is the shape parameter and σ^* the GPD scale parameter and u the threshold level

The block maxima method divides up the data into equally sized samples called 'blocks' and records the largest observed peak in each block. A GEV distribution (Weibull, Gumbel, Fretchet) is then fitted to this data set. The block size is typically set to the exposure time of interest so that the distribution of extremes $F_e(x)$ can be calculated directly, this does not have to be the case however.

$$F_e(x) = exp\left(-\left[1+\frac{\varepsilon(x-\mu)}{\sigma}\right]\right)^{-\frac{1}{\varepsilon}} \tag{2.15}$$

where μ, σ and ε are the location, scale and shape parameters respectively.

In each case the distribution of the extremes for a given exposure time, typically one or three hours, can be calculated by raising the CDF of the peaks ($F_p(x)$) to the power of the expected number of peaks.

$$F_e(x) = F_p(x)^n \tag{2.16}$$

The expected number of peaks n occurring in a given exposure time can be estimated (as shown later). Alternatively a MC simulation could be used to estimate this value, for a three hour storm 1000 peaks are often assumed (e.g. Hunt-Raby et al. (2011)).

It is found that POT and block maxima methods require an order of magnitude more data than the other two methods to function properly. While caution is recommended in the method of distribution fitting chosen as they all have performance trade-offs, the Weibull tail fit is recommended to have a good balance between accuracy, low variance and efficient usage of data. The authors warn that this conclusion may not hold for different sea spectra or if non-linearities are included in the model. The 95% confidence intervals for the expected value of the extreme response are presented for each distribution fitting method so that the effect of data set size on the uncertainty can

be seen in Fig.2.1. The black solid line is the expected value of the empirical "true" I-hour extreme distribution, black dashed lines are the bounds of the 95% interval. The expected values and 95% bounds from the different methods are shown in blue. APW = all peaks Weibull, WTF = Weibull tail fit. The number following the name of the distribution fit on the x axis indicates the number of hours of data used.

The confidence intervals at the higher percentiles of the distributions where the design load is determined will be significantly wider. This raises the questions of how much data is required to narrow the confidence intervals to an acceptable level, and what is an acceptable level at what stage of the design process?

Fig.2.1 has been removed due to Copyright restrictions.

Figure 2.1: A comparison of the expected values of the extreme value distributions of the PCC load using all peaks Weibull, Weibull tail fit, POT and block maxima methods. Reproduced from Michelen and Coe (2015).

The GPD and GEV distribution describe the same set of distributions (Weibull, Gumbel, Fretcht), with the GPD applying to the tail. Their parameters are therefore linked and

obey the following relation (Doherty et al. (2011)):

$$\sigma^* = \sigma + k(u - \mu) \tag{2.17}$$

where k is identical to both.

2.2.2 Short term extreme value distributions from spectra

A rough approximation of the short term EVD is commonly estimated using a linear response spectrum and assuming a Gaussian underlying process leading to Rayleigh distributed peaks. This Gaussian assumption for sea surface elevation is found to be largely empirically accurate (Ochi (1998)). Response conditioned methods are based on these assumptions, as is the scaling of the amplitude for focused waves and so an outline of the theory is given below.

The response spectrum is calculated from the response amplitude operators (RAOs) and sea spectrum.

$$Sr(\omega) = RAO^2 S(\omega) \tag{2.18}$$

The response can be modelled as a random process given by a summation of cosine functions

$$x(t) = \sum_{j=1}^{N} b_j \cos(\omega_j t + \varepsilon_j) \tag{2.19}$$

where ε_j is the phase term which is the sum of the random phase of the wave ϕ_j and the phase of the RAO, t is time. The spectral amplitude of the response spectrum is:

$$b_j = \sqrt{2Sr(\omega_j) \triangle \omega_j} \tag{2.20}$$

The zero mean Gaussian process is calculated using the spectral amplitude of the response spectrum:

$$f_{X_m}(x) = \left(\frac{1}{\sigma\sqrt{2\pi}} e^{\frac{-x^2}{2\sigma^2}} \right) \tag{2.21}$$

$$\sigma^2 = \sum_{j=1}^{N} \frac{1}{2} b_j^2 \tag{2.22}$$

where σ is the standard deviation of the process. If the sea spectrum $S(\omega)$ and spectral amplitude a_j are used rather than the response spectrum $Sr(\omega)$ and amplitude b_j in eqns 2.19 to 2.22 the distribution of surface elevation process is approximated rather than that of the response.

To approximate the distribution of the extremes the number of independent samples of the process dependent on the exposure time m needs to be found, what follows is set out in Kim (2012). This can be done from the standard normal CDF (where $\Phi(x)$ denotes the evaluation of the standard normal CDF at the value x) and the target extreme value (TEV)

$$m = \frac{1}{\Phi(TEV)} \tag{2.23}$$

where TEV is the response divided by the standard deviation of the Gaussian process so that a TEV of four is a response value at four times the standard deviation of the process.

$$TEV = \frac{\hat{x}}{\sigma} \tag{2.24}$$

It can also be related to the expected number of peaks n assuming a Rayleigh distribution.

$$TEV = \left[2 \ln \left(\frac{2\sqrt{1-\varepsilon^2}}{1+\sqrt{1-\varepsilon^2}} n \right) \right]^{\frac{1}{2}} \tag{2.25}$$

The bandwidth parameter is defined as

$$\varepsilon = \sqrt{1 - \frac{m_2^2}{m_0 m_4}} \tag{2.26}$$

where the spectral moments are

$$m_k = \int_0^\infty \omega^k S(\omega) d\omega \tag{2.27}$$

ε represents two exteme cases, a value of zero represents a narrow band spectrum and a value of one a wide-band spectrum. An approximation of the expected number of peaks for a non-wide-banded spectrum, defined as $\varepsilon < 0.9$, is

$$n = \frac{1}{4\pi}\left(\frac{1+\sqrt{1-\varepsilon^2}}{\sqrt{1-\varepsilon^2}}\right)\sqrt{\frac{m_2}{m_0}} \tag{2.28}$$

Finally the distribution of the extremes from m samples of the Gaussian process can be calculated from

$$f_{X_m}(x) = m\left(\frac{1}{\sigma\sqrt{2\pi}} e^{-\frac{x^2}{2\sigma^2}}\right)\left(\Phi(\frac{x}{\sigma})\right)^{m-1} \tag{2.29}$$

TEV, n and m are all ways of quantifying the exposure time. Alternatively the Rayleigh distribution from n samples of the peaks is given by

$$f_{X_n}(x) = n\left(\frac{x}{\sigma^2} e^{-\frac{x^2}{2\sigma^2}}\right)\left(1 - e^{-\frac{x^2}{2\sigma^2}}\right)^{n-1} \tag{2.30}$$

The short term EVD predicted by this method using the Gaussian distribution of the process is slightly different, but asymptotically similar, to that predicted from the Rayleigh distribution of the peaks. This implies that as the exposure time is increased the distributions become ever more similar (Kim (2012)).

2.2.3 Full long term method

If the short term EVDs for a range of sea states are estimated then they can be combined to calculate the long term extreme response distribution. This is commonly done

in the WEC design literature using equation 2.31.

$$\bar{F}X_{3hr}(x) = \int_h \int_t \bar{F}X_{3hr||(t,h)}(x||(Te,Hs))f_{(Te,Hs)}(t,h)dtdh \tag{2.31}$$

where $f_{(Te,Hs)}$ is the occurrence probability distribution for the given sea state and $\bar{F}X_{3hr||(t,h)}$ is the short term survival function for the response of interest, X, in a particular sea state. This short term survival function is otherwise known as the complimentary cumulative distribution function (CCDF) and is used as an alternative to the CDF as it makes the tail region more visible. It can be defined as one minus the CDF.

$$\bar{F}X(x) = 1 - F(x) \tag{2.32}$$

This method requires the selection of a number of representative sea states to model to determine the corresponding short term EVDs. One such method for the selection of the sea states is covered in Coe et al. (2018) and implemented in the WDRT where H_s T_e space is converted to standard normal space and samples taken using areas of equal probability before being converted back to H_s T_e space. This method is widely considered the most accurate method for predicting design loads and is frequently used as a benchmark against which other methods are judged (e.g. Van Rij et al. (2018), Drummen et al. (2009), Coe et al. (2018), Coe et al. (2017)). It is also however, the most time consuming. Coe et al. (2018) numerically studied the long-term heave response of a simplified WEC, consisting of a buoy of $3.6m$ height, by simulating 50, 100, 200 and 400 sea states. They found that there was a significant trade off between simulation time and accuracy as the 95% confidence interval reduced from approximately $6m$ for 50 sea states to $2m$ for 400.

2.3 Environmental characterisation and contour methods

An environmental contour method is an approximate method widely used to estimate a design load which involves the determination of an x year return period contour in H_sT_p

space (DNV (2014)). The short term extreme response distributions for the responses of interest are determined for several sea states along the contour. It is then assumed that the largest median short term extreme response from the sea states along this x year contour corresponds to the x year extreme load. However, if the approach were to be applied in this way it would be neglecting the variation in the response as the short term EVD is different for every sea state, when this is taken into consideration a larger percentile than the median needs to be chosen to represent the design load. Alternatively the contour may be inflated to a longer return period (Winterstein et al. (1993)), (Yu et al. (2015) uses a 20% inflated contour.) and the median selected or a multiplication factor may be applied to it (DNV (2014) and NORSOK (2017) – as referenced in Ross et al. (2020)). The selection of this percentile requires response modelling and different selection methods have been developed (Saranyasoontorn (2006)). Fig.2.2 following Haver et al. (2013) illustrates the inverse first order reliability method (IFORM) process for a 1 in 100 year extreme response where the x and y axis give the H_s and T_p values and the z the percentile of the short term EVD (X_{3hr}) of the response, with 0 representing the $50th$ percentile. The environmental contour method only considers the environmental variables and neglects the response (z axis) and so the 100 year return period is represented by the red circle in the x y plane and the $50th$ percentile of the EVD selected. However, in reality a larger response with an equal probability of ocuurance is likely to exist on a smaller return period contour but at a higher percentile of the EVD (X_{3hr}), shown in the figure by the blue ellipses. To compensate for neglecting the response variability, a larger percentile of the EVD can be selected for the sea state along the 100 year environmental contour (red circle), or the environmental contour can be inflated to a longer return period. The figure illustrates this later approach with the dashed red circle.

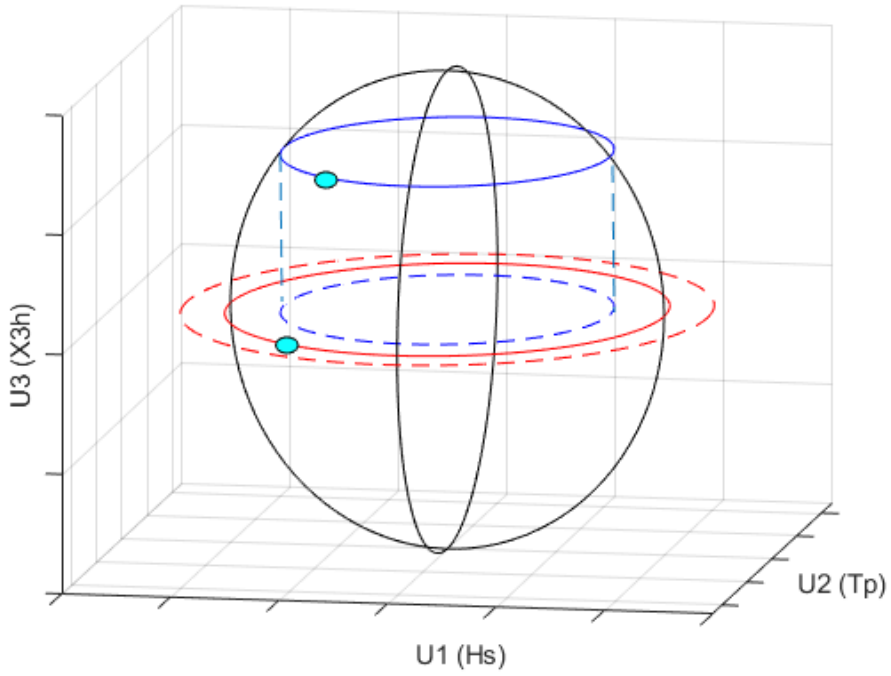

Figure 2.2: Environmental contour method using IFORM, following Haver et al. (2013).

In the absence of a response model, empirical data from other offshore engineering applications can be used to select a percentile to represent the design load. The WDRT recommends a percentile between 75 and 99 be used for the contour (Coe et al. (2018)) based on empirical data from offshore engineering applications (figure from Haver et al. (2013)), but estimates for more exact values will not be possible until real world data for WECs becomes available. The $90th$ percentile is thought to be a reasonable value for the one in 100 year response in locations in the North Sea based on empirical deployment data from other offshore engineering applications (Haver et al. (2013)).

The fitting of the contour itself is not simple and several different methods have been developed. The most common approach is to use an IFORM after fitting a joint distribution to H_s and T_p. A Weibull distribution is fitted to H_s, being the marginal distribution then a conditional lognormal or normal distribution to $T_p|H_s$ (DNV (2014)) as these distributions are observed to best describe the empirical distribution of T_p given H_s.

$$f_{H_s T_p}(h,t) = f_{H_s}(h) f_{T_p|H_s}(t|h) \tag{2.33}$$

The IFORM process (DNV (2014)) then transforms the joint distribution to standard normalised Gaussian space

$$\Phi(u_1) = F_{H_s}(h_s), \Phi(u_2) = F_{T_p|Hs}(t_p) \tag{2.34}$$

The return period of interest is then drawn as a circular contour before converting back to the sea state parameter space. For a 3 hour exposure time this results in

$$\sqrt{u_1^2 + u_2^2} = \beta = -\Phi^{-1}\left[\frac{1}{50x365x8}\right] = 4.5 \tag{2.35}$$

$$h_s = F_{H_s}^{-1}(\Phi(u_1)), t_p = F_{T_p|H_s}^{-1}(\Phi(u_2)) \tag{2.36}$$

The WDRT comprised a comparative study (Coe et al. (2017)) using IFORM fitting different joint distributions which concluded that the distribution chosen has a significant impact on the location and shape of the contour as seen in Fig. 2.3.

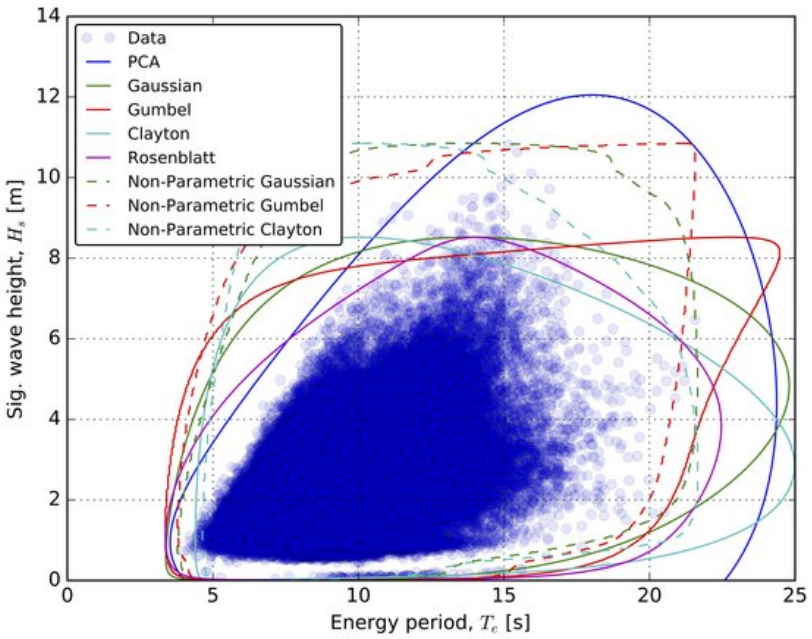

Figure 2.3: Comparison of different contour fitting methods for a 50 year return period, taken from Coe et al. (2017).

The principal component analysis (PCA) was recommended in Edwards and Coe (2019) as all the observed data points, representing 20 years of data were contained within the 50 year contour. This was not true of any of the other methods. However, the PCA was found to be overly conservative at the higher energy period sea states. Subsequent work has highlighted difficulties with the PCA method which make it an inappropriate choice when the joint distribution is bi-modal or displays other unique characteristics (Martin (2016)). They have since suggested kernel density or adaptive bandwidth kernel density approaches may be better, where However, kernel density is often not viewed as a good choice when extrapolating. Contrary to this point, Eckert et al. (2020) show in their contour comparison paper that the kernel density method performed favourably compared with traditional IFORM and PCA.

The Environmental Contours for SAfe DEsign of Ships and other marine structures (ECSCADES) project was a three year partnership between the DNV, Shell UK and the University of Oslo developing contour methods and guidance on their use (Ross et al.

(2020)). Several different methods of producing the contour are outlined from literature and MATLAB scripts provided. It is pointed out that covariates such as direction and season likely alter the joint distribution and that producing separate contours for these covariates may be more appropriate. For example, direction may have a significant impact on the joint distribution due to fetch limited seas in some directions.

They surveyed environmental contour users in industry and highlighted the uncertainty with which the environmental contour is applied. They stress that users should remember that it is an approximate method and set out the following advice for when to use the approach:

- The nature of responses and environmental variables are known: The dominant structural responses of interest and the environmental variables which cause them are understood. They are driven by the long term variability of the environmental variables rather than the short term response variation within sea states.
- Response-based analysis is not possible: Either because there are no accurate, computationally efficient response models available or there are computationally expensive models but no resource to develop approximate models or statistical emulators.
- At outline design stage: The specifics of the device may not be finalised at the initial design stage and so sea states along an environmental contour may provide useful extreme conditions to compare and evaluate design choices.

In regard to the selection of the percentile chosen to be the design load, they point out that an accurate response model would have to be used to determine this and if such a model is available then a response based approach should probably be used instead of a contour approach.

Neither the WDRT or ECSCADES papers discuss how the contour may be unrealistic for low T_p values due to the wave limiting steepness whereby a limit in H_s is reached

due to wave breaking. This steepness limit is defined in DNV (2014) fom the average sea state steepness:

$$S_A = \frac{2\pi}{g}\frac{H_s}{T_p^2} \tag{2.37}$$

where the limiting steepness is defined as $S_A = 1/15$ for $T_p \leq 8s$.

For some devices and response types this high steepness region is likely important. Drago et al. (2013) study this question and propose a modification to the method of fitting a lognormal distribution to T_p where they shift the T_p value by the steepness limit for each bin, $T_p' = T_p - T_{plim}$. This makes use of the property of the lognormal distribution that it cannot go negative to ensure that non-physical sea states are excluded. Further to this the authors note that defining the joint probability distribution in this way may also have an impact on the fatigue life calculations.

The $2D$ contour method can be taken a step further, though at great computational expense, by accounting for the response variability using the short term extreme response distributions. In standard normal space the failure surface is now described as a sphere (as represented in Fig.2.2) with the Z axis representing the variation in the response, as Z increases with decreasing H_s and T_p the percentile of the short term extreme response distribution representing equal probability of occurrence increases. In practice this requires modelling far larger regions of the parameter space than the $2D$ contour to the extent that the simulation time would be similar to that of the full long term approach requiring hundreds of hours of time series to be simulated. The further problem exists of the difficulty in estimating the larger percentiles (> 99) of the short term extreme response distributions. The larger the percentile the larger the confidence intervals and so the more data that is required to make accurate estimates. Contours of equal probability required for the $3D$ contour method are illustrated in Fig.2.4 taken from Rendon and Manuel (2014) for a fixed offshore wind turbine studying fore-aft tower bending moment at the mud line, where the monopile meets the sea bed, and the out-

of-plane bending moment at the blade root. This illustrates how as the likelihood of the contour increases, so to does the percentile of the response (p_3) required to maintain a constant probability.

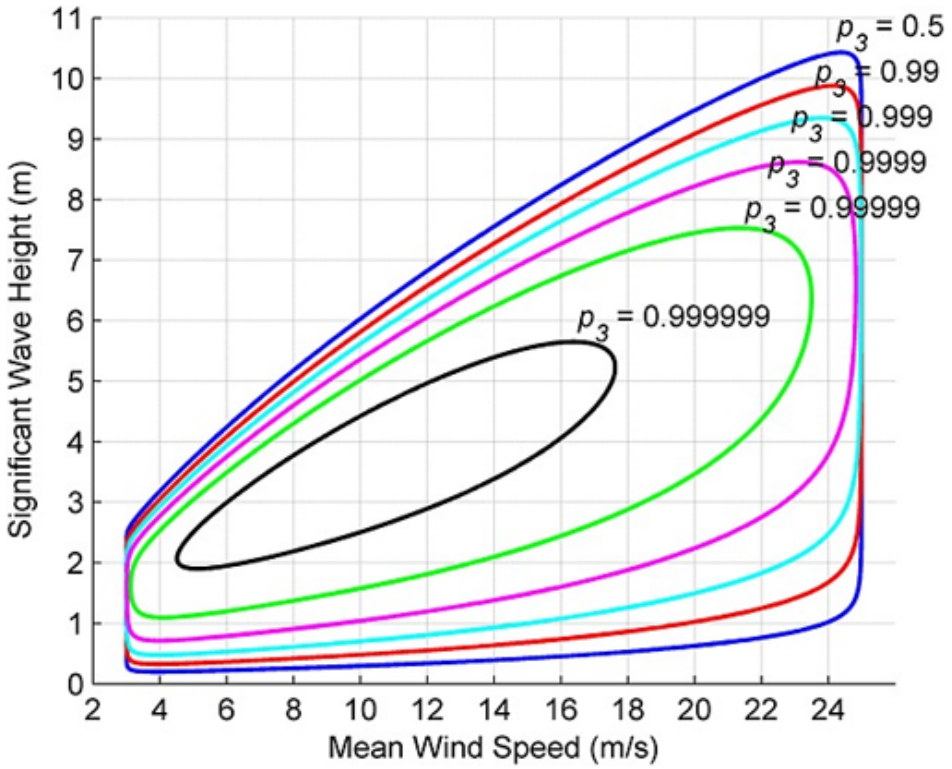

Figure 2.4: Response percentile (P_3) of the EVDs for different contours of equal probability, taken from Rendon and Manuel (2014).

The $3D$ IFORM process for this example (Rendon and Manuel (2014)) may be described with the following

$$l(P_T, v, h) = F^{-1}_{L|Hs,V}(p_3(P_T, v, h)) \tag{2.38}$$

$$l_T = max_{allv,h} l(P_T, v, h) \tag{2.39}$$

$$p_3(P_T, v, h) = \Phi\left(\sqrt{\Phi^{-1}(1-P_T)^2 - (\Phi^{-1}(F_V(v)))^2 - (\Phi^{-1}(F_{H_s|V}(h|v)))^2}\right) \tag{2.40}$$

where $F^{-1}_{L|H_s,V}(.)$ is the inverse cumulative distribution function of the load variable, L that must be estimated from simulations. p_3 is the non-excedance load percentile for L

conditional on V and H_s. $F_V(v)$ is the CDF for the hub height wind speed and $F_{H_s|V}(h|v)$ is the CDF of H_s conditional on V. l_T is the target return period load, $l(P_T, v, h)$ is the long term load for a particular sea state (H_s, V).

In summary, the $3D$ IFORM and full long term methods require the generation of a significant amount of data and therefore a fast and accurate response model. The low number of sea states needed for the $2D$ contour approach make it the only method which can be run quickly enough to be compatible with physical tank testing. It is also most closely aligned with the design load cases approach recommended in design standards, this point will be expanded upon later in section 2.5.

2.4 Short design waves

Focused waves are widely used in three ways in the literature: to study extreme responses in a generic way; for characteristic load prediction; and in the prediction of the EVD. Extremes are most often studied in a generic way in the sense that there is no explicit comparison to an EVD or design load other than in the scaling of the focused wave amplitude to the most probable maximum (MPM) (e.g. Quon et al. (2016)). They are used to study the device responses under an extreme condition and the results can be used as inputs to dynamic structural analysis models. Single focused waves may be used or they may be constrained into random irregular wave backgrounds. Occasionally responses produced by single focused waves have been compared to other methods for predicting design loads in an ORE context in place of irregular wave series (e.g. Van Rij et al. (2018)). Outside of ORE in the fields of ocean engineering and naval architecture, constrained focused wave methods have also been used to predict the short term EVD of the response instead of irregular waves. The constrained NewWave (CNW), conditional random response wave (CRRW) and design load generator (DLG) methods were all developed for this purpose (Taylor et al. (1997), Dietz (2005), Kim (2012)).

The NewWave approach developed by Tromans et al. (1991) treats the generation of a sea state profile as a Gaussian process and uses the spectral density to generate

the average profile of the extreme wave by scaling the different frequency components according to their energy contribution. The same profile would be generated if a very large number of irregular wave simulations were run and the mean profile calculated from the overlay of the largest wave from each run. The wave profile is found to match the autocorrelation function of the spectrum

$$r(t) = \frac{\sum_{p=1}^{N} [S(\omega_p)\delta\omega]\cos(\omega_p t)}{\sigma^2} \tag{2.41}$$

The surface elevation of the NewWave η_N is then scaled to the target crest elevation, η_R, by $\eta_N(t) = \eta_R r(t)$

The amplitude is typically scaled to be the modal value of the extreme for the exposure time e.g. the three hour storm (Tromans et al. (1991)). Or

$$\eta_R = \sqrt{2m_0 ln(n)} \tag{2.42}$$

where n is the expected number of peaks in the exposure time, usually 3 hours. n is often assumed as 1000 when a three hour exposure is used (Hann et al. (2015)). When the peaks are Rayleigh distributed η_R is at the $38th$ percentile approximately, meaning that 62% of the time the three hour storm is run the amplitude η_R is exceeded (Ochi (1990)). The amplitude of each wave component is scaled in accordance with Bennett et al. (2012) using the following:

$$A_p = \eta_R \frac{S(\omega_p)\delta\omega}{\sum_{p=1}^{N} S(\omega_p)\delta\omega} \tag{2.43}$$

Fig.2.5 shows an example of the NewWave amplitude generated at $1:50$ scale, $H_s = 14.4m, T_p = 18.8s$ for a 14 minute exposure time in relation to a histogram of the largest wave amplitudes from $10,000$ realisations. It can be seen that the NewWave amplitude corresponds to the peak of the distribution indicated by the histogram. The underpinning assumption is that the most likely extreme wave in a three hour storm is likely to

produce the most likely extreme device response/load. However, whilst this may hold true for fixed structures such as monopiles, it is not necessarily the case for dynamic floating bodies. Experimental and numerical studies have confirmed this for Jack-ups (Taylor et al. (1997)) and WECs (Hann et al. (2018)). Several studies have applied the NewWave to WECs (Rafiee et al. (2016), Orszaghova et al. (2016), Hann et al. (2018), Santo et al. (2017)) .

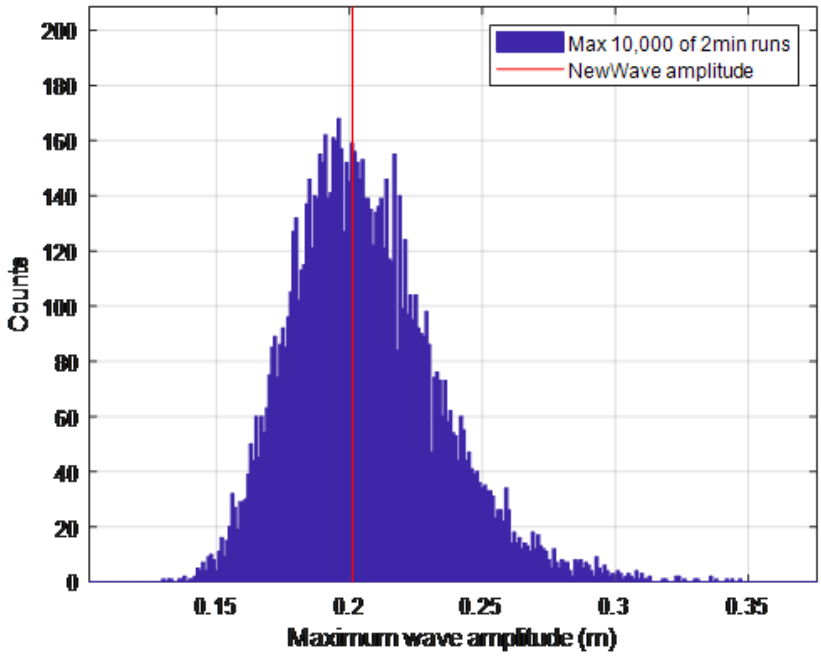

Figure 2.5: NewWave amplitude comparison to histogram of the maximum wave amplitudes occurring in a 14 minute exposure time (2 minutes at 1:50 scale).

In Rafiee et al. (2016) and Orszaghova et al. (2016) a phase shifted NewWave, where the phase no longer aligns at zero, was used to excite the extreme responses of Carnegie's CETO submerged point absorber WEC. Their scale model experiments focused on the extreme PTO extension response using irregular wave time series tests to identify the seven largest responses. The wave profiles which produced these responses were then analysed and compared to a phase shifted NewWave. The NewWave was shifted by the average phase angle of the RAO of the PTO response that dominated the energetic part of the underlying wave spectrum considered so that

the shape of the wave would produce a larger response. This short wave profile was then run and found to produce an extreme PTO response comparable to those generated by the seven extreme responses recorded during the long IW runs. The authors conclude, unlike the studies of the previous paragraph, that the focused wave can be used successfully to estimate the extreme response of the WEC accurately. This illustrates that methods for predicting extremes may depend on the device and response being studied. The responses produced were not compared to the EVD for the sea state studied.

The MLER wave developed in Adegeest (1998) follows a similar method but the profile is calculated from the response spectrum of the response of interest and the amplitude is often scaled according to the response rather than the wave amplitude. It is therefore based on the assumption that the non-linear response is a small perturbation from the linear one. Quon et al. (2016) scaled the MLER wave profile according to the most likely expected wave height, the same height which the NewWave is commonly scaled to. Other response conditioned wave profiles have been developed, such as the most likely response wave (MLRW) or the NewWave in response method applied to the M4 device (at that time a three float WEC) in Santo et al. (2017), but the MLER is the one which most commonly occurs in the WEC literature (Quon et al. (2016), Rosenberg et al. (2019), Coe et al. (2019), van Rij et al. (2019)). The WDRT produced an open toolbox with python scripts for its implementation (Coe et al. (2016b)). The ability of a MLER profile to reproduce target extreme responses however, is like the NewWave, limited by a device's dynamic behaviour (Quon et al. (2016), Rosenberg et al. (2019), van Rij et al. (2019)).

Regular wave methods have also been extensively investigated where waves of height $1.9 \times H_s$ are often used in place of focused waves (Yu et al. (2015), van Rij et al. (2019), Coe et al. (2019), Rosenberg et al. (2019)). This follows guidance found in NORSOK (2017), DNV (2014). For fixed offshore wind turbines non-linear regular waves have been embedded into linear irregular wave time series to predict design loads as in

Rainey and Camp (2007). The effects of non-linear vs linear waves on fixed offshore wind turbines has been studied extensively in the DERISK project comparing linear irregular, non-linear irregular and constrained waves (Wang et al. (2021b), Pierella et al. (2021)).

Attempts to reconcile the NewWave approach for more dynamic applications when the preceding wave time history is important have been made by constraining the focused wave into random background sea states. Taylor et al. (1997) developed the embedded or constrained NewWave (CNW) to evaluate the extreme responses of a jack-up and found that the extreme loads are not always produced by the extreme wave amplitude, the device memory effects are also very important. They conclude that the NewWave underestimated the extreme response as it neglects the random background and therefore for dynamically responding structures, CNWs are required.

The process of constraining the NewWave into a random irregular background as outlined in Bennett et al. (2012) is as follows

$$\eta_C = \eta_I + r(t)[\eta_R - \eta_I(t_1)] + \left(\frac{-\dot{r}(t)}{m_2/\sigma^2}\right)[\dot{\eta}_R - \dot{\eta}_I(t_1)] \tag{2.44}$$

Recall that r is the autocorrelation function (equation 2.41) and η_R the target crest amplitude. η_I is the random background wave defined as

$$\eta_I(t) = \sum_{p=1}^{N} A_p \cos(\omega_p t + k_p x + \phi_p) \tag{2.45}$$

Göteman et al. (2015) constrained the NewWave into several regular wave backgrounds to investigate the wave loads on a single point moored point absorber WEC and how background waves influence these loads. four different frequency waves and several phase backgrounds were considered totalling 32 cases. A large variability in the load was reported which further highlights the importance of history effects and the preceding waves.

The CNW was studied in relation to WECs in Hann et al. (2018) where a generic representation of a point absorber WEC was exposed to irregular wave time series; a NewWave was constrained into 180 unique irregular wave backgrounds and 24 CNWs in two regular wave backgrounds were also tested. The experiments were carried out in a physical wave tank. It was found that the target CNW time series were not easily reproducible experimentally, a finding also reported in Bennett et al. (2012). The irregular CNWs were found to experience larger mooring loads and surge motions than the regular CNW. The study compared the responses of the WEC to NewWaves, regular CNWs, irregular CNWs and long irregular wave time series simulations and did not attempt to reproduce the EVD with the embedded cases.

Embedding MLER waves in a random background leads to the conditional random response wave (CRRW) developed in Dietz (2005). Sagging and hogging responses of ships were studied. The surface elevation is calculated in a slightly different manner to that discussed up until now, where the phase randomization is accounted for by coefficients rather than phases. Equations 2.46 - 2.52 detail the approach.

$$\zeta(t) = \sum_{n=1}^{N} a_{\zeta;n}[V_n \cos(-\omega_n t) + W_n \sin(-\omega_n t)] \tag{2.46}$$

where N is the number of wave components, V_n and W_n are independent standard normal random variables and $a_{\zeta;n}$ is the spectral amplitude. The method follows a Slepian model process which describes the conditional behaviour of a stochastic process (See appendix A), where the conditioned values of V_n and W_n used to constrain the desired response conditioned focus wave are $V_{n;c}$ and $W_{n;c}$

$$\begin{aligned} V_{n;c} = V_n &- \frac{a_{M;n}}{m_2 m_0 - m_1^2}(m_2 - \omega_n m_1)S_1 \cos(\theta_{M;n}) - M_c(m_2 - \omega_n m_1)\cos(\theta_{M;n}) \\ &+ (\omega_n m_0 - m_1)S_2 \sin(\theta_{M;n}) + (\omega_n m_1 - m_2)S_3 \sin(\theta_{M;n}) + (\omega_n m_0 - m_1)S_4 \cos(\theta_{M;n}) \\ &- M_c \omega_M(\omega_n m_0 - m_1)\cos(\theta_{M;n}) \end{aligned} \tag{2.47}$$

$$W_{n;c} = W_n - \frac{a_{M;n}}{m_2 m_0 - m_1^2}[(m_2 - \omega_n m_1)S_1 \sin(\theta_{M;n}) - M_c(m_2 - \omega_n m_1)\sin(\theta_{M;n}) \\ -(\omega_n m_0 - m_1)S_2 \cos(\theta_{M;n}) - (\omega_n m_1 - m_2)S_3 \cos(\theta_{M;n}) + (\omega_n m_0 - m_1)S_4 \sin(\theta_{M;n}) \\ - M_c \omega_M (\omega_n m_0 - m_1)\sin(\theta_{M;n})] \tag{2.48}$$

$$S_1 = \sum_{n=1}^{N} a_{M;n}[V_n \cos(\theta_{M;n}) + W_n \sin(\theta_{M;n})] \tag{2.49}$$

$$S_2 = \sum_{n=1}^{N} a_{M;n}\omega_n[V_n \sin(\theta_{M;n}) - W_n \cos(\theta_{M;n})] \tag{2.50}$$

$$S_3 = \sum_{n=1}^{N} a_{M;n}[-V_n \sin(\theta_{M;n}) + W_n \cos(\theta_{M;n})] \tag{2.51}$$

$$S_4 = \sum_{n=1}^{N} a^e_{M;n}\omega_{e;n}[V_n \cos(\theta^e_{M;n}) + W_n \sin(\theta^e_{M;n})] \tag{2.52}$$

where $a_{M;n}$ is the spectral amplitude of the response spectrum, M_c is the target response amplitude and $\omega_M = \frac{m_1}{m_0}$. The conditioned values $V_{n;c}$ and $W_{n;c}$ are then substituted in place of V_n and W_n in (equation 2.46) to produce the embedded wave time series. The MLER wave is obtained by defining V_n and W_n as Gaussian random variables with zero mean and standard deviation equal to $a_{M;n}$ rather than one.

A similar approach to the CNW in Taylor et al. (1997) was adopted in Dietz (2005) whilst studying extreme hogging and sagging responses of ships and extended to uncondition the response conditioned profile in order to estimate the EVD. 15 batches of 100 CRRW simulations were performed to achieve consistent data fitting at $250MNm$ bending moment intervals between $2500-6000MNm$ according to the linear EVD. GEV distributions were fitted to each of the 15 sets of 100 non-linear responses, the non-linear short term EVD for the sea state was then approximated using:

$$FX_{3hr,NL}(x_{NL}|h_s,t_z) = \int_0^\infty FX_{3hr,NL}(x_{NL}|X_{3hr,L} = x_L, h_s, t_z) f_{X_{3hr,L}}(x_L|h_s,t_z) dx_L \tag{2.53}$$

where x_{NL} is the non-linear response given the linear response level x_L. $FX_{3hr,NL}(x_{NL}|X_{3hr,L} = x_L, h_s, t_z)$ is obtained by simulation of the 100 CRRW profiles for a linear target response. $f_{X_{3hr,L}}(x_L|h_s,t_z)$ is the Rayleigh short term EVD as calculated from the linear response spectrum (Dietz (2005)). The calculation of the long term extreme response distribution from CRRW waves (or CNWs) would require thousands of simulations for the short term EVD of each sea state. This method on its own does not therefore reduce the computational effort required in calculating the short term EVD (for a three hour exposure time) compared to the method of extrapolation and its success is dependent on the non-linear responses being small perturbations from the linear responses. Drummen et al. (2009) conclude that the CRRW method for determining the short term EVD is unworkable experimentally due to the large number of required simulations.

Directionality may also be important for the extreme loads on ORE devices and so a focused wave approach that can be adapted to short crested seas would be useful. Cassidy (2011) considered the short crested NewWave and Mirzadeh et al. (2016) the short crested CNW. Pastoor (2002) developed the directional MLER model. To the best of the author's knowledge the CRRW hasn't been made directional. These all use double summation methods, where each frequency component is not uniquely defined by one direction, thus rendering the calibration with a single WG a formidable challenge, if not impossible.

Kim (2012) points out in a review chapter on focused waves that one potential draw back of the constrained focused waves is that the focused wave of a particular amplitude has to be produced independently of the irregular background wave that it's embedded in. This limitation is addressed in Kim (2012) and Alford (2008) in the development of the design loads generator (DLG) which is the subject of the next chapter. The DLG was developed by the University of Michigan for use in ship design and offshore engineering. It presents a method which may be useful in the determination of

wave profiles leading to WEC design loads and to the author's knowledge has not yet been applied to ORE. It is explained and applied using a case study in chapter 3 but for more detail see Alford (2008), and Kim (2012). For discussions of the development of focused wave approaches see Kim (2012), Hann et al. (2018), Dietz (2005).

2.5 Design standards

There are various offshore engineering design standards available to FORE developers with those produced by DNV and the IEC being regularly cited. Summarising the standards is not necessarily straight forward as there are different device types and responses involved. Broadly, there are two methods for the characteristic load prediction which will be termed here the average of maxima and high percentile approaches (DNV (2018), IEC (2019)). The average of maxima method is used for the majority of responses in the IEC standards and for the mooring loads by the DNV. It consists of running several phase seeds for the design wave method, either irregular waves or constrained waves, and comparing the average of the maxima from each run between each sea state studied. Often this is the mean of the maxima but for mooring loads it is the most probable maximum (mode) which is used assuming a Gumbel distribution. In practice this is calculated using the mean and standard deviation of the maxima of the seeds by Eq.2.54 below. DNV (2015) state the most probable maximum of the Gumbel EVD corresponds to the $37th$ percentile and the expected value to the $57th$. The high percentile method is used in DNV documents for most other types of response.

$$MPM = \mu - 0.45x\sigma \tag{2.54}$$

For the characteristic mooring load the prediction is split into static and dynamic components and separate safety factors applied to each according to a consequence class. For consequence class two the failure of the component could lead to possible loss of human life or the subsequent damage of other structures and so a large partial safety factor is applied. For consequence class one these things are not true and a smaller

safety factor can be used. Typically floating ORE devices will be deployed in arrays and so the moorings are likely to come under consequence class two requiring a higher safety factor.

The IEC standard for fixed offshore wind IEC (2014), permits the use of constrained wave methods where a non-linear regular wave or stream function wave is embedded in a linear irregular background. This is done in the absence of the device where the particle velocities are used in the Morison equation to determine loading.The DNV fixed offshore wind guidance also permits constrained wave methods by referencing the IEC standard (DNV (2016)). The IEC floating wind standard IEC (2019), does not recommend this approach as diffraction can be important for large volume structures and so determining particle velocities in the absence of a structure is inappropriate.

However, this does not mean a different constrained wave approach would not be valid. The DNV floating wind standard makes no reference to constrained methods (DNV (2018)). The IEC wave and tidal standards (IEC (2016), IEC (2015)) allow constrained wave methods for both the device and mooring responses if the designer can demonstrate they are at least as conservative as the characteristic loads estimated from irregular waves.

Table 2.1 summarises the post processing methods used in the standards.

Table 2.1: Characteristic load prediction comparisons for different standards. Details column indicates either the average used or the minimum percentile. AM = average of maxima, HP = high percentile, M = mean, MPM = most probable maximum.

Response type	Standard	Method	Details	Seeds
Device response/load	IEC (2016)	AM	M	> 6
	DNV (2014) DNV (2018)	HP	$> 75\%$	
Dynamic Mooring load	IEC (2015)	AM	MPM	> 6
	DNV (2015) DNV (2018)	AM	MPM	> 10

The standards give a list of explicit DLCs which should be assessed to calculate design loads and that include sea states where a device is in normal operation and those

where they are in survival mode. A full set of these requires thousands of simulations and so a mid-fidelity numerical model is necessary. The DLC most relevant to extremes is DLC 6.1 which uses a contour approach at the 50 year return period (IEC (2016), IEC (2014)) to assess extreme sea states.

In the IEC fixed wind standard IEC (2014), variations on the mean of maxima method also exist where the mean of the upper half of the maxima are used when investigating DLCs relating to control system failure and emergency stops.

Haselsteiner et al. (2022) published a comparison of different contour methods to the long term approach using OpenFAST for the bending moment response of a fixed OWT. They found that contour methods using the IEC post processing method, selecting the mean response from the maxima of the seed realisations, under predicted the characteristic load by between 17% and 28% but by applying the higher percentile approach as in DNV (2014) better agreement was found. However, the selection of the contour method produced differences in the percentile found to accurately represent the characteristic load when compared to the full long term approach.

This chapter has presented the background literature and theory necessary to evaluate the ability of focused and constrained focused waves to predict design loads using methods in line with existing standards. The following chapters will apply many of these methods and much of this theory in physical and numerical model case studies.

Chapter 3

X-MED

Chapter summary

A numerical model is calibrated and validated against 1:50 scale experimental data for a single point moored point absorber termed the X-MED buoy. Different methods of using short design waves to predict the EVD in the 100yr extreme sea state are then compared with the traditional irregular wave approach. The impact of history effects and nonlinearities are discussed with the aid of numerical models. Suggestions are then made as to how focused and constrained focused waves may be used for characteristic value predictions in line with the IEC standards.

3.1 Introduction

The aim of this chapter is to investigate the uses of short design waves using response conditioned methods in relation to dynamic FORE. The extent to which mid-fidelity models such as WEC-Sim are able to accurately model extreme responses is often questioned and so an extensive model validation is undertaken before the model was then used to investigate the EVDs and design loads. There are three main parts to this chapter, the first is a calibration and validation of a WEC-Sim model for use in the modelling of extreme mooring responses. The second is an assessment of the validity of CRRW and DLG response conditioned methodologies for prediction of the short term EVDs for dynamic, floating ORE applications. The third section is a discussion of the practical application of short design waves, their selection for use in physical experiments and whether or not a single or small number of cases can be used in the prediction of design loads.

3.2 Introduction to the Xmed buoy model

Hann et al. (2018) carried out experiments in the University of Plymouth's COAST lab using a generic point absorber, the X-MED buoy, illustrated in Fig.3.1.

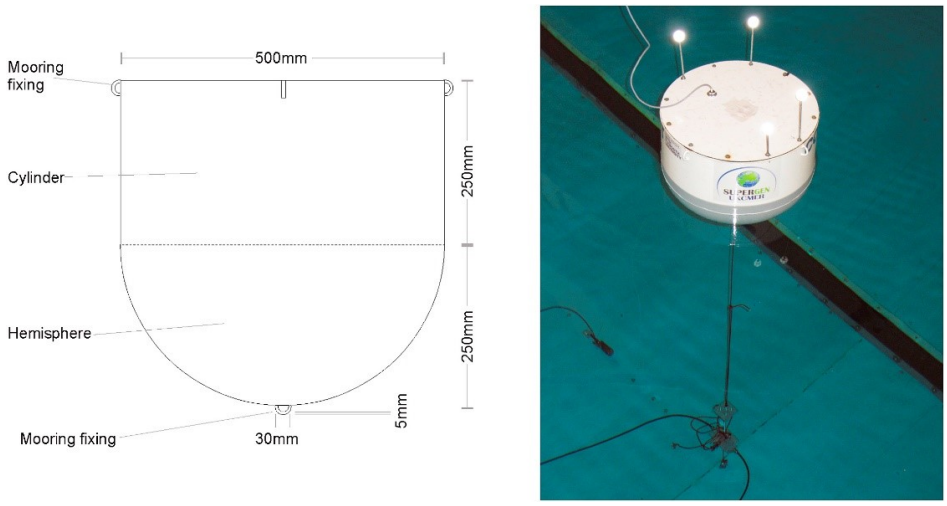

Figure 3.1: Photo of the X-MED buoy and dimensions. Taken from Ransley (2015).

The device was used to investigate snatch loading in 100 year extreme storm conditions at the wave hub demonstration site off the coast of Cornwall in the UK. The tests were performed at $1:50$ scale with target full scale significant wave height and peak period of $H_s = 14.4m$, $T_p = 18.8s$. The device has subsequently been used in numerous studies, experimentally to investigate CNWs and numerically to validate CFD models and in code comparison projects (Ransley et al. (2020)). The large amount of available experimental data and numerical studies make it a useful starting point in investigating extreme responses of point absorbers. The lack of a PTO further simplifies the numerical and physical modelling required as does the relatively simple single point mooring configuration. WECs are commonly assumed to be in survival mode during extreme response modelling and so PTOs are usually excluded from the analysis.

The X-MED buoy was designed for the EPSRC project (Hann et al. (2015)) Extreme loading of marine energy devices due to waves, current, flotsam, and mammal impacts. It was designed to be a generic representation of a heaving point absorber for use in

a set of experiments on extreme responses and so is not representative of any one particular full scale commercial WEC.

The experimental set up consisted of a $43.2kg$ buoy in $2.8m$ water depth secured to a spring by, $35kN/m$ stiffness Dyneema rope. The spring is then fixed to the tank bottom by a universal joint so that the buoy can move in 6DoF. The X-MED buoy geometry consists of a $0.5m$ diameter $0.25m$ high cylinder atop a $0.25m$ radius hemisphere (Fig.3.2)

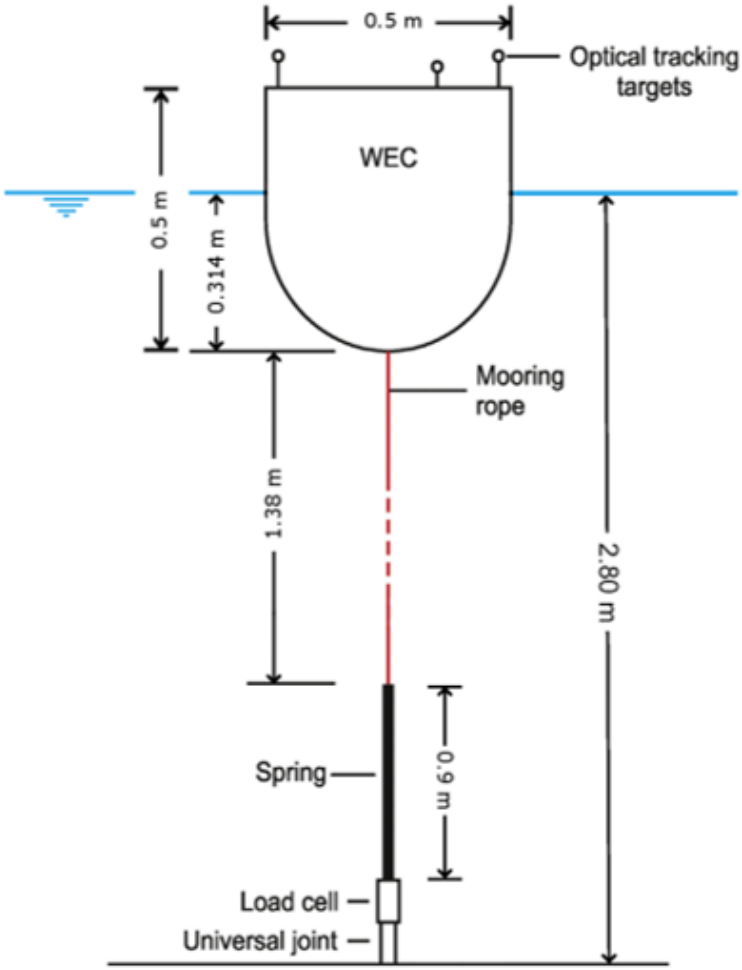

Figure 3.2: Experimental set up for the X-MED buoy. Taken from Musiedlak et al. (2017).

The experiments carried out in this work are in deep or the deep end of intermediate water depth. The irregular waves require a frequency dependent amplitude correction to make sure the target significant wave height, peak period and spectrum are physi-

cally realised in the tank. In this work there is no attempt to correct for error waves as this is not standard practice for wave basins.

The POT method will be used in this thesis for fitting EVDs to response time series as it makes use of a large amount of the data and is flexible enough to produce a good fit to different families of distributions. The characteristic mooring loads have been evaluated using a mean of maxima approach applied to the total mooring load values without separating into mean and dynamic components and without applying equation 2.54. This decision was made so as to more easily facilitate comparisons with other response types and because no design load prediction is actually being made for any device, the focus is on the comparison of different methods for determining characteristic loads for ultimate limit states.

3.3 Numerical model calibration

The use of CFD models in the determination of EVDs is inappropriate due to the large number of one to six hour simulations required (Van Rij et al. (2019b)). For this reason a mid-fidelity model based on potential flow and the Cummins equation such as WEC-Sim is necessary. However, the model must be able to reproduce the responses of the device with reasonable accuracy and there is likely to be a trade-off between reducing the simulation time and maintaining an acceptable degree of accuracy. The level of accuracy required to maintain the partial safety factors prescribed in design standards IEC (2016) is still an open question. For this reason the model needs to be calibrated and validated against experimental data before carrying out any analysis of the EVD. The response of interest studied in this chapter is the extreme mooring load which is here inferred from the spring extension calculated from the heave, surge and pitch positions.

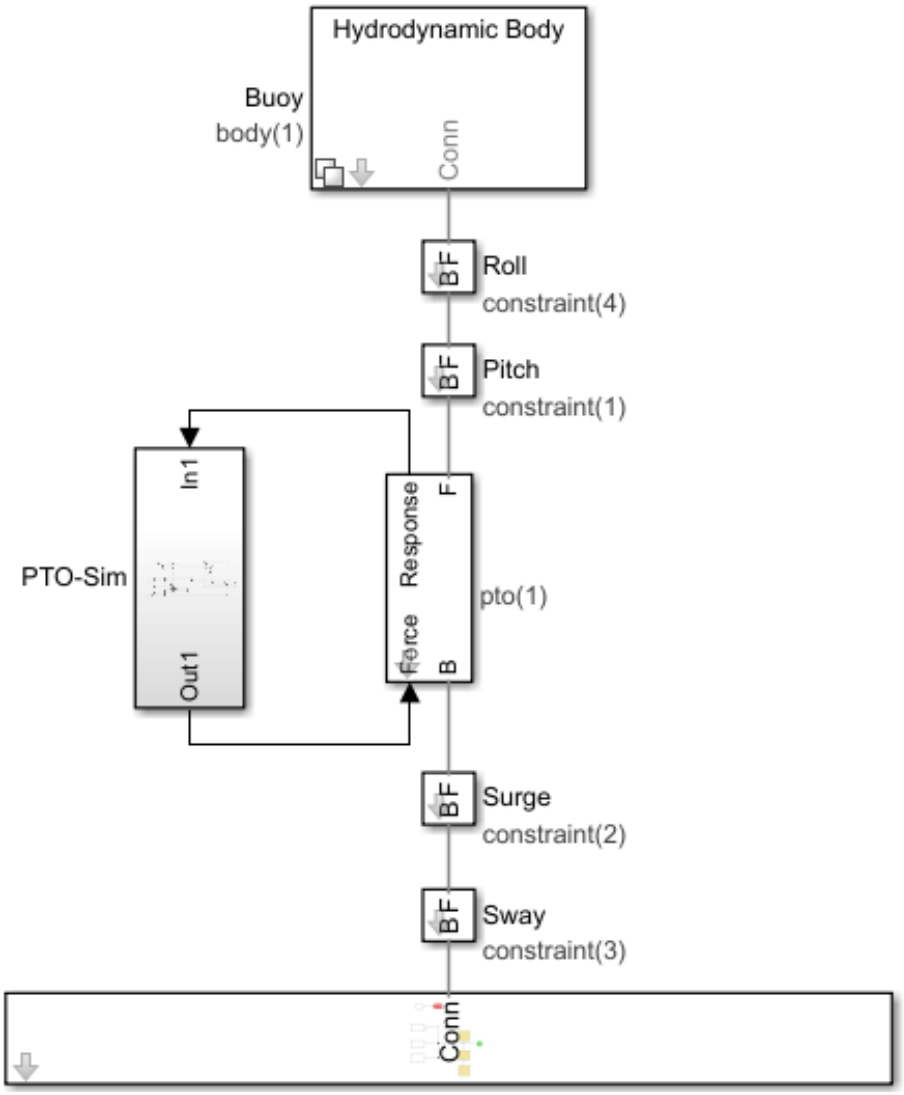

Figure 3.3: Simulink model used for the WEC-Sim simulations.

The WEC-Sim model uses constraints to allow movement in five degrees of freedom (DOF), surge, sway, heave, roll and pitch (Fig.3.3). There are only very limited motions in roll and sway as all waves are unidirectional and so these DOF are excluded from all analysis in this thesis. The spring is represented by a PTO block with a stiffness term of $66.3N/m$, the pre-tension enacted by the initial extension of the spring is modelled at the PTO using a pre-tension of $23.4N$ to be in agreement with the physical model.

173 irregular CNW and 3.8 hour duration (model scale) irregular wave physical runs carried out by Hann et al. (2018) provide useful calibration data which can be used

to validate the WEC-Sim models ability to simulate extremes, quantify errors in the numerical results, and determine the physical conditions under which the model is accurate. The factors which greatly improve the accuracy of the linear WEC-Sim model are the inclusion of weak nonlinearities, in the form of a changing hydrostatic stiffness term and Froude-Krylov (FK) force, along with the calibration of the viscous drag coefficients (Lawson et al. (2014a)). The FK force makes up part of the wave excitation force and has a significant impact on the low frequency surge motions of the device. It is calculated by integrating over the pressure at every time step, this requires an STL mesh input and significantly increases the computation time. Therefore, it is important to make the mesh as coarse as possible without reducing the accuracy to an unacceptable level. Two meshes are required, mesh one is used by NEMOH to calculate the linear hydrodynamic coefficients used as inputs to the WEC-Sim model (added mass, radiation damping etc) and mesh two to calculate the weak nonlinearities from the wetted volume. Fig.3.4 shows the spring extension produced by two versions of the WEC-Sim model, one using very fine meshes consisting of 2969 and 22708 pannels for meshes one and two respectively. The other shows the meshes selected for use in the numerical case study which consisted of 1190 and 902 pannels for meshes one and two respectively. The wave used for this study was an MLER wave for the spring extension using a three hour exposure time. The percentage difference in the spring extensions produced by the two WEC-Sim models was 0.37% and the absolute difference was $0.97mm$. The WEC-Sim model using the finest meshes took 1166.2 seconds to run vs 67.5 seconds for the meshes selected for use in the case study. The simulation with the selected meshes therefore ran approximatly 17 times faster than that using the finest combination, but there was only a 0.37% difference in the extreme spring extension. Fig.3.5 illustrates the two STL meshes used in this comparison to calculate the weak nonlinearities.

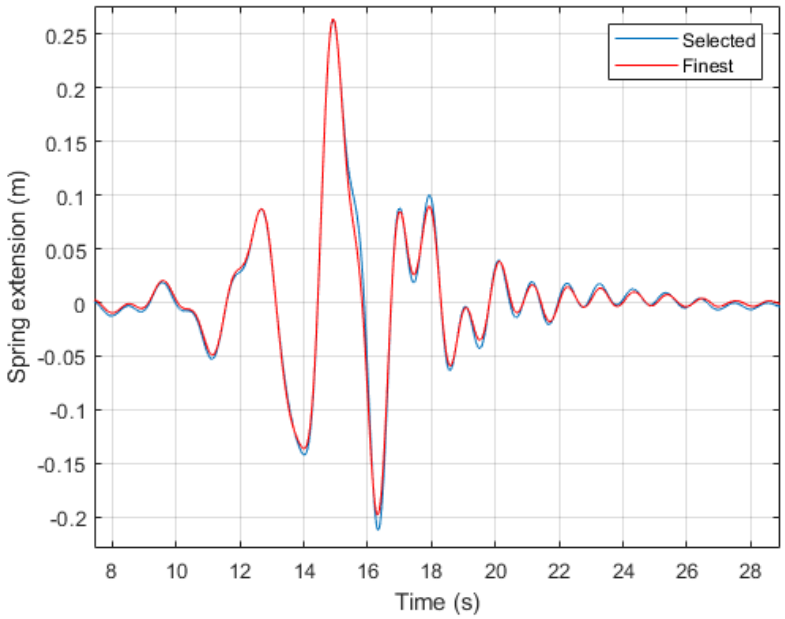

Figure 3.4: WEC-Sim time series of extreme spring extension in response to an MLER wave for different mesh sizes

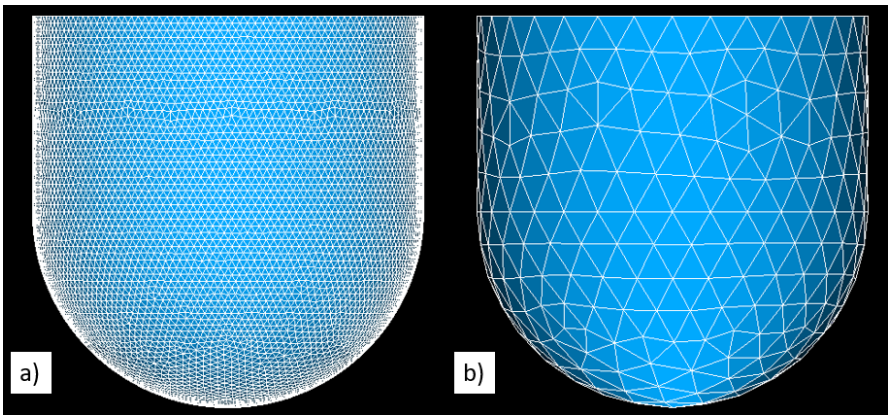

Figure 3.5: WEC-Sim STL meshes used in the calculation of the wetted volume at each time step. a) was the finest mesh tested which has 22708 pannels, b) is the mesh selected for use in the numerical case study and has 902 pannels.

The drag coefficients used to best replicate the experimental test motions were $CDx = 0.3$, $CDz = 0.085$, $CDpitch = 0.05$. CDz was determined from heave decay test data following a least squares curve fitting method where the WEC-Sim model was run for 0.05 increments of CDz between 0.075 and 0.1 and the CDz value providing the

best fit identified. Fig.3.6 shows a comparison of the normalised heave displacement time series between the physical experiments, the WEC-Sim model with no quadratic damping term ($CDz = 0$) and the identified best fit value ($CDz = 0.085$).

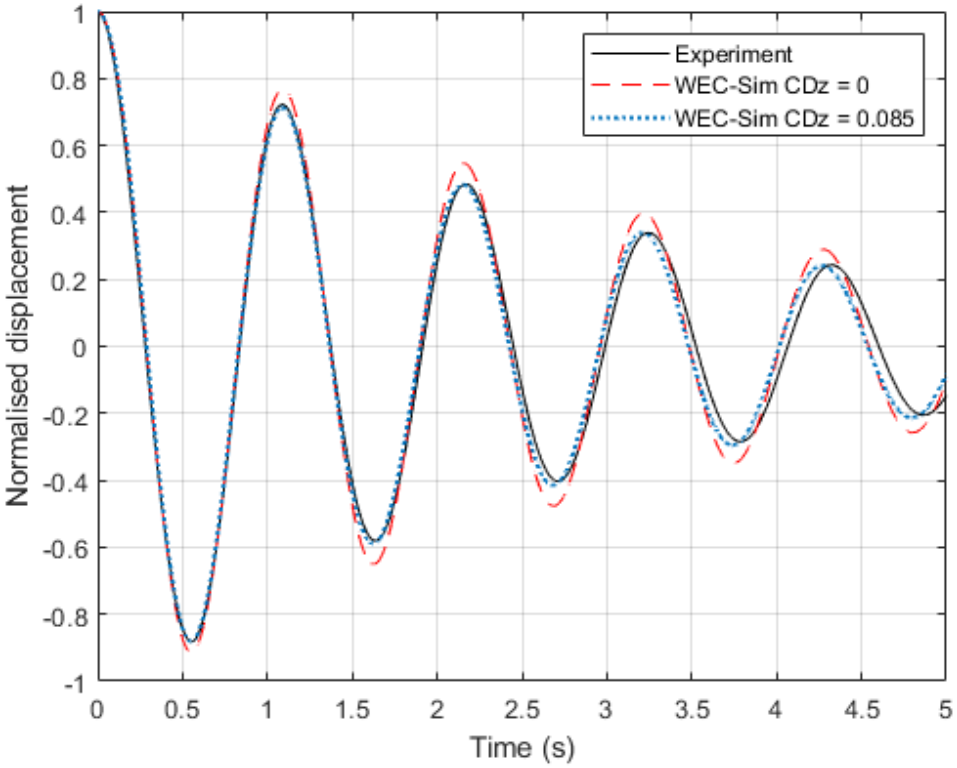

Figure 3.6: Comparison of the normalised heave displacement during a heave decay test between the experiments and WEC-Sim with and without viscous drag.

CDx was estimated from several constrained NewWave experimental runs. The value of CDx is approximate as different values would be optimum for different wave runs, a fact exhibited in van Rij et al. (2019) who as part of the CCP-WSI X-MED blind comparison study tuned the drag coefficients to CFD runs for each individual focused wave case. Their WEC-Sim model took approximately 4 minutes to run per case where as the CFD simulations took 6 days each ($55000CPUhr$) and the optimal CDx varied from 0.6 to 0.8. In the present work a single value is used as tuning the coefficient on a wave by wave basis is deemed too time consuming to be of practical use. Therefore CDx was estimated from 3 of the CNW cases. Drag is implemented through the Morison

equation.

The 173 CNWs were run using the calibrated WEC-Sim model with the drag coefficients stated above. The model error of the peak spring extension is presented by the boxplots in Fig.3.7 and Fig.3.8 where it can be seen that the response is approximately over and under predicted an equal number of times. The boxplots show the median result with a solid red line, the box then gives the 25th and 75th percentiles (q1 and q3), the protruding lines or 'whiskers' then show the maximum and minimum values excluding outliers which are indicated by the red crosses. Outliers here are defined as being one point five times the interquartile range (q3-q1) above q3 or one point five times the interquartile range below q1. The most significant errors occur when the WEC-Sim model over predicts. The magnitude of the median percentage error is 9.6% which corresponds to $2.8cm$, this case is shown in Fig.3.9.

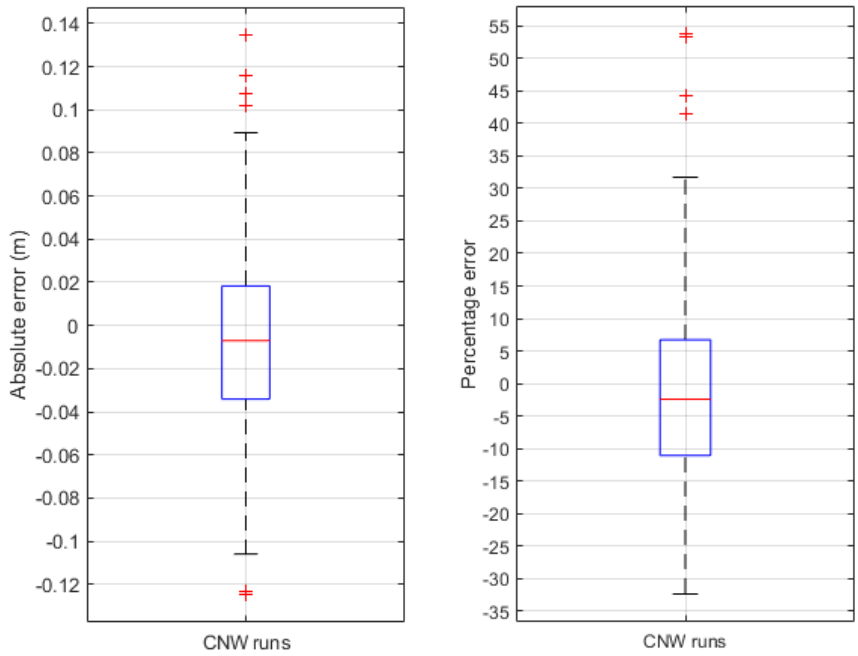

Figure 3.7: Box plots showing the percentage and absolute error of the WEC-Sim model

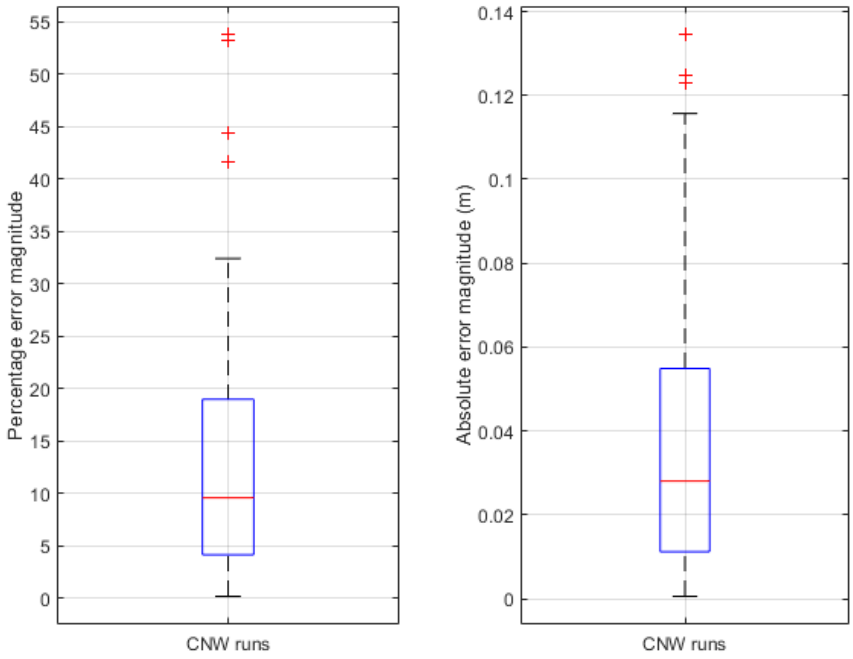

Figure 3.8: Box plots showing the percentage and absolute error magnitudes of the WEC-Sim model

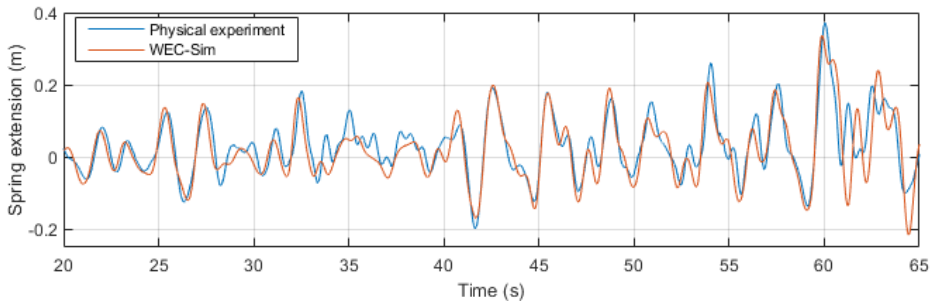

Figure 3.9: Experiment and WEC-Sim model time series for case giving the median error in spring extension.

It is noted that the percentage error appears to be independent of wave amplitude but there is a negative correlation between the percentage error and response magnitude, as demonstrated in Fig.3.10(d), implying that the WEC-Sim model tends to underpredict the larger responses and overpredict the smaller ones. It can be seen in Fig.3.10(c) that the cases with the largest overprediction were the cases with a smaller wave am-

plitude. Fig.3.10(a) shows that the extreme spring extension is only weakly positively correlated with the NewWave amplitude for both the WEC-Sim model and the physical experiments. Fig.3.10(b) shows that the extreme spring extensions measured in the physical experiments and simulated in WEC-Sim largely cluster in the $0.2 - 0.4cm$ region. The CDFs for the experimental and numerical data created by fitting a generalised extreme value distribution to the maximum response amplitude in each run produced similar results with the same range of extreme values between the 10th and 90th percentiles. This indicates that the WEC-Sim model can be used to evaluate short design wave methods (Fig.3.10(e)).

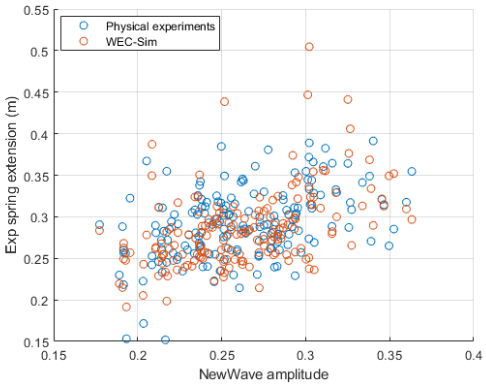

(a) Wave amplitude vs extreme spring extension for each CNW

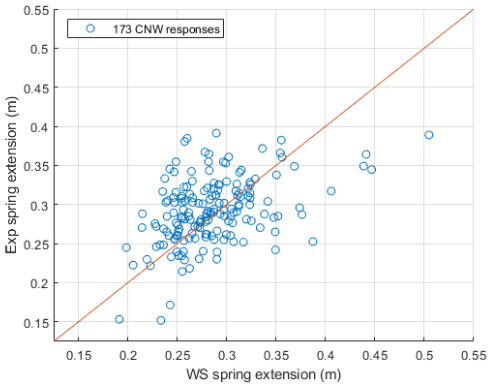

(b) WEC-Sim vs physical experiments, the red line shows equivalence

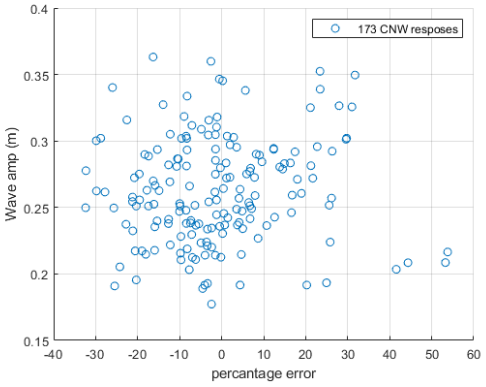

(c) Wave amplitude vs percentage error in extreme spring extension

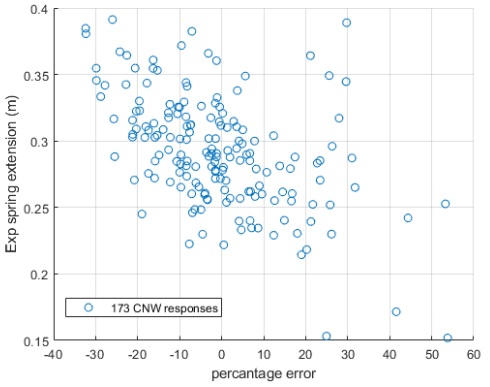

(d) Extreme spring extension vs percentage error

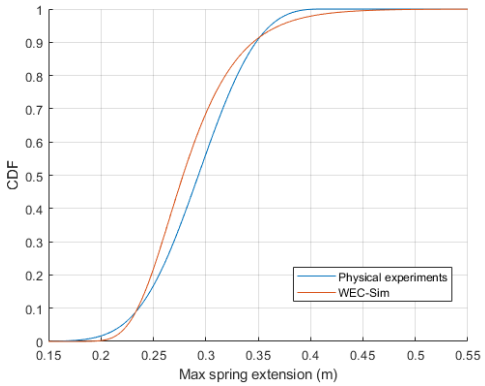

(e) Fitted CDFs for the CNW responses comparing WEC-Sim and the physical experiments

Figure 3.10: Plots comparing the WEC-Sim model responses to those of the physical experiments.

Fig.3.11 shows that the five largest spring extensions predicted by the WEC-Sim model, indicated by the red markers with an extreme spring extension above 0.4, are primarily caused by an over prediction of the surge response. This can be seen by the five red points at the top of Fig.3.11(a) which have a much larger spring extension than heave position. This may be partially due to the use of a constant viscous drag coefficient CDx but investigating this is outside the scope of this thesis.

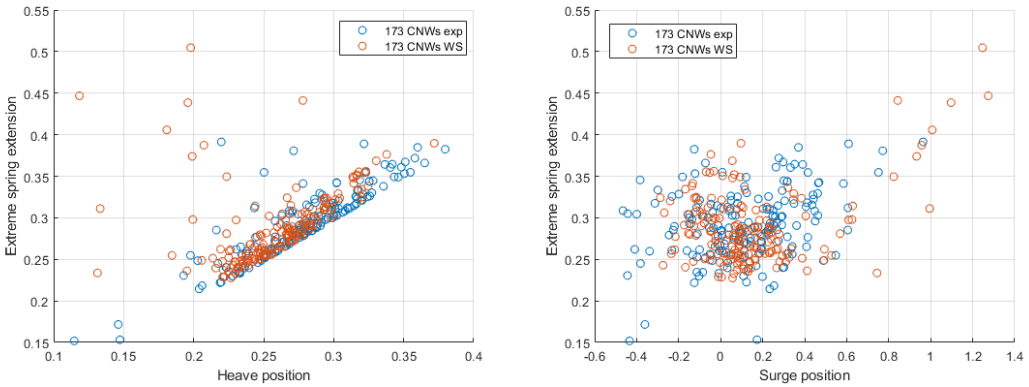

(a) Extreme spring extension vs heave at time step of the CNW

(b) Spring extension vs surge at time step of the CNW

Figure 3.11: Numerical and physical model comparisons of spring extension, surge and heave at the time step of the extreme spring response for 173 CNWs.

3.4 Single focused waves

The weakly nonlinear WEC-Sim model was used to run 500, two minute, irregular wave time series (14.14 minutes at full scale) corresponding to approximately 118 hours of waves at full scale so that an empirical 'true' CDF of the extremes could be created to assess different methods for determining design loads. The input wave spectrum used was that measured by the wave gauges during the physical long irregular wave runs. This enabled a direct comparison to be drawn between the physical and numerical data. The error associated with the measured wave data was assessed in Hann et al. (2018) who report that the root mean square error (RMSE) in the wave elevation time series of a CNW repeated five times was $0.012m$, indicating a good level of repeatability in wave generation. Such small errors in wave generation indicate that the variation in

the response is dominated by the different background waves which the focused waves are embedded in.

Both NewWave and MLER focused waves, scaled to the most likely maximum wave amplitude and spring extension respectively, were run in WEC-Sim for a 14.14 minute full scale exposure time. This short exposure time was initially chosen instead of the three hours commonly used when modelling extremes so that a large amount of data could be quickly generated for an initial study. For the device and response of interest studied it can be seen that the linear focused waves were a very similar shape (Fig.3.12).

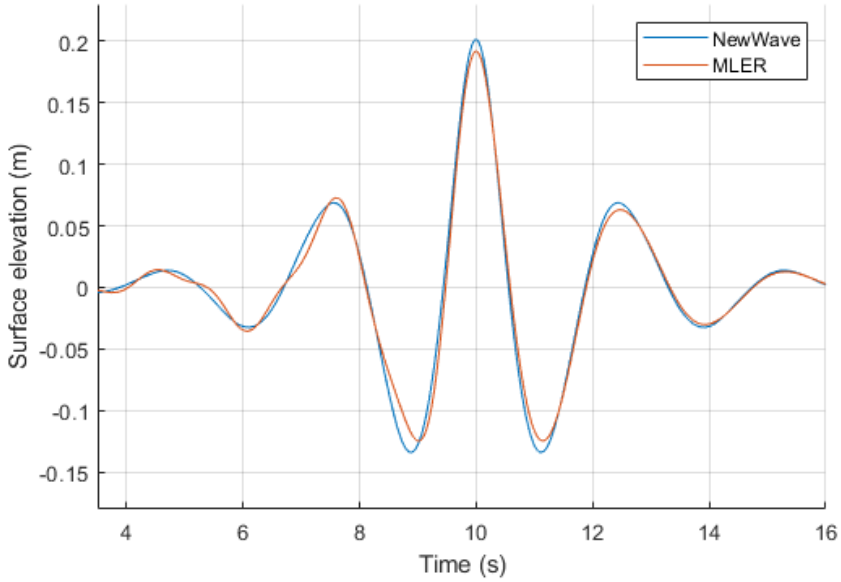

(a) Surface elevation

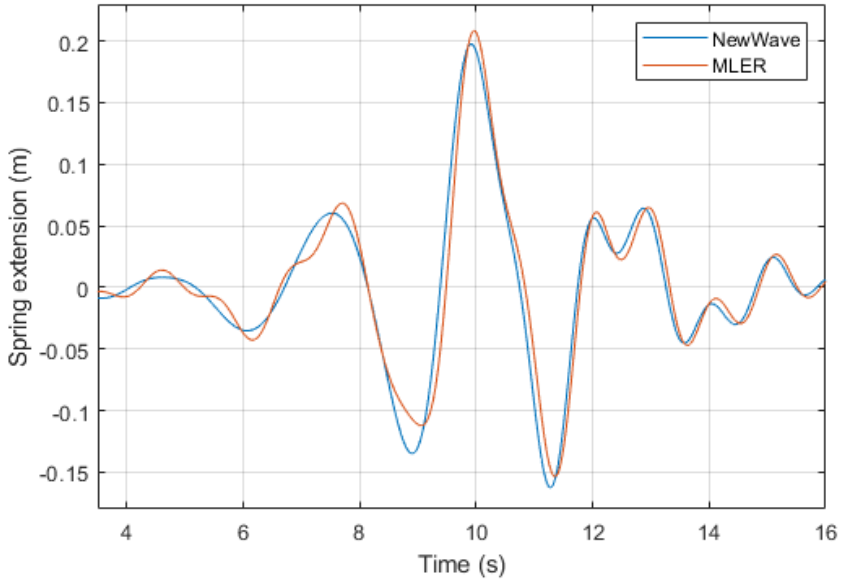

(b) Spring extension

Figure 3.12: NW MLER comparison from the WEC-Sim model.

The NewWave produced a spring extension response of $0.195m$. The MLER wave produced a response greater than the $0.201m$ which was predicted from the response spectrum but fell short of the peak of the histogram of the extremes from the 500 weakly

nonlinear WEC-Sim runs (Fig.3.13). The fact that the single focused waves under predict can be seen from the red and black lines which are at smaller spring extension response magnitudes than the peak of the histogram.

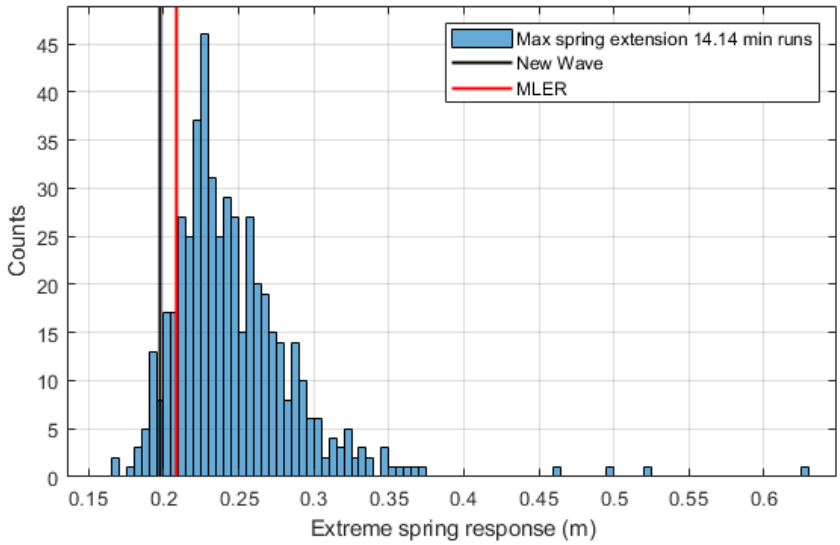

Figure 3.13: Histogram of the five hundred, 14.14 minute WEC-Sim responses with those from the equivalent single event MLER and NW focused waves overlaid.

MLER and NewWave methods were tested as they appear most commonly in the literature although other methods exist which condition the wave on the device response. The fact that the dynamic behavior of the WEC invalidates the focused wave approach to some extent has been reported on in Hann et al. (2018) and Quon et al. (2016). Constrained focused waves have therefore been applied to try to circumvent this problem by Göteman et al. (2015) and Hann et al. (2018), though without reference to the EVD, and both reported large variations in the extreme responses of interest.

3.5 Analysis of short term extremes

Atcheson et al. (2019) note that a key problem in extrapolating to the extreme responses from a peak distribution is the lack of guidance or goodness of fit parameters. NREL's WDRT suggests when applying a POT method using a threshold value of the mean plus 1.4 times the standard deviation as used in the wind industry (Michelen and

Coe (2015)). A threshold at the $90th$ percentile was adopted in this study as it approximately matches this threshold and ensures the amount of data used in the peak analysis remains constant for equal sized samples.

The statistical uncertainty introduced by the sampling and extrapolation can be investigated using the five hundred 14.14 minute runs and bootstrapping, where values are sampled with replacement. Sampling with replacement means that a sampled value can be selected multiple times. 1000 random samples of response peaks equating to six times the exposure time each were used in the estimation of confidence intervals. Additional confidence intervals for 60 hour samples (20 seeds for a three hour exposure time) are calculated for the 3 hour exposure time. Fig.3.14 shows the CDFs and 90% confidence intervals for a 14.14 minute and three hour full scale exposure time calculated from the WEC-Sim data. Also shown are the equivalent CDFs calculated using the full 26.9 hours (3.8 model scale) of experimental data from the irregular wave runs. Their close agreement serves as further validation of the WEC-Sim model, for this device in this sea state, and suggests that additional WEC-Sim runs could be used in place of physical experiments to increase the sample size and narrow the confidence intervals.

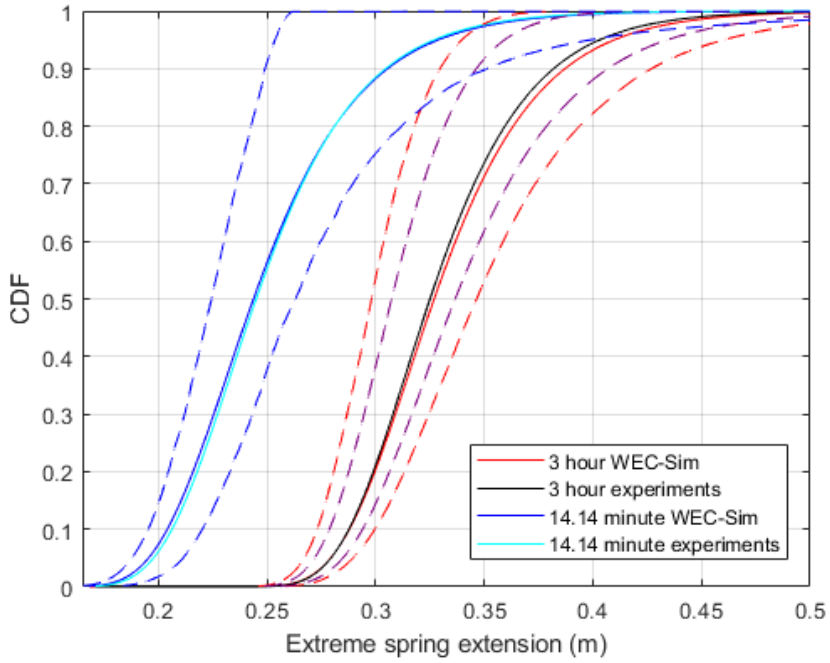

Figure 3.14: CDFs for 2 different exposure times comparing physical and WEC-Sim data. Exposure times given are for full scale. Dashed lines show 90% confidence intervals from bootstrapping 6 seed samples for both exposure times. The 90% confidence intervals using 20 seed samples are also shown for the 3 hour exposure time by the purple dashed lines.

3.6 Design Loads Generator

An alternative to the traditional extrapolation approach developed for ship design and offshore engineering by the University of Michigan is the DLG (Kim (2012), Alford (2008)). This approach assumes wave surface elevation as a Gaussian random process and combines a brief exposure time, response spectrum and Monte Carlo (MC) simulations in order to create an ensemble of wave profiles to excite extreme responses for much larger exposures. This approach has the advantage of creating surface elevation time series which can be used as inputs to numerical or physical model test runs to produce a prediction for the EVD of the response of interest. It is distinct from the constrained focused wave approach in terms of the generation of the wave profiles as the background wave frequencies are used to produce the extreme surface elevation at a particular time step, rather than producing a background wave profile and embedding

the separately generated focused wave within it. This means that the amplitude of the wave at the time step of the extreme response is not scaled to be the same for each run.

Whether this approach can be applied to something as dynamic as a point absorber WEC is uncertain as, similar to the CRRW method, one of the key conditions for its successful implementation is that nonlinearities produce small perturbations from the predicted linear responses. To try and understand this a numerical model case study is performed on the X-MED buoy. For the purposes of the case study an initial two minute exposure time was chosen corresponding to roughly 14.14 minutes full scale. This was to reduce the computation time required to run the large number of simulations which were necessary, by a factor of roughly 764, compared to running three hour simulations.

The main achievements of the DLG method are that:

1. It can produce a realistic wave profile around a particular extreme response.
2. It reduces shortcomings associated with the statistical extrapolation used in the traditional irregular wave approach in the estimation of an EVD.
3. It is applicable to short-crested seas.
4. It creates a method whose speed is independent of the exposure time.

The DLG is broken down into several stages and applied to the X-MED buoy for its extreme sea state below:

1. A sea state and number of frequency components (201 are used here for illustrative purposes) are chosen and a linear model used to determine the magnitude and phase of the RAOs of the response of interest, in this case the spring extension is the response chosen. The RAOs are then squared and multiplied by the sea spectral density $S(\omega)$ to produce a response spectrum $Sr(\omega)$ as in equation 3.1.

$$Sr(\omega) = RAO(\omega)^2 * S(\omega) \tag{3.1}$$

The wave and response spectra are illustrated in Fig.3.15, and the natural period in heave can be seen at 1.1 seconds.

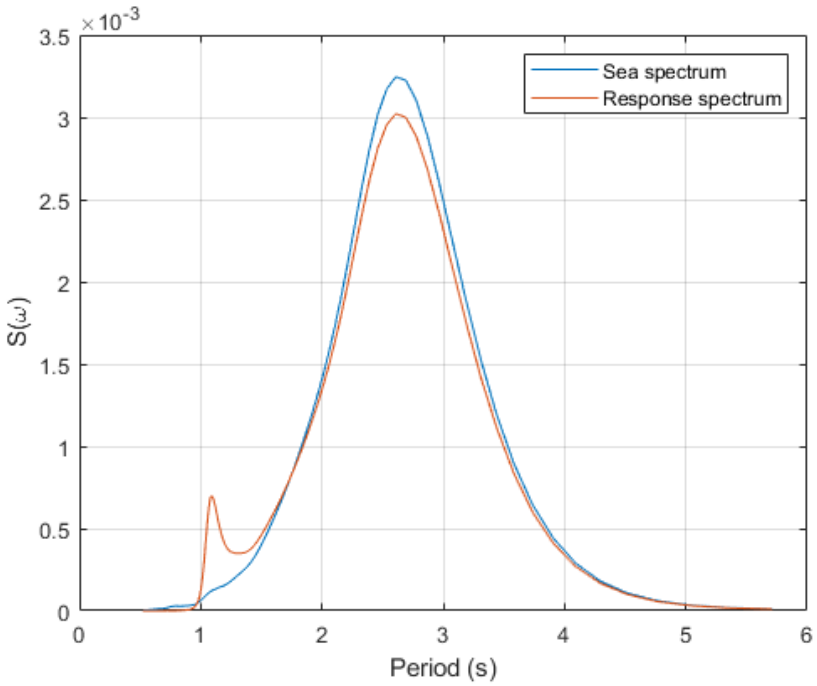

Figure 3.15: Plot of sea and response spectra.

2. The spectral moments of the response spectrum and an exposure time are used to calculate a target extreme value (TEV) which corresponds to the peak of the EVD normalised by the standard deviation (equation 3.2). This means that a TEV of 3 refers to an EVD with a peak at a value of 3 times the standard deviation of the underlying Gaussian process describing the response. A TEV corresponding to a small exposure time is initially chosen.

$$TEV = \frac{\hat{x}}{\sigma} \tag{3.2}$$

where $\hat{x}$ is the peak value of the EVD.

3. The spectral amplitude of the response spectrum a_j is used in equation 3.3 to predict the extreme response in a chosen exposure time (14.14 minutes in this instance). Surface elevation is assumed to be a zero mean random Gaussian

process and so a number of realisations m of equation 3.3 can be used to represent the responses for a time series of a given length. The number of realisations is calculated from the CDF of the standard normal distribution using equation 3.4 and for the 14.14 minute exposure time equates to 210 realisations. ε_j is the random phase angle and φ_j the phase of the RAO of interest.

$$x(t) = \sum_{j=1}^{N} a_j \cos(-\omega_j t + \varepsilon_j + \phi_j) \tag{3.3}$$

$$m = \Phi(\frac{\hat{x}}{\sigma})^{-1} \tag{3.4}$$

4. This is repeated a large number of times, 25000 in this study, and the largest value in 210 realisations recorded each time for each frequency component. These 25000 realisations are based on equation 2.19 and so take on the order of a few minutes to calculate. These 25000 extreme values are then used to produce a probability distribution of the phase angles (Fig.3.16) at the time step of the extremes for each frequency component. Fig.3.17. Shows each of these 201 distributions, as in Fig.3.16, side by side.

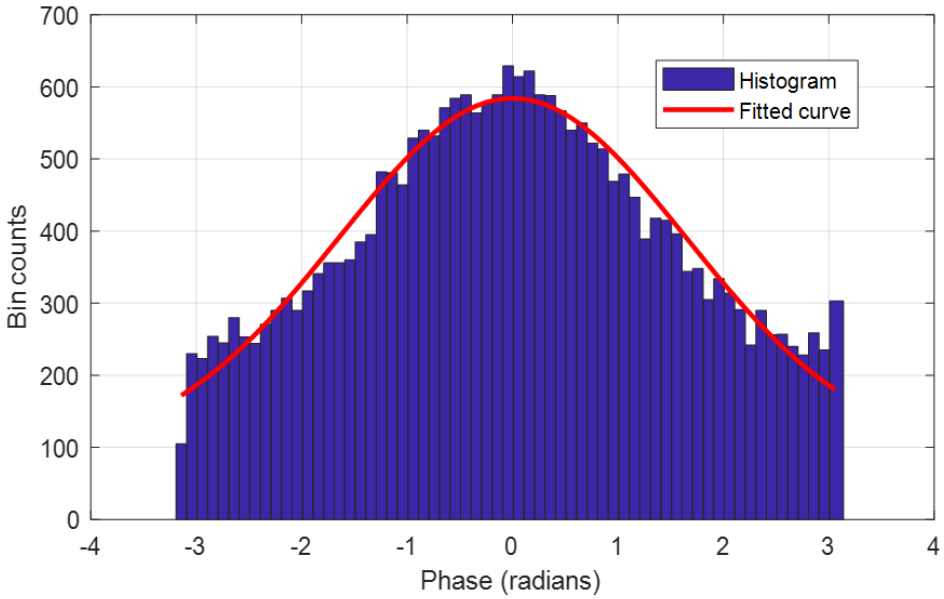

Figure 3.16: Histogram of $25,000$ values for the phase angle of a single frequency component at the time step of the extreme response.

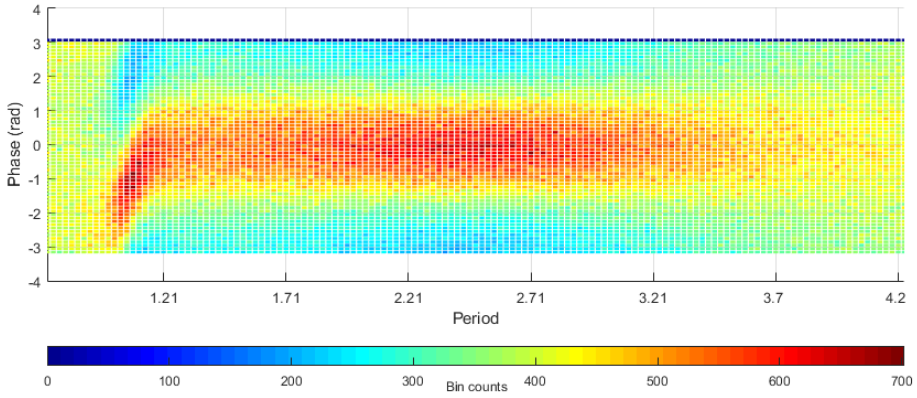

Figure 3.17: Histograms for each of the 201 frequency components showing the bin counts for the phase angle at the time step of the extreme response.

5. Each distribution can be described by a modified Gaussian distribution defined by the parameter λ between zero and ten (equation 3.5). The closer lambda is to zero the more peaked the distribution, the closer to 10 the more uniform it becomes (Fig.3.18). These values of λ are calculated from the histograms.

$$fE_{mj}(z) = \frac{1}{\lambda_j\sqrt{2\pi}} e^{-\frac{z^2}{(2\lambda_j^2)}} + \frac{1}{2\pi}(1 - erf(\frac{\pi}{\lambda_j\sqrt{2}})) \tag{3.5}$$

where $-\pi \leq z < \pi$

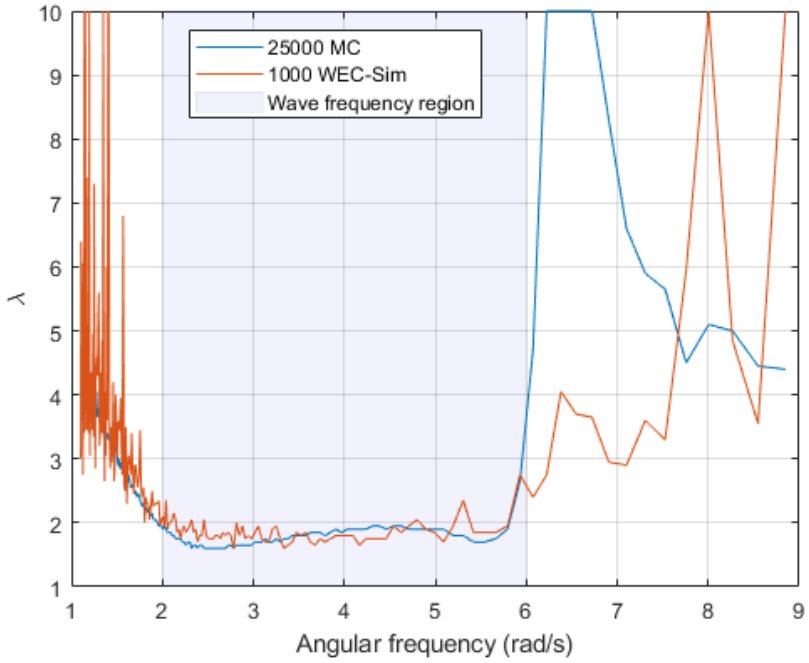

Figure 3.18: Lambda values calculated from MC simulations using transfer functions and $1000, 14.14$ minute WEC-Sim runs. The sea state frequency range was approximately $2 - 6 rads^{-1}$.

6. Responses corresponding to a longer exposure time can then be realised by altering the parameter λ, achieved in this work through trial and error and MC simulations rather than using characteristic functions and optimisation required for longer exposure times as in Kim (2012).

7. These distributions of the phase angles can then be sampled from to produce random time series leading to extreme responses at a chosen time step using equation 3.3. However, information regarding the dependence of the phase angles between the different frequency components has been lost. The resulting profiles therefore do not necessarily lead to extreme responses without additional sampling.

8. A large number of linearly predicted responses are generated using step 7 and an acceptance rejection algorithm used to sample from these to the theoretical EVD. A uniform random number u between zero and one is generated and if

$u \leq f_X(y)/cg_Y(y)$, y is accepted as a sample x from the random variable X. $g_Y(y)$ is the distribution of linearly predicted responses calculated in step seven, $f_X(y)$ is the linear target EVD and c is a constant. Fig.3.19 demonstrates the sampling with the PDF. A specific number of profiles are chosen to reproduce the EVD. Kim (2012) recommends between 500 and 1000, for this initial analysis 250 have been used to reduce the simulation time.

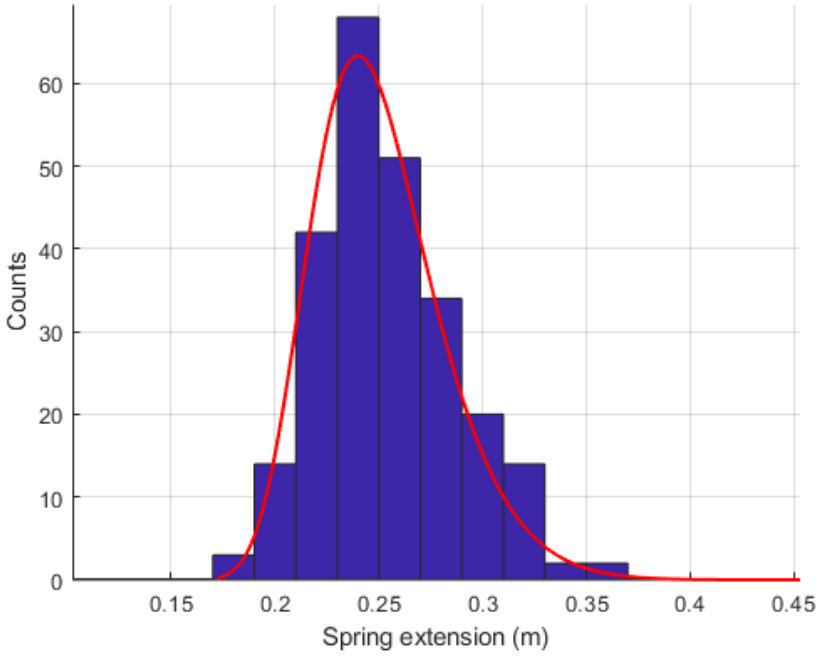

Figure 3.19: Sampled histogram of 250 extreme spring extension values for the 14.14 minute exposure time. Red curve gives the target distribution to sample.

9. The 250 profiles are then run in a weakly nonlinear response model and their empirical CDF produces an estimate of the EVD. An example of a few DLG profiles is given in Fig.3.20 with the extreme response set to occur at $100s$. This plot shows 4 different DLG profiles, each conditioned to produce a different target spring extension.

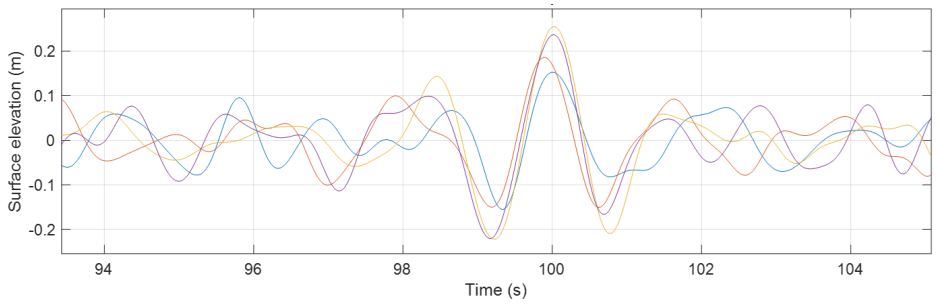

Figure 3.20: Example DLG profiles.

3.7 Application of the short design wave methods in the prediction of the EVD

The DLG was applied as outlined above but using 1001 frequency components. An exposure time of 14.14 minutes was used to be directly comparable to the 500 WEC-Sim simulations so the validity of the approach could be determined. The results are plotted in Fig.3.21 and show the target CDF calculated by the TEV, the 250 DLG runs as actually achieved when run through weakly nonlinear WEC-Sim and the 'true' CDF from the 500 weakly nonlinear WEC-Sim runs. The responses are also included from the MLER and NW profiles which hit the $12th$ and $5th$ percentiles of the 'true' distribution respectively.

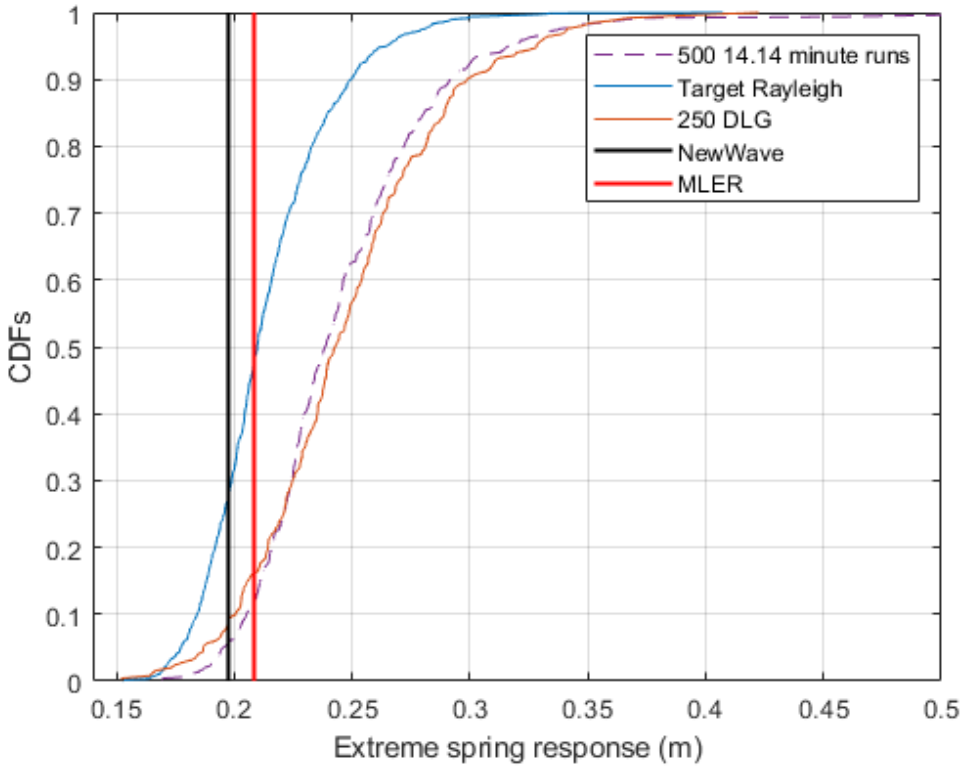

Figure 3.21: 14.14 minute exposure DLG irregular wave CDF comparison.

This initial result suggested the DLG approach may be valid for floating ORE. However, the three hour exposure times of interest are much longer and so a further validation effort was made. Fig.3.22 shows the results for a three hour exposure time. The 250 DLG runs under predicted the EVD for the three hour exposure.

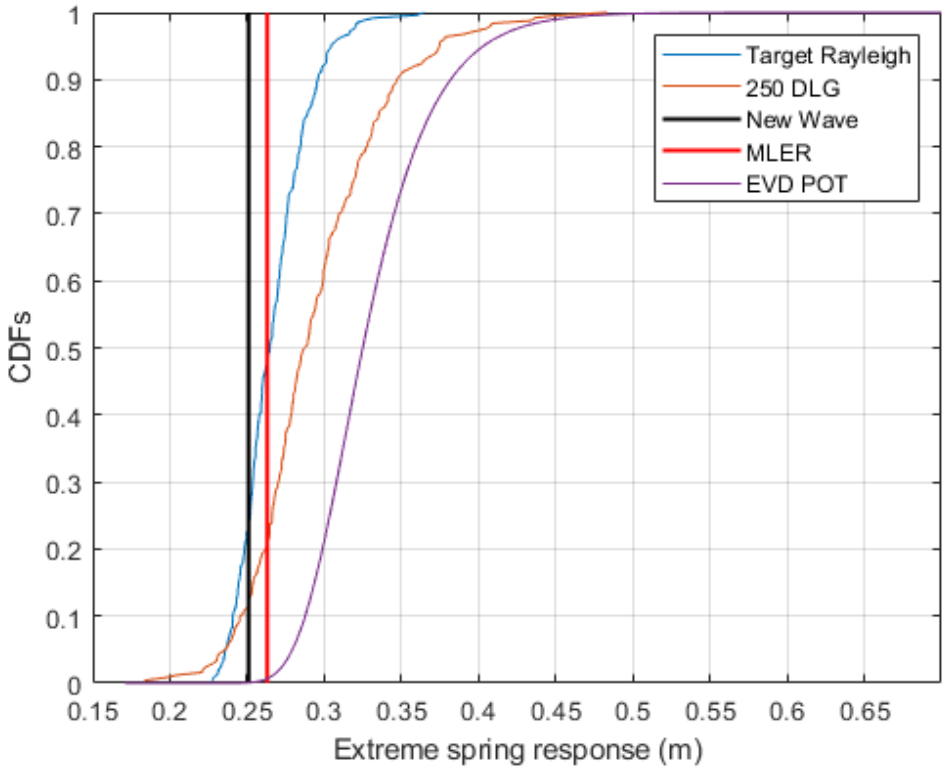

Figure 3.22: 3 hour exposure DLG irregular wave CDF comparison.

The CRRW method, as outlined in section 2.4, was also run through WEC-Sim for comparison and produced similar results to the DLG. 450 WEC-Sim runs were performed by discretizing the linear Rayleigh EVD into 9 points and running 50 CRRW profiles for each. However, the discretization is somewhat arbitrary and so the predicted nonlinear EVD of the response may well improve slightly with a different discretization, larger number of discretized points (e.g. 20 instead of 9) or a larger number of CRRW (e.g. 200 rather than 50). A second discretization of five points again running 50 simulations for each was tested for comparison to check this, the resulting estimate of the CDF of the EVD was not significantly altered. The five point discretization went from $23cm$ to $35cm$ of the spring extension in $3cm$ increments, the nine point discretization used $1.5cm$ increments over the same range. The EVD prediction from the CRRW method is shown in Fig.(3.23) with the Rayleigh EVD in red and the dashed lines showing five of the nine discretization points used and the corresponding distributions produced by the

50 CRRW profiles. It can be seen that for each of the five CRRW ensembles shown the target values fall between the $30th$ and $40th$ percentiles of their respective distributions. It should be noted that the CDF produced by the CRRWs at the $32cm$ target response is very similar to that predicted from the irregular waves.

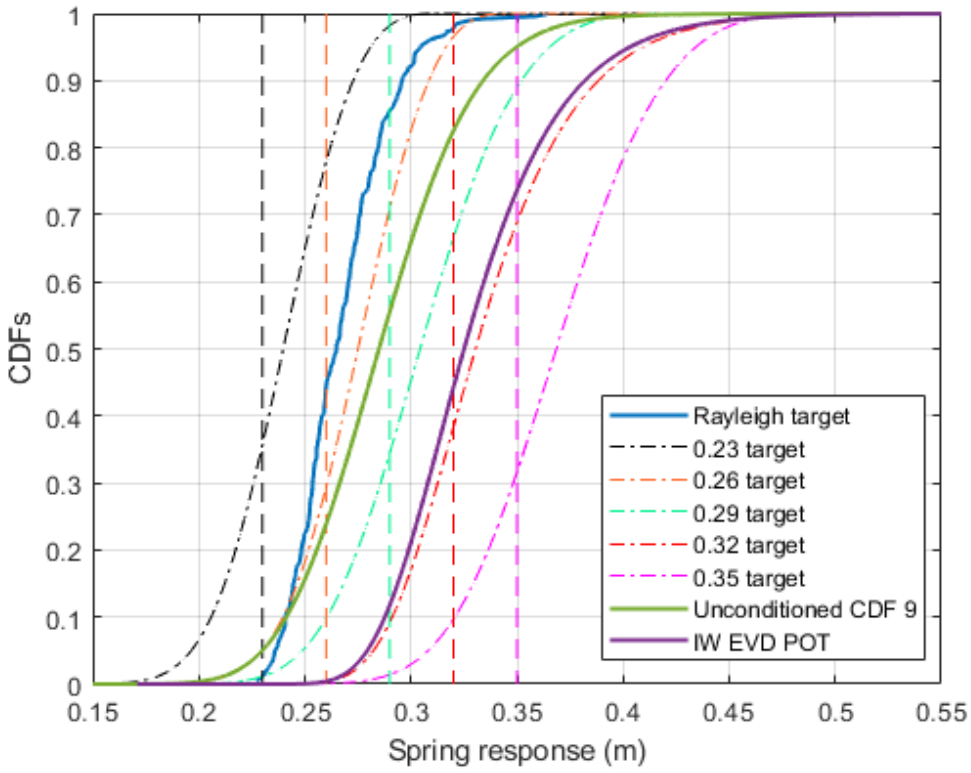

Figure 3.23: 3 hour exposure EVD predicted from the CRRW approach using 9 discretizations, 5 of which are shown. Each dashed line shows a linear target response and the CDFs of the corresponding colour are produced by the 50 CRRW profiles run through weakly nonlinear WEC-Sim. IW stands for irregular wave.

Fig.(3.24) shows that the CRRW and DLG approaches produce similar predictions of the short term EVD but both are significant under predictions.

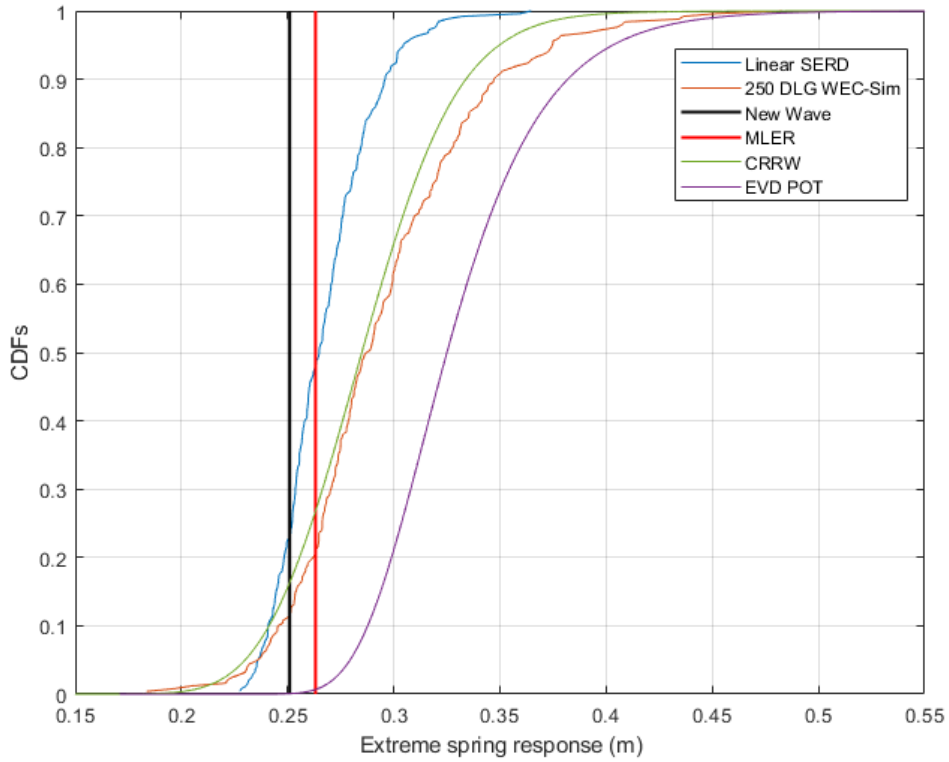

Figure 3.24: 3 hour exposure irregular wave, CRRW, DLG, target EVD CDF comparison.

The DLG and CRRW runs did not reproduce the true CDF for the same reason that the solitary focused wave approaches did not recreate the responses around the peak of the EVD. The time history is important for dynamic cases such as this. By focusing on one DLG wave run and starting the simulation at different time steps this point can be illustrated (Fig.3.25).

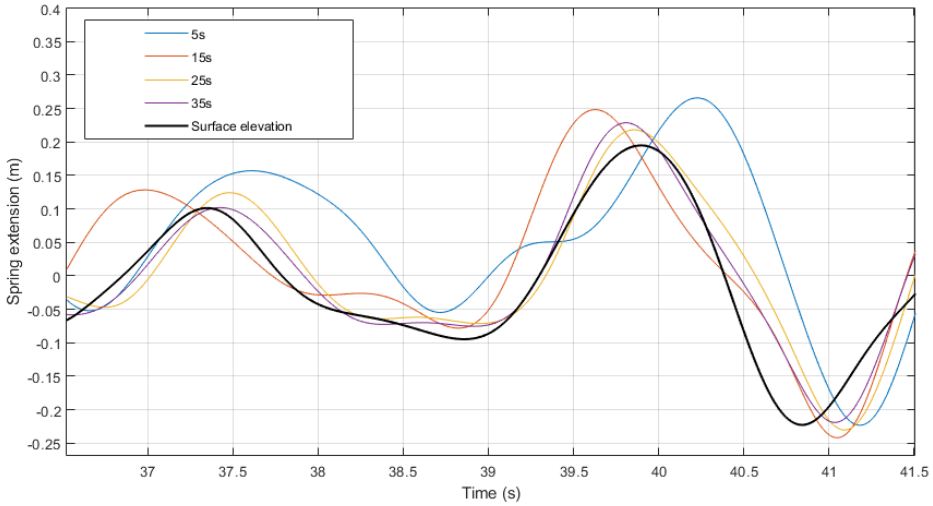

Figure 3.25: Preceding wave impact on spring extension.

Ten cases were considered with preceding wave times increasing from 5 to 35 seconds in 10 second increments. Fig.3.26 shows how the extreme spring extension is begining to converge with each 10 second increase in the simulated wave time series.

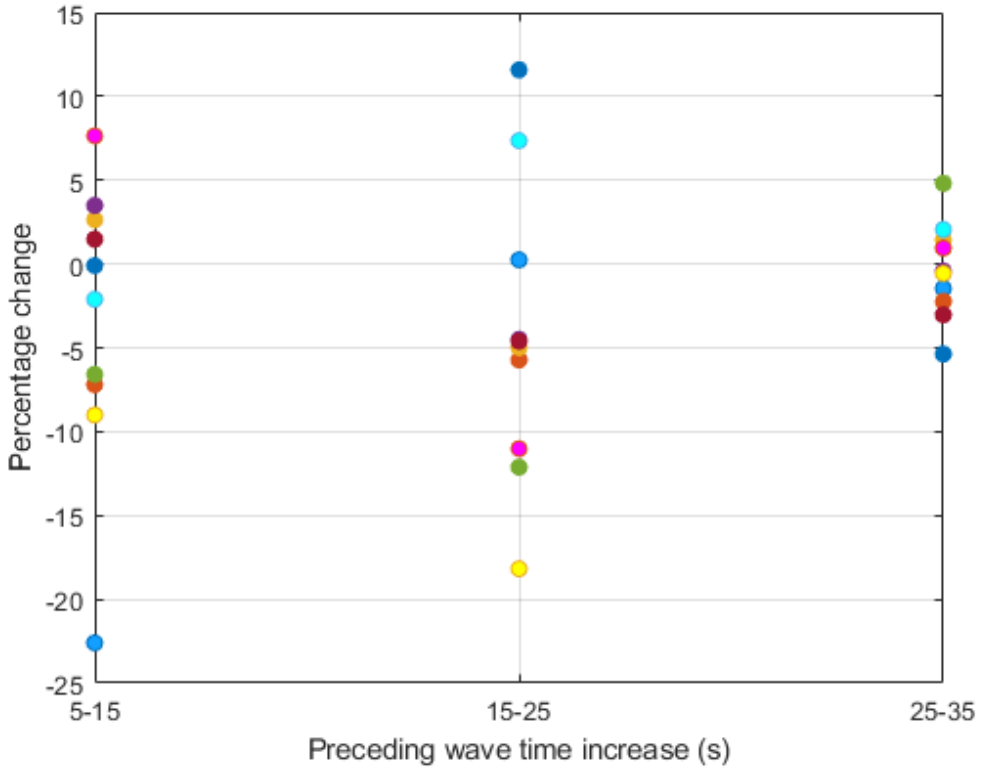

Figure 3.26: Change in percentage difference of extreme spring extension for 10 second increments in the preceding wave time series.

As a result of this analysis on the impact that the preceding wave history has on the spring extension, 40 seconds was chosen as the target time step for the extreme event to occur so as to keep the time series short but also allow enough time to capture the history effects. This is evidenced by the small, $+-5\%$ change in the extreme spring extension observed when the varying the length of the background wave from 25 to 35 seconds.

The discrepancy between the CDFs produced by the long irregular waves and the short design wave methods raises the question of why the true nonlinear response is different to the linearly predicted one? The 450 CRRW profiles and irregular waves were run for several iterations of the WEC-Sim model increasing in complexity to determine why the constrained wave methods for predicting the EVD are not suitable. It can be seen in Fig.3.27 that when the model is limited to just heave or to $3DoF$ without the

weak nonlinearities, the predicted CDF matches the target Rayleigh distribution well and the CRRW approach gives a similar prediction of the EVD to the irregular waves. It's the impact of the nonlinear Froud-Krylov force on the surge position which changes the shape of the distribution and results in larger extremes. The remaining differences between the CDFs for the CRRW and irregular wave predictions are then due to shortfalls of the short design wave method, in particular the assumption that the nonlinear response is a small perturbation from the linear one is no longer met. History effects are important and lead to different model positions and velocities at the time step of the design event, which strongly influence the response of interest for this device.

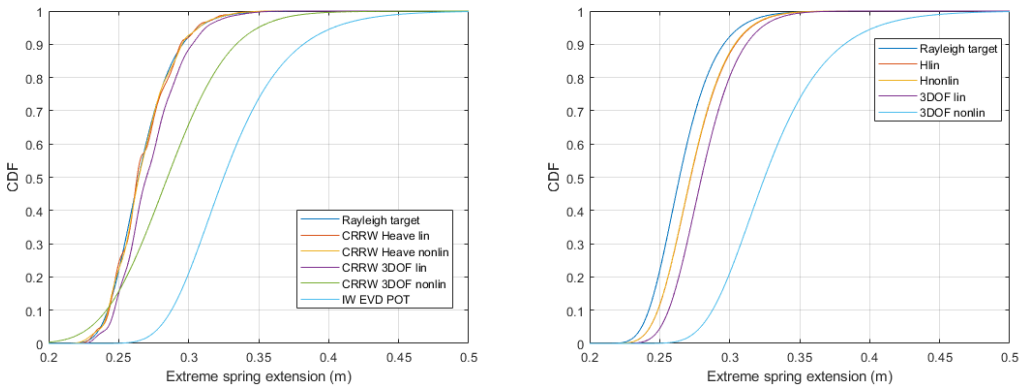

(a) CRRWs *(b)* Irregular waves

Figure 3.27: CRRW EVD predictions for WEC-Sim models of increasing complexity.

Plotting the CRRW spring extension vs heave in Fig.3.28 for the different WEC-Sim models reveals that whilst the increase in the surge position for the nonlinear $3DoF$ model does lead to an increased spring extension, the increased contribution from heave is more important. The spring extension for the nonlinear heave model is equal to the heave position since that is it's only degree of freedom and the values are lower than those produced by the nonlinear $3DoF$ model. The large spring extension, low heave cases far from the 1:1 line are caused by large surge values but a much larger number of the largest spring extension cases are close to the line suggesting the contribution of the surge position is not as significant as the increase in heave for the nonlinear model.

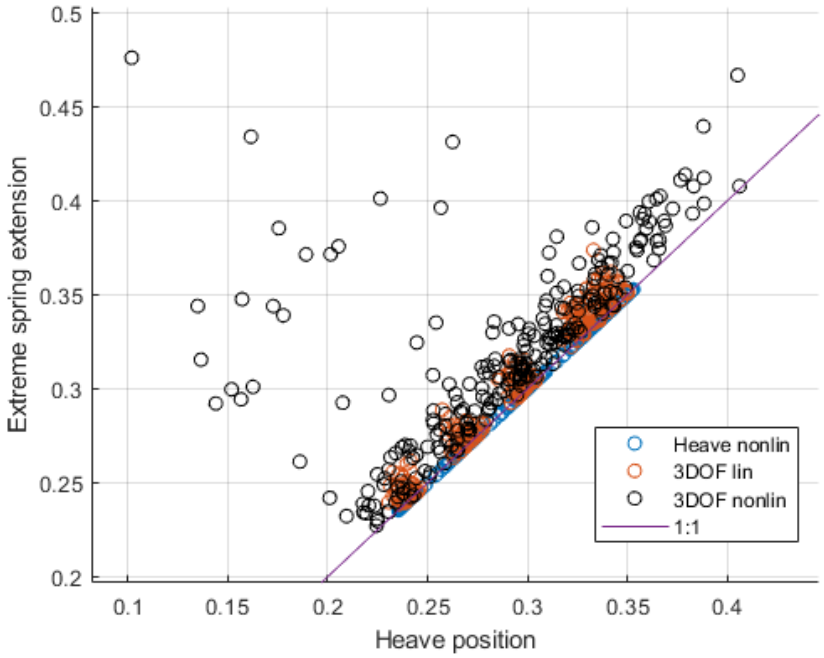

Figure 3.28: CRRW spring extension vs heave at time step of extreme spring extension.

Using data from the physical experiments, Fig.3.29 shows the average of ten empirical wave profiles (given by the thick red and black lines) leading to the largest spring response from the irregular waves. The average responses generated confirm the importance of heave and surge position and demonstrate that the pitch has little influence over the extreme spring extension.

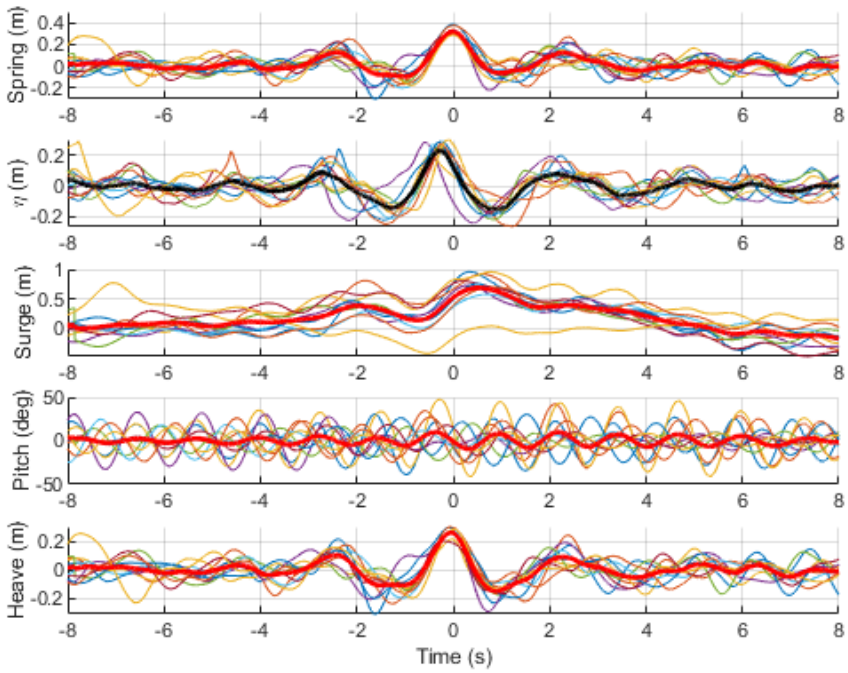

Figure 3.29: Average surface elevation and responses leading to the 10 largest spring extensions, defined at $Time = 0$, from the irregular wave data during the physical experiments.

The fact that all the CDFs in Fig.3.24 and Fig.3.27 are produced in WEC-Sim using linear wave theory means that the Rayleigh distribution of the wave amplitudes is adhered to and all errors are independent of wave theory. This means they are entirely due to the EVD prediction method. Errors such as deviations of the extreme wave amplitude from linear theory of concern to high fidelity numerical and physical modellers, will be discussed in later chapters.

Having to use a weakly nonlinear model is somewhat limiting as, although it runs fast relative to other methods such as CFD, it takes far longer than using transfer functions or just applying the Morison equation (As can be done for fixed wind turbines). To quantify this time difference, Van Rij et al. (2019b) report that linear models such as WEC-Sim typically run on the order of real time and CFD models on the order of 10^4 to 10^8 times real time, depending on the model complexity. There is also no guarantee that such a model will accurately reproduce the motions of more complex devices

which include PTOs, more complex moorings, power cables, control strategies or other complex physics such as slamming or overtopping.

3.8 Characteristic load prediction and extreme profile selection

The response-conditioned, short design wave methods implemented for predicting the EVD were not suitable for this device's response of interest due to the incompatibility with the condition that weakly nonlinear runs remain minor perturbations from linear predictions. The responses of this WEC, and the mooring load in particular, were significantly impacted by nonlinearities. Other floating ORE devices may follow linear predictions more closely and so this result is not necessarily generalizable to other devices or responses.

To what extent the numerical model error would impact the experimentally produced EVD can be examined by replacing the responses to sample from, calculated using MC simulation and transfer functions, with a number of nonlinear WEC-Sim simulations. For the X-MED example step 7 of the DLG method was used to create and run 1000 profiles. From the results of these 1000 simulations 250 were sampled to recreate the extreme value distribution calculated from a peak over threshold method using the five hundred, 14.14 minute runs. A CDF of the percentage error from the 173 CNW cases was created, randomly sampled and applied to the DLG run responses to give some indication of what might be achieved if these cases were run physically in the basin or with a higher fidelity model (Fig.3.30). The assumption is made here for illustrative purposes that the CDF of the percentage errors will be broadly the same for the CNW cases as for the DLG runs and is independent of response magnitude. This last point is not strictly true as evidenced by Fig.3.10(b).

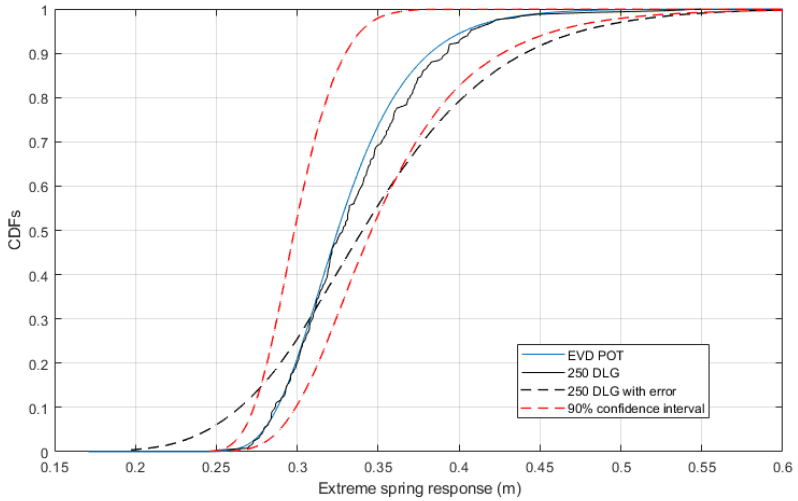

Figure 3.30: 3 hour exposure DLG predicted experimental spring response.

Clearly if the target EVD must first be estimated from a large number of numerical simulations then there is no point in using a constrained wave method to reproduce that same EVD. The purpose of doing so here is to illustrate that whether trying to estimate the whole EVD, a part of it or just a single percentile as in the design standards there will be errors impeding accurate prediction due to model error as well as due to nonlinearity of response. This is also true if attempting to use a single profile, constrained or otherwise even when neglecting the error in the target wave profile as done in this analysis so far. All these points make it highly unlikely that a single short design wave, regardless of the method, will be able to identify and then produce the response at a specific percentile with high accuracy, such as the $95th$ which is used for some responses in some standards. It may still be possible however in cases with highly nonlinear responses to produce an average value of the extreme response from a small number of constrained waves corresponding to the same method applied to long irregular waves as widely used in the IEC standards. The implications for the more generic uses of focused waves, to produce extremes but not necessarily characteristic load predictions, are that it may be useful to scale to larger percentiles. The solitary MLER and NW focused waves are often scaled to reproduce the peak of the

EVD which is usually around the $38th$ percentile (Ochi (1990)). However, it may be more useful to scale to a higher percentile which is more likely to be closer to the characteristic response. Using the CRRW or DLG methods a number of profiles could be used to represent a target percentile of the linear response prediction for the exposure time and be run experimentally or using CFD and a range of responses around the upper percentiles produced. In this way these approaches can be used to estimate a particular wave profile producing an unspecified (with respect to a percentile of the EVD) large response which may be useful to structural modellers.

Characteristic load predictions using the average of maxima approach from irregular waves for the physical and numerical data are presented in Fig.3.31. For both sets of data it can be seen from the empirical distributions of the peaks, specifically how they deviate from the orange EVD curve at the upper percentiles, that using a threshold above the $90th$ percentile for the POT fit would produce a longer tailed distribution. This emphasises the point that if selecting a characteristic load from the upper percentiles (> 75) the selection of the threshold is important and a larger data set may be necessary. The maxima from each three hour seed is given by a dashed line.

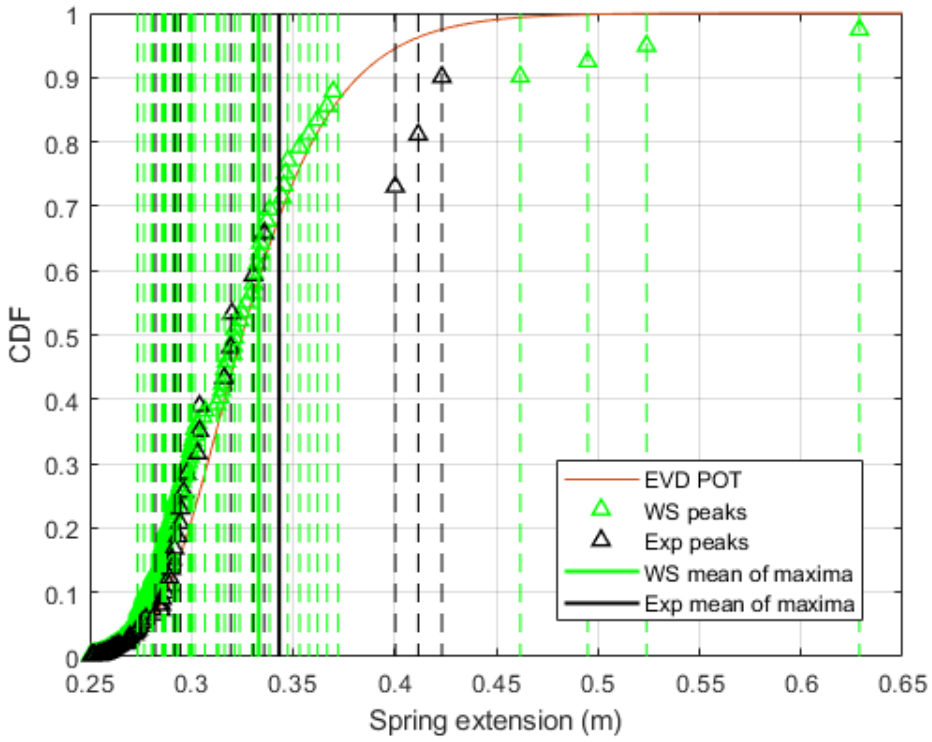

Figure 3.31: Comparison of the characteristic load predictions from the mean of maxima from the physical and WEC-Sim models. The dashed lines show the maxima from each irregular wave seed. The EVD from the WEC-Sim irregular wave data is shown.

Using CRRW profiles, consideration was given to which percentile the response amplitude should be scaled to from the linear EVD, either to produce extreme responses at the upper percentiles, or an estimate of the characteristic load in line with the average of maxima approach. What follows is a discussion of the average of maxima method for predicting the characteristic value where the mean of the maxima from each seed is taken as the characteristic value. The 50 CRRW profiles with a target spring extension of $32cm$ were used to fit a GEV distribution which was then randomly sampled 1000 times to give 90 and 50 percent confidence intervals for the mean of various sized samples. These are shown by the red shading in Fig.3.32 and illustrate how increasing the sample size improves confidence in the prediction of a characteristic value. The dashed black vertical line gives the mean response produced from the CRRW ensemble using the WEC-Sim model. The linear target of this ensemble was $32cm$ and represented a

target linear percentile of 97.9. Fig.3.23 shows that the characteristic response prediction from the irregular waves is in line with the mean of the CRRW responses from the $32cm$ linear target which is approximately at the $98th$ percentile of the Rayleigh EVD. This is evidenced by the proximity of the lines giving the mean of maxima (solid vertical black and green lines) to the second rightmost dashed vertical line. This shows that by scaling the focused waves to the $98th$ percentile of the Rayleigh linear target EVD, extremes of similar magnitudes to those of characteristic load predictions from irregular waves could be generated.

The degree of inflation of the linear target necessary to produce a characteristic load estimate in agreement with the irregular wave method is likely to be dependent on what extent the response deviates from linear assumptions. For very linear responses the inflation will produce an over estimate and there may be responses for which even the constrained focused waves scaled to an inflated target will produce an under prediction. How generalisable this finding is will need to be tested against other device and response types, a task which will take up much of the remainder of this thesis. Scaling beyond the $99th$ percentile is generally not considered a good idea due to how rapidly values change in the tail of a distribution above this point. For this reason the $99th$ percentile will be adopted as the linear target to scale to.

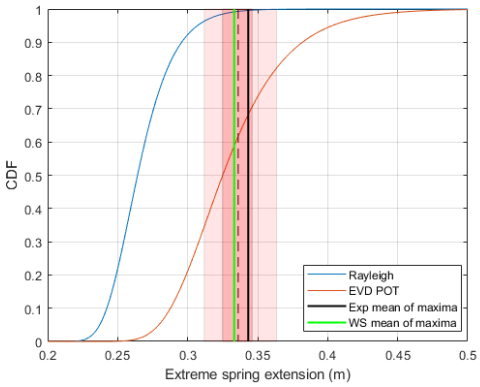

(a) Characteristic load predictions from 6 samples

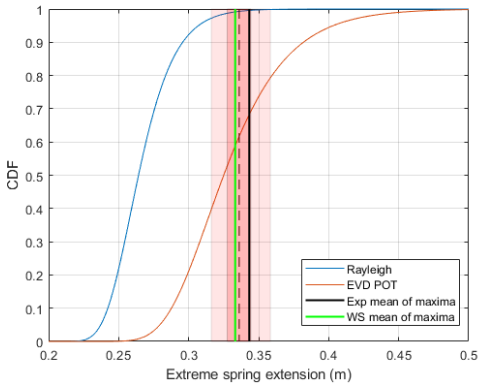

(b) Characteristic load predictions from 10 samples

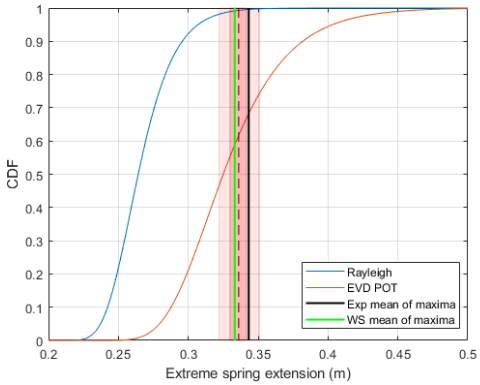

(c) Characteristic load predictions from 20 samples

Figure 3.32: 50% and 90% confidence intervals for characteristic load predictions from CRRW profiles are given by the red shading, darker shading indicates 50%. Dashed vertical line gives the mean of the 50 CRRW runs for the linear target spring extension of $32cm$.

Experimental data was used to validate a WEC-Sim model for the X-MED buoy, the magnitude of the median percentage error of the model for extreme responses during the three hour, 100 year storm was 9.6% and the averaged measured residual in the optical tracking system was $+-1.15mm$ (Hann et al. (2018)). This validated model was then used to judge the suitability of DLG and CRRW methods for determining the EVD, neither were very accurate in this instance due to the significant influence of nonlinearities on the response of interest. However, the constrained wave methods were still useful in the identification of a series of short wave profiles which could,

when scaled to large percentiles, be used for characteristic load prediction following the average of maxima method and linear response prediction. The next section, rather than using linear response predictions, explores the use of the nonlinear WEC-Sim model in the selection of cases to run during physical experiments to produce a range of responses around specific percentiles of the EVD and discusses the error due to the physical realisation of the target wave time series.

3.9 Reproduction of an extreme response in physical experiments

500 DLG runs were simulated in WEC-Sim and the profiles whose responses roughly corresponded to two percentiles of the true EVD, the $33rd$ and the $92nd$, were selected to run in physical tests. The experiments were carried out with a set up as close to that used in Hann et al. (2018) as was practically possible. A shorter spring with a stiffness of $66N/m$ was used and the line connecting the buoy to the spring lengthened to compensate. Fig.3.33 shows the experimentally achieved extreme responses, indicated with vertical dashed lines, which had a target response according to the WEC-Sim model of $0.31m$ given by a solid vertical black line. These values are overlaid on the CDF with the dotted vertical line indicating the mean of the experimentally achieved extremes (dashed vertical lines). The median numerical model error of 9.6% means that approximately half of the extreme responses are expected to be within $0.03m$ of the $0.31m$ target indicated by the solid vertical red lines. It is observed that four of the nine responses are within this range. There is a 10.2% error between the target response and the mean of the nine DLG generated values.

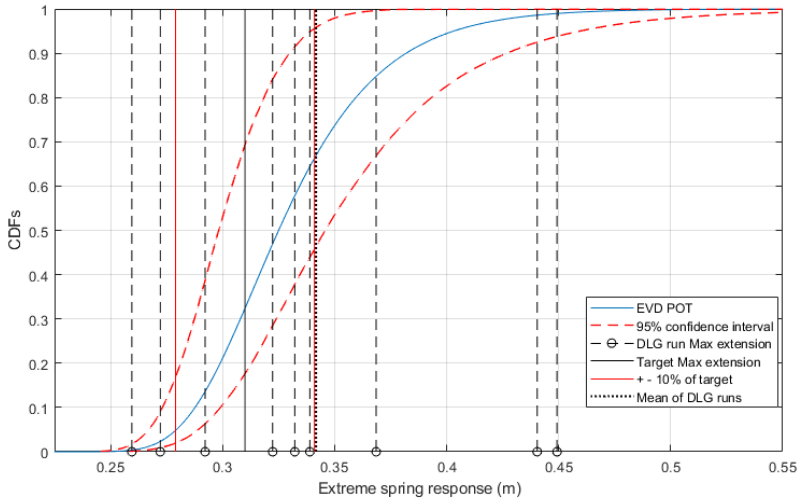

Figure 3.33: 9 DLG profile responses around the $33rd$ percentile target.

Fig.3.34 gives the experimentally achieved extreme responses around roughly the 92nd percentile of $0.39m$ shown by the solid black line. This target was chosen somewhat arbitrarily to produce responses at the upper percentiles. 9 out of the 15 profiles were above the 75th percentile where the characteristic loads for some responses are sometimes selected from in offshore engineering applications (Coe et al. (2018)). 7 of the 15 responses were within 9.6% of the target response indicated by the solid red lines. There is a -1.9% error between the target response and the mean of the 15 DLG generated values.

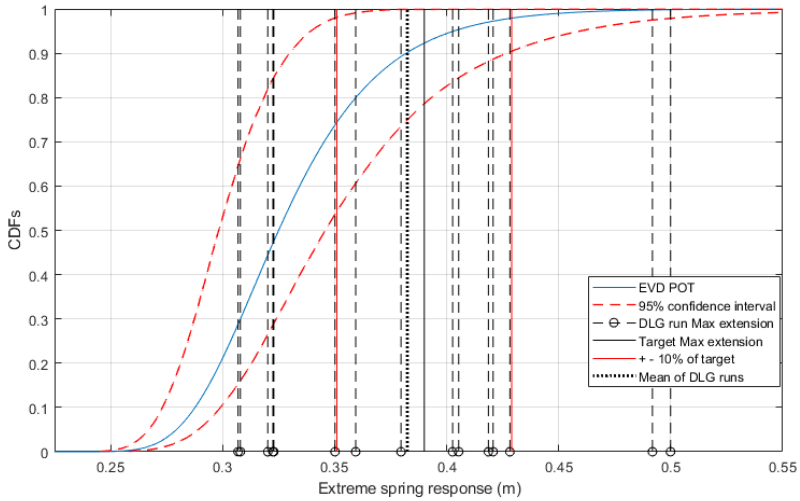

Figure 3.34: 15 DLG profile responses around the $92nd$ percentile target.

For comparison, Fig.3.35 shows the CDF with the CNW responses from Hann et al. (2018) overlaid. The NewWave in that study was designed on an expected number of peaks of 1000 and scaled according to the most probable maximum. The mean spring extension was $0.292m$ corresponding to the $13th$ percentile of the true short term EVD.

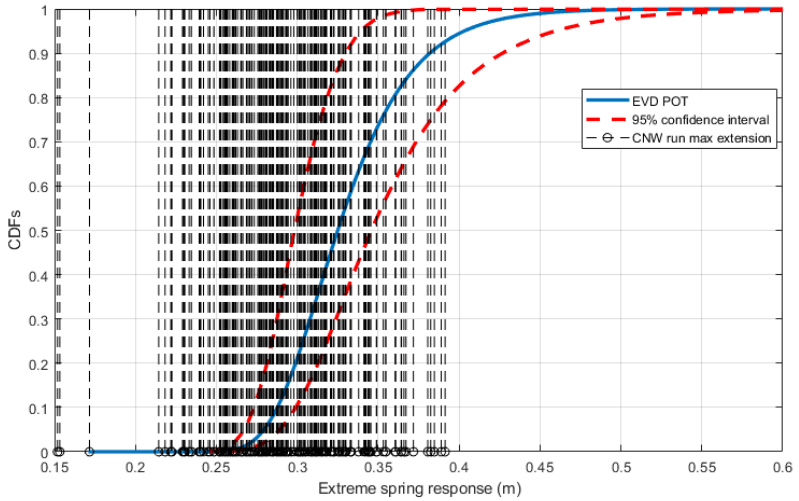

Figure 3.35: CDF comparison with 173 CNW responses.

The error in achieving the desired wave profile also has an impact on the validity of this approach as it is not always easy to reproduce an exact time series in a wave

basin. The wave profiles leading to the responses shown in Fig.3.33-Fig.3.35 were run without calibration. Calibration was initially attempted by altering the gain of different frequency components as is common practice for long irregular wave time series and for regular waves and although this led to slight improvements in some parts of the time series it led to increased error in others. As a result no calibration was implemented for the cases reported here. Alford and Maki (2015) highlight the difficulty in the realization of DLG profiles, generated using linear theory, in numerical and physical wave tanks. The development of a calibration approach will be discussed in the following chapter. Breaking waves were also found to exacerbate this issue. Fig.3.36 shows the percentage error of the experimentally achieved main crest amplitude from the DLG runs, the median error is just under 12%. Although this appears to be a large error, surprisingly it doesn't appear to have significantly impacted the results as the majority of the recorded extreme responses are still within the expected range. It should also be noted that the under predictions are affected by wave breaking. In this vein it should be clarified that this graph is for the fifteen 92nd percentile waves; when the nine $33rd$ percentile cases are included the magnitude of the median error drops to 7.5%.

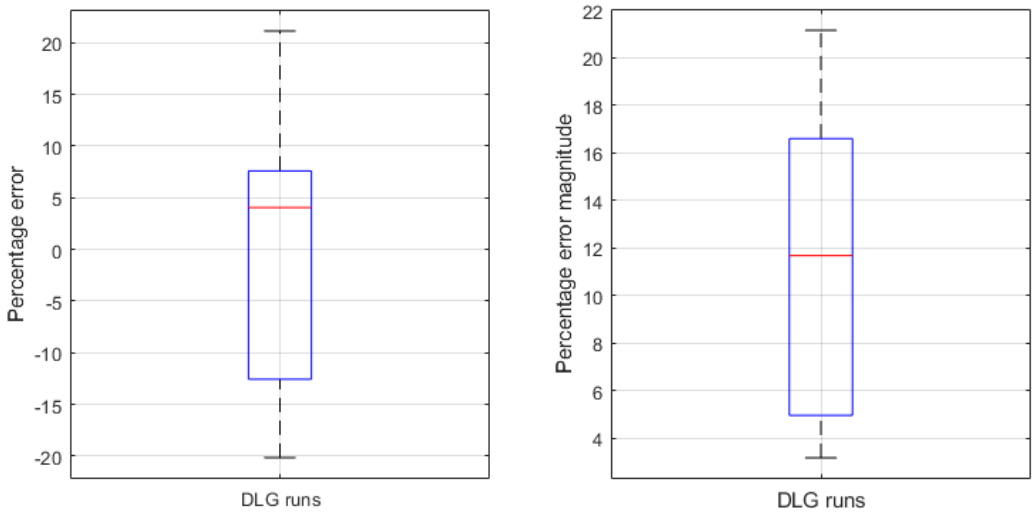

(a) Wave amplitude percentage error

(b) Wave amplitude percentage error magnitude

Figure 3.36: DLG wave profiles percentage error for $92nd$ percentile.

The wave profile in Fig.3.37 below illustrates the median percentage error magnitude in the experimentally achieved constrained wave amplitude. This sea state has a low steepness relative to those tested in later chapters and so it can be seen that even though no calibration was attempted the phase and magnitude of the physically produced wave profile is reasonably good. A detailed summary of the statistics on the physical CNW experiments is given in Hann et al. (2018).

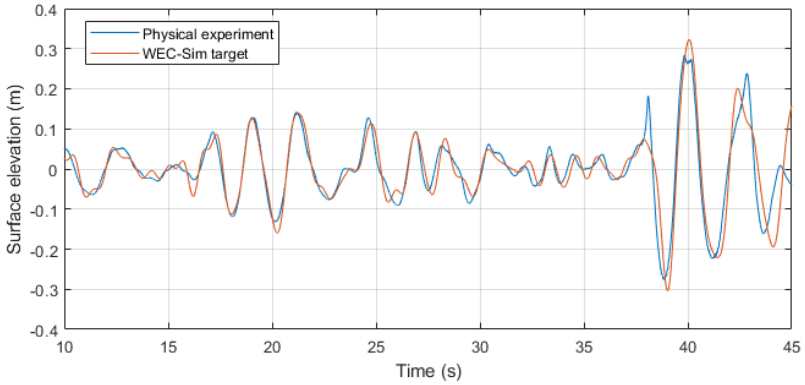

Figure 3.37: Physical and target surface elevation time series representing the median error in the achieved extreme wave amplitude.

Based on the findings for the mooring response in this chapter the objectives of using focused wave based methods in a floating ORE context have been limited over the remainder of the thesis to producing generic extremes or characteristic load predictions from an average of maxima approach. A question remains over which method CNW, CRRW or DLG profiles would best serve this purpose. In the case of CNWs it would first seem that for most devices and responses they would probably have a disadvantage over response based methods as the phase of the response is unlikely to be zero. However, this was found to not always be the case and will be discussed over the next few chapters. There are advantages to DLG profiles over CRRWs such as being able to create them in short-crested seas and creating the extreme responses in a wider range of different ways. For the remaining chapters the CRRW approach is used however as only unidirectional waves are being considered and it is more straight forward and can produce a single focused wave, the MLER wave, which has been applied in an ORE

context previously Quon et al. (2016). Applying the approach developed over the next few chapters using DLG profiles in short crested conditions is left for future work.

In light of the dynamic nature of the mooring responses of floating ORE devices it seems unreasonable to expect that a characteristic load can be deduced from a single focused wave run, even if it is embedded. It also appears that the DLG and CRRW methods for approximating the EVDs of the responses are unlikely to work in dynamic cases due to their common underpinning linear assumptions. For many ORE device types the mooring loads are very sensitive to the surge drift motion which is generally a $2nd$ order effect not captured by the linear response spectrum. Other devices and responses which are better described by linear and frequency domain models will likely have more success when implementing CRRW or DLG approaches to predicting the EVD and, potentially, single focused waves for the prediction of characteristic values.

3.10 Conclusions and future work

Experimental data was used to validate a WEC-Sim model for the X-MED buoy, the magnitude of the median percentage error of the model for CNW responses during the three hour, 100 year storm was 9.6 percent. The surge position was sometimes over predicted by the model with the drag coefficients used, despite this, the predictions of the spring extension EVD from the numerical and physical data were in reasonably good agreement. This validated model was then used to determine the suitability of DLG and CRRW methods for determining the EVD, they did not work in this instance due to the significant influence of nonlinearities. Short design waves however appear promising in the prediction of a characteristic load when using an average of maxima approach. The average of the response maxima produced by the CRRWs suggests that profiles need to be scaled to the region of the $97th - 99th$ percentile of the linear EVD prediction for the spring extension to produce characteristic values in line with the true nonlinear EVD. This may or may not be generalisable to other devices and responses of interest and so will be explored in later chapters. The WEC-Sim model runs fast enough that it could be used to run irregular waves alongside future physical

experiments to reduce the statistical uncertainty of the EVD prediction. It could also be used to select for extreme profiles to run in physical experiments or higher fidelity numerical models to produce responses of interest. Though model error and the accurate realisation of wave time series in the physical wave tank will limit this application, particularly for steep sea states that deviate from linear wave theory.

Short crested seas may be the source of extreme responses for ORE devices and so extending the CRRW or DLG profiles to short crested seas could potentially be useful. This has not been done for CRRWs before but is straightforward for DLG profiles. However the accurate, physical realisation of specific short crested time series in a wave basin presents its own challenges so this is left for future work. Unanswered questions on constrained focused wave calibration and the applicability of the use of CRRW profiles scaled to the $99th$ percentile to other devices and response types will be addressed in the next two chapters.

Chapter 4

Mocean

Chapter summary

Physical experiments were conducted comparing characteristic value estimates using constrained waves and the traditional irregular wave method. Pitch angle and mooring load were studied for a 1:20 scale model of Mocean energy's Blue Star WEC. A method for quickly calibrating the constrained waves using a single focused wave was developed. The impact of snatch loading and wave breaking on the characteristic value prediction are discussed.

4.1 Introduction

The previous chapter showed that for the mooring response of the Xmed buoy, using CRRW profiles scaled to the $99th$ percentile of the EVD produces an EVD close to that predicted from the traditional irregular wave approach. This observation will be used in this chapter to determine whether CRRW profiles scaled to the $99th$ percentile can be used to produce characteristic response / load predictions in line with irregular waves, using the approach recommended in the IEC standards. The study is carried out with physical experiments only as the mooring has a large bending stiffness, which could not be modelled in Moordyn, the code used by WEC-Sim, at the time of writing this thesis.

4.2 Device description

A $1:20$ scale model of Mocean Energy's Blue Star WEC was used to study the extreme mooring loads and relative pitch response. This is a 2 body hinged raft type WEC which

was moored using a 'Lazy S' arrangement (Fig. 4.1) at a water depth of $3m$. The model did not contain any power take off (PTO) in line with the envisaged survival strategy that involves switching off the PTO (i.e. free hinge). The Lazy S mooring consisted of 6 evenly spaced $1.6 \times 10^{-5} m^3$ floats and 5 evenly spaced $3.8g$ masses with a line length between fairlead and tank bottom of $4.5m$. The line had a high axial stiffness, so as can be considered inelastic, and a bending stiffness of $1.3 \times 10^{-3} N/m^2$. See Fig.4.2 for mooring details. The device responses selected for study were the mooring load and maximum relative pitch angles (hogging and sagging). The hogging and mooring load responses, that were measured using a load cell at the fairlead position, are presented in this chapter with their magnitudes obscured for commercial confidentiality. Further details of a previous iteration of the device can be found in Caio et al. (2021). The device has a moon pool in the back raft.

Figure 4.1: Subsurface view of model WEC and Lazy S mooring line - experimental setup

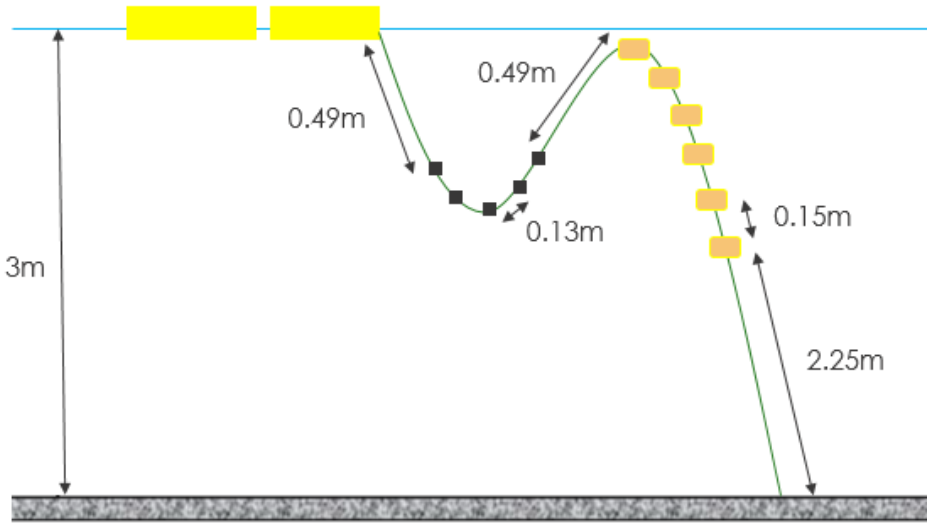

Figure 4.2: Sketch of the Lazy S mooring (not drawn to scale), distances between masses and floats are constant and given from centre to centre of each mass/float

4.3 Contour method

The EVD is defined here as the distribution of the single largest value occurring in a three hour exposure time and is determined from a peak over threshold (POT) method, where the peaks data is gathered using irregular wave time series. All irregular waves in this study were generated using a JONSWAP spectrum with gamma equal to one, equivalent to a Pierson-Moskowitz spectrum, with a run time of one hour. A three hour exposure time was used for the EVD and characteristic load / response prediction and so the one hour seeds are grouped into threes when needed. The contour method was utilised in this work as other, potentially more accurate long-term methods require too much data to be collected to make them suitable for use in physical modelling.

The CRRW and CNW profiles in these experiments were scaled to the $99th$ percentile of their respective EVDs for several reasons:

- History effects are important but unaccounted for in the response conditioned focused wave methods and by scaling to a higher percentile the profiles are more likely to produce responses in line with the extremes from the irregular waves.

- The distributions of the extreme wave and response amplitudes are based on linear theory and so likely to be under predictions due to neglecting the nonlinear evolution of waves. The Rayleigh distribution is found to under predict extremes from field measurements (Christou and Ewans (2014)) and in wave tanks.

- There are discrepancies between the target and physically realised wave amplitudes due to experimental error, deviations from linear wave theory and wave breaking and so a range of values around the target will be generated in practice. This point and the competing effects of wave breaking and nonlinear amplification are illustrated in Fig.4.3.

The significant steepness S_p is reported for each sea state in the labels of Fig.4.3 and illustrates how the wave amplitude distributions deviate from linear theory with increased steepeness.

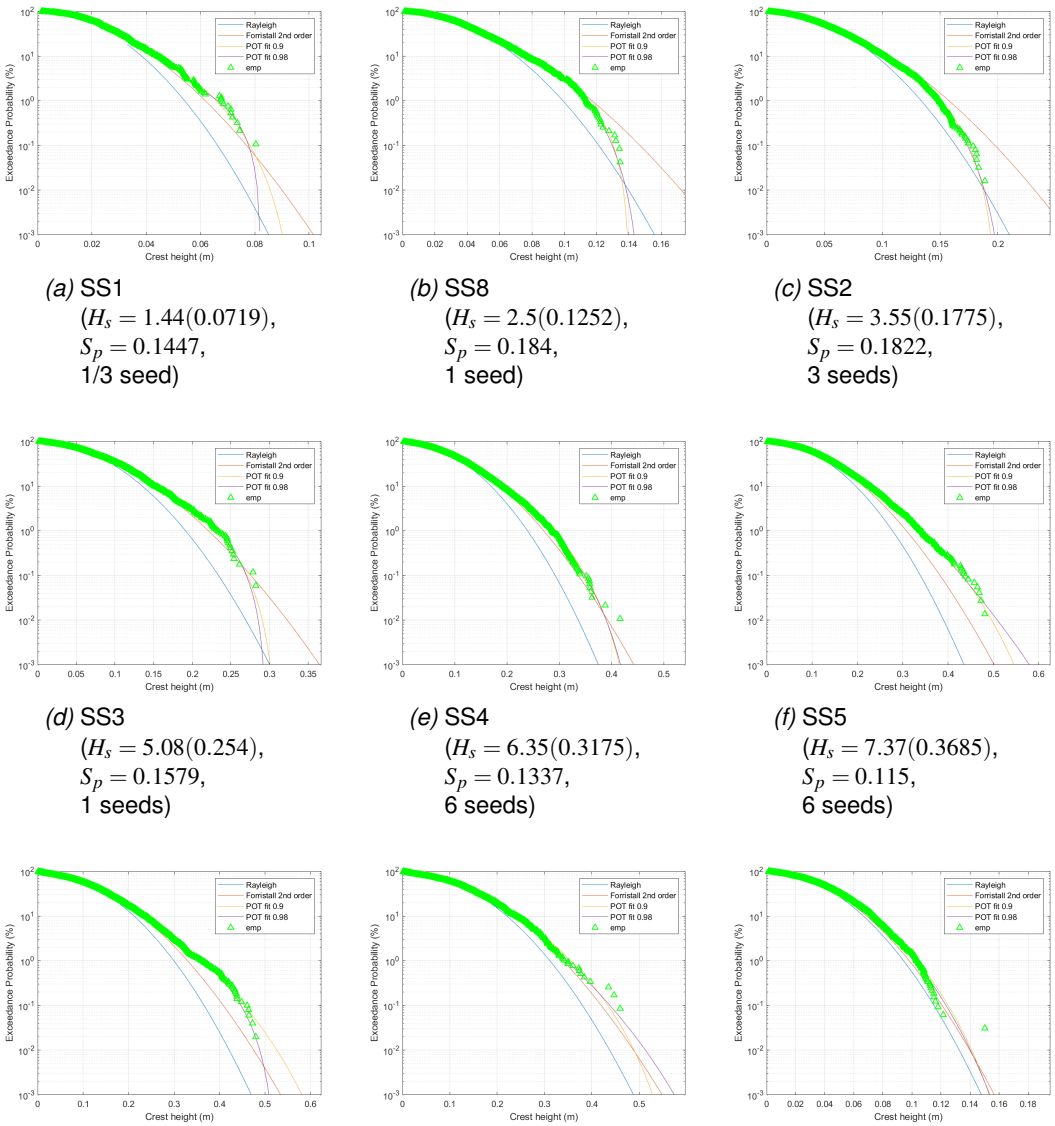

(a) SS1
($H_s = 1.44(0.0719)$,
$S_p = 0.1447$,
1/3 seed)

(b) SS8
($H_s = 2.5(0.1252)$,
$S_p = 0.184$,
1 seed)

(c) SS2
($H_s = 3.55(0.1775)$,
$S_p = 0.1822$,
3 seeds)

(d) SS3
($H_s = 5.08(0.254)$,
$S_p = 0.1579$,
1 seeds)

(e) SS4
($H_s = 6.35(0.3175)$,
$S_p = 0.1337$,
6 seeds)

(f) SS5
($H_s = 7.37(0.3685)$,
$S_p = 0.115$,
6 seeds)

(g) SS6
($H_s = 7.96(0.398)$,
$S_p = 0.1039$,
4 seeds)

(h) SS7
($H_s = 8.27(0.4135)$,
$S_p = 0.093$,
1 seed)

(i) SS9
($H_s = 2.63(0.1317)$,
$S_p = 0.0391$,
6 seeds)

Figure 4.3: Exceedance plots of the wave amplitude distributions for various sea states. The green triangles show the empirical EVD of the peaks from the irregular waves which the EVD is predicted from. Hs values in metres are given as full scale (model scale).

Fig.4.4 shows the percentage error in H_s and it can be seen how the steeper sea states (e.g. 2 and 8) where wave breaking occurs produce values of Hs smaller than the target.

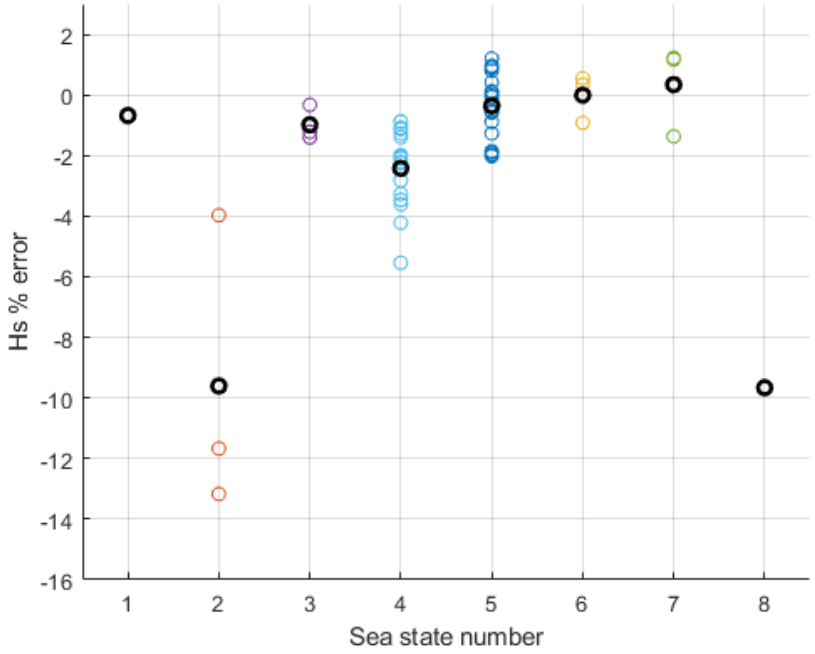

Figure 4.4: Scatter plots of the Hs percentage error for each 1 hour seed in each sea state. The black markers show the means.

4.4 Test site and wave climate

The environmental characterisation was performed on the EMEC site off Scotland using 30 years of hindcast data. The estimation of the environmental contour is based on IFORM, together with a Weibull distribution for H_s and conditional log-normal distribution for $T_p|H_s$ (DNV (2014)). The limiting steepness defines the green curve in Fig.4.5 to the left of which wave breaking renders the sea states unphysical following DNV (2014) and Drago et al. (2013). The closer a sea state is to this limit the more difficult it is to physically reproduce the target surface elevations of the constrained focused wave runs due to an increased frequency of wave breaking as the target focused waves may be unphysical. The increased steepness also leads to greater deviations from linear wave theory. 8 sea states along the contour were studied. It should be pointed out that the contour fitting close to the steepness limit is not accurate as evidenced by the fact that the 50 and 100 year contours go beyond the limit. Therefore the 1 year contour shown here is actually for a much higher return period along much of its length.

A contour approach following Drago et al. (2013), as discussed in section 2.3 of the literature review, where the lognormal distribution is adjusted by the steepness limit is plotted in Fig.4.5 to illustrate this limitation and give an idea of more accurate return period contours at low values of T_p.

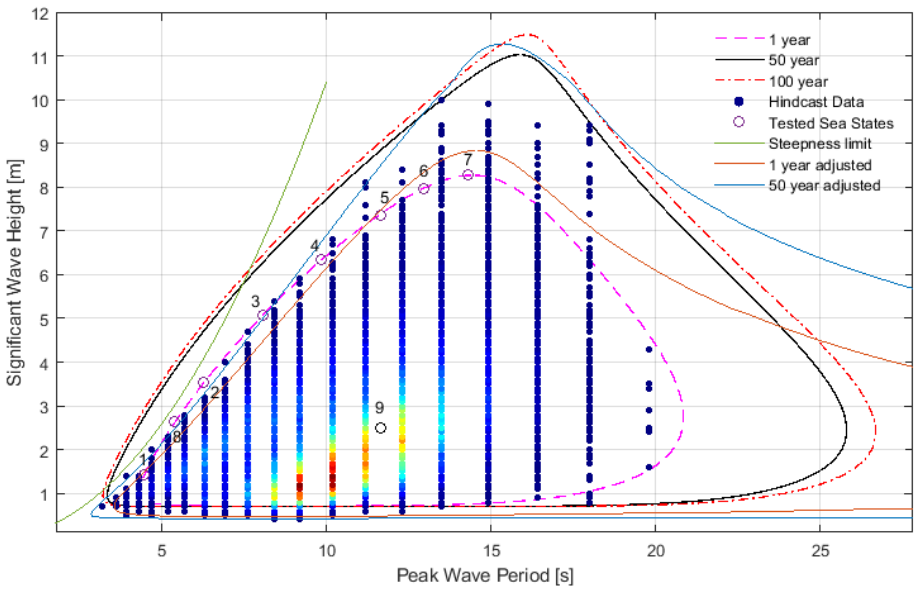

Figure 4.5: EMEC full scale site data, numbered sea states correspond to those in table 1

4.5 Wave Calibration

It is important to assess the accuracy of the physical realisation of the constrained focused waves and apply some form of calibration. Time series calibration is usually applied using a phase amplitude iteration scheme such as in Schmittner et al. (2009) in the frequency domain. This is potentially very time consuming if a large number of iterations is required or a large number of time series used. Preliminary tests suggested that a single, frequency specific phase correction resulted in a large improvement in the accuracy of the generated focused wave profile. The NW and MLER profiles were therefore calibrated in this way by taking an FFT of the target and measured surface elevations and adding the phase difference to the input signal of the wave paddles.

Two types of calibration were compared for CRRWs scaled to the $80th$ percentile re-

sponse of the Rayleigh EVD in SS4 ($H_s = 0.318m$, $Tp = 2.2s$). The selection of the 80th percentile was somewhat arbitrarily chosen as a high percentile response. The first method tried, termed the individual calibration, was based on a section of the surface elevation defined as the time step of the focused wave, $52s$, plus/minus $4s$. This small portion of the time series was selected for calibration as it contains the embedded focused wave, the rest of the time series is random and so its accurate reproduction is less important. An FFT was then performed on this section of the measured wave and compared to the FFT of the corresponding section of the target wave. The phase difference was then added to the input signal and the wave rerun; this process needed repeating for every individual CRRW and so increases the lab time required relative to no calibration by a factor of more than 2. The second method applied the phase correction from the single MLER wave to the CRRW runs and so did not increase the lab time needed, this is termed the single focused wave calibration.

An important source of error affecting the device response is the error between the target and physically generated wave surface elevation. Not only is accuracy important but so too is the amount of time required for the calibration. There does not appear to be a standard way of assessing the accuracy of the generated wave profiles. Collins et al. (2018) discusses metrics for the evaluation of waves in basins and recommend several types of skill score; in this work the Brier skill score is selected to compare different calibration approaches. It is the accuracy of the focused wave constrained at 52 seconds which is of most importance as the background is random. To assess the improvement in the accuracy due to the calibration method the surface elevation was analysed from $52 - T_t$ to $52s$ where T_t is the time step of the trough preceding the focus time ($52s$). The mean square error (MSE) of the uncalibrated and calibrated waves are then calculated and the profiles shifted in time by up to $1.5s$ so that the values are minimised. This time shift was appropriate as the exact time that the focused wave occurs was not important within a few seconds and an example is illustrated in Fig.4.6.

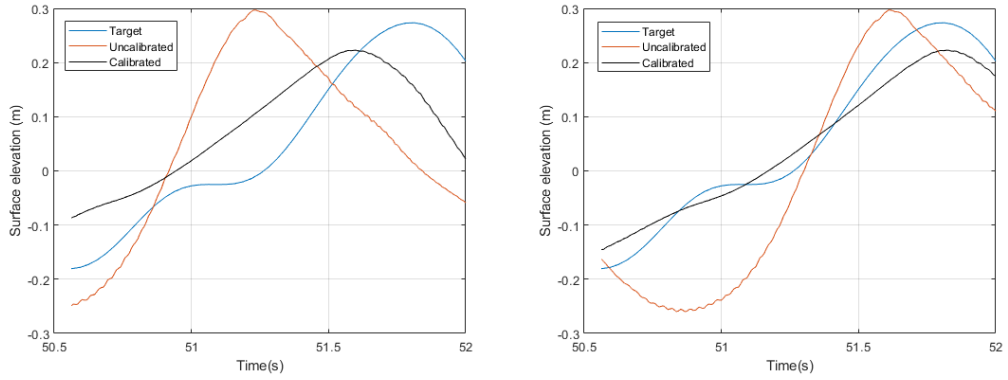

(a) Original timeseries *(b)* Time series after timeshift

Figure 4.6: Illustration of the preprocessing for the BSS calculation.

The Brier skill score (Sutherland et al. (2004)) is then calculated to determine whether the calibration has produced an improvement on the uncalibrated wave. A positive value means the calibration was a better fit to the target with a value of 1 being an exact fit. A negative value means the uncalibrated wave was a better fit.

$$BSS = 1 - \frac{MSE(Y,X)}{MSE(B,X)} \tag{4.1}$$

Here the baseline prediction is taken as the uncalibrated surface elevation so $MSE(Y,X)$ is the mean square error of the calibration to the target and $MSE(B,X)$ the mean square error of the uncalibrated wave relative to the target.

4.6 Results and discussion

4.6.1 Searching the contour

The full scale equivalent of a minimum of three hours of irregular waves were run for sea states $2-7$ shown in Table 4.1. SS5 was identified as the one most likely to be the design state for the mooring load and 18 hours of data (full scale equivalent) collected in line with Commission et al. (2015). In the interest of time SS5 was also used to study the extreme hogging angle although it was unclear whether SS5 or SS6 produced the extremes (See Fig.4.8). Fig.4.7 gives the EVD predictions using all the irregular wave

Table 4.1: Surge offset by sea state at model scale

Sea state	$H_s(m)$	$T_p(s)$	Mean surge position (m)
1	0.072	1	1.15
8	0.132	1.2	1.38
2	0.178	1.4	1.49
3	0.254	1.8	1.41
4	0.318	2.2	1.34
5	0.369	2.6	1.32
6	0.398	2.9	0.89
7	0.413	3.2	0.65

data. Fig.4.7 can be understood in the context of Table 4.1, SS5 produces the largest mooring loads due to the combination of large surge drift position and H_s. The average surge position significantly reduces for SS6 and SS7. The EVD predictions for SS3-5 were larger due to the presence of snatch loads which occurred when the mooring line became taut, leading to much higher loads.

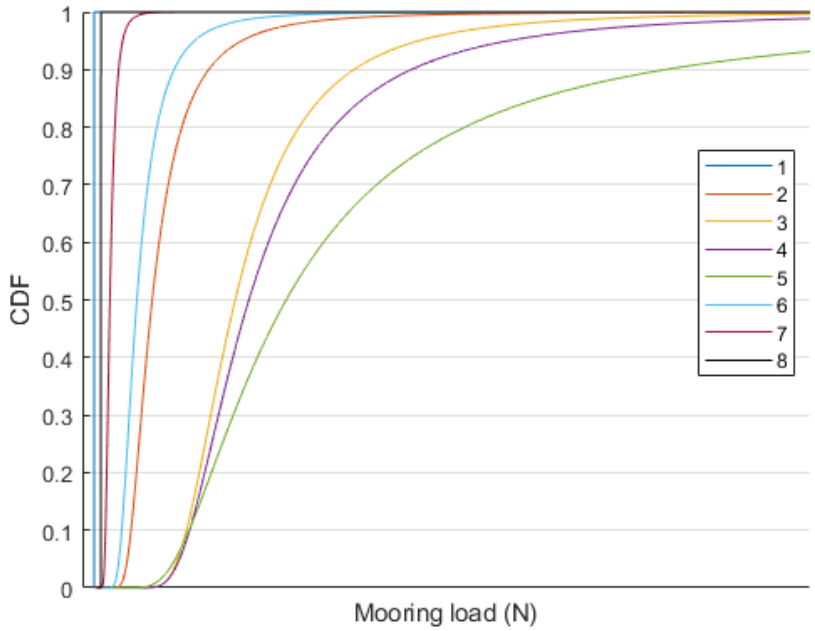

Figure 4.7: EVD force at fairlead. The full scale equivalent of 18 hours of irregular wave data was used in the estimation of the EVD of SS4 and SS5, 3 hours for SS2, SS3, SS6 and SS7 and 1 hour for SS1 and SS8.

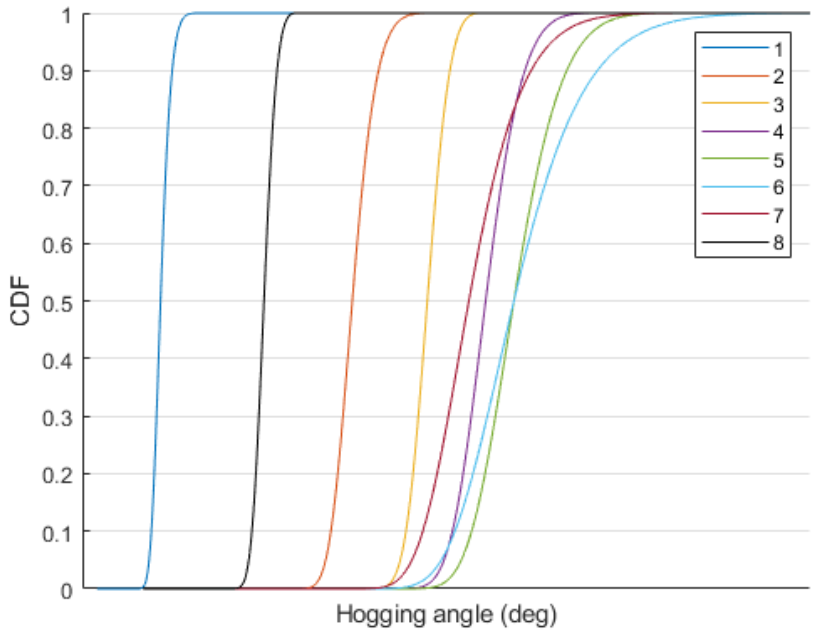

Figure 4.8: EVD hogging angle. The full scale equivalent of 18 hours of irregular wave data was used in the estimation of the EVD of SS4 and SS5, 3 hours for SS2, SS3, SS6 and SS7 and 1 hour for SS1 and SS8.

4.6.2 Impact of preceding wave

By identifying a wave profile resulting in a snatch load event and varying the amount of preceding wave time series generated the importance of the history effects and the surge drift position in particular can be demonstrated, see Fig. 4.9. As the amount of preceding wave generated is increased so too is the surge drift position, there is not a significant increase after around 35 seconds in the example shown. Here the surge position is given according to the position of the hinge connecting the rafts.

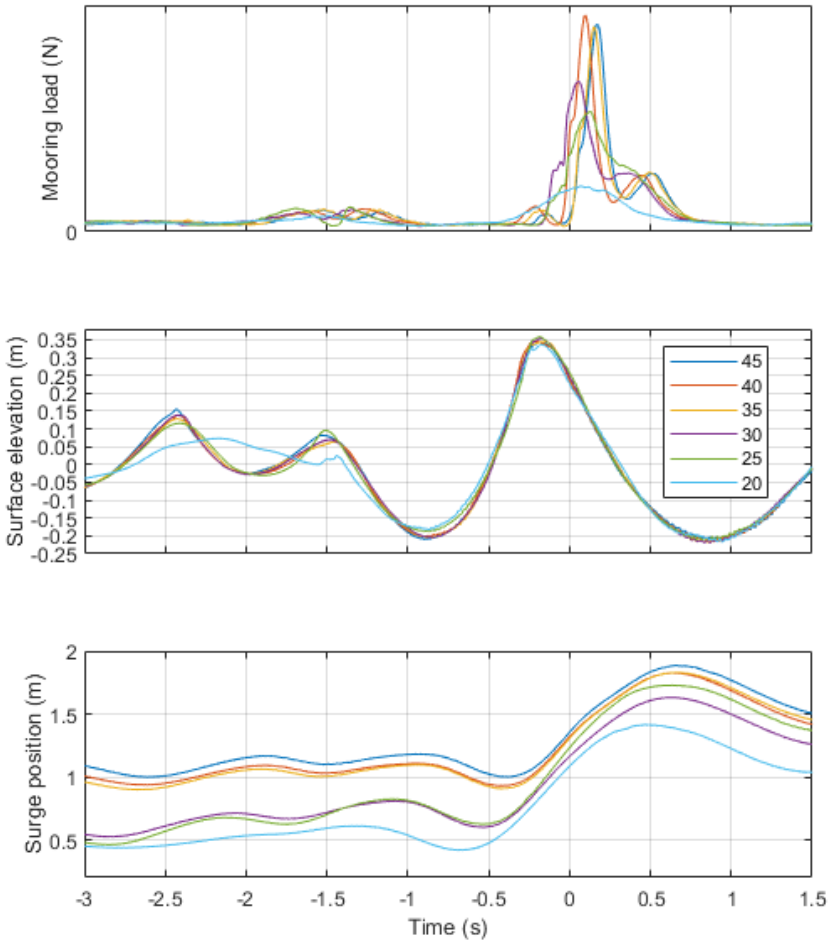

Figure 4.9: Effect of varying the length of the irregular wave background on the mooring load, the amount of preceding wave in seconds is given by the legend. The first 7 seconds of each run consists of paddle inactivity and ramp time. The surface elevation is given from a wave gauge located at $1.47m$ from the zero surge position. The surge position given is that at the hinge.

To allow for the surge drift to establish, all the focused waves were constrained at $52s$ and each run lasted $57s$. The drift has a significant effect on the mooring loads and is a second order effect. It illustrates why single focused waves do not produce extremes for the mooring load, why any estimate of an EVD based on the linear RAOs will be inaccurate and why the same focused wave embedded in different backgrounds will produce a wide range of mooring loads.

4.6.3 Wave calibration

Fig. 4.10 shows that to produce accurately the profiles with large amplitudes it is necessary to perform some form of calibration. In the cases considered here the extreme response occurs at 45 seconds so it is the accurate reproduction of the profile up to $45s$ which is of primary concern.

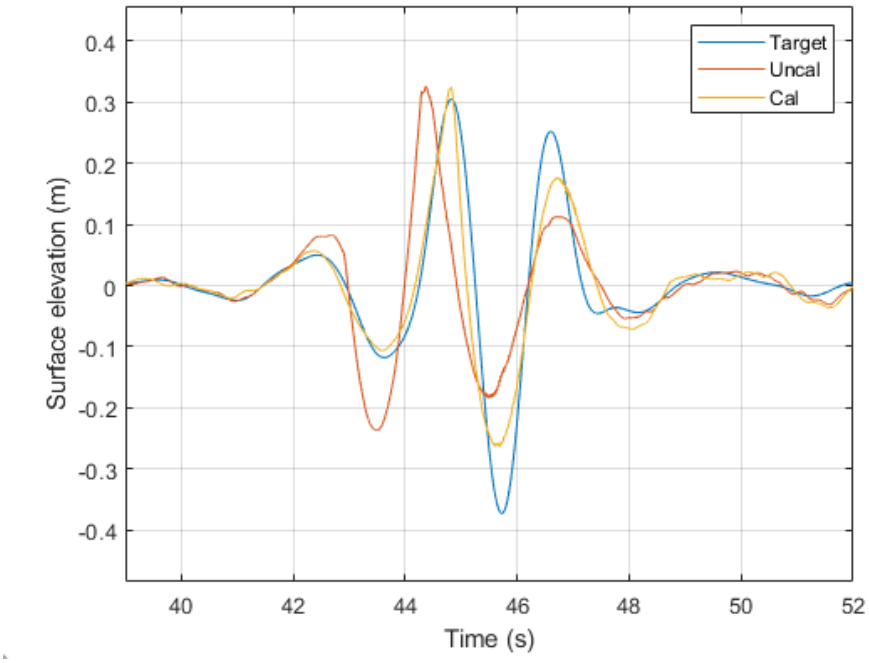

Figure 4.10: Single mooring load MLER wave calibration SS5, scaled to the $99th$ percentile of the linear response EVD. The calibration method applied was using a single, frequency dependant phase correction.

It can be seen in Fig.4.11 that the calibration produced an improvement (A BSS above 0) in $8/10$ cases for the individual calibration runs and $9/10$ for the single focused wave calibration runs.

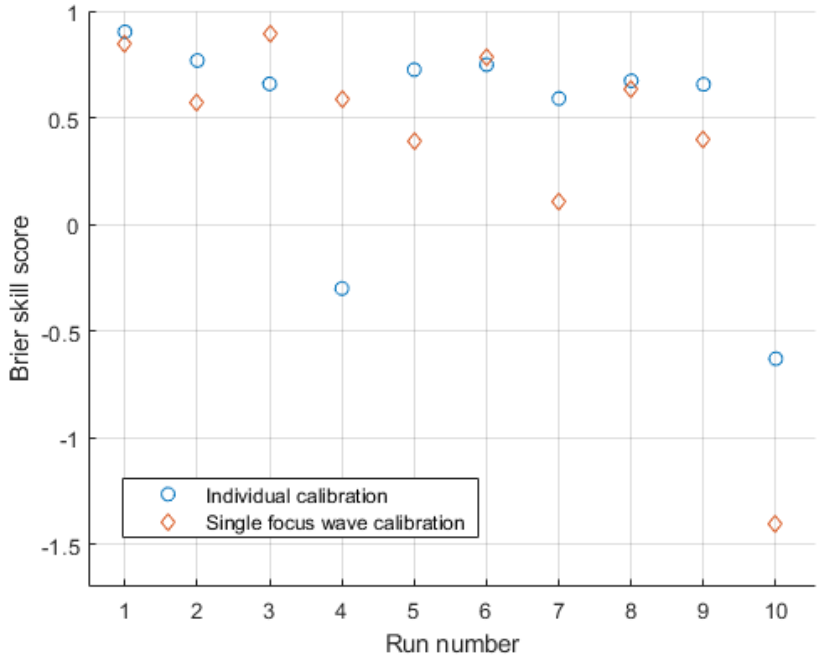

Figure 4.11: Brier skill score calibration comparison, 80th percentile CRRW profiles for SS4.

The instances where the calibration was not an improvement were due to wave breaking as illustrated in Fig.4.12 below. There was no significant difference in the improvement using the individual compared to the single focused wave calibration but there was a substantial difference in the time requirement. Therefore the single focused wave calibration method was used for the constrained focused wave profiles.

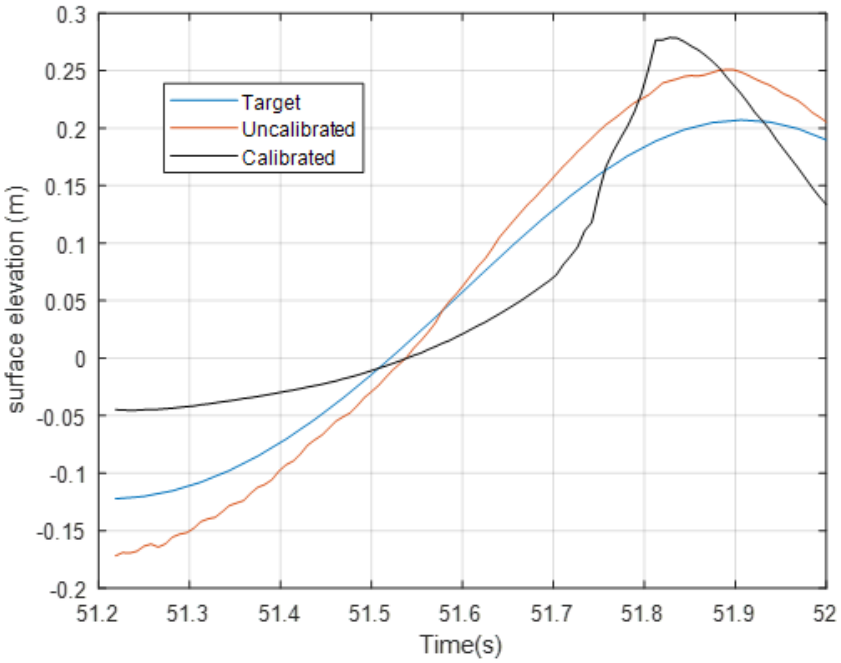

Figure 4.12: Negative Brier skill score example for a breaking wave case $BSS = -1.4$

4.6.4 SS5 mooring load

The empirical extreme wave profile for SS5 was calculated from the average of the 6 profiles which resulted in the largest mooring load during the 18 hours of irregular wave data. Fig.4.13 shows the sudden increase in surge, relative pitch and mooring load caused by the extreme profile. The bold black line shows the mean surface elevation from the six extremes and the bold red lines indicate the average response.

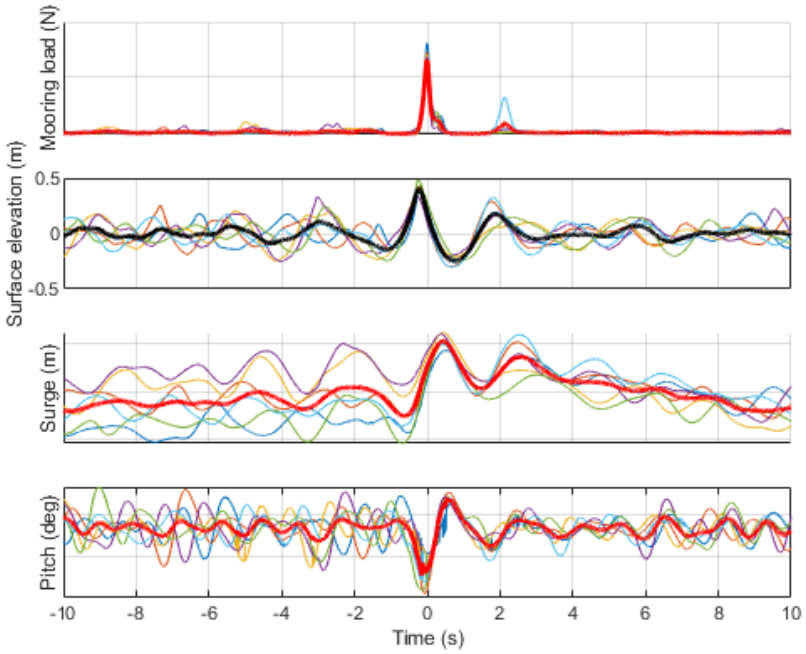

Figure 4.13: Average profiles of the surface elevation and response for the empirical extreme profile.

20 CRRW (black line Fig.4.14a) were first run for SS5 but it was apparent that the extreme amplitude did not match the average profile (red line Fig.4.14a and 4.14b) which led to the extreme mooring loads from the irregular wave time series. 30 CNWs (black line Fig.4.14b) were then run as they were found to more closely resemble the empirical average profile in the second before the extreme load (-1 to 0 seconds) Fig.4.14b. A phase shifted CNW which was a better fit was tried also, but is not shown here as the loads generated were not significantly different to those of the CNW.

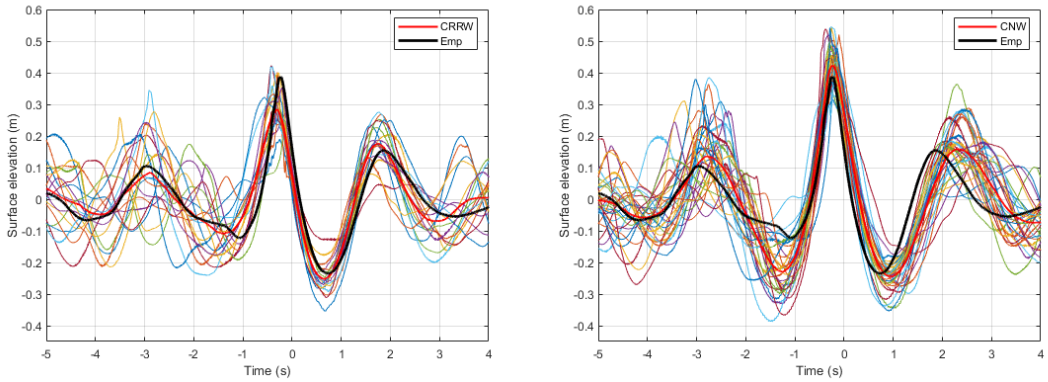

(a) CRRW *(b)* CNW

Figure 4.14: (a) 20 CRRW profiles with red giving the average and black the average for the 6 empirical extremes from the $18hrs$ of irregular waves. (b) 30 CNW profiles with red giving the average and black the average for the 6 empirical extremes from the $18hrs$ of irregular waves.

The mooring loads generated by the CRRW, CNW and empirical runs are compared to the EVD predicted from the irregular waves in Fig.4.15. It can be seen that the CNWs produced a small number of extremes at the higher end of the EVD. The effects of wave amplitude on the mooring load generated are demonstrated in Fig.4.16. The range of CNW amplitudes about the $99th$ percentile target of $0.443m$ can also be seen. There is no shared target surface elevation amplitude for the CRRWs to compare with as the response peak occurs after the surface elevation peak and it is the linear prediction of the response which the amplitude is scaled to rather than a surface elevation. The CRRWs failed to produce extremes as large as the CNWs likely due to the abrupt change in system behaviour brought on by the snatch loads, as seen in the irregular wave time series in Fig.4.13, and by the discrepancy between the average of the CRRW and empirical profiles due to nonlinear wave development and wave breaking. The CRRWs are based on linear RAOs and because the system behaviour departs from those RAOs, the CRRWs no longer produce the extremes. This result serves as a reminder that response conditioned methods are only as valid as the linear RAOs they are calculated from and that in steep sea states nonlinear wave development may further complicate the analysis. The mean of the upper half of the maxima from the

CNWs was found to produce a characteristic load estimate more in line with the irregular waves and is given by the blue vertical line in Fig.4.15. This presents a potential adjustment for studying highly chaotic, nonlinear effects such as snatch loading but more cases should be studied before commenting on its general applicability.

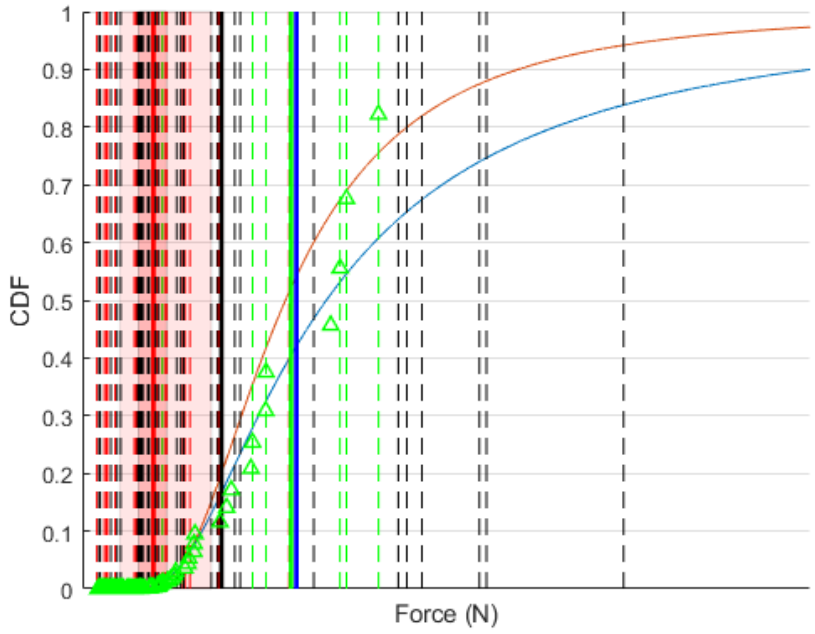

Figure 4.15: CRRW, CNW, EVD comparison. CNW responses are given by red dashed vertical lines, CRRWs black and the 6 empirical 1 in $3hr$ extremes from the irregular waves are green. The mean of each ensemble is given by its respective colours solid vertical line and the mean of the upper half of the CNW responses are given by the solid vertical blue line. The EVD CDF for threshold 1 is given in blue, threshold 2 is given by the solid red curve. Threshold 2 uses a larger threshold. Force magnitudes have been obscured by removing the x axis values.

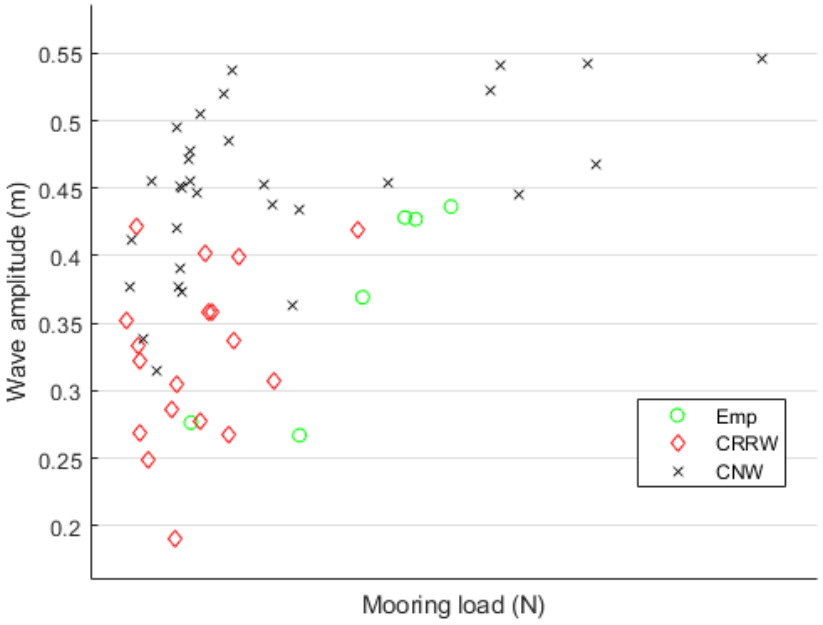

Figure 4.16: Largest mooring load vs largest wave amplitude for the 20 CRRWs and 30 CNWs occurring approximately at the selected time step of the extreme ($52s$) and the empirical profiles producing the largest responses for SS5.

Fig.4.17 demonstrates how the selection of the target wave amplitude at the $99th$ percentile of the EVD using linear wave theory produces similar results as seen for the response amplitude and distributions. The CNW amplitudes produced in the physical experiments cover the range of the estimated 'true' nonlinear amplitude EVD and the mean is around the $70th$ percentile. This fact highlights the decision to apply a phase correction only to the focused and constrained focused waves. If an iterative calibration procedure were applied insisting on the linearly predicted target wave being recreated then the resulting wave would not be representative of the extremes produced during the physical irregular wave runs and so any resulting characteristic load calculation would also be an under prediction. The NewWave profile has been extended to second order theory (Jensen (1996)) but as Fig.4.3(f) and Fig.4.17 show even second order theory is exceeded and linear wave maker theory is used in most basins and numerical models.

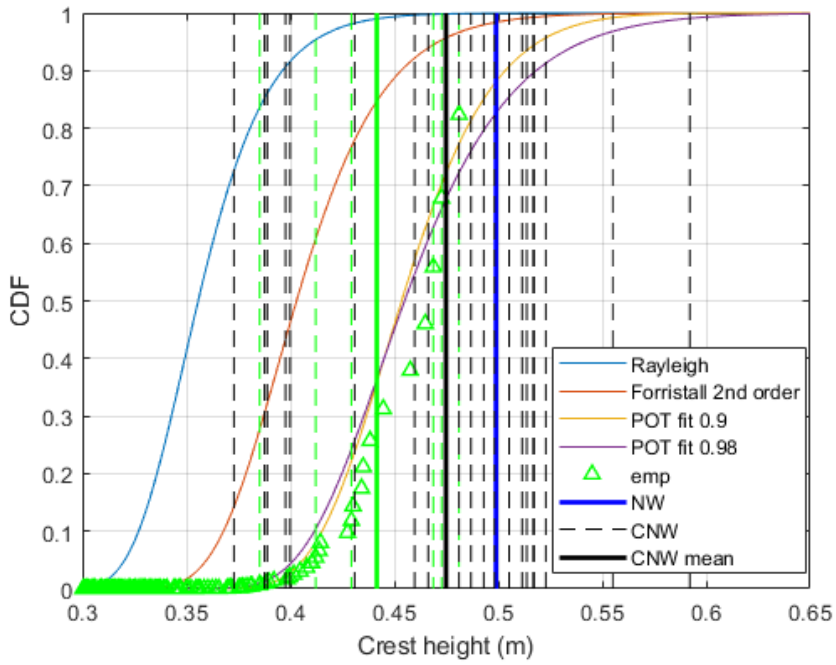

Figure 4.17: NW, CNW, EVD comparison. The 6 empirical 1 in $3hr$ extremes from the irregular waves are green with the solid line showing the mean.

The CNWs produced some higher percentile responses on the predicted EVD. However, considering the wave amplitudes were scaled to the $99th$ percentile of the predicted extreme wave amplitude distribution, few higher percentile values were observed. This is likely due to the difficulty in producing snatch loads as they are dependent on chaotic history effects, but also because the snatch loading complicates the prediction of the EVD as they likely change the shape of the distribution above a threshold. The EVD prediction for the sea state containing snatch loads therefore would be improved by determining the threshold to fit the distribution by the definition of the snatch loads, as is done in Hsu et al. (2017). Defining the snatch load cases for stiff cables however is not straightforward. A classification using the separation distance of the fairlead and anchor positions was attempted but it was found that this distance being at a maximum was no guarantee of a large mooring load. The definition of the threshold then becomes somewhat arbitrary. Threshold 1 in Fig.4.15 is based on the mean and standard deviation, the same as that used to compare the

sea states in Fig.4.7. Threshold 2 is taken at a larger mooring load chosen to define the snatch loads as a high value which occurs when the separation distance of anchor and fairlead is at a maximum. Threshold 1 corresponds to the $96.7th$ percentile of the data and so the EVD is calculated from 271 peaks, threshold 2 to the $98.6th$ percentile using 106 peaks. Threshold 2 therefore uses much less data in the prediction of the EVD. The problem of threshold selection is present even in the absence of a change in system behaviour and it would seem prudent to impose a mooring design criteria that precludes the possibility of snatch loading to the greatest extent possible as they result in significantly increased mooring loads. For these reasons the accuracy of the EVD is not considered further here.

4.6.5 SS5 hogging angle

The focused waves for the hogging angle are presented in Fig.4.18. It can be seen that the CRRWs don't give an estimate in line with the IWs, that the CNWs give a better fit and that the empirical profile is very similar to that leading to the extreme mooring loads in Fig.4.14. This is most likely due to the pitch angle of the front raft spiking during snatch load events. The Characteristic load estimates presented in Fig.4.19 show a similar trend to those of the mooring loads in Fig.4.15 with the upper half of the CNW responses giving an estimate in line with the irregular waves.

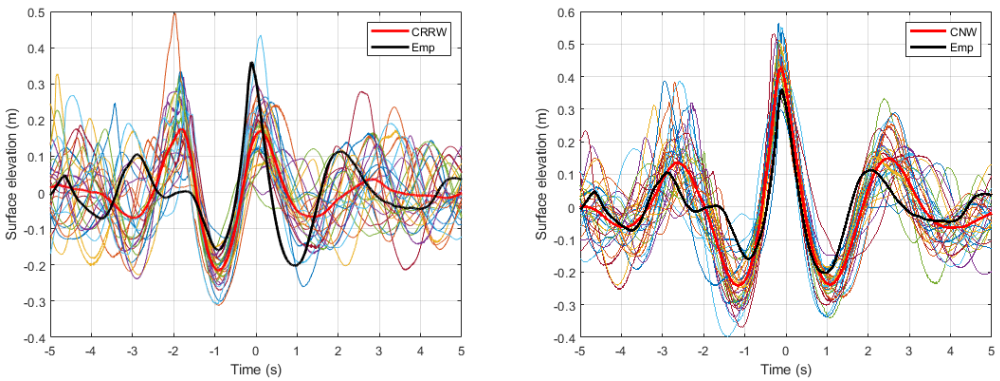

(a) CRRW *(b)* CNW

Figure 4.18: CRRW, CNW and empirical extreme (Emp) wave profile comparisons for the hogging response, each individual run is given by the thin lines.

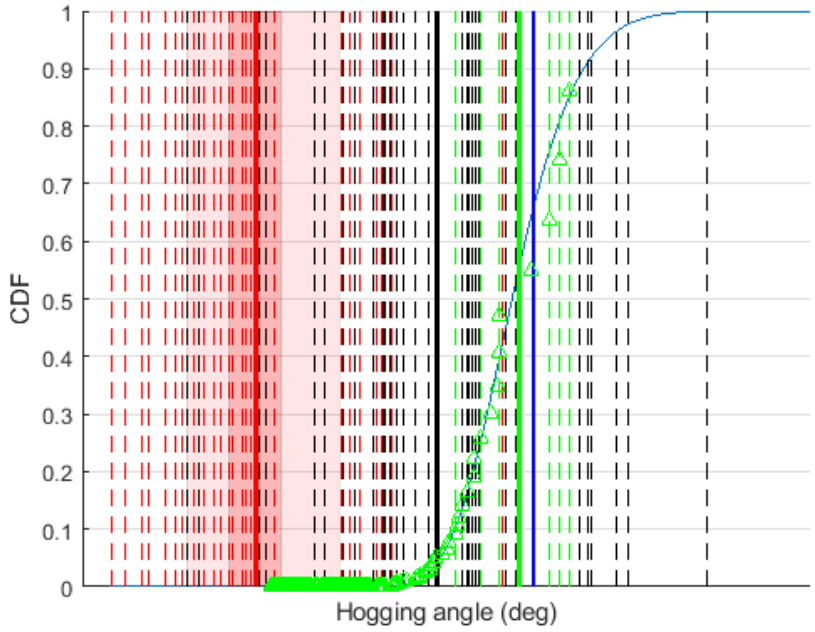

Figure 4.19: CRRW, CNW, EVD comparison. CRRW responses are given by red dashed vertical lines, CNWs black and the 6 empirical 1 in $3hr$ extremes from the irregular waves are green. The blue vertical line shows the response to the MLER wave. Response magnitudes have been obscured by removing the x axis values. The solid blue vertical line gives the mean of the upper half of the CNW responses.

4.6.6 SS9 mooring load

To remove the complicating effects of snatch loading a less extreme sea state with the same T_p as SS5 but a much smaller H_s is studied for comparison. The full scale equivalent of 12 hours of irregular waves, 30 CNW and 30 CRRW profiles were run for a smaller sea state with the same peak period as SS5, $T_p = 2.6s, H_s = 0.1252m$ which will be referred to as SS9. The EVD was calculated based on the POT method using the threshold calculated from the mean and standard deviation. In Fig.4.20 it can be seen that the average CRRW profiles are in agreement with the average of the 4 empirical extremes. Fig.4.21 and Fig.4.23 demonstrate that the 30 CRRWs produced mooring loads larger than the 30 CNWs and at the upper percentiles of the EVD.

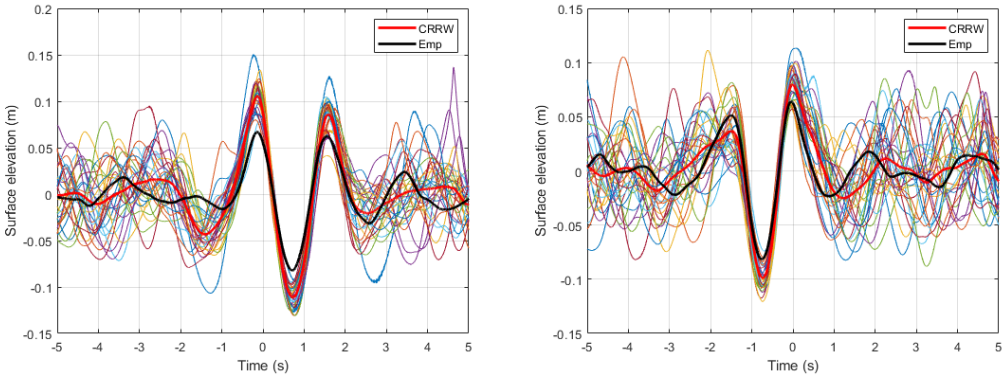

(a) Force at fairlead

(b) Hogging angle

Figure 4.20: CRRW and empirical extreme (Emp) wave profile comparisons, each CRRW run is given by the thin lines.

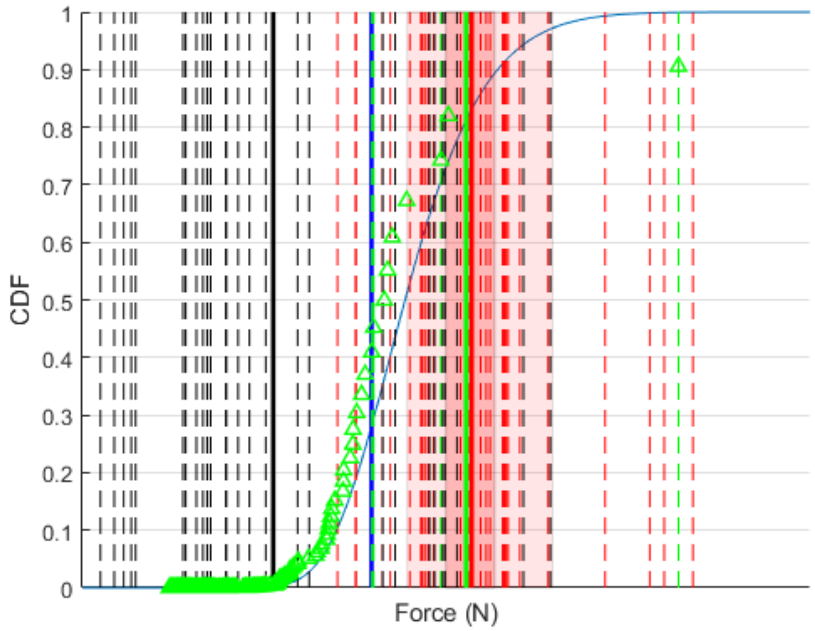

Figure 4.21: CRRW CNW EVD comparison. CRRWs are red, CNWs black and the 4 empirical 1 in $3hr$ extremes from the irregular waves are green. The response to the MLER wave is given by the vertical blue line. The EVD CDF is calculated based on the full scale equivalent of 12 hours of irregular waves. The x axis values are obscured.

The CNW amplitudes produced, shown in Fig.4.22, reveal that when scaling the amplitude to the Rayleigh EVD for a less steep sea state, the extremes produced are at the

tail of the distribution rather than spread over the EVD as in Fig.4.17.

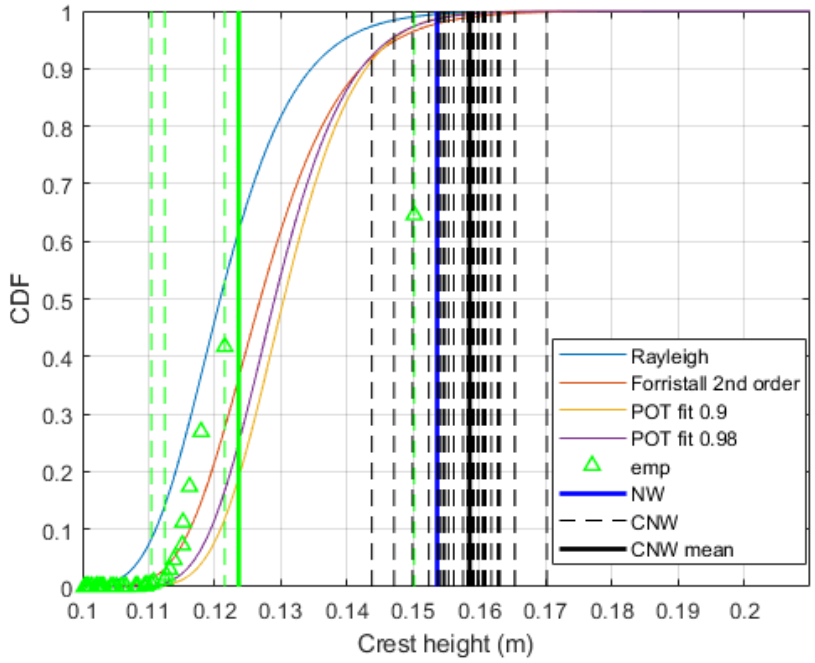

Figure 4.22: NW, CNW, EVD comparison. The 4 empirical 1 in $3hr$ extremes from the irregular waves are green with the solid line showing the mean.

The target CNW amplitude was $0.151m$. It can be seen from Fig.4.23 that even in the absence of snatch loads CNWs with virtually identical amplitudes produce a wide range of mooring loads due to the importance of history effects.

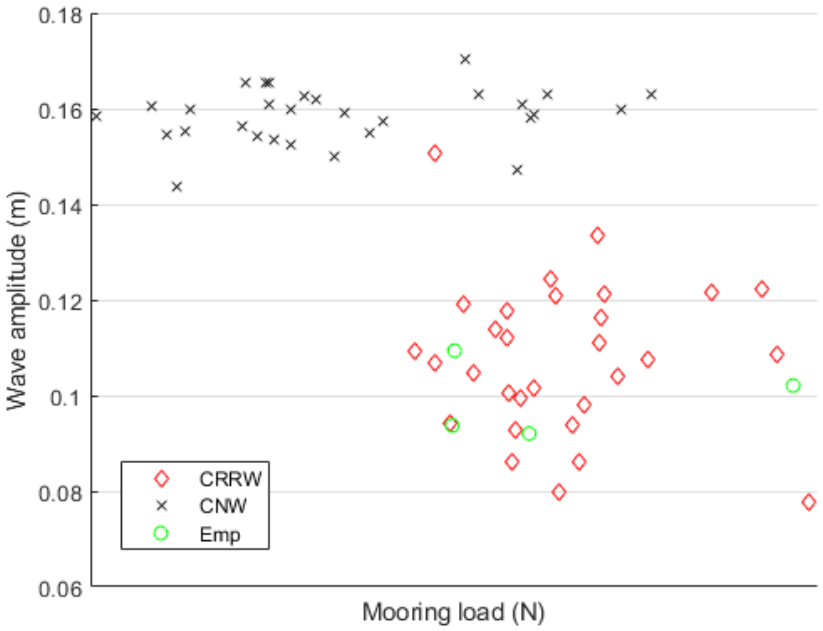

Figure 4.23: Largest mooring load vs largest wave amplitude for the 30 CRRWs and 30 CNWs occurring approximately at the selected time step of the extreme ($52s$) and the empirical profiles producing the largest responses for SS9.

4.6.7 SS9 hogging

Fig.4.24 demonstrates that the response conditioned waves perform as expected in the smaller sea state and the MLER wave produces a conservative estimate.

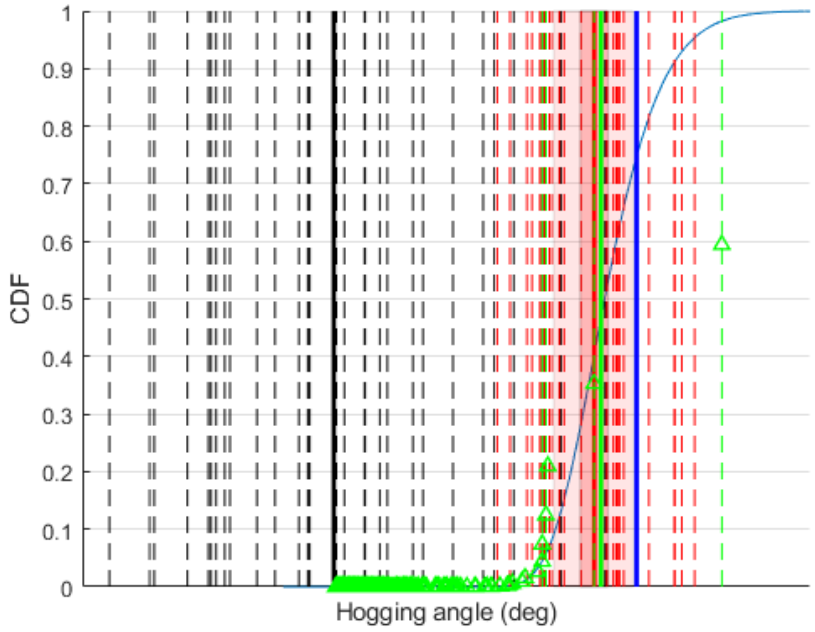

Figure 4.24: CRRW, MLER, CNW, EVD comparison for the hogging response. CRRWs are red, CNWs black and the 4 empirical 1 in $3hr$ extremes from the irregular waves are green. The EVD CDF is calculated based on the full scale equivalent of 12 hours of irregular waves. The x axis values are obscured.

Table 4.2: Design load prediction comparisons. FL = Fairlead, Hog = hogging angle. FL$(\%)$ refers to the percentile of the EVD CDF, FL$(95th/\%)$ the ratio of the response at the percentile in the previous column to that at the $95th$ percentile.

Sea state	Wave type	FL $(\%)$	FL $95th/\%$	Hog $(\%)$	Hog $95th/\%$
SS4	IW	44.1	2.7	57.6	1.09
SS5	IW	40.0	4.94	55.3	1.12
	MLER	0	-	0	-
	CRRW	0	-	0	-
	NW	0	-	0	-
	CNW	0	-	4	-
	CNW 1/2	42	-	66	-
SS9	IW	81.2	1.03	46.7	1.13
	MLER	28	-	74.7	-
	CRRW	83.1	-	40	-
	NW	0	-	0	-
	CNW	0	-	0	-

4.6.8 Wave breaking

It is worth mentioning that wave breaking in sea states close to the steepness limit result in significant problems for physical testing. In particular, the proximity of SS1, SS8 and SS2, to the steepness limit made it impossible to produce accurately any surface elevation profiles for constrained focused waves in these sea states. The profile of the wave producing the extreme response cannot scale up indefinitely due to the occurrence of ever more wave breaking as the amplitude is increased. The impact of wave breaking on the prediction of the EVD is uncertain; there is currently no upper limit and how to impose one is an open question. Being able to accurately determine the point at which a wave becomes unphysical would be useful in attempting to solve these issues as would knowing the true nonlinear crest height distribution.

4.7 Conclusions and future work

The CRRW profiles produced extremes at the higher end of the EVD and in line with the characteristic load predictions from irregular waves in the benign sea state where snatch loading did not occur. However, the extreme responses in sea states in which snatch loading did occur were more successfully produced by CNWs. Although the characteristic load prediction from the CNWs was still an under estimate compared to the irregular waves. An equivalent estimate could be arrived at by taking the mean of the upper half of the CNW responses but this may not be generally applicable. The same was true for the hogging response. This result serves as a reminder that response conditioned methods are only appropriate when the behaviour of the system is unchanging over the range of possible wave sequences for the sea state. It is a likely constraint on mooring design to minimise the risk of snatch loading and so it is perhaps not worth spending too much time on this problem. On the other hand, other events which may cause abrupt changes in device behaviour exist, snap loads of tension leg or catenary moored platforms or the end stops of a PTO being reached for example, which make this kind of event worthy of future study. Snatch loads have also been found to produce extreme mooring loads for other existing WEC devices and mooring

arrangements (Sirigu et al. (2020)).

This chapter demonstrates how constrained focused waves can be used during physical testing to produce useful data on the extreme responses of ORE devices around the characteristic load or response. It is worth reiterating that the EVD in SS5 has a large associated uncertainty due to threshold selection caused by snatch loading, more data would be required to reduce this. Spending large amounts of precious lab time on calibration to improve the physical reproduction of the constrained focused waves would seem unwise, particularly as the variation in the response appears to have more to do with chaotic history effects than with the errors in the physical realisation of the target embedded wave profiles. This is demonstrated most clearly by the range in responses produced by similar amplitude CNWs in Fig.4.16 and Fig.4.23. $20-30$ profiles can be run in an hour using the phase correction calculated from the single focused wave calibration. Care should be taken when using response conditioned methods as changes in system behaviour, or wave breaking resulting in the target profiles being unphysical, may render them invalid. The effects of wave breaking on the prediction of the EVDs and physical realisation of constrained focused waves is an important area for future work.

Chapter 5

VolturnUS-S experimental

Chapter summary

Experiments using a $1:70$ scale model of a semi-sub FOWT to assess the suitability of the CRRW approach for characteristic load prediction are described and results presented. Limitations of the environmental characterisation and of the accurate realisation of target wave profiles in a physical basin are discussed. A method for constraining wave groups is applied to predict characteristic mooring loads.

5.1 Device description and experimental setup

The FOWT tested in this chapter is a semi-sub design; the VolturnUS-S platform and IEA 15MW reference turbine shown in Fig.5.1. This device benefits from extensive publicly available data including an OpenFAST model. It is moored with 3 catenary chains.

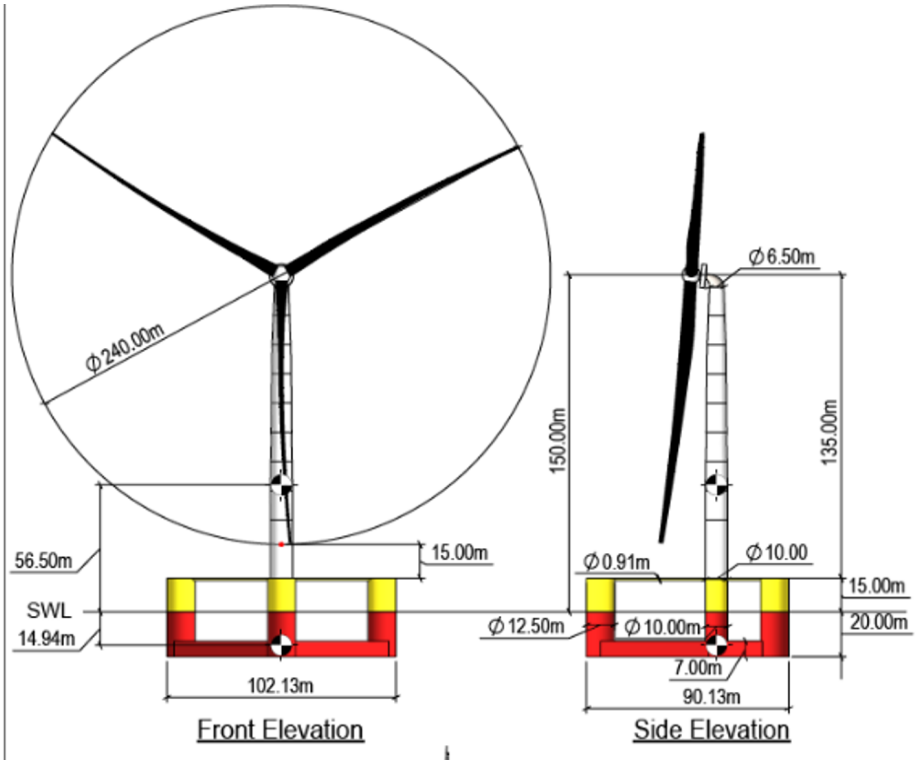

Figure 5.1: Diagram of the reference device taken from Allen et al. (2020).

The focus of this thesis is on hydrodynamic loading and the inclusion of turbulent wind would greatly complicate the characteristic load predictions. Therefore the wind loading for this model uses a thruster generating constant thrust so that the wind loading can be incorporated in a basic way without incurring the risk that so many parameters are considered that the hydrodynamic effects are masked. Turbulent wind can have an impact on the low frequency surge motions of a FOWT (DNV (2018)) and so this limitation should be kept in mind when interpreting the results.

The locations in the basin of the three wave gauges and device are given in table 5.1.

Table 5.1: Locations of model and probes in the basin, x is relative to the paddles, y to the basin centre line

Position	Model	Probe 1	Probe 2	Probe 3
$x(m)$	17.3	7.3	9.8	17.3
$y(m)$	0	0	0	-1.5

The mass density of the three catenary chains was $0.14kg/m$, the back two chains had a length of $8.94m$ and the front of $9.69m$. They were each attached to one of the columns positioned at 120 degrees to one another. The mass properties of the device presented in table 5.2 deviate from those of the reference documents (Gaertner et al. (2020), Allen et al. (2020)) in order to maintain the correct draft in fresh water.

Table 5.2: Model details estimated from a solid works model, moments of inertia are taken about the centre of mass, vertical centre of gravity (VCG) is taken from the model base and the centre of gravity in x (XCG) from the tower centre. * Note that the -791.667% difference seems large but is only $-3.8mm$ as an absolute value.

Mass properties	Target	Achieved	Difference	Percentage difference
Ixx (kgm^2)	26.495	26.550	0.055	0.207
Iyy (kgm^2)	26.451	26.551	0.099	0.373
Izz (kgm^2)	14.206	14.120	-0.086	-0.609
VCG (mm)	255.14	261.57	6.43	2.458
XCG (mm)	4.28	0.48	-3.8	-791.667*
$Mass$ (kg)	58.123	56.23	-1.893	-3.367

Fig.5.2 is a photo the model in the basin with labels indicating the ducted fan thruster system, reflective markers used by the Qualisys motion capture software and the location of one of the load cells which measures the mooring force. There are two additional load cells not shown, one on each column.

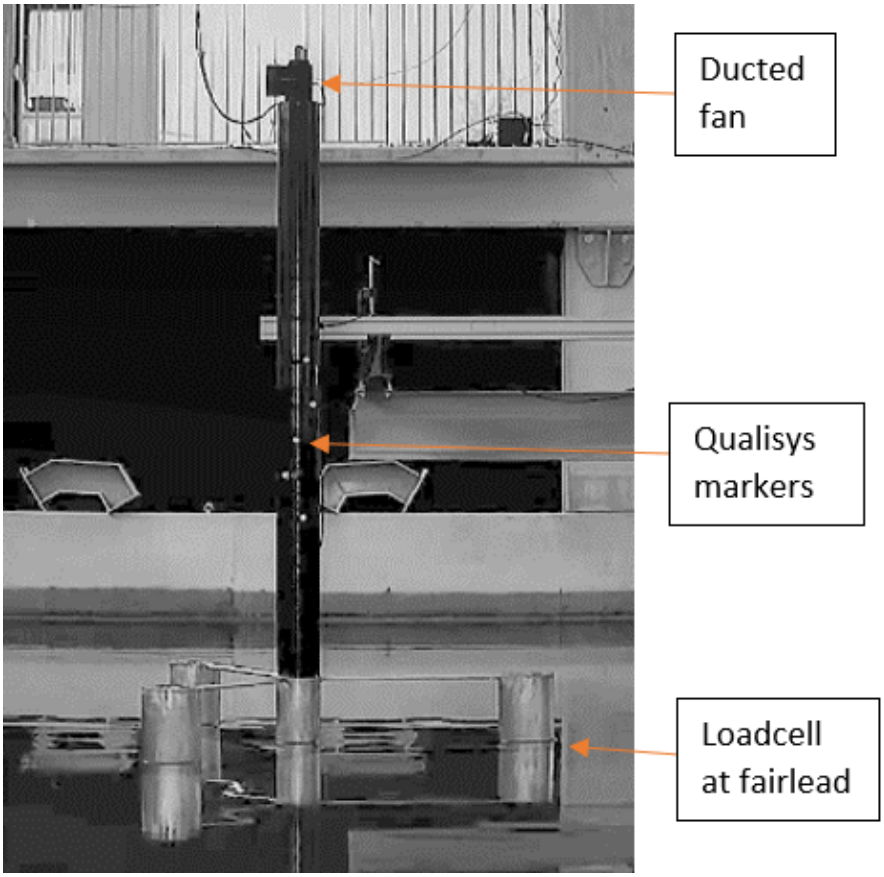

Figure 5.2: Anotated photo of the VolturnUS model in the basin.

Results from the physical experiments should be interpreted in the context of measurement uncertainty. Wave gauges were calibrated each morning before testing began and a maximum error of 0.61% was recorded in the calibration files over the campaign. The Qualisys motion tracking software recorded a mean average residual from the irregular wave runs of $1mm$. The uncertainty in the single axis load cell readings was inferred from the noise in the signal and gives an uncertainty of 3.2% at a load chosen to be representative of an extreme response of $12.5N$. The load cell reading at the models equilibrium position in the absence of waves was around $7.6N$ and so the uncertainty at smaller values such as this is larger, judged to be around 5%.

5.2 Environmental characterisation and selection of sea states

Aqua Ventus 1 will see a similar VolturnUS design supporting an $11MW$ turbine deployed at the University of Maine deepwater offshore test site on the north east coast of the USA in 2024 (University of Maine (2022)). The deployment location selected for this study is close to this site at the NOAA 44005 buoy location with a water depth of $200m$. 30 years of hindcast data was used to perform the environmental characterisation in this chapter. The site benefits from 30 years of buoy data and a detailed environmental characterisation study (Viselli et al. (2015)).

A $1hr$ exposure time is commonly used for FOWTs as a compromise between the $3hr$ stationary sea states and 10 minute stationary wind conditions (e.g. Li et al. (2017)). When considering wind loading it makes sense to search contours associated with particular wind speeds such as the cut-out and rated (maximum thrust) wind speed as well as the extreme H_s conditions. DNV (2018) states that it is often the rated wind speed condition which produces the extreme responses. When the wind loading is the dominant driver of the response there is less reason to assume a high percentile along the contour will represent the characteristic load as the same wind conditions will occur far more frequently in less severe sea conditions. Li et al. (2017) developed a modified contour approach where they search lower return period contours and use a higher percentile response from the EVD using OpenFAST to try and address this issue. This is a response based method similar to that of 3D IFORM requiring a much larger dataset to reduce the confidence intervals to a satisfactory level, and so it is not compatible with a physical modelling approach.

The method applied in Li et al. (2013) is frequently cited when investigating extreme responses of FOWTs. They characterised the joint U, H_s, T_p distributions using hindcast data for 18 sites and gave the distribution parameters for five reference sites so the distributions can quickly and easily be generated. They used U as the marginal then $H_s|U$ then $T_p|H_s|U$. U is chosen as the marginal distribution as it has a significant impact on the extreme responses. However, while using U as the marginal distribution makes

sense for contours relating to operating conditions, it appears to produce a contour with unreasonably large H_s values when the turbine is idling ($U > 25m/s$). E.g. The marginal H_s fit for the Wave hub site gave the 50yr H_s value as $10.22m$ where as the contour based on marginal U gave a value of $14m$. Applying this 3 parameter method ($T_p|H_s|U$) to the site off the coast of Maine also produces an extreme H_s far larger than the 50yr extreme sea state estimate given by the characterisation study in Viselli et al. (2015). A joint distribution is not fitted; instead, H_s is used to calculate the 50yr sea state paired with the mean T_p through a POT method, with only extreme events separated by at least 4 days being included. In contrast the contour method uses all the 1 hour sea states available in order to have sufficient data to fit the joint distribution to T_p. The H_s of the 50 year sea state using the three parameter fit ($T_p|H_s|U$) corresponds to approximately the 600 year H_s using the two parameter contour model ($T_p|H_s$) used previously applied to the hindcast data. Despite this, for the idling conditions we chose to mostly focus on a 50 year contour produced in line with the 3 parameter method in Li et al. (2013) as that is the approach most commonly applied. Also because data was already available for the 50 year sea state determined in Viselli et al. (2015), from previous tests using the same model setup conducted by other researchers at the University of Plymouth. Additionally, the method for selecting the extreme conditions used in Viselli et al. (2015) has its own flaws which can be seen by the unrepresentative location of the corresponding case, here referred to as the '50yr Viselli' sea state, relative to the hindcast data in Fig.5.3. Only sea states tested with multiple seeds are named on this plot and discussed in this chapter although others were studied.

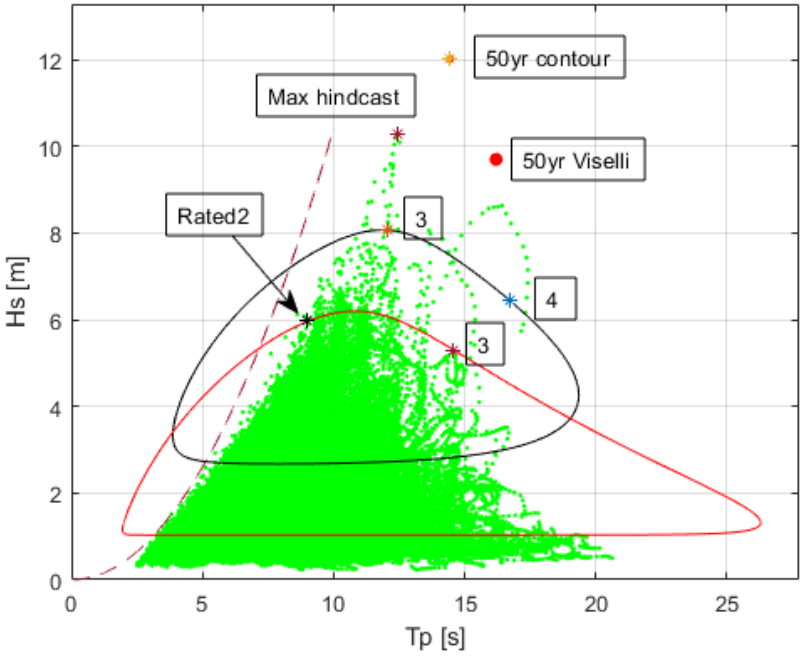

Figure 5.3: Sea states chosen for study with 1hr hindcast data points underlaid in green. The red line shows the 2D H_sT_p contour at rated wind speed (maximum thrust) and the black shows the cut out windspeed contour. The dashed line shows the theoretical steepness limit.

Additionally, an extreme sea state from the hindcast data was selected as there are further issues using established methods when fitting the contour resulting in a 50 year sea state which does not well represent the site as discussed previously. Briefly, these are caused by the extrapolation of the joint distribution to extreme sea states using the bulk of the data which give invalid results at the extremes. This is probably not solvable with descriptive statistics alone and would need a physics based model to generate hundreds or thousands of years of synthetic sea state data and that would produce its own problems. A move towards a method such as this appears to be happening in the oil and gas industry with the NS1200 data set which uses a climate model to generate 1200 years of synthetic data for the north sea (Gibson (2020b)).

An initial JONSWAP spectrum with $\gamma = 3.3$ was chosen for all sea states and then once the potential design seas had been identified values of 1 and 5.5 were used for the Rated 2 sea state and 1 and 3.3 for the 50 year contour sea to judge the impact of

gamma. The larger values were chosen to be roughly in line with the DNV recommendation on how gamma varies with significant steepness (equations 5.1-5.3) where a maximum value of 5 is recommended (DNV (2014)). In this work 5.5 is used to increase the difference between the gamma values for comparative purposes.

$$\gamma = 5 \quad for \quad T_p/\sqrt{H_s} \leq 3.6 \tag{5.1}$$

$$\gamma = exp(5.75 - 1.15\frac{T_p}{\sqrt{H_s}}) \quad for \quad 3.6 < \frac{T_p}{\sqrt{H_s}} < 5 \tag{5.2}$$

$$\gamma = 1 \quad for \quad 5 \leq \frac{T_p}{\sqrt{H_s}} \tag{5.3}$$

The environmental characterisation has a significant effect on the characteristic load prediction if wind cases are not considered as can be seen in the substantially different locations of the 50yr contour and 50yr Viselli sea states in Fig.5.3. However, if the Rated 2 sea state turns out to be the design sea containing the largest responses then the issue is largely mitigated as it is close to the steepness limit and so any increase in the steepness of this sea state will result in reduced extreme responses due to increased wave breaking. It may however call the validity of the contour approach into question as a small deviation in H_sT_p space results in a large change to the return period as pointed out in Li et al. (2017). This is particularly true of sea states close to the steepness limit. A numerical model combined with an IFORM approach would be required to confirm this, and careful consideration of wave breaking would be of utmost importance. This is because the tail of the EVD of the response would likely reach an asymptote due to wave breaking in a similar manner as the crest height exceedance plots appear to for the steeper sea states in Fig.4.3.

5.3 Wind loading

A thrust curve needed to be calculated using a numerical model so that the wind loading could be simulated. Several wind speed cases were run using the reference model in OpenFAST to produce a new thrust curve which we then used as the physical input.

This model was used 'out of the box' with no changes to give an approximate value for the mean aerodynamic thrust experienced for different wind speeds, the existing reference open source controller (ROSCO) was used with no additional tuning

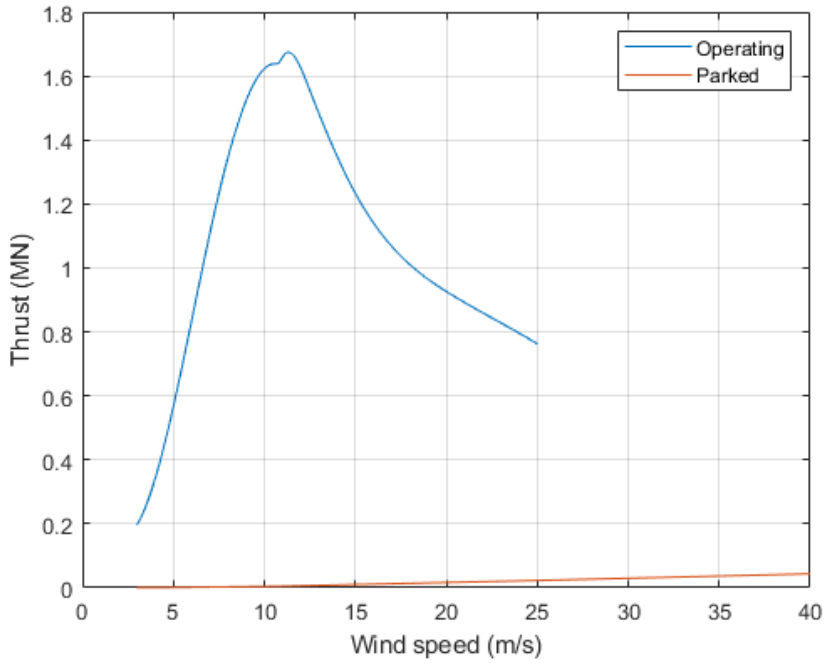

Figure 5.4: Full scale aerodynamic thrust curves from OpenFAST calculations. The thrust curve is calculated in the absence of wave loading.

Angle offsets against suspended masses attached to the centre of the turbine nacelle were tested and were consistently around one degree off compared with the same target force produced by the thruster. It was later found that the thruster was incorrectly calibrated due to friction with the beam it was sat on and so the thrust values were approximately $1.2N$ less than the target. $4.78N$ was the target thrust for the rated wind speed but a value closer to $3.5N$ was estimated from the pitch and surge offsets of the numerical model to have been produced in practice. Details of the sea states tested along with target and estimates of the achieved thrust values are given in table 5.3. Unfortunately the effects of this under prediction of thrust on the EVDs would be difficult to investigate with the numerical model due to the under prediction of the mooring loads and pitch responses discussed in the next chapter. The mean differences could

however be reliably estimated and it is found that approximately an additional $1.1N$ would need to be added to the front mooring load and 1.3 degrees to the pitch if the target thrust had been achieved.

Table 5.3: Sea state details, brackets are model scale values. The achieved thrust is an estimate from pitch and surge offsets.

Sea state	γ	Seeds	$H_s(m)$	$T_p(s)$	Thrust target $(MN(N))$	Thrust achieved $(MN(N))$
50yr contour	1	18	12 (0.171)	14.44 (1.73)	-	-
50yr contour	3.3	18	12 (0.171)	14.44 (1.73)	-	-
50yr Viselli	3.3	24	9.7 (0.139)	16.2 (1.94)	-	-
Max hindcast	3.3	10	10.28 (0.147)	12.44 (1.49)	-	-
Rated 2	1	6	5.95 (0.085)	9 (1.08)	1.64 (4.78)	1.2 (3.5)
Rated 2	3.3	10	5.95 (0.085)	9 (1.08)	1.64 (4.78)	1.2 (3.5)
Rated 2	5.5	6	5.95 (0.085)	9 (1.08)	1.64 (4.78)	1.2 (3.5)
Rated 3	3.3	6	5.25 (0.075)	14.54 (1.74)	1.64 (4.78)	1.2 (3.5)
Cut Out 3	3.3	5	8.07 (0.115)	12.04 (1.44)	0.76 (2.22)	0.34 (1)
Cut Out 4	3.3	6	6.45 (0.092)	16.71 (2)	0.76 (2.22)	0.34 (1)

It can be seen in Fig.5.4 that the aerodynamic thrust on the turbine is very low in parked conditions. However, if the drag on the tower were also to be included then substantial surge and pitch offsets could be observed. When wind speeds get to $50m/s$ and over this could be expected to produce offsets as large as those in rated conditions (Vigara et al. (2019b)). Wind loading when the wind speed rose above $25m/s$ has not been modelled in the physical experiments due to uncertainty in how these should be applied with a single thruster located at the top of the tower but will be investigated in future work.

It is worth restating that the inclusion of turbulence intensity (varying wind speed) will have an effect on the low frequency surge motions and mooring loads, but has not been included in these experiments and the thrust values produced are lower than the target values. For these reasons the results presented for operating conditions in this chapter give an indication only of the sea states likely to produce the extremes.

5.3.1 Effects of wind compared to no wind

Seed one of the Rated 2 sea state with $\gamma = 3.3$ was run with and without thrust to judge the effects of constant thrust on the device responses. It can be seen from Fig.5.5 that the thrust has a large effect on the mean position of the positive pitch angle, surge and the front mooring load and that the low frequency response appears to change slightly with thrust whilst the font mooring load increases.

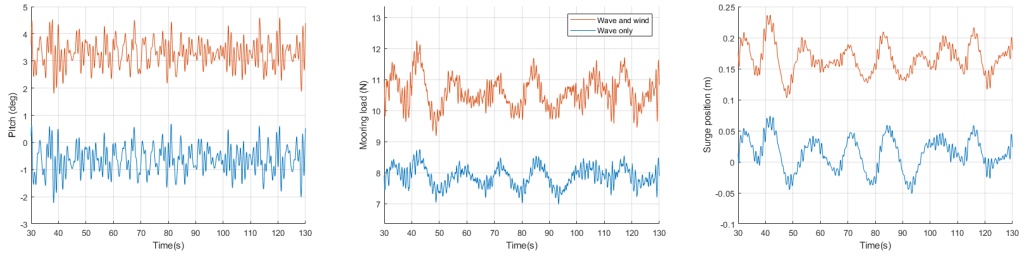

(a) Pitch *(b)* Front mooring load *(c)* Surge

Figure 5.5: Wind / no wind responses for the Rated 2 sea state, $\gamma = 3.3$

Fig.5.6 confirms that the low frequency pitch and surge motions are slightly altered in the presence of constant thrust and the front mooring load is increased. The wave PSD is for wave gauge 3 in the presence of the model.

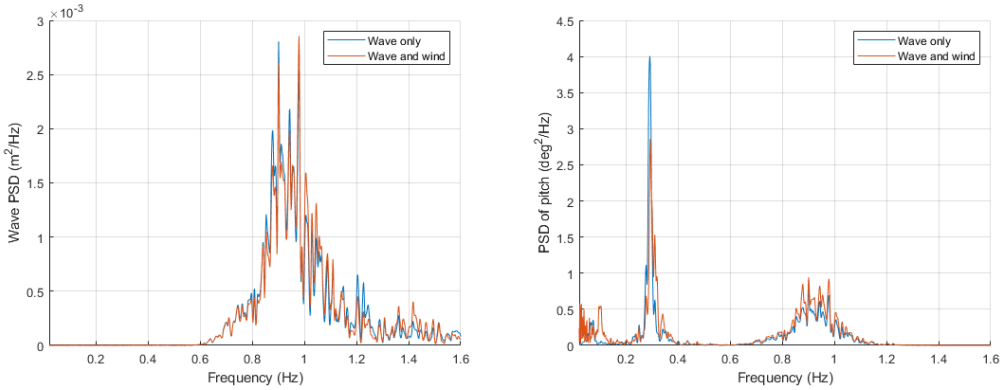

(a) Wave

(b) Pitch

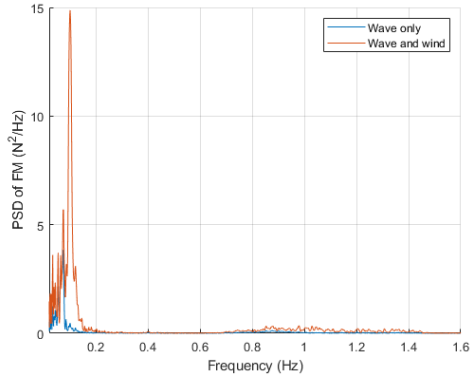

(c) Front mooring load

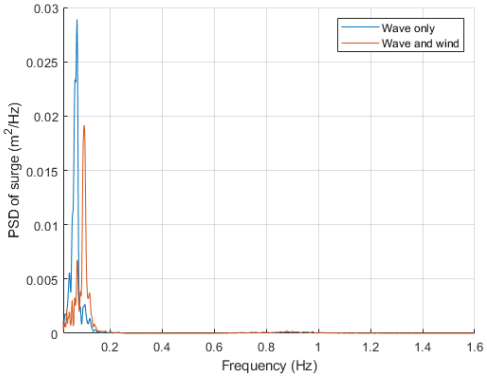

(d) Surge

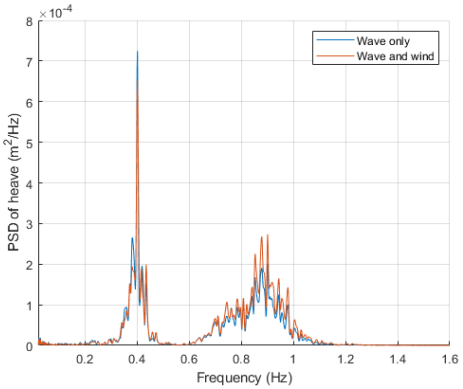

(e) Heave

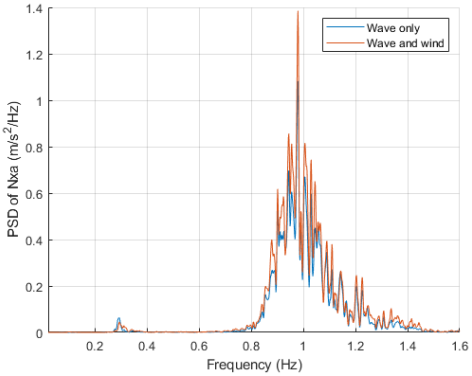

(f) nacelle x acceleration

Figure 5.6: Wind / no wind response spectra for the Rated 2 sea state, $\gamma = 3.3$

For sea states where the turbine is in operating conditions identified as producing extremes it is acknowledged that there may be easily enforcible mitigation strategies which aren't an option when the turbine is idling or parked. For example an alarm

system can be used so that if the platform drifts in surge past a specified point then the turbine shuts down and the platform returns to its zero surge position and so avoids large mooring loads and surge offsets. This kind of system is mentioned in Vigara et al. (2019a). However, presumably this mitigation strategy should be avoided where possible as it would lead to the undesirable outcome of loss of revenue.

5.4 Extreme distributions based on long IW runs

The extreme responses selected for study were the maximum positive and negative pitch angles, the x and z nacelle acceleration components (The nacelle acceleration components are a common design consideration for FOWTs calculated in e.g. Vigara et al. (2019a)) and the front and back mooring loads at the fairleads. It should be noted that the nacelle accelerations had to be heavily filtered and in reality will be strongly impacted by turbulent wind loading and the control strategy in operating cases, as found in Vigara et al. (2019a), neither of which were considered in these experiments. However the nacelle accelerations in x are reported here as they were produced by an interesting wave profile and may still give an indication of the suitability of short design wave methods for the response. Although all the waves studied here are unidirectional and head on, the back mooring load will most likely be at a maximum for a sea state with a different mean wave direction and with directional spreading. It is studied here regardless as being representative of a category of response where the extreme will occur during a small surge offset. The tower base bending moment is typically also considered in design load predictions but is neglected here due to lack of instrumentation.

The EVDs of the responses of interest for each sea state were compared to give an indication of which sea states lead to extremes. The 50 yr contour, maximum hindcast and Rated 2 sea states were identified as producing the largest pitch, surge and front mooring load responses Fig.5.7. Based on this data the 50yr contour and Rated 2 sea sates were selected for further study with short design waves. It should be remembered that a full comparison of which sea states are the design seas, that is those leading to

the largest extremes for this device in this location, cannot be made with confidence due to the discussed limitations of the achieved thrust and the lack of wind loading for the parked condition cases.

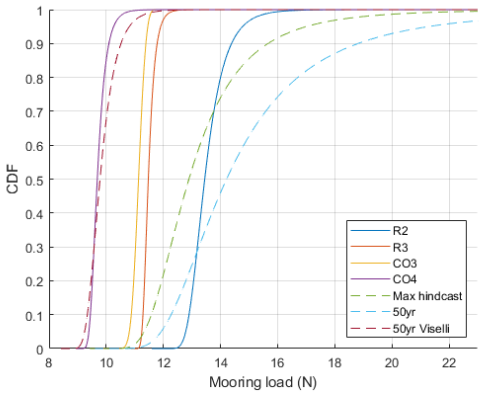

(a) Front mooring load

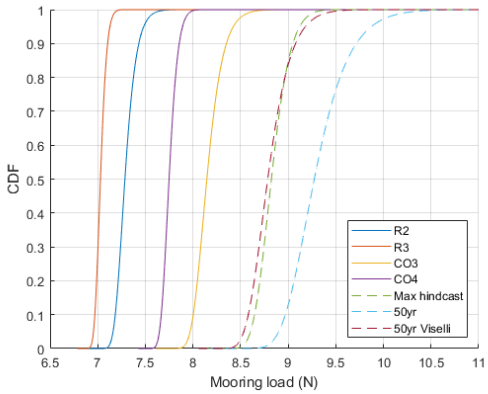

(b) Back mooring load

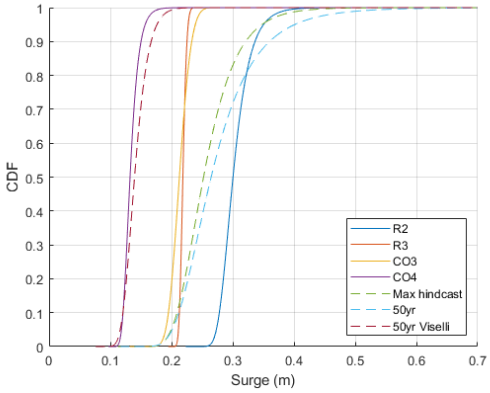

(c) Surge

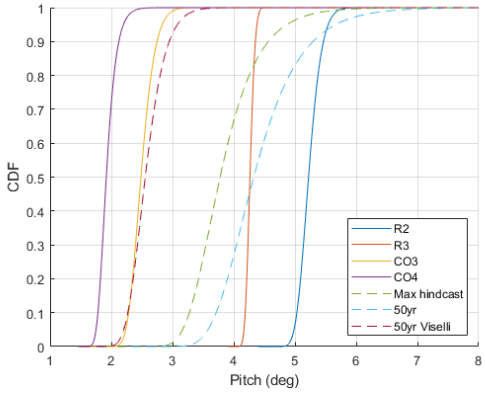

(d) Pitch

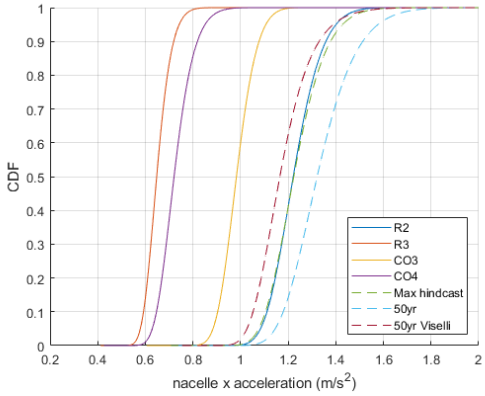

(e) nacelle x acceleration

Figure 5.7: EVD CDF comparisons for the different responses and sea states with $\gamma = 3.3$.

The effect of varying gamma on the distributions was then investigated. Values of 3.3

and 1 are widely used and so investigated, 5.5 is also studied for the Rated 2 sea state as a likely upper limit. The EVD estimates for the IW data using different gamma values for the sea states Rated2 and 50yr contour are presented in Fig.5.8. It can be seen that in general the extreme responses increase with increasing gamma for the chosen sea states.

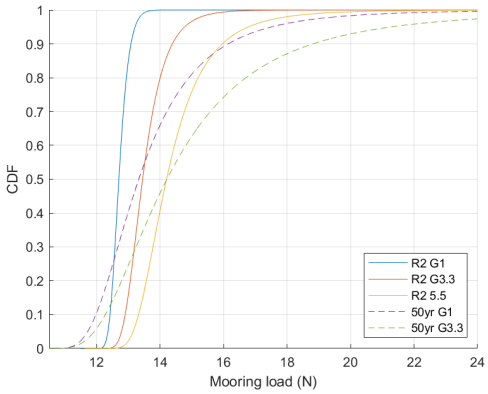

(a) Front mooring load

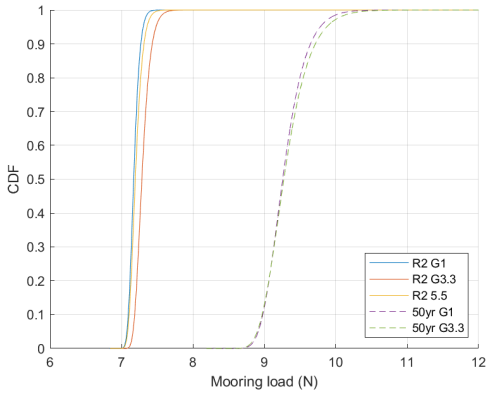

(b) Back mooring load

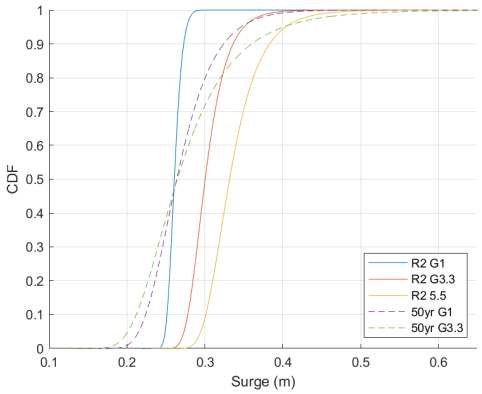

(c) Surge

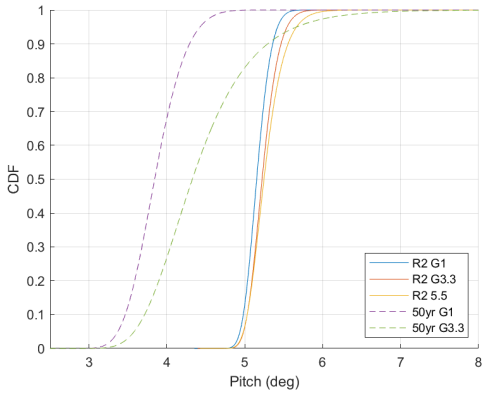

(d) Pitch

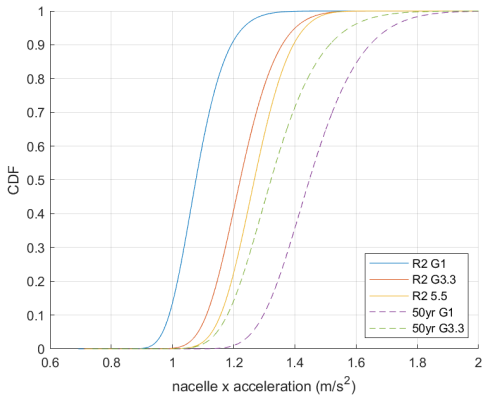

(e) nacelle x acceleration

Figure 5.8: EVD CDF comparisons for the different gamma values for the Rated2 and 50yr contour sea states.

The effect of gamma is clear from the EVDs, particularly for the front mooring load

whose 90th percentile response increase from $15N$ to nearly $19N$. The front mooring is significantly impacted by the surge drift position.

5.4.1 Amplitude distributions

Before discussing the short design waves it is worth comparing the extreme wave amplitude distributions of the different sea states tested to give an indication of deviations from linear theory as they have varying steepness and the focused wave methods employed here are based on linear wave theory. The Rated 2, 50yr contour, 50yr Viselli and Max hindcast EVDs are given below for all tested gamma values. The figures below are presented in order of increasing S_p and where S_p values are equal, increasing gamma. Extreme amplitude distributions published in Latheef and Swan (2013) suggest that $S_p > 0.024$ will result in deviations from the Rayleigh extreme amplitude distribution and linear theory. Increasing S_p also indicates an increasing amount of wave breaking which was observed in the Rated 2 and Max hindcast sea states and a tiny amount for the 50yr contour sea.

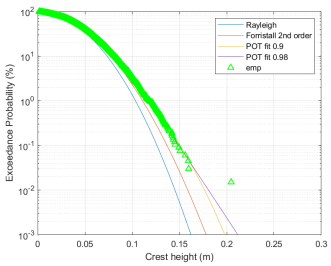

(a) 50yr Viselli ($\gamma = 3.3$, $H_s = 9.7(0.139)$, $S_p = 0.0747$, 24 seeds)

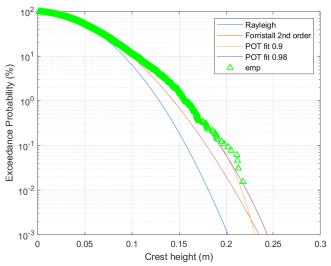

(b) 50yr contour ($\gamma = 1$, $H_s = 12(0.17)$, $S_p = 0.1163$, 18 seeds)

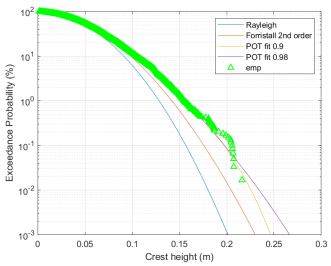

(c) 50yr contour ($\gamma = 3.3$, $H_s = 12(0.17)$, $S_p = 0.1163$, 18 seeds)

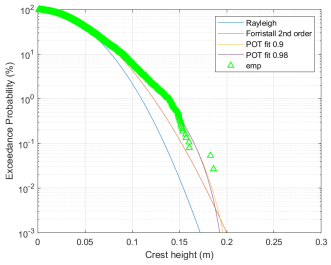

(d) Maximum hindcast ($\gamma = 3.3$, $H_s = 10.28(0.1469)$, $S_p = 0.1337$, 10 seeds)

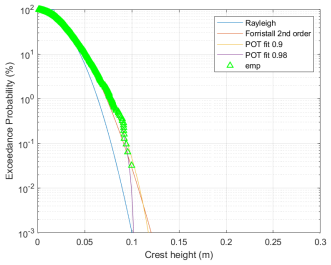

(e) Rated2 ($\gamma = 1$, $H_s = 5.95(0.085)$, $S_p = 0.1478$, 6 seeds)

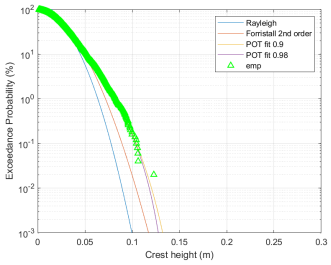

(f) Rated2 ($\gamma = 3.3$, $H_s = 5.95(0.085)$, $S_p = 0.1478$, 10 seeds)

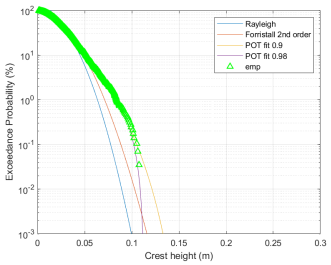

(g) Rated2 ($\gamma = 5.5$, $H_s = 5.95(0.085)$, $S_p = 0.1478$, 6 seeds)

Figure 5.9: Exceedance plots of the wave amplitude distribution for various sea states. The green triangles show the empirical EVD of all the peaks from the irregular waves from which the EVD is predicted. H_s values are given as full scale (model scale).

5.4.2 Short design waves

The extreme sea states selected for the constrained focused wave study were the 50yr contour and the Rated 2 cases ($\gamma = 3.3$). The nacelle accelerations, back mooring load and negative pitch angle were largest for the 50yr contour sea state, the positive pitch angle was largest in the Rated 2 sea state, the front mooring load was largest for 50 yr and Rated 2 Fig.5.7. The responses of interest studied using the CRRW profiles were chosen accordingly using $\gamma = 3.3$ for both sea states.

Before deciding on the time step in the short irregular background to constrain the focused waves at, an extreme mooring load was identified from an irregular wave run and the preceding wave varied to study the impact of history effects. This was done for both sea states and presented in Fig.5.10. It can be seen that, after 40 seconds, the maximum mooring load ranged from 14.31 to $14.88N$ for the 50yr contour sea state and 13.72 to $14.14N$ for the Rated2 sea state.

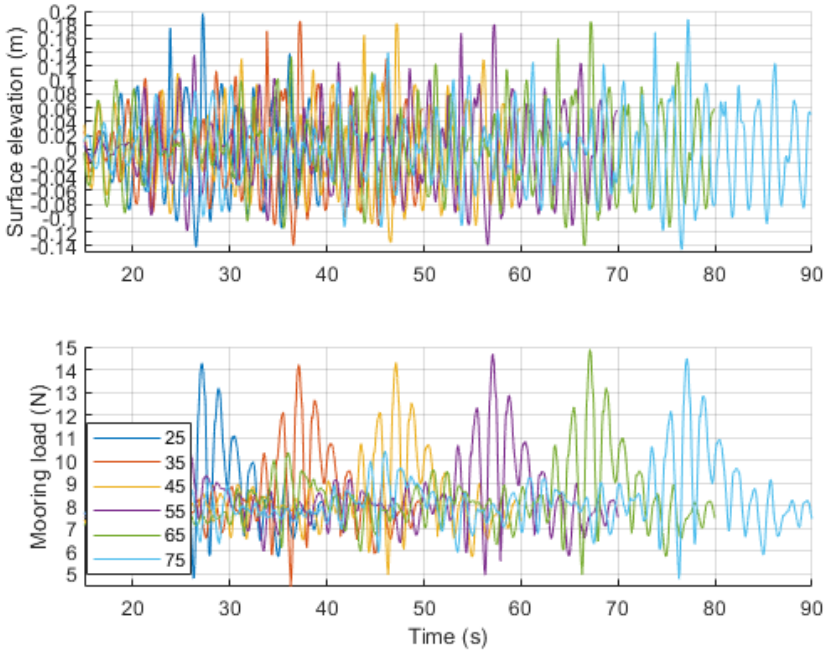

(a) 50yr contour

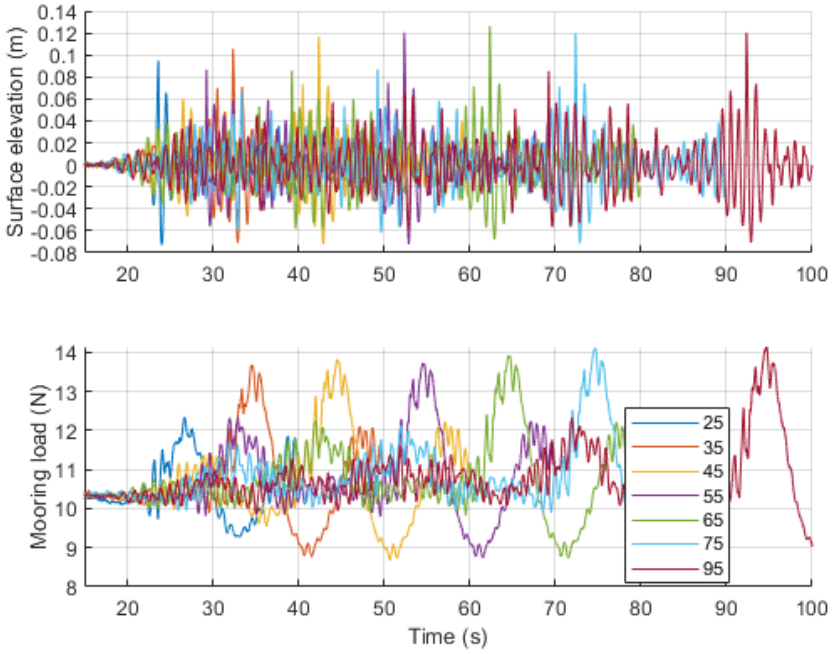

(b) Rated2

Figure 5.10: Time series comparison to show what the effect of varying the seconds of preceding wave has on the front mooring load for an extreme response during (a) the 50yr contour and (b) Rated2 sea states. The numbers in the key indicate the amount of time the preceding wave was run for.

While there was some variation in the surface elevation and mooring load recorded there was not significant fluctuation after 40 seconds. Some of this may also be due to repeatability. For this reason five repeats are compared for seed 1 of the 50yr contour sea state, the largest mooring response is shown in Fig.5.11. For this figure the time axis has been removed and each run is shifted by ten seconds to give a clearer comparison, but in each case the extreme occurred at $59s$.

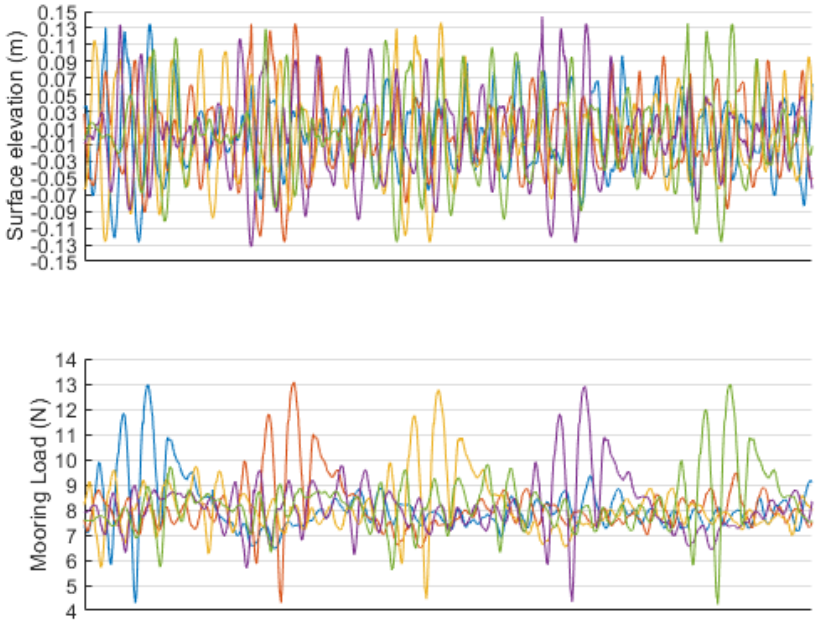

Figure 5.11: Time series comparison to show the effect of repeatability on the front mooring load for an extreme response during the 50yr contour sea state seed 1 with $\gamma = 3.3$. The time axis has been removed as each case has been shifted by 10 seconds to make the comparison clearer.

Although it is not possible to unpick with confidence what the uncertainty contribution due to the repeatability is compared to the length of irregular background before the constrained wave using such a small data set, the percentage differences in the front mooring loads are given as an indication. The percentage difference between the smallest and largest recorded mooring loads was 2.3% for the five repeated irregular waves (max $12.95N$) and for the preceding wave cases with more than $40s$ of preceding

wave they were 3% for R2 (max $14.14N$) and 3.9% for the 50yr contour case (max $14.88N$). Based on this data all the design waves were constrained at a chosen time of $50s$.

The assessment of the effects of uncertainty in physical modelling campaigns is an active area of study and it is important to consider the relative contributions of the different sources. Robertson et al. (2018) note that some sources of uncertainty which include the processes of data conversion, time sampling, time averaging, time synchronization and the numerical precision of the data acquisition system can generally be assumed to be insignificant compared with other sources. In this work where extreme values are of most concern, the differences in device position and velocity due to background wave conditions preceding an extreme event appear to influence the extreme responses much more than repeatability. The percentage difference in the maximum front mooring load represented by the $5th$ and $95th$ percentiles of the EVD in the 50yr contour sea state for example is approximately 59%. It can be argued therefore, that running a larger number of constrained wave cases in a shorter time period should take priority over waiting a significant amount of time between each run for the water to settle. This of course would not be true if a numerical comparison were the primary objective of the tests, in which case stationary initial conditions would be a priority.

5.4.3 Rated2 sea state

The CRRW responses and 50% and 95% confidence intervals for the mean estimate based on a sample of six CRRW profiles are overlayed on the figures below and compared to the characteristic load estimates and EVDs from the long irregular waves.

Fig.5.12 shows that there are large low frequency surge, pitch, heave and front mooring line responses outside of the wave frequencies. This finding is in agreement with other semi-sub FOWT device tests most notably the international code comparison project, OC5 (Robertson et al. (2017)) and the MaRINET2 round robin experiments conducted at a range of different facilities (Gueydon et al. (2021)). The exact nature of these non-linear effects are still being debated and investigated (Robertson and Wang (2021))

and, to the authors knowledge at the time of writing, have not yet been successfully reproduced using mid fidelity numerical models Robertson et al. (2020).

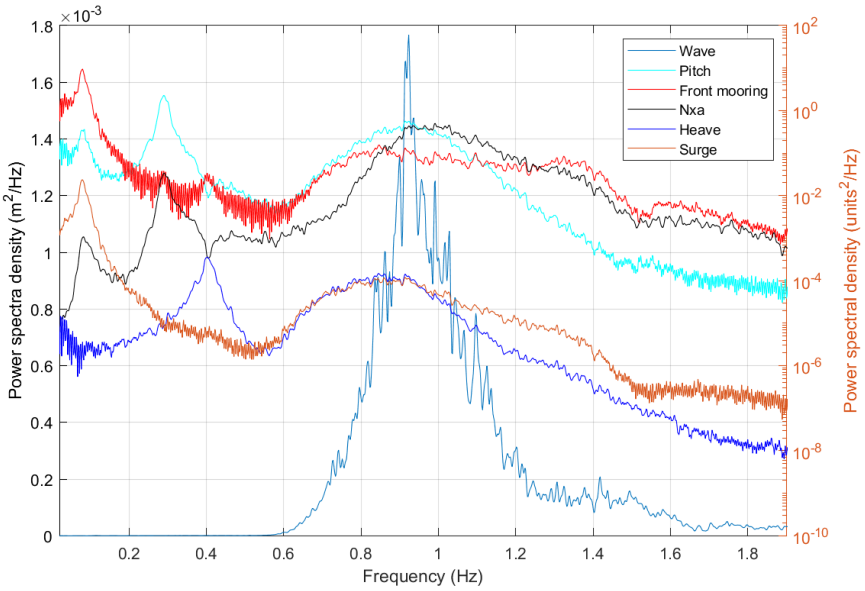

Figure 5.12: Spectral density plots for the responses of interest in the Rated 2 sea state ($\gamma = 3.3$). The wave spectral density magnitude is given by the left y axis while a log scale is used for the response spectra on the right y axis.

For semi-subs, viscous effects are thought to be responsible as outlined in the EXWAVE JIP (Improved procedures to calculate slowly varying wave drift forces on floating units in extreme seas, Ma et al. (2020)) on mobile offshore drilling units. This so called 'viscous drift' in surge is attributed to a third order effect (proportional to the wave amplitude cubed) due to drag acting above the still water surface (Ma et al. (2020)).

Fig.5.13 presents the results of testing CRRW profiles for the pitch response scaled to the $50th$ (black) and $99th$ (red) percentiles. It is interesting that both appear to be under predictions but the $99th$ percentile MLER wave produces a better estimate, and despite the fact there was a small amount of breaking observed during the $99th$ percentile run. This means the background waves reduced the likelihood of producing an extreme pitch response in the $99th$ percentile case. However, there was a large discrepancy between the target and achieved surface profile as can be shown in Fig.5.14. It should also be pointed out that the difference between the IW and CRRW characteristic load

prediction is small in magnitude being less than $.4$ of a degree for the $99th$ percentile case.

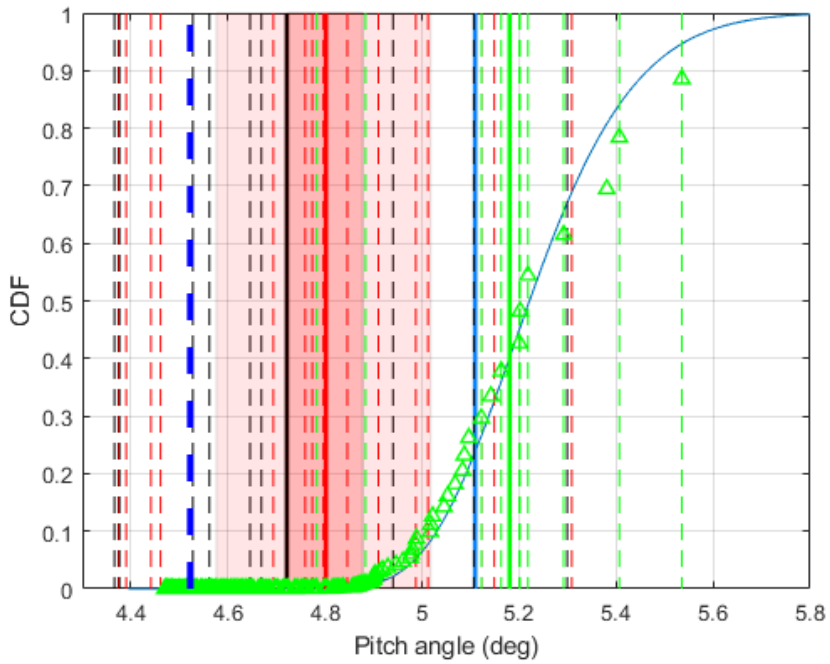

Figure 5.13: EVD of pitch for Rated2 sea state ($\gamma = 3.3$), CRRW responses overlayed in dashed red lines. Red shading shows 50 and 95% confidence intervals. Red filled line gives mean of 15 CRRW responses for 99% target. 9 CRRW profiles at 50% target given by black lines. Green dashed lines give single largest response from each of 10 irregular wave runs and the filled line gives their mean. Green triangles show empirical EVD of peaks from irregular waves from which the EVD is predicted. Solid blue vertical line shows response from $99th$ percentile MLER wave, dashed blue line for $50th$ percentile

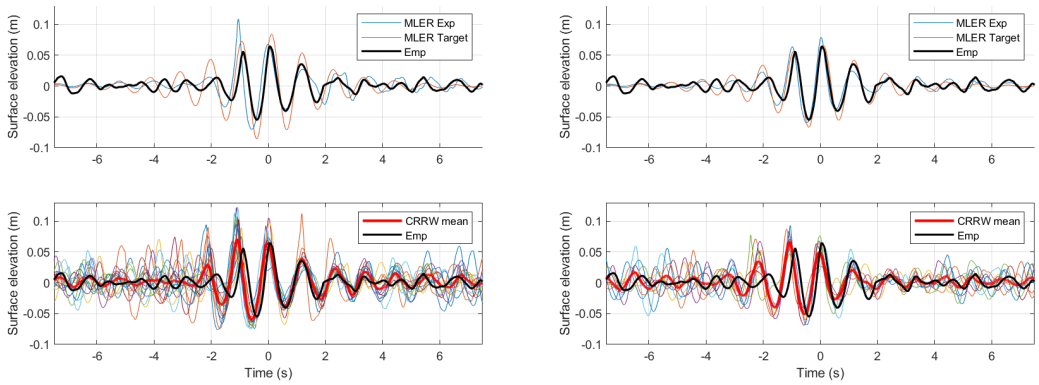

(a) 99th percentile

(b) 50th percentile

Figure 5.14: Comparison of the pitch MLER theoretical target and physically achieved (after a single phase correction) profiles and CRRW profiles to the empirical average of the 10 profiles leading to the largest responses in the 10 Rated 2 sea state seeds.

It is worth checking how the MLER profile scales with increasing target amplitude as shown in Fig.5.15 to understand the discrepancy between the target and physically achieved wave in Fig.5.14a). The agreement of the surface elevation achieved for the $99th$ percentile wave with the empirical profile in this figure is notably worse than for the $50th$ percentile and the constrained cases also reveal some marked differences. In particular, there is a difference in the phase and a large wave peak occurring at -2 seconds before the focus time which appears to be a discrepancy between the target MLER wave and the observed empirical profile suggesting the importance of history effects. This is thought to be the main cause of the CRRWs producing responses which are too small. There is also a deviation from the target due to nonlinear wave development and breaking. The phase difference between the target MLER wave and the average of the CRRW profiles observable in Fig.5.14b) suggests that nonlinear wave development is responsible for the discrepancy rather than any phase difference in the calibration due to wave breaking that occurred during the uncalibrated wave run. This example further highlights the difficulties in applying short design waves in steep seas due to the discrepancies between the target and achieved surface elevations that are quickly achievable using linear wave and wave maker theory.

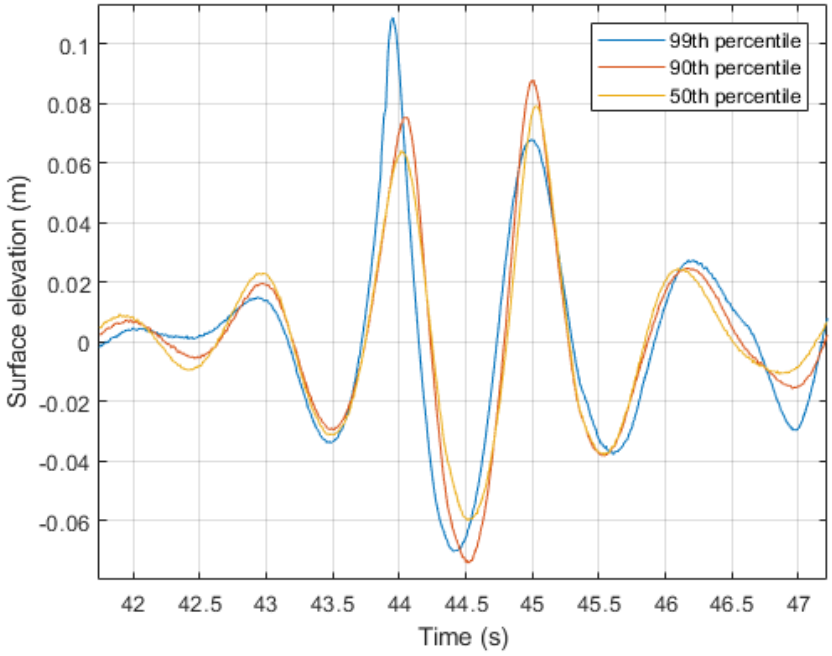

Figure 5.15: Comparison of the pitch MLER physically achieved (after a single phase correction) profiles of several percentiles of the linear RAO prediction for a 1 hour exposure time in the Rated 2 sea state ($\gamma = 3.3$).

Fig.5.16 and Fig.5.17 show that the empirical wave profiles leading to the extreme pitch response are all very similar despite varying gamma, and so gamma does not have a significant influence.

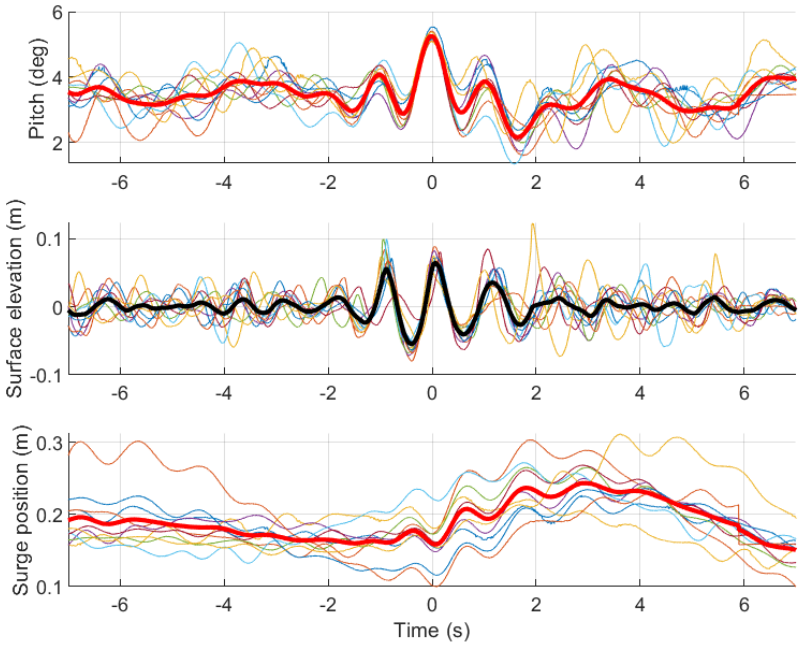

Figure 5.16: 10 profiles of surface elevation, surge position and pitch leading to the largest pitch responses for the 10 seeds in the Rated 2 sea state ($\gamma = 3.3$). Averages of the 10 extremes are given by the thick lines.

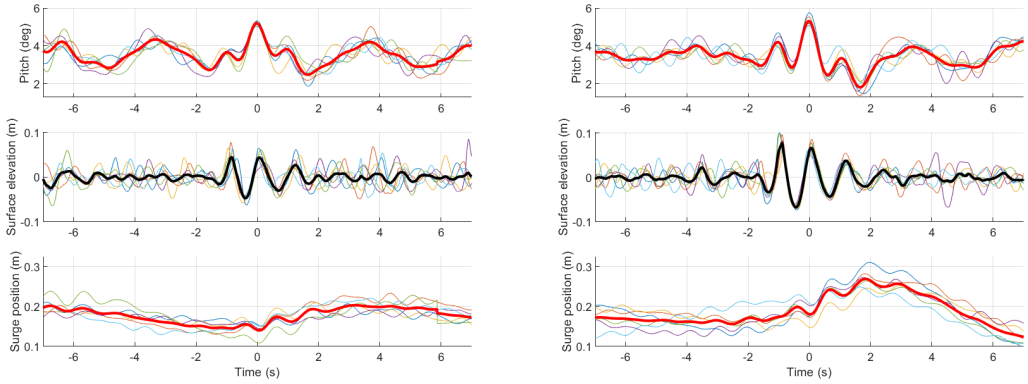

(a) $\gamma = 1$ *(b)* $\gamma = 5.5$

Figure 5.17: 6 profiles of surface elevation, surge position and pitch leading to the largest pitch responses for the 6 seeds in the Rated 2 sea state for different gamma values. Averages of the extremes are given by the thick lines.

The CRRWs conditioned on the front mooring load response also do not reliably produce loads as large as those from the irregular waves in the Rated2 sea state as seen

in Fig.5.18.

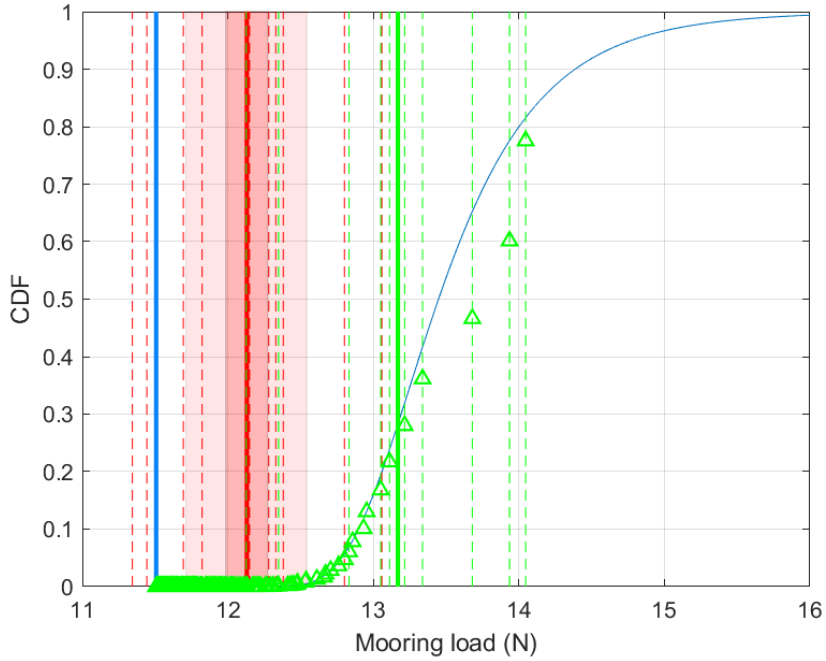

Figure 5.18: EVD of the front mooring load for the Rated2 sea state ($\gamma = 3.3$), CRRW responses are overlayed in dashed red vertical lines. The red shading shows the 50 and 95% confidence intervals. The red filled line gives the mean of the 10 CRRW responses. The green dashed vertical lines give the single largest responses from the 10 irregular wave runs and the filled line gives the mean. The green triangles show the empirical EVD of the peaks from the irregular waves from which the EVD is predicted. The solid blue vertical line shows the response from the MLER wave.

The average of the empirical profiles leading to the extreme mooring responses in the irregular waves do not agree with the MLER and CRRW profiles seen in Fig.5.19. It is interesting that the CRRWs were more accurate to the target MLER profile than the MLER which was produced in the physical experiments. This suggests that even if nonlinear wave development makes the MLER profile unachievable it might more accurately be realised by some of the CRRW runs.

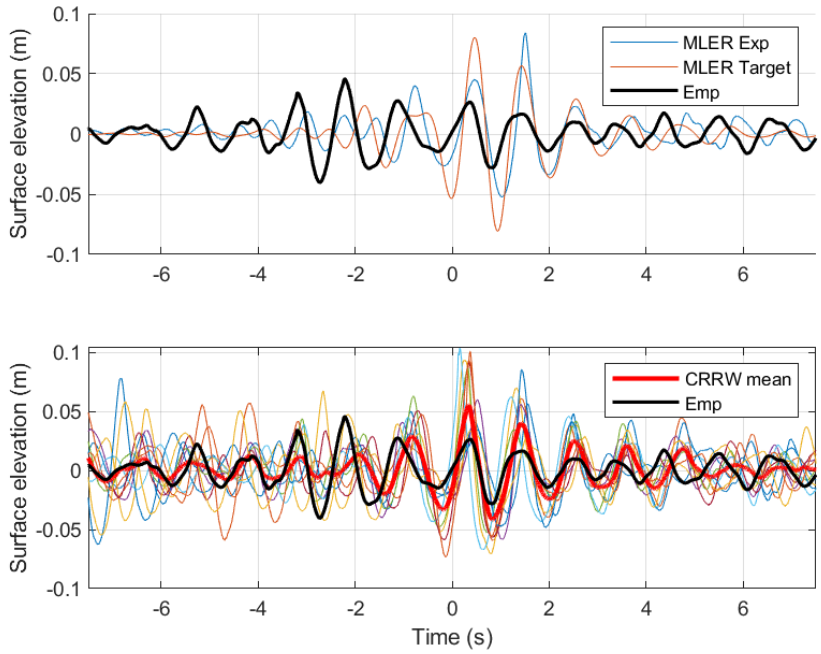

Figure 5.19: Comparison of the front mooring load MLER theoretical target and physically achieved (after a single phase correction) profiles and CRRW profiles to the empirical average of the 10 profiles leading to the largest responses for the 10 seeds in the Rated 2 sea state ($\gamma = 3.3$).

Plotting the overlay of the responses and surface elevations leading to the 10 extreme front mooring loads in Fig.5.20 shows that there is a large wave occurring between approximately -2 and -4 seconds which leads to a low frequency surge response and has a large effect on the mooring load. This effect is made clearer in Fig.5.21 where it can be seen that for $\gamma = 1$ there is more of an impact of the wave at 0 seconds whereas for $\gamma = 5.5$ the large wave sequence which precedes the extreme response is of more significance, $\gamma = 3.3$ is somewhere in between.

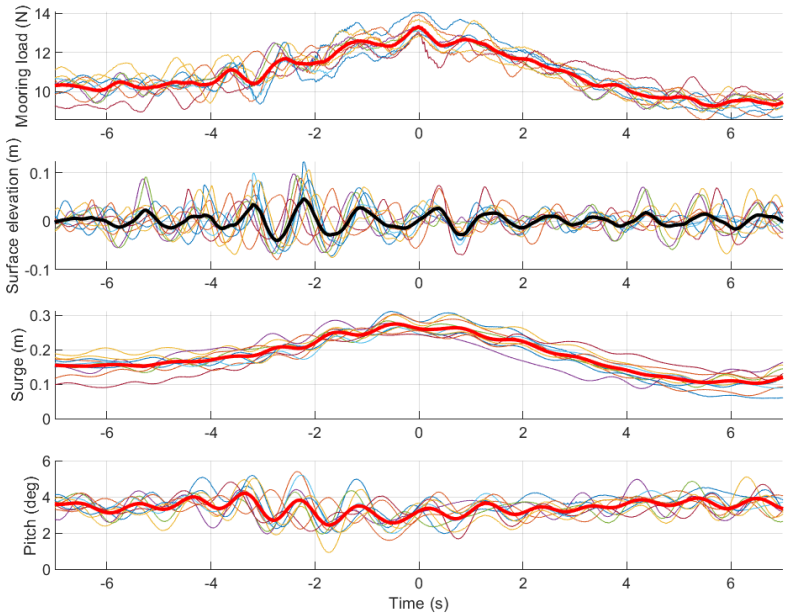

Figure 5.20: 10 profiles of surface elevation, surge position and front mooring load leading to the largest front mooring load responses for the 10 seeds in the Rated 2 sea state ($\gamma = 3.3$). Averages of the 10 extremes are given by the thick lines.

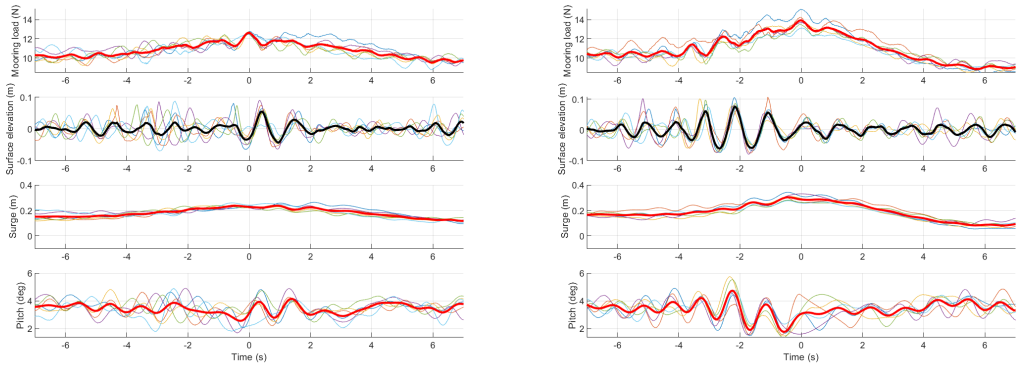

(a) $\gamma = 1$ *(b)* $\gamma = 5.5$

Figure 5.21: 6 profiles of surface elevation, surge position and front mooring load leading to the largest front mooring load responses for the 6 seeds in the Rated 2 sea state for different gamma values. Averages of the extremes are given by the thick lines.

The mooring load and surge response increase with gamma which can also be seen in the frequency domain through the spectral density in Fig.5.22 where the low frequency

mooring load at the surge natural frequency increases with gamma.

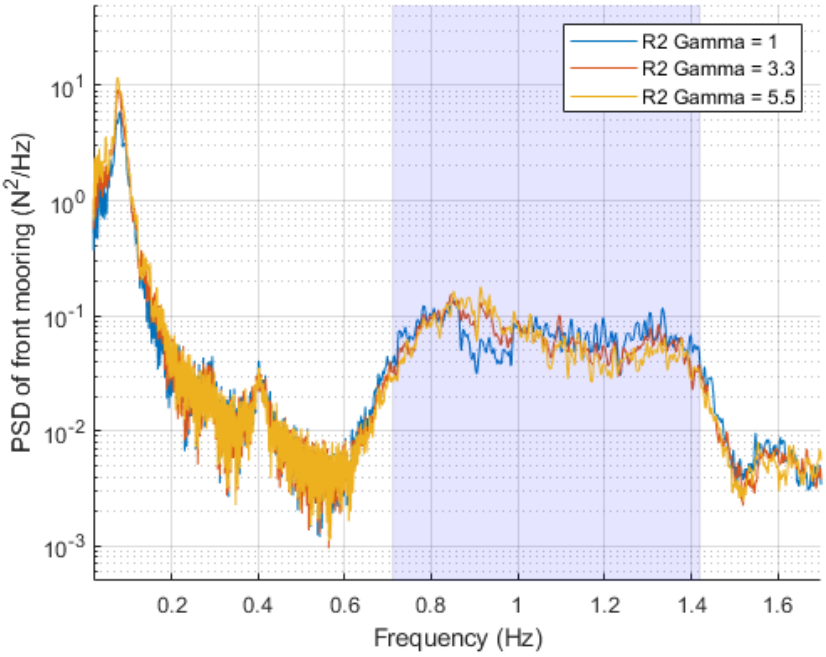

Figure 5.22: Spectral density plot of the front mooring load response in the Rated 2 sea state ($\gamma = 1$, $\gamma = 3.3$, $\gamma = 5.5$). The approximate wave frequency region is indicated by the grey background shading.

The wave profile in Fig.5.21 for $\gamma = 5.5$ does not compare well with the front mooring MLER wave in Fig.5.19 and looks more like a sequence of 3 large waves. This considered alongside the fact that a large surge offset caused by viscous drift makes a significant contribution to the extreme mooring load and that increasing gamma increases this effect suggests it may be a wave group of three large waves that is most likely to produce the extremes. A derived process z_k was defined in Kim and Troesch (2013) to search a surface elevation time series for such groups. They were found to occur for large values of z_k.

$$z_k(t) = \sum_{p=1}^{k} \eta(t + (p-1)\tau) \tag{5.4}$$

where τ is a predefined period of interest, here set to T_p, and k is the wave group

index. A k value of three is selected here due to the observation that a series of three large wave amplitudes appear to lead to the extreme front mooring load (see Fig.5.21). In Seyffert et al. (2016) and Seyffert (2018) the occurrence of these rare wave groups were studied using wave buoy data and their average (most probable maximum) shape reproduced successfully using a scaled shifted autocorrelation function (recall the NewWave is the shape of the autocorrelation function) given by equation 5.5.

$$E|\eta(t)|z_k(0) = \frac{\hat{z}_k(t)}{\sigma_{zk}^2} \sum_{p=1}^{k} r_{\eta\eta}(t_p) \tag{5.5}$$

The average wave profile for a group of k large peaks, conditioned on the kth derived process being a maximum, is proportional to the sum of k autocorrelation functions of the wave elevation, separated in time by $(p-1)\tau, p = 1...k$. The most probable maximum value of the derived process $\hat{z}_k$ is calculated in the usual way with equations 2.26 - 2.28 and 2.42. The scaled in scaled shifted autocorrelation function refers to the constant of proportionality ($\frac{\hat{z}_k(t)}{\sigma_{zk}^2}$), which is the maximum of the derived process, with group index k, divided by its variance. The shifted refers to the shift in time, τ.

Fig.5.23 compares a target wave group of three peaks scaled to the $99th$ percentile, to the average of the empirical profiles observed to produce the extreme front mooring loads. The wave group has been shifted by $-1.09s$ so it's peak aligns with the empirical profile. The $99th$ percentile is estimated in the usual way (equations 2.26 - 2.28 and 2.30) but using the spectral moments of the derived process rather than the wave or response spectra. Seyffert et al. (2016) note that the assumption of independent and identically distributed peaks is not strictly valid in this instance as the dependence of successive local maxima increases with the wave group index, k. For this reason the EVD of the derived process will be plotted alongside the empirical distribution of 100 one hour samples from linear wave theory for comparison whenever the derived process EVD is shown.

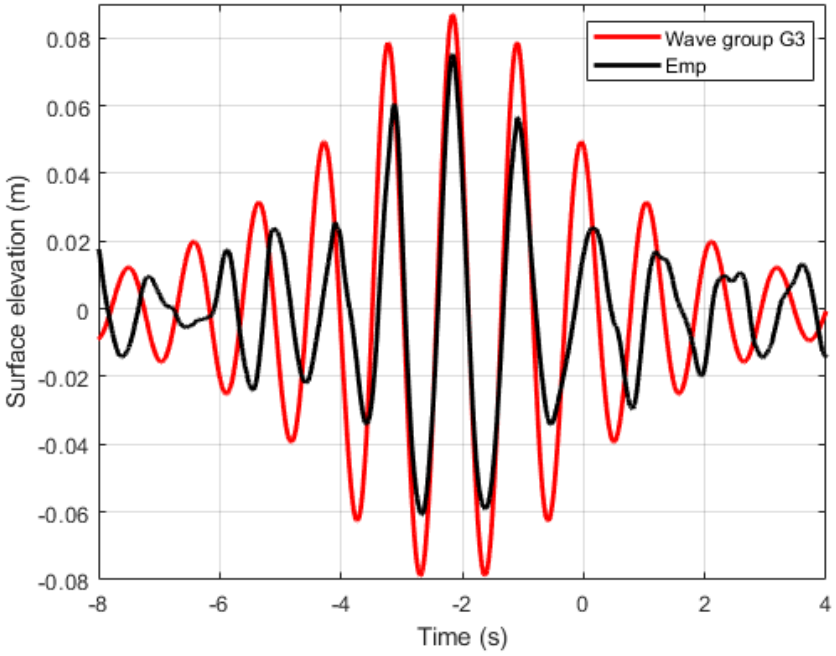

Figure 5.23: Comparison of the average of the 6 wave profiles leading to the extreme front mooring load from the irregular waves (Emp) to the target wave group based on 3 peaks for the Rated 2 sea state ($\gamma = 5.5$).

This derived process (equation 5.4) was adopted for each value of γ to select the ten 'groupiest' CNW profiles out of a sample of 200 to use in the physical model tests. These will be referred to here as CNWG3s. The CNWG3 profiles were then compared to those of CNWs produced in the usual way. Fig.5.24 shows how the CNWG3s were able to produce mooring loads at larger percentiles in line with the EVD prediction from the irregular waves.

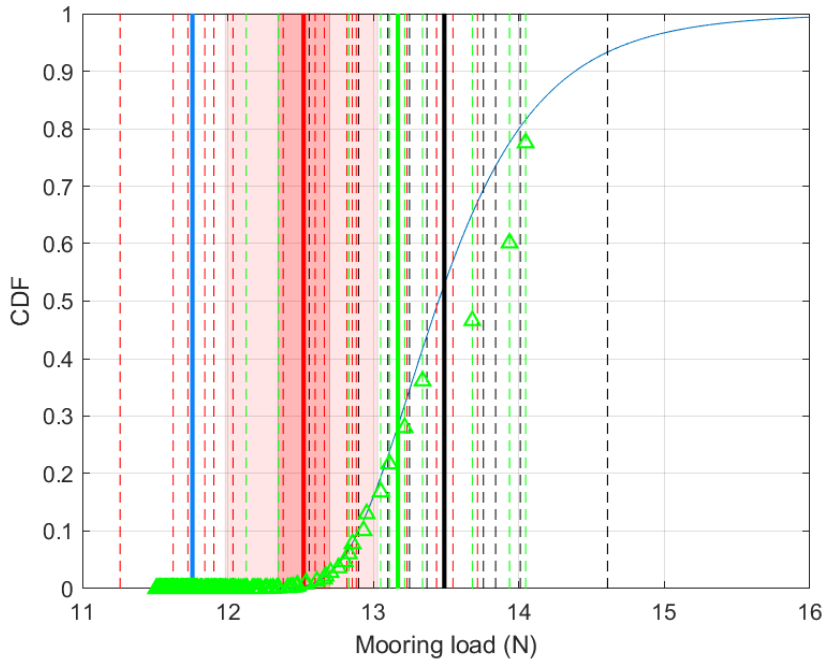

Figure 5.24: EVD of the front mooring load for the Rated2 sea state ($\gamma = 3.3$), 20 random CNW responses are overlayed in dashed red vertical lines. The 10 groupiest CNWs are given in black. The red shading shows the 50 and 95% confidence intervals. The red filled line gives the mean of the 20 random CNW responses. The green dashed vertical lines give the single largest responses from the 10 irregular wave runs and the filled line gives the mean. The green triangles show the empirical EVD of the peaks from the irregular waves from which the EVD is predicted. The solid blue vertical line shows the response from the focused wave.

It's possible however that this could just be due to the largest amplitude in the CNWG3 profiles being larger; Fig.5.25 shows that not to be the case.

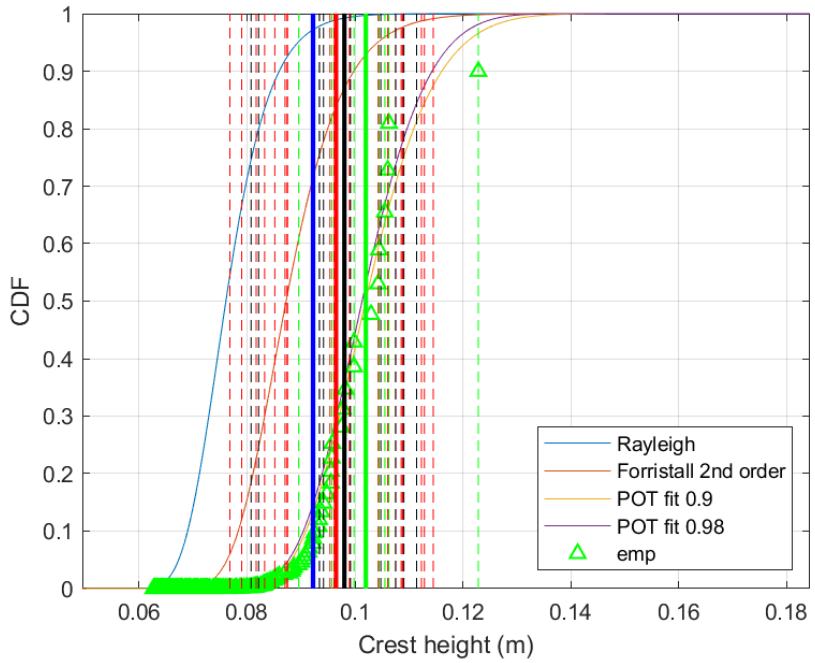

Figure 5.25: EVD of the wave amplitude distribution for the Rated2 sea state ($\gamma = 3.3$), 20 random CNW amplitudes are overlayed in dashed red vertical lines. The 10 groupiest CNWs are given in black. The red filled line gives the mean of the 20 random CNW amplitudes. The green dashed vertical lines gives the single largest wave amplitude from each of the 10 irregular wave runs and the filled line gives their mean. The green triangles show the empirical EVD of the peaks from the irregular waves from which the EVD is predicted. The solid blue vertical line shows the amplitude of the NewWave.

Although this approach of selecting the ten 'groupiest' CNW cases out of sample of 200 loses it's grounding in the occurrence statistics, Fig.5.26 shows that the derived process maxima from the irregular waves compare favourably with those produced by the ten CNWG3 profiles and their ranges roughly coincide suggesting that scaling to the $99th$ percentile is appropriate and in keeping with the NewWave. Nevertheless the process will be improved in the next section to be more in line with occurrence statistics by constraining the focused wave into a short irregular background as done for the CNWs and CRRWs. The method was applied in this suboptimal way initially as the analysis was done and approach developed 'on the fly', by necessity hastily, alongside carrying out the physical experiments. Presenting the $\gamma = 5.5$ EVD of the derived process in

Fig.5.26 as an example, it can be seen from the proximity of the Rayleigh EVD, given in blue, to the empirical linear EVD calculated from 100 one hour irregular wave time series, given by the orange curve and green triangles, that taking the $99th$ percentile target from Rayleigh is reasonable. The $99th$ percentile from Rayleigh corresponds to the $99.9th$ percentile of the empirical linear EVD.

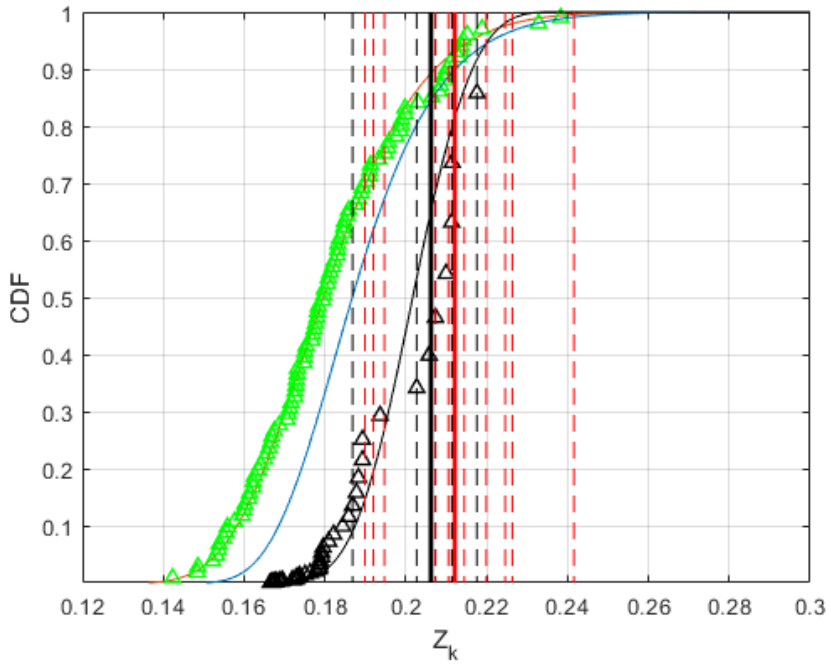

Figure 5.26: EVD of the derived process for 3 peaks in the Rated2 sea state ($\gamma = 5.5$), the 10 CNWG3s are given in red. The red filled line gives the mean. The black dashed vertical lines gives the single largest derived process maxima from the 6 irregular wave runs and the filled line gives the mean. The green triangles show the empirical EVD of the derived process maxima produced from 100 one hour irregular wave time series using linear wave theory. The blue curve shows the Rayleigh distribution from the spectral moments of the derived process.

It can be seen in Fig.5.27 and Fig.5.30 that for the CNWG3s the wave occurring at approximately -2.5 seconds is larger on average than for the CNWs. Several effects of nonlinear wave development may help to explain this. Tang et al. (2021) note the tendency for the largest wave in a packet to move to the front of the group and how this effect increases with an increasing Benjamin-Feir (BF) index. The BF index being the ratio between the wave steepness and spectral band width (Serio et al. (2005)).

Vyzikas et al. (2018) note the downshifting of the spectral peak due to nonlinear wave development. Myrhaug (2018) show how individual wave steepness increases with gamma. It could be that increasing gamma and selecting the 'groupiest' CNW cases effectively reduces the spectral bandwidth and so increases the BF index of the wave group signifying an increase in non-linear wave development. It should be noted that such large deviations in the 2nd order amplitude distribution prediction, which have led here to the largest, steepest waves due to non-linear amplification, are thought to be significantly reduced in more realistic directionally spread seas (Latheef and Swan (2013)) according to a complex relationship between wave steepness, spectral shape, directional spreading and water depth (Swan (2020)). This means that characteristic load predictions for the front mooring in unidirectional waves are likely to be overly conservative.

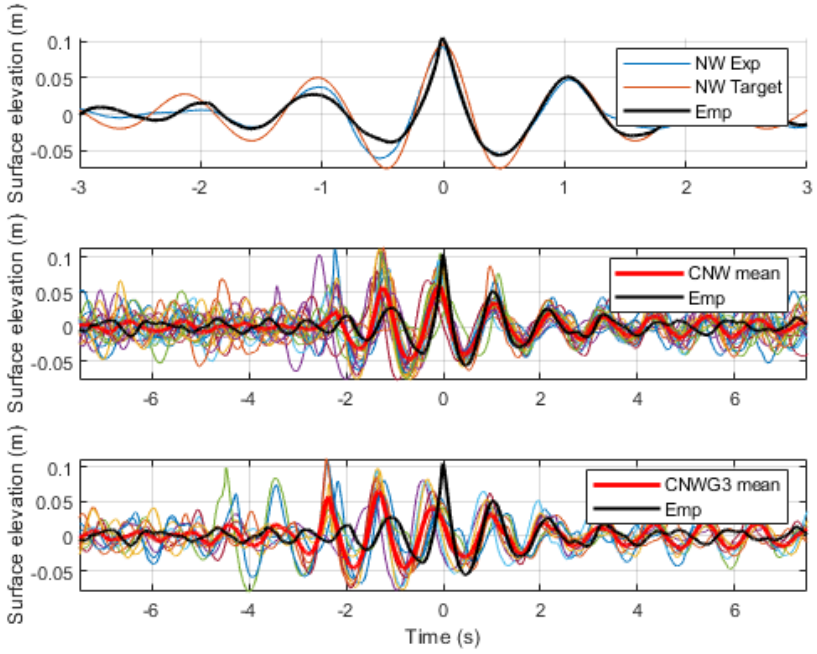

Figure 5.27: Comparison of the 10 CNWG3 and 20 CNW profiles to the empirical average of the 10 largest wave profiles for the Rated 2 sea state ($\gamma = 3.3$).

The $\gamma = 5.5$ case reveals similar findings in Fig.5.28 through Fig.5.30 with the possible exception that it appears the average largest amplitude occurring for the CNWG3s is

slightly larger than for the regular CNW cases. The difference between the average CNW and CNWG3 profiles is also less striking than for the $\gamma = 3.3$ case. Running CNWG3s for $\gamma = 1$ produced a characteristic load estimate much lower than the irregular waves as Fig5.21 would suggest. Therefore, no CNWs were run for comparison.

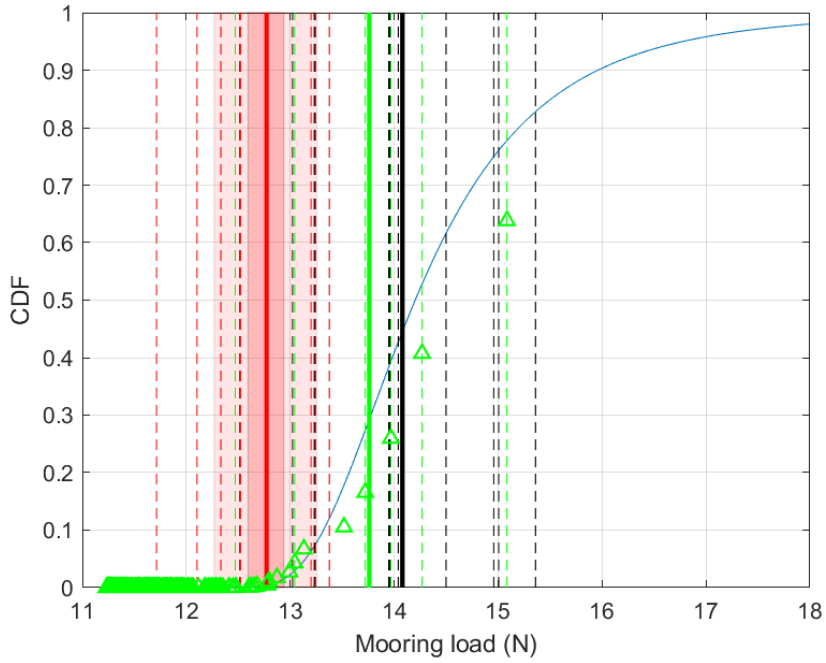

Figure 5.28: EVD of the front mooring load for the Rated2 sea state ($\gamma = 5.5$), 10 random CNW responses are overlayed in dashed red vertical lines. The 10 groupiest CNWs are given in black. The red shading shows the 50 and 95% confidence intervals. The red filled line gives the mean of the 10 CNW responses. The green dashed vertical lines give the single largest responses from the 6 irregular wave runs and the filled line gives the mean. The green triangles show the empirical EVD of the peaks from the irregular waves from which the EVD is predicted. The solid blue vertical line shows the response from the focused wave.

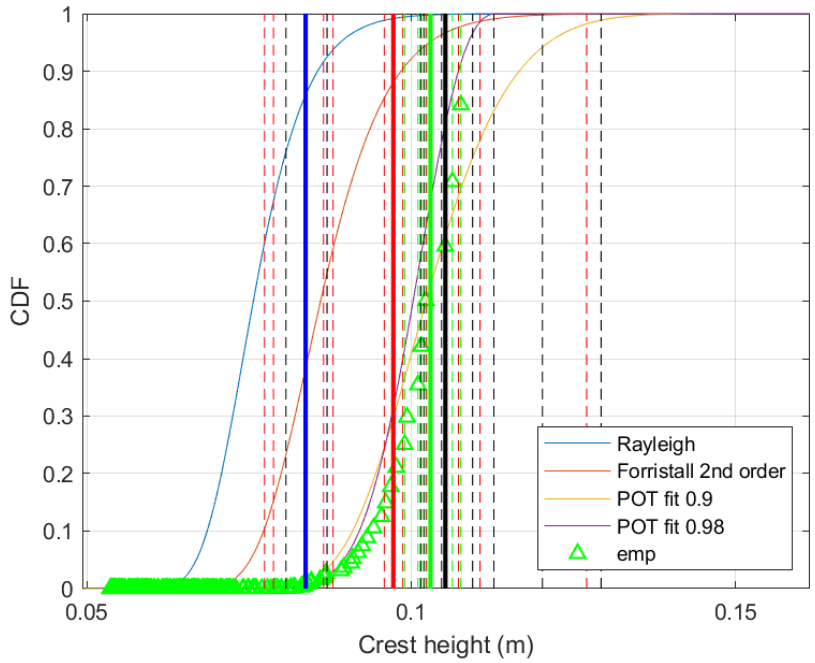

Figure 5.29: EVD of the wave amplitude distribution for the Rated2 sea state ($\gamma = 5.5$), 10 random CNW amplitudes are overlayed in dashed red vertical lines. The 10 groupiest CNWs are given in black. The red filled line gives the mean of the 10 random CNW amplitudes. The green dashed vertical lines gives the single largest wave amplitude from the 6 irregular wave runs and the filled line gives the mean. The green triangles show the empirical EVD of the peaks from the irregular waves from which the EVD is predicted. The solid blue vertical line shows the response from the focused wave.

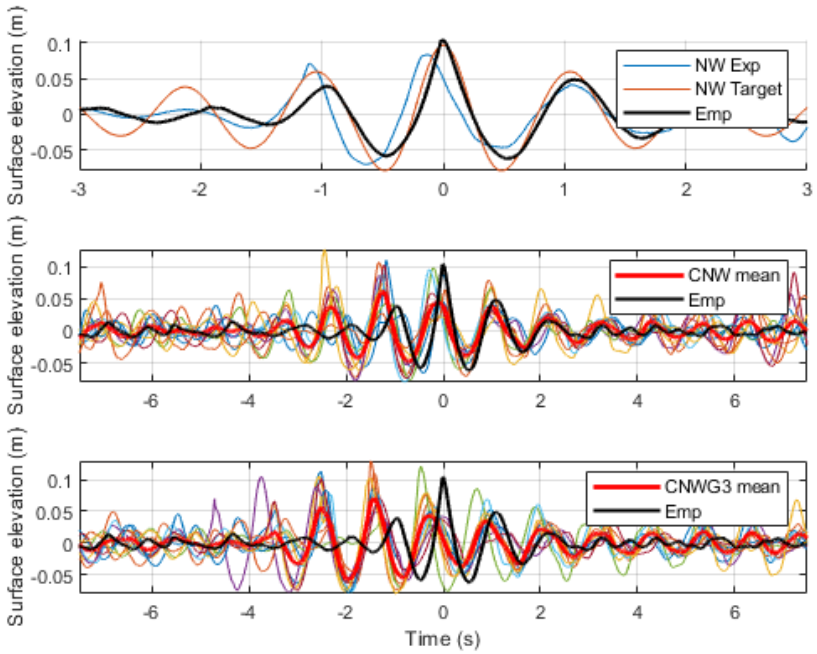

Figure 5.30: Comparison of the 10 CNWG3 and 10 CNW profiles to the empirical average of the 10 largest wave profiles for the Rated 2 sea state ($\gamma = 5.5$).

Comparing the empirical average wave profile leading to extreme mooring loads to the average CNW and CNWG3 profiles in the physical experiments shifted in time to facilitate a better comparison in Fig.5.31, it is somewhat striking how similar they are considering that the average CNW profile produced is so different to the target shown in Fig.5.30.

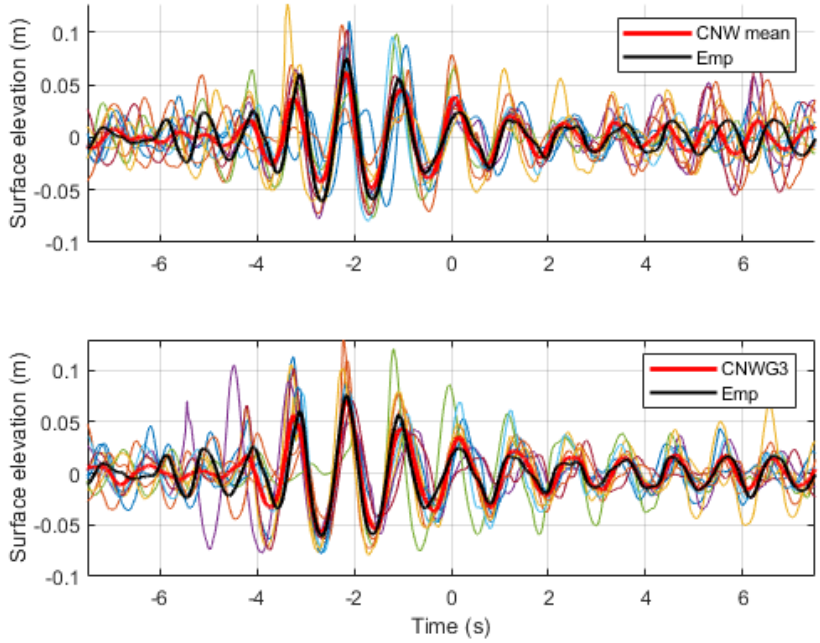

Figure 5.31: Comparison of the CNWG3 profiles to the empirical average of the 6 profiles leading to the largest responses during the 6 seeds in the Rated 2 sea state ($\gamma = 5.5$). The CNWs and CNWG3s have been shifted by 0.93 seconds and 0.73 seconds respectively to allow a better comparison of the wave profiles.

In summary, the physics which complicates the use of focused and constrained focused waves discussed in the previous chapter of nonlinear wave development in steep seas, breaking and deviations from the linear RAOs due to history effects, drift and other higher order effects also appear to complicate the analysis for the Rated 2 sea state presented here. The realisation of the extremes of the pitch response using CRRWs appears to be hampered by the occurrence of a large wave immediately preceding the main crest (at approximately $-2s$). It seems likely that the extreme mooring load may be better produced using a wave group, this will be discussed further in the next section.

5.4.4 50 year contour sea state

The frequency domain analysis of the 50yr contour sea state for $\gamma = 3.3$ in Fig.5.32 shows the front mooring, surge and pitch responses all have substantial low frequency

content similar to the Rated 2 case in Fig.5.12.

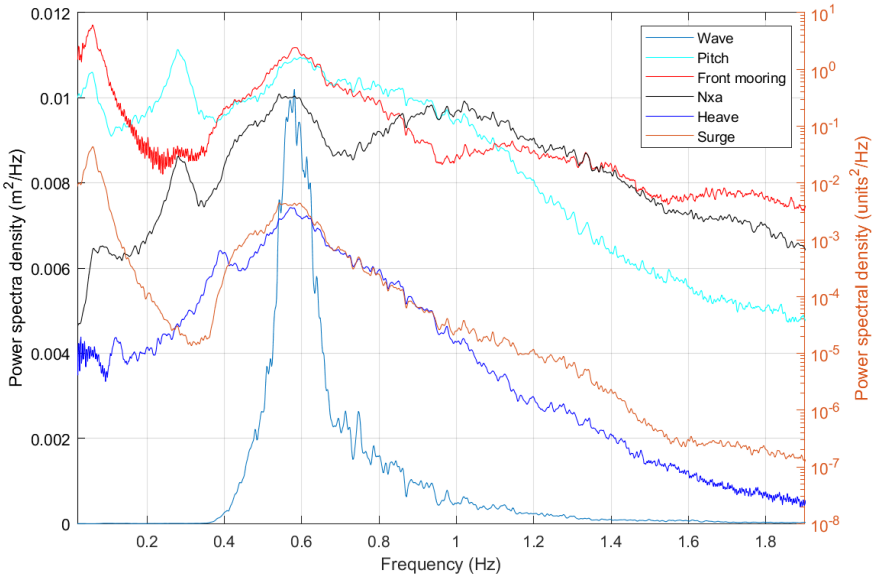

Figure 5.32: Spectral density plots for the responses of interest in the 50yr contour sea state ($\gamma = 3.3$). The wave spectral density magnitude is given by the left y axis while a log scale is used for the response spectra on the right y axis.

For the back mooring load the average of the CRRW profiles produces a characteristic load estimate more in line with the IW prediction compared to the responses in the Rated 2 sea (see Fig.5.33), but it is still an under prediction. It is not surprising that the MLER wave produces a larger response than the constrained waves as an increased surge position decreases the back mooring loads in unidirectional waves. Figs.5.34-5.35 demonstrate the average wave and response profiles leading to the extreme back mooring loads are highly consistent.

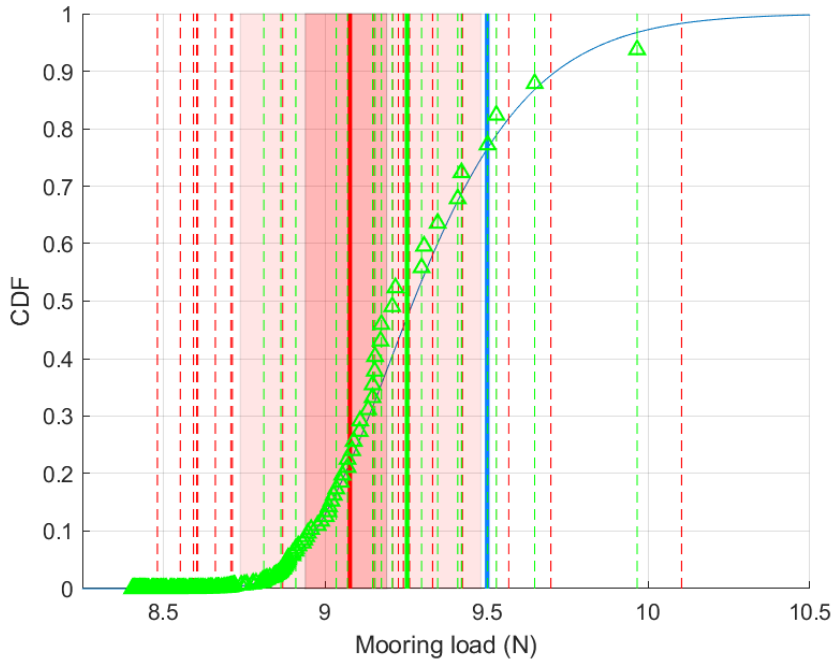

Figure 5.33: EVD of the back mooring load for the 50yr contour sea state ($\gamma = 3.3$), CRRW responses are overlayed in dashed red vertical lines. The red shading shows the 50 and 95% confidence intervals. The red filled line gives the mean of the 20 CRRW responses. The green dashed vertical lines give the single largest responses from the 18 irregular wave runs and the filled line gives the mean. The green triangles show the empirical EVD of the peaks from the irregular waves from which the EVD is predicted. The solid blue vertical line shows the response from the MLER wave.

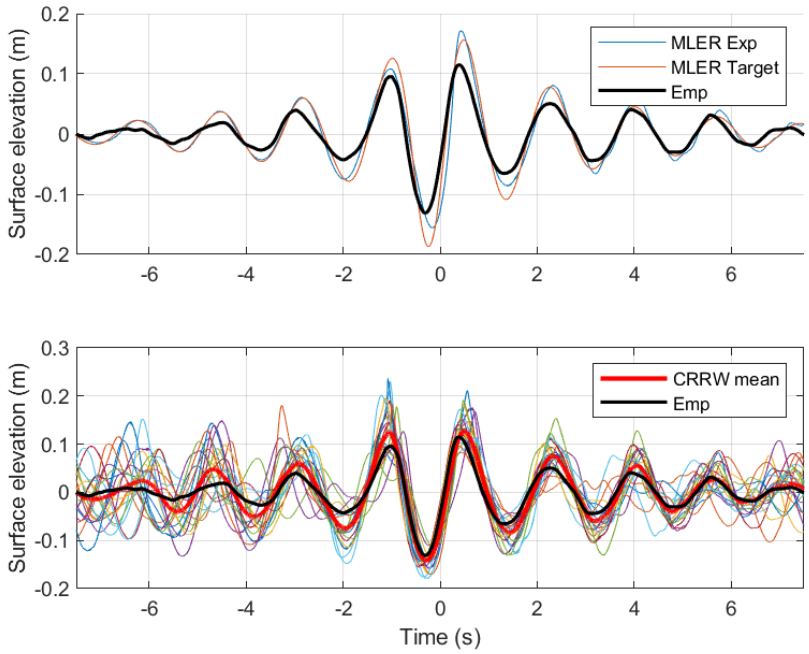

Figure 5.34: Comparison of the back mooring load MLER theoretical target and physically achieved (after a single phase correction) profiles to the empirical average of the 18 profiles leading to the largest responses for the 50yr contour sea state ($\gamma = 3.3$).

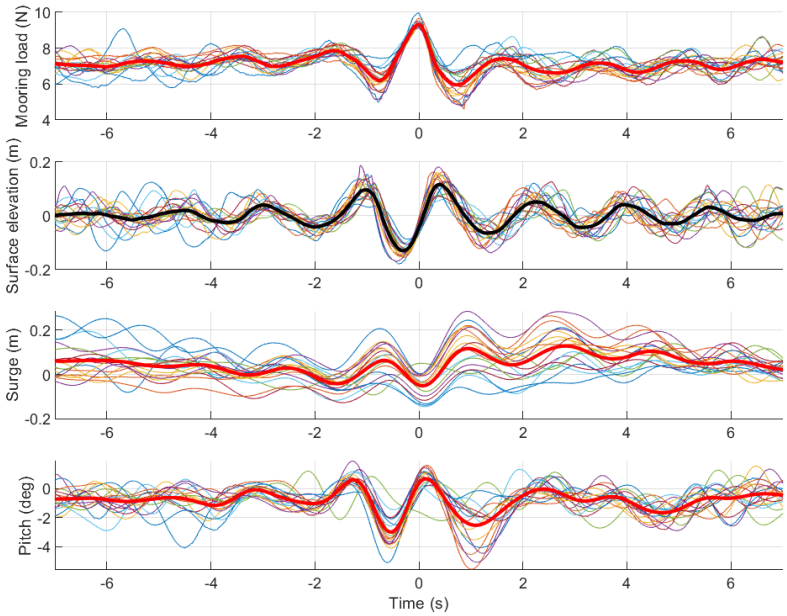

Figure 5.35: 18 profiles of surface elevation, surge position and back mooring load leading to the largest back mooring load responses for the 18 seeds during the 50yr contour sea state ($\gamma = 3.3$). Averages of the 18 extremes are given by the thick lines.

It is apparent from Fig.5.36 that two IW seeds produce loads much higher than the others, at around $18 - 20N$, and so drastically change the shape of the EVD of the front mooring load. This serves as a reminder of why it is necessary to obtain response data from a large number of seeds. It also raises interesting questions on the post processing methodology behind the characteristic load prediction. If the mean of the maximum values from each seed is used then a substantially different characteristic value is arrived at compared to if a high percentile is selected; $13.56N$ vs $21.62N$ (though recall no standard actually recommends this processing method for mooring loads). This would imply that for responses where the distribution is likely to have a long tail, using the average of maxima post processing methodology may require significantly larger partial safety factors than selecting a high percentile.

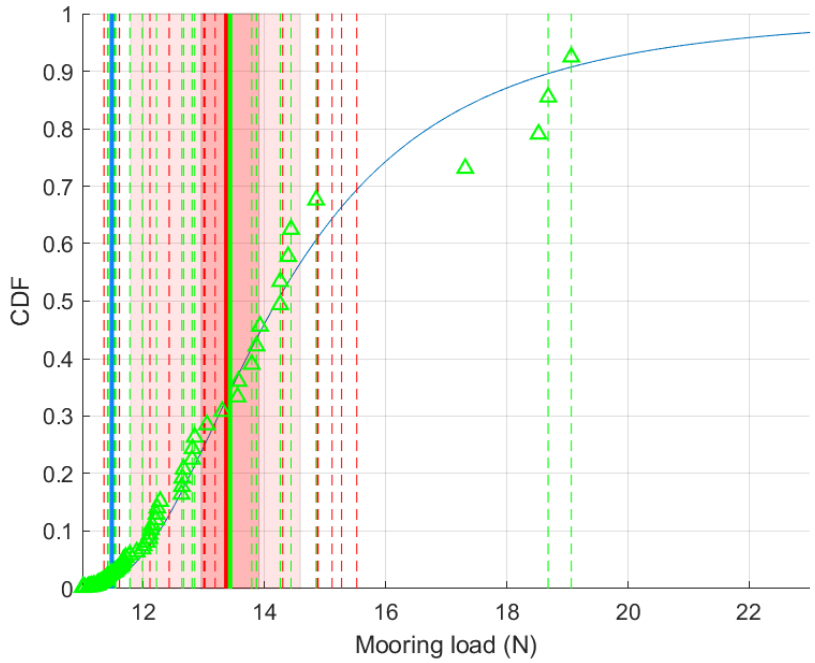

Figure 5.36: EVD of the front mooring load for the 50yr contour sea state ($\gamma = 3.3$), CRRW responses are overlayed in dashed red vertical lines. The red shading shows the 50 and 95% confidence intervals. The red filled line gives the mean of the 15 CRRW responses. The green dashed vertical lines give the single largest responses from the 18 irregular wave runs and the filled line gives the mean. The green triangles show the empirical EVD of the peaks from the irregular waves from which the EVD is predicted. The solid blue vertical line shows the response from the focused wave.

The MLER profile conditioned on the linear RAOs is not in agreement with the empirical profile seen to produce the extreme responses in Fig.5.37. As with the Rated 2 sea state, there is still a significant low frequency response as seen in Fig.5.32 and the profiles in Fig.5.38 appear to show that the extremes are caused by two large waves of approximately equal amplitude rather than a single large wave. Also gamma does not have a significant impact on the profile leading to the extreme.

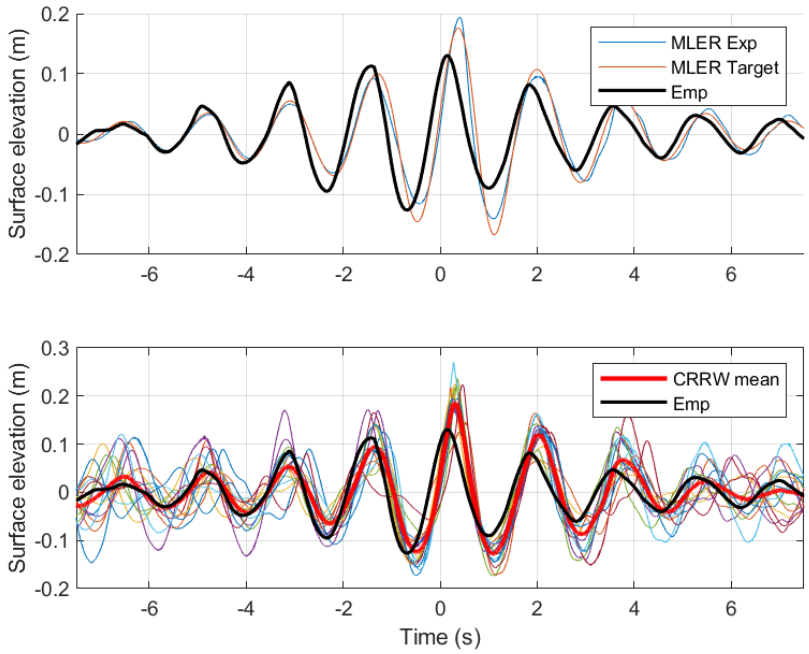

Figure 5.37: Comparison of the front mooring load MLER theoretical target and physically achieved (after a single phase correction) profiles to the empirical average of the 18 profiles leading to the largest responses for the 18 seeds in the 50yr contour sea state ($\gamma = 3.3$).

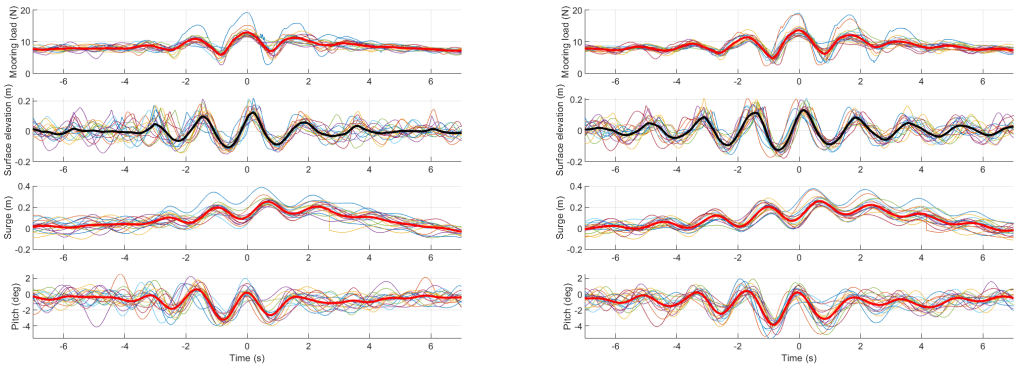

(a) $\gamma = 1$ *(b)* $\gamma = 3.3$

Figure 5.38: 18 profiles of surface elevation, surge position and front mooring load leading to the largest front mooring load responses for the 18 seeds in the 50yr contour sea state for different gamma values. Averages of the extremes are given by the thick lines.

A wave group conditioned on the maximisation of the derived process in equation

5.4 was also run along with constrained cases, but this time based on maximising two peaks in accordance with the empirical profile presented in Fig.5.37 and Fig.5.38. These will be referred to as G2 and CG2. Again it can be seen that the CG2 profiles produced loads along the length of the EVD and at the higher percentiles (Fig.5.39). The method used was improved by using the focused wave for the group of two large waves given by equation 5.5, scaled to the $99th$ percentile and constraining it into a random background as presented in Fig.5.40.

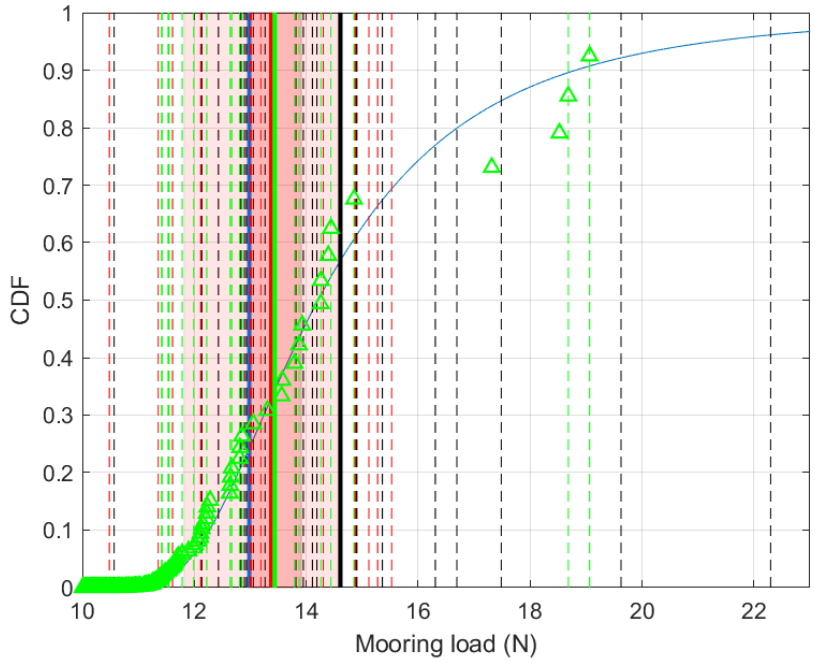

Figure 5.39: EVD of the front mooring load for the 50yr contour sea state ($\gamma = 3.3$), 20 random CRRW responses are overlayed in dashed red vertical lines. The 20 groupiest CNWs (2 peaks) are given in black. The red shading shows the 50 and 95% confidence intervals for the CRRWs. The red filled line gives the mean of the 20 random CRRW responses. The green dashed vertical lines give the single largest responses from the 18 irregular wave runs and the filled line gives the mean. The green triangles show the empirical EVD of the peaks from the irregular waves from which the EVD is predicted. The solid blue vertical line shows the response from the focused wave.

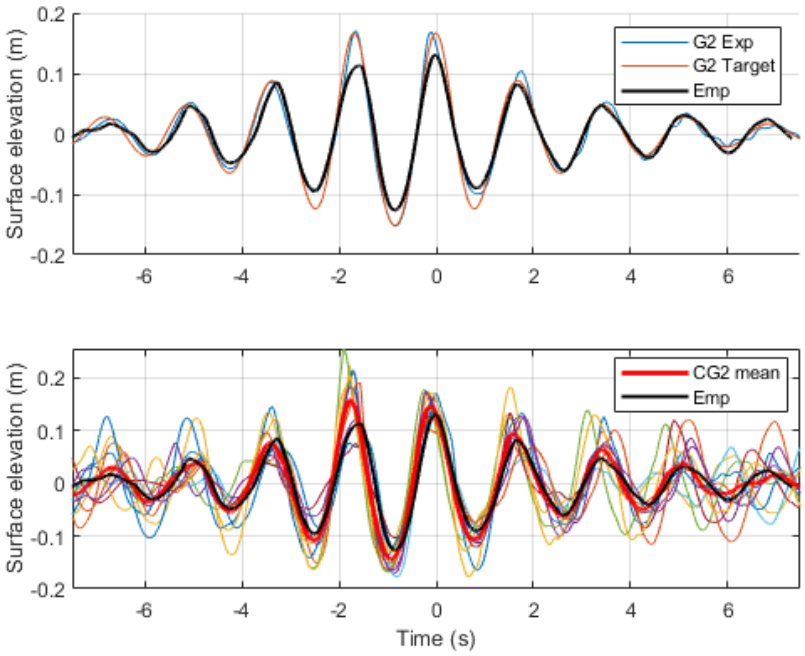

Figure 5.40: Comparison of the front mooring load G2 theoretical target and physically achieved (after a single phase correction) profiles to the empirical average of the 18 profiles leading to the largest responses for the 18 seeds in the 50yr contour sea state ($\gamma = 3.3$). The constrained G2 profiles are shown in the bottom plot along with the average.

Whilst this approach better represents the statistics than the method used for the Rated2 sea state, where 200 CNWs were produced and the ten 'groupiest' cases selected, it is not as rigorous as for the CRRWs or CNWs. It is only the surface elevation of the second wave peak being constrained so although the average CG2 profile is close to that of G2, the value of the maximum derived process (Z_k) of the target surface elevations is not the same in every case as can be seen in Fig.5.41.

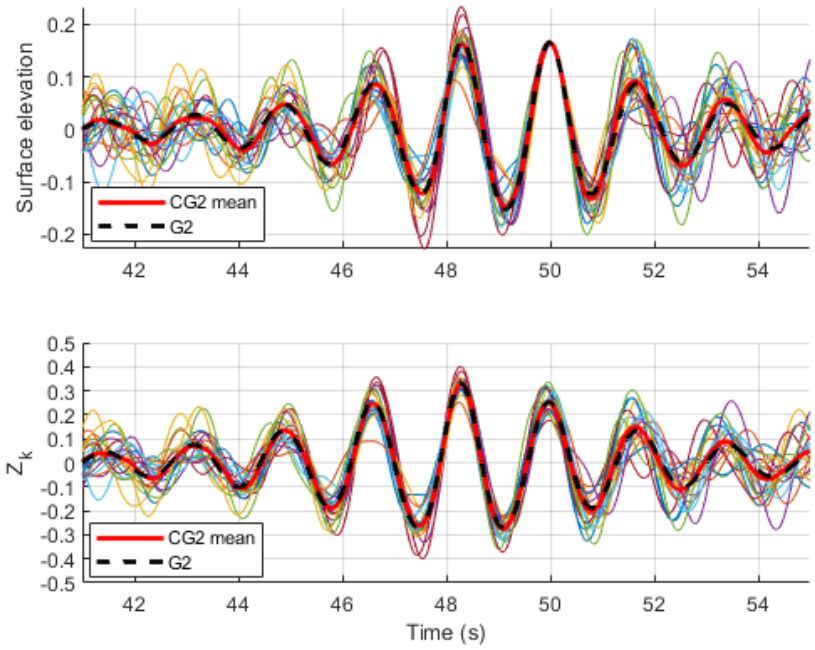

Figure 5.41: Comparison of the target wave profiles and derived process values for the G2 and 20 CG2s in the 50yr contour sea state ($\gamma = 3.3$).

To improve on this method in future a number of cases could be generated at different percentiles for the constrained profiles then searched according to equation 5.4. The cases matching the desired value of Z_k could then be selected so that a range of peak target wave amplitudes conforming to the desired Z_k could be run. Despite this limitation however, Fig.5.42 confirms that the derived process maxima achieved by the CG2 profiles using the current method are reasonably close to those from the irregular waves, though a bit more conservative.

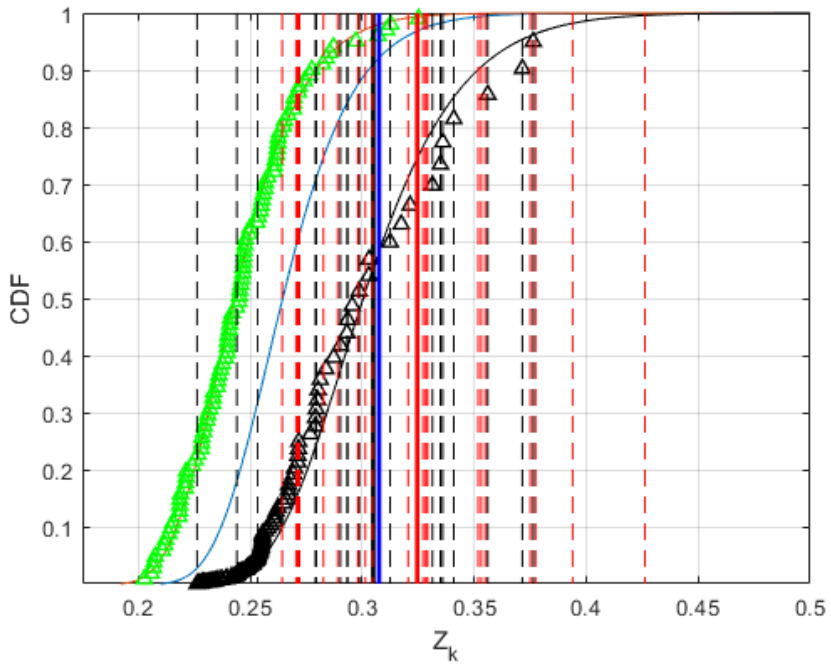

Figure 5.42: EVD of the derived process for 2 peaks in the 50 yr sea state ($\gamma = 3.3$), the 20 CG2s are given in red. The red filled line gives the mean. The black dashed vertical lines give the single largest derived process maxima from the 18 irregular wave runs and the filled line gives their mean. The green triangles show the empirical EVD of the derived process maxima produced from 100 one hour irregular wave time series using linear wave theory. The blue curve shows the Rayleigh distribution from the spectral moments of the derived process. The solid blue vertical line shows the value achieved experimentally from the G2 focused wave.

The nacelle *x* acceleration is largely dependent on pitch and so it is perhaps unsurprising that the MLER wave produced the largest characteristic estimate in Fig.5.43. However the mean response from the CRRWs gave an under prediction relative to the irregular waves. This was partly due to the mean CRRW profile being smaller than the target due to wave breaking as can be seen if Fig.5.44.

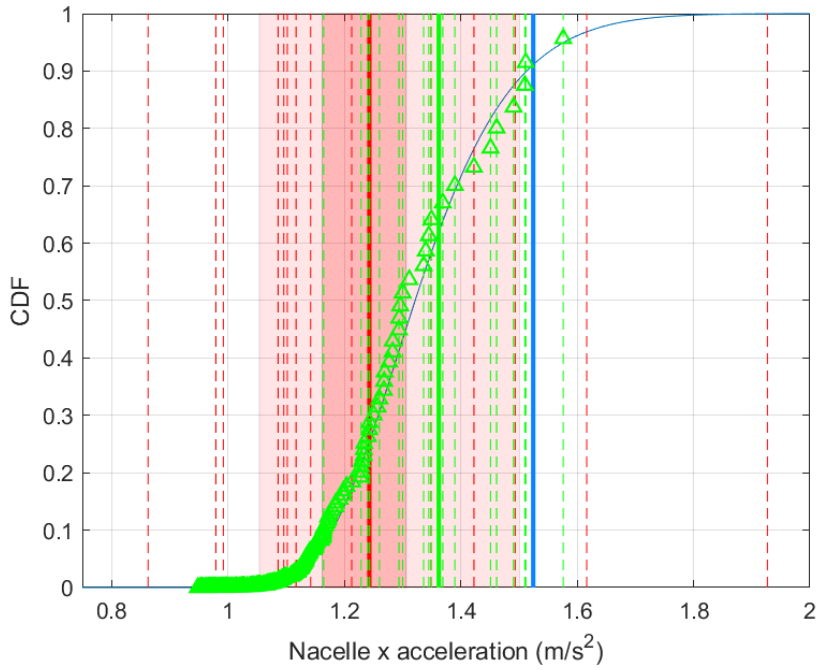

Figure 5.43: EVD of the nacelle *x* acceleration for the 50yr contour sea state ($\gamma = 3.3$), CRRW responses are overlayed in dashed red vertical lines. The red shading shows the 50 and 95% confidence intervals. The red filled line gives the mean of the 15 CRRW responses. The green dashed vertical lines give the single largest responses from the 18 irregular wave runs and the filled line gives the mean. The green triangles show the empirical EVD of the peaks from the irregular waves from which the EVD is predicted. The solid blue vertical line shows the response from the MLER wave.

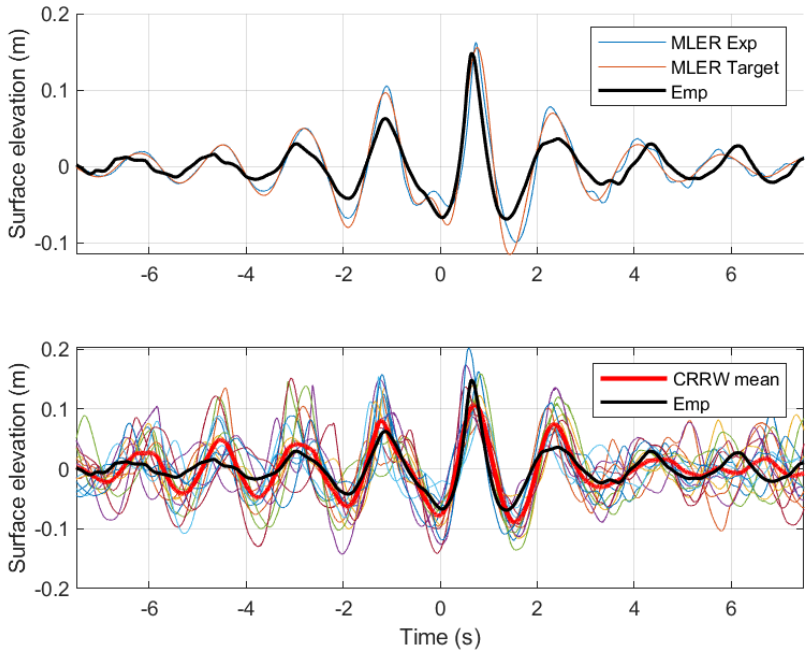

Figure 5.44: Comparison of the nacelle x acceleration MLER theoretical target and physically achieved (after a single phase correction) profiles to the empirical average of the 18 profiles leading to the largest responses for the 18 seeds in the 50yr contour sea state ($\gamma = 3.3$).

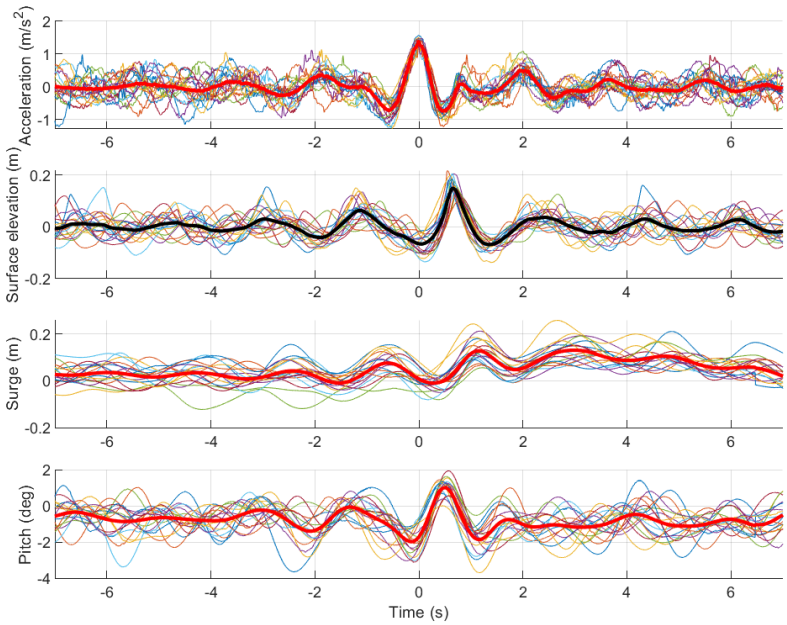

Figure 5.45: 18 profiles of surface elevation, surge position and nacelle *x* acceleration leading to the largest nacelle *x* acceleration responses for the 18 seeds in the 50yr contour sea state ($\gamma = 3.3$). Averages of the 18 extremes are given by the thick lines.

The extreme pitch which occurred in the 50 year contour sea state was negative in the sense that it was into the waves in the absence of wind loading. Fig.5.46 presents the comparison between the CRRW responses and those from the IWs, the MLER wave produced an estimate of the characteristic load comparable to the mean of the largest responses from the irregular waves. The MLER profile in Fig.5.47 was a good match to the empirical average wave from the irregular wave seeds which led to the extreme pitch responses. Gamma had no significant impact on the profile in Fig.5.48.

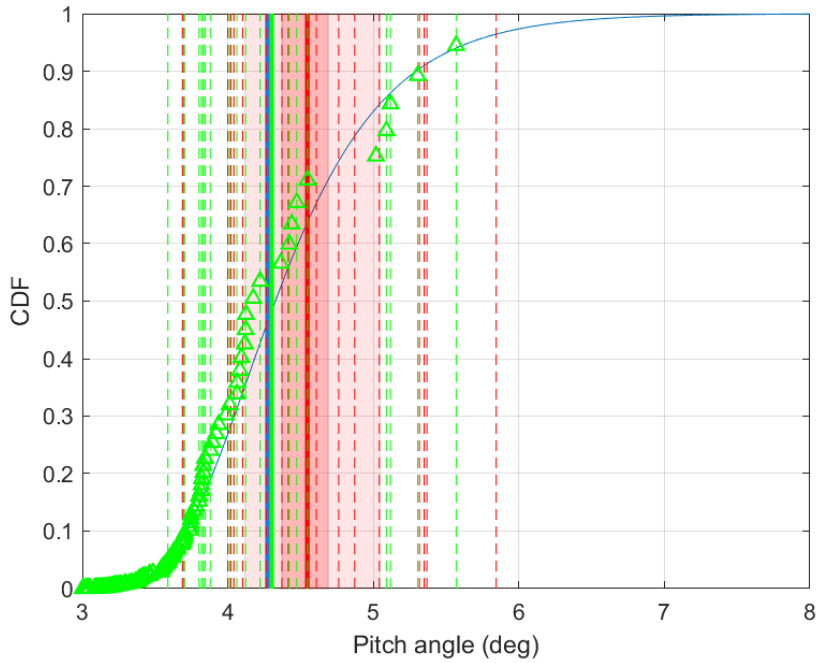

Figure 5.46: EVD of the negative pitch for the 50yr contour sea state ($\gamma = 3.3$), CRRW responses are overlayed in dashed red vertical lines. The red shading shows the 50 and 95% confidence intervals. The red filled line gives the mean of the 20 CRRW responses. The green dashed vertical lines give the single largest responses from the 18 irregular wave runs and the filled line gives the mean. The green triangles show the empirical EVD of the peaks from the irregular waves from which the EVD is predicted. The solid blue vertical line shows the response from the MLER wave.

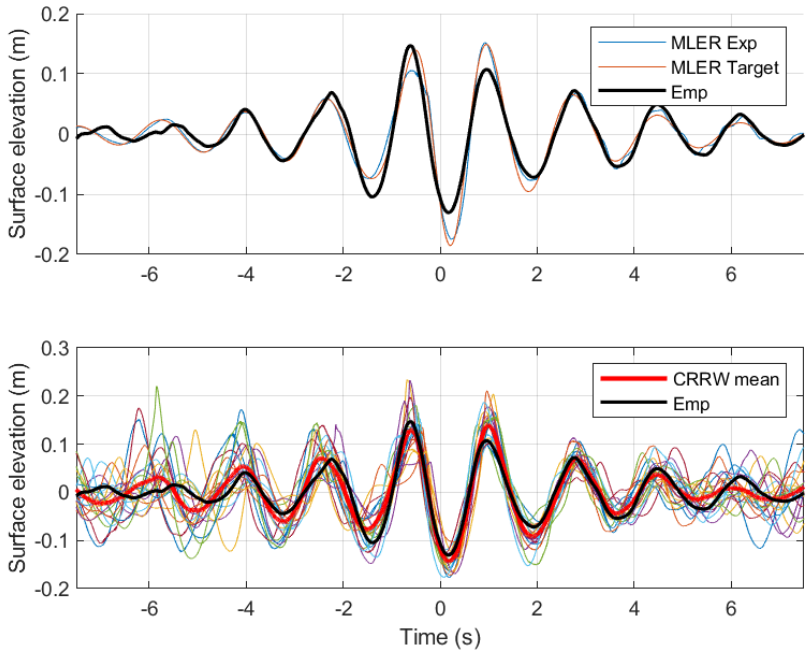

Figure 5.47: Comparison of the negative pitch MLER theoretical target and physically achieved (after a single phase correction) profiles to the empirical average of the 18 profiles leading to the largest responses for the 18 seeds in the 50yr contour sea state ($\gamma = 3.3$).

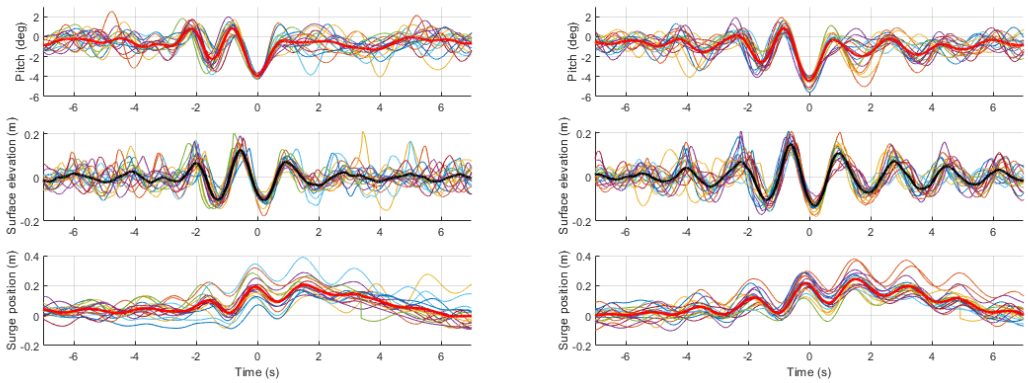

(a) ($\gamma = 1$) *(b)* ($\gamma = 3.3$)

Figure 5.48: Profiles of surface elevation, surge position and negative pitch leading to the largest negative pitch responses for the 18 seeds in the 50yr contour sea state for different gamma values. Averages of the extremes are given by the thick lines.

The data in table 5.4 and table 5.5 shows how the percentiles representing the char-

acteristic load fluctuate using the mean of the maximum responses from the CRRWs and IWs. The characteristic load/response predictions from the CRRWs and IWs are in approximate agreement for the front mooring and pitch responses in the 50yr contour sea state. The MLER was found to produce equivalent or larger estimates for pitch, back mooring load and nacelle x acceleration. For the steep Rated 2 sea state, the analysis was complicated by non-linear wave development, wave breaking and the reliance on linear wave and wave maker theory. The CRRWs and CNWs under predicted the characteristic load for the front mooring but by selecting wave groups based on the maximisation of a derived process a more accurate prediction in agreement with the IWs was made.

There are large differences between the characteristic load predictions using the different post processing methods. The largest of these occurred for the front mooring response as the distribution has a long tail. Interestingly this is a response where the IEC (2015) and DNV (2015) standards are in agreement that the most probable maximum (MPM) value should be taken as the characteristic load for the dynamic part of the tension which would give a value less than the mean reported in table 5.4 (even after subtracting the mean tension). This would explain why a larger safety factor (2.2 in DNV (2013)) is then used to compensate.

Table 5.4: Characteristic load prediction comparisons. FM = front mooring, P = Pitch. FM(%) refers to the percentile of the EVD CDF, FM(N) the magnitude. $95th$ refers to the magnitude of the response at the $95th$ percentile of the EVD CDF.

Sea state	γ	Wave type	FM (%)	FM (N)	FM $95th(N)$	P (%)	P (deg)	P $95th(deg)$
50yr contour	1	IW	31.4	12.85	17.87	49.7	3.84	4.43
	3.3	IW	34.3	13.44	21.28	48.2	4.30	5.70
	3.3	MLER	1.4	11.49	-	46.2	4.27	-
	3.3	NW	0	11.16	-	-	-	-
	3.3	CRRW	33.0	13.38	-	63.7	4.55	-
	3.3	CNW	23.3	12.94	-	-	-	-
	3.3	G2	24.2	12.98	-	-	-	-
	3.3	CG2	56.9	14.61	-	-	-	-
50yr Viselli	3.3	IW	33.1	9.61	10.93	47.3	2.54	3.08
Max hindcast	3.3	IW	23.5	12.06	17.13	55.7	3.85	4.87
Rated 2	1	IW	23.7	12.54	13.21	37.0	5.10	5.42
	1	CNW G3	0	12.23	-			
	3.3	IW	28.3	13.17	14.77	40.2	5.18	5.54
	3.3	MLER	0	11.51	-	23.8	5.11	-
	3.3	NW	0	11.76	-	-	-	-
	3.3	CRRW	0	12.13	-	0	4.80	-
	3.3	CNW	0	12.52	-	-	-	-
	3.3	CNW G3	52.9	13.49	-	-	-	-
	5.5	IW	29.2	13.76	16.78	48.1	5.24	5.66
	5.5	CNW	0	12.78	-	-	-	-
	5.5	CNW G3	44.5	14.08	-	-	-	-

Table 5.5: Characteristic load prediction comparisons. BM = back mooring, Nxa = nacelle *x* acceleration. BM(%) refers to the percentile of the EVD CDF, BM(N) the magnitude. $95th$ refers to the magnitude of the response at the $95th$ percentile of the EVD CDF.

Sea state	γ	Wave type	BM (%)	BM (N)	BM $95th(N)$	Nxa (%)	Nxa (m/s^2)	Nxa $95th(m/s^2)$
50yr contour	1	IW	38.0	9.18	9.72	60.6	1.48	1.71
	3.3	IW	47.5	9.26	9.87	62.0	1.35	1.58
	3.3	MLER	76.6	9.50	-	91.1	1.52	-
	3.3	CRRW	22.2	9.08	-	25.5	1.24	-
50yr Viselli	3.3	IW	47.5	8.77	9.12	17.6	1.08	1.39
Max hindcast	3.3	IW	47.5	8.82	9.06	51.3	1.26	1.43
Rated 2	1	IW	55.7	7.18	7.25	50.9	1.08	1.23
	3.3	IW	30.0	7.18	7.42	57.1	1.24	1.40
	5.5	IW	38.8	7.11	7.30	57.2	1.28	1.43

For some response cases (nacelle *x* acceleration and back mooring load) the CRRWs under performed relative to the irregular waves but the MLERs were at least as conservative. Therefore it is recommended that the CRRW and MLER should be run and where the MLER prediction exceeds that from the CRRWs, the MLER prediction should be used as the characteristic value. This is not thought to be a common scenario, however, as the back mooring load is not actually a response of interest and was only studied here as an example of a case where the preceding wave may produce a surge response acting to reduce the extreme.

5.5 Region of applicability

Based on the limitations observed in these experiments due to wave breaking it would be useful to try and specify some regions of applicability for the constrained wave method in physical experiments. The simplest way to do this would be with steepness limits showing the limitations due to wave breaking and nonlinear development. Fig.5.49 indicates the extreme sea states modelled in physical experiments throughout this thesis. Regions of suggested applicability of the proposed focused wave method in deep water are indicated with red, amber and green shading. Red regions representing

zone 3 are considered inapplicable, amber (zone 2) will be challenging experiencing some wave breaking and green (zone 1) should be straightforward to apply. It is likely the applicability of FNPF models to numerically model the constrained focused waves will follow a loosely similar pattern with increasing difficulty outside the green region.

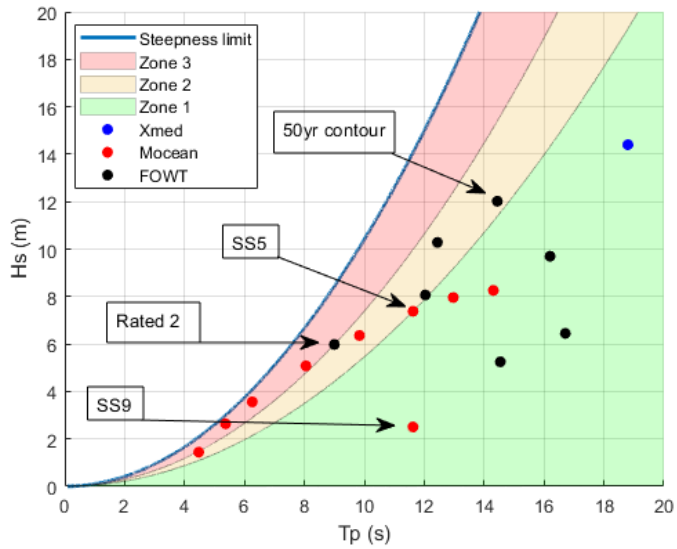

Figure 5.49: Sea states tested and suggested regions of applicability for the developed focused wave approach

A further caveat is that the design methods applied here to physical experiments are using unidirectional waves. This is common practice and shouldn't undermine the comparison between irregular and constrained wave methods, but as such wave conditions lead to nonlinear wave amplification, the characteristic value predictions will likely be overly conservative.

5.6 Conclusions and future work

The Rated 2, 50 year contour and Max hindcast sea states were the ones which resulted in the largest pitch and front mooring load responses. Wind loading on the tower for idling cases and turbulent wind will need to be modelled in future to draw more certain conclusions about which sea state is the design sea for each response. For the 50yr contour sea state the post processing methodology used in the characteristic load

prediction of the front mooring load had a significantly larger impact on the result than for all other sea states and responses. Gamma has a substantial effect on the surge, mooring load and to a lesser extent, pitch responses.

The response conditioned focused waves perform worse in the Rated 2 sea state due to non-linearity of wave development and response, although it should be pointed out that the difference in the pitch prediction between CRRWs and IWs is less than 0.4 degrees. Selecting the 'groupiest' CNWs based on 3 peaks improved the front mooring load prediction for the Rated 2 sea state and a wave group consisting of 2 large peaks produced a profile more in line with the empirical one for the 50yr contour sea state.

For the pitch, nacelle *x* acceleration and back mooring load responses in the 50 year contour sea state a MLER wave scaled to the $99th$ percentile produced characteristic response values in line with or more conservative than the irregular waves and for the nacelle *x* acceleration and back mooring load larger than for the CRRWs. For this reason it is recommended to run MLER and CRRW profiles and use the larger of the two characteristic estimates.

Nonlinear wave amplification is curtailed by directional spreading. It would therefore be interesting to know how directional spreading varies with significant steepness and what the joint distribution of H_s, T_p, gamma and spreading would be. The effect of turbulent wind on the EVD and characteristic load predictions should be investigated further, though this greatly complicates the statistics and experimental set up requiring a software in the loop approach for the thruster. Extending the short design episode approach to combined wind and wave loading would be very interesting.

The underlying physics leading to the extreme responses will be discussed in the next chapter with the aid of a numerical model.

Chapter 6

VolturnUS-S numerical

Chapter summary

A WEC-Sim model was calibrated against the data from physical experiments. It was found that an additional drag term in the Morison equation can improve the accuracy of the low frequency surge motions. A fully nonlinear potential flow model (REEF3D::FNPF) was used to explore the possibility of creating realistic nonlinear wave time series as inputs to the WEC-Sim model and the implications of using linear modelling and wave theory were investigated.

6.1 WEC-Sim and OpenFAST models

The WEC-Sim model was constructed in the usual way with one key difference that a non-hydro body was added atop the tower at the location of the thruster and a constant thrust force option added. The mooring properties and drag coefficients were then calibrated. It was found that to achieve the static mooring load in still water, for the wind and no wind cases, the mass of the catenary chains needed to be increased from $0.14kg/m$ to $0.154kg/m$. The measured mass density of the lines was $0.14kg/m$ so it is likely that errors in the measurement of the anchor or fairlead connection points is the real source of the discrepancy. The OpenFAST model was taken directly from the IEA reference case on github (IEAWindTask37 (2021)) and has slightly different model properties to those of the one used in the physical experiments. Errors asociated with the experiments are discussed in the previous chapter.

Several mesh sizes were tested to select an appropriate size for use in the numerical model. The selected mesh used to calculate the hydrodynamic coefficients in NEMOH

had 1525 panels, the most refined mesh consisting of 2529 panels was also tested. When the finest mesh and the selected mesh were assessed by comparing the maximum mooring loads produced in response to a NewWave for the 50yr contour sea state by a linear WEC-Sim model, the difference was found to be 0.07%. This difference was considered acceptable and the time series is presented in Fig.6.1.

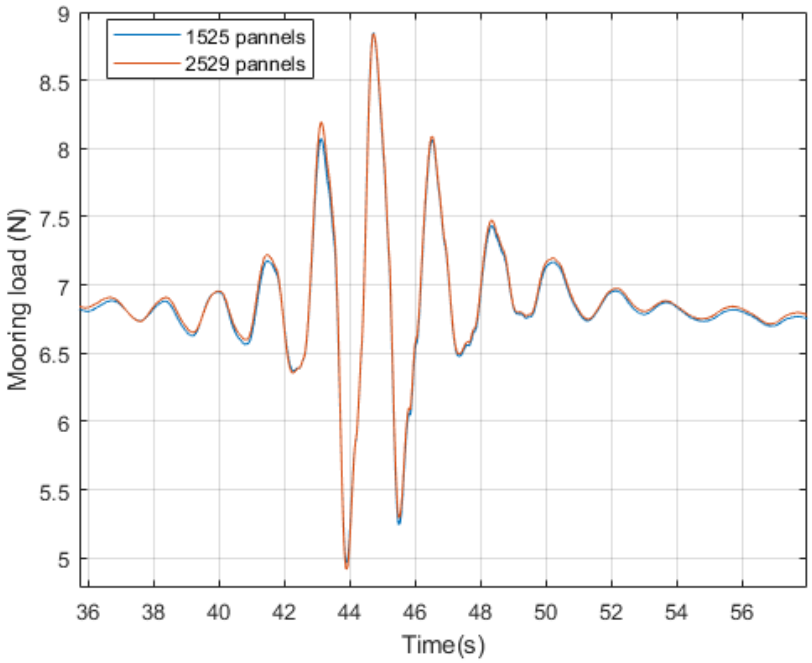

Figure 6.1: hlComparison of the front mooring load response to a NewWave for the 50yr contour sea state between 2 WEC-Sim models with different numbers of pannels.

If the large surge drift was caused by dynamic pressure effects it would be modelled by the non-linear Froude-Krylov force in the WEC-Sim model. However as Fig 6.2 shows, the drift is not accurately modelled in this way in WEC-Sim and nor is it captured any better by the QTFs in OpenFAST. This has important implications for the design of moorings and dynamic power cables.

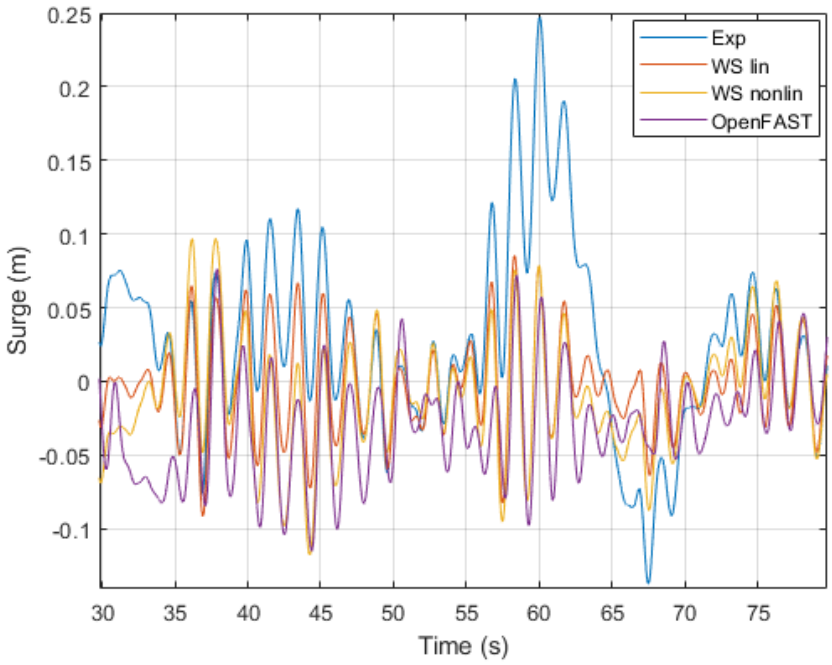

Figure 6.2: Comparison of the experimental and numerical model surge predictions for an extreme surge response during the 50yr contour sea state. The OpenFAST model results were for full scale but have been scaled down.

As the surge drift is observed to occur most severely in the steeper sea states it is likely due to more complex nonlinear effects such as slap loading or viscous drag. WECSim and FAST don't currently have a way of modelling slap loading as standard although a slamming formulation has been implemented by Cruz-Acheson (Atcheson et al. (2019)) and the method outlined in Laporte Weywada et al. (2019) though the model itself has not been made public. The OC5 and OC6 code comparison projects (Robertson et al. (2017), Robertson and Wang (2021), Robertson et al. (2020)) show how the modelling of the low frequency motions of semi-sub FOWTs is an ongoing area of study. A comparison of many different numerical models in Robertson et al. (2020) concluded that none were validated as the low frequency surge and pitch responses were not well captured. Wang et al. (2021a) tried to further understand the additional excitation force and conclude that the source is likely the result of viscous drag rather than wave diffraction. Experiments on some other FOWT types, for example the spar model in Meng et al. (2020), do not report large discrepancies between the physical

and numerical results for extreme responses in design sea states. Ma et al. (2020) discuss the low frequency surge motion of a semisub as part of the EXWAVE JIP in the context of mobile offshore drilling units and refer to it as viscous drift, caused by drag.

Slamming has been studied in regard to WECs recently (Katsidoniotaki (2021)) using CFD and is also considered important in relation to fixed offshore wind. Notably the Derisk project (Pierella et al. (2021)) has attempted to improve the extreme loading estimates of fixed structures due to nonlinear wave development and slap loading. Swan (2018) points out that in Norge (2007), physical model testing following a contour approach is recommended for very non-linear actions. Twenty $3hr$ phase seeds are recommended due to the potentially rare occurrence of large extremes due to non-linear effects, with the need for physical modelling emphasised. It is highlighted that the design load is not likely to occur in the sea state matching the annual exceedance probability. This is the same point as made about the effect of wind loading in Li et al. (2017) and is a warning against the validity of the contour approach for FOWTs. Although the slap loads considered most important for wave in deck loading are due to wave breaking (Swan (2018)), which don't appear to produce loads that are significantly different to steep non-breaking waves in the current study as discussed later. It is then recommended that a large number of sea states are evaluated. Whilst this would undoubtedly result in a more accurate design load prediction it would also result in large increases in time and resource requirements. This lends further weight to the argument that for the implementation of many probabilistic design approaches to be of practical use, fast numerical models need to be used and made accurate enough to model extremes or computing technology needs to improve to speed up high fidelity models.

To model how these loads influence the global motions of the device a crude drag term was added to the Morison equation in WEC-Sim. WEC-Sim and OpenFAST use the device velocity rather than relative velocity in the Morison equation, for this additional

term it was found that the calculation of the relative velocity between the platform and fluid flow at the location of the centre of mass was required. It should be noted that the way these loads were implemented here would not be of use to structural modellers interested in local loading as it is just an extra force applied at the COM. The advantage of applying the additional excitation force in this way is that the model still runs fast and can be used to determine the positions and mooring loads of the device, which is of most relevance to this work.

The drag modification was implemented in the Morison equation by adding an extra force term proportional to the square of the relative velocity between the device and fluid. This additional force acts in the positive x direction in line with the device motions and so leads to an increase in the excitation force, it is set to zero when the device moves in the negative *x* direction (into the waves). The *x*, *y* and *z* components of the orbital velocity were calculated at the position of the model CoM (calculated from surge and heave position neglecting any pitch correction, this is considered sufficient here as the pitch of the device is so small). The constant was then calibrated against the 50yr contour $99th$ percentile NewWave and the first 100 seconds of the irregular wave for seed 1. It was found that if the orbital velocity rose above $1.2m/s$ the surge became far too large and so whilst on the rare occasions the orbital velocity exceeds this value the force is reduced by a factor of 0.125, this was a somewhat arbitrary decision as some other combination of cut off velocity and reduction factor could possibly yield similar results. These unrealistic spikes in orbital velocity are likely due to two factors, the absence of a stretching being applied to the wave particle velocities, and instances where the CoM is above the water surface. However these calibrated values were found to produce reasonably accurate results in all the sea states tested.

The orbital velocity calculation was adapted from that in the Morison elements function within WEC-Sim which applies linear theory. This means the velocity above the mean water level will be over predicted, Wheeler stretching is often employed to mitigate this effect. Gibson (2020a) discusses the limitations of calculating the wave kinematics

from linear theory and stretching methods and recommends 2nd order theory be used to avoid over prediction from linear theory and under prediction above the mean water line from Wheeler stretching. Although they also recommend using full non-linear methods for very steep waves. It is possible then that using a stretching or 2nd order prediction would negate the need for the applied force reduction factor of 0.125. For the purposes of this thesis the present model formulation is considered adequate and so these questions are left for future work.

All tested sea states were run with this drag correction and found to be in reasonably good agreement with the surge from the experiments as shown for selected time series in Fig.6.3. This formulation will be further evaluated later in the chapter using EVD CDFs and response spectra, the advantage of this correction is it can be calibrated against a single sea state and produce reasonable results in sea states of differing steepnesses.

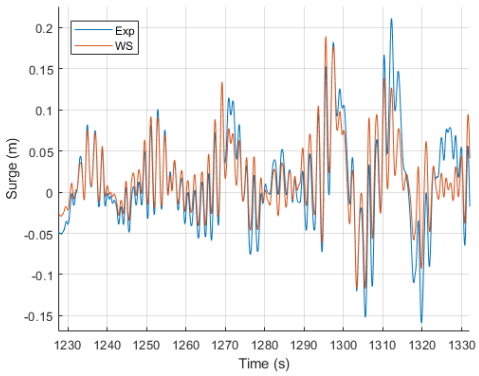

(a) 50yr Vesilli

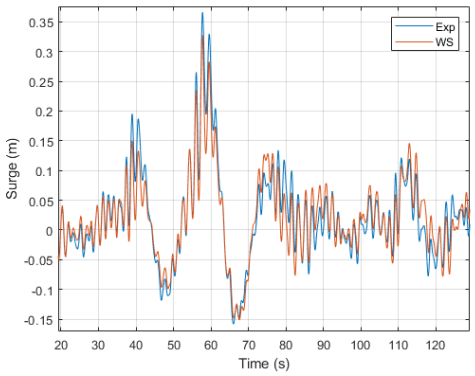

(b) 50yr contour

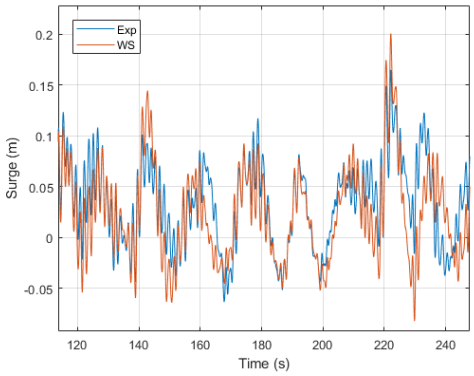

(c) Max hindcast

Figure 6.3: Experiment vs modified drag surge comparisons, Exp shows data from physical experiments, WS from the WEC-Sim model.

When the Rated 2 sea state was modelled with wind however the drag modification resulted in slightly less of an improvement relative to the no wind case. This was thought to be partly due to the additional drag being calibrated in a less steep sea state and partly to the fact that the wave, using the measurement made at the wave gauge in the physical tests, is propagated according to linear wave theory in the model. To assess the effect of this and try to mitigate it the surface elevation produced in the WEC-Sim model at the device taken from the wave gauge in the physical experiments was recalculated at the mean surge offset of $16cm$. This resulted in a slight improvement shown in Fig.6.4. The justification for this is that the discrepancy in the surface elevation due to linear wave propagation is larger than if the target location is shifted. This issue

due to linear wave propagation in the steepest sea states could be reduced in future by placing more wave gauges around the model to use as the wave input e.g. at the mean surge position of $16cm$. While the effect here is relatively minor, it is a source of error and one which will be larger for devices which experience a larger drift in surge.

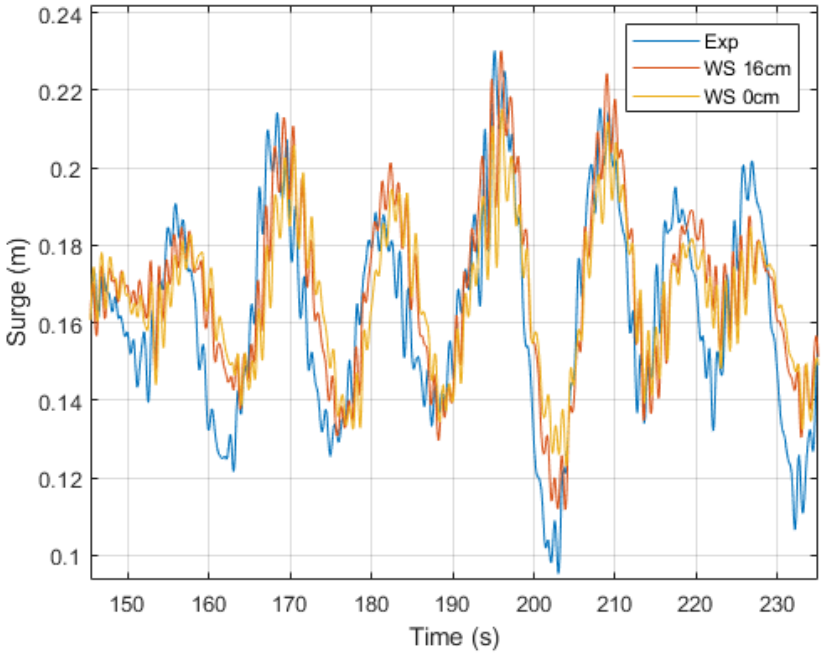

Figure 6.4: Comparison of the experimental and numerical model surge predictions for the Rated 2 sea state when the target surface elevation position is shifted to $16cm$.

This drag modification was found to dominate the surge motions to such an extent that the weak non-linearities of the WEC-Sim model didn't substantially alter the surge or front mooring load predictions. This meant that the weak nonlinearities of the WEC-Sim model could be 'switched off' which resulted in a very fast run time. If 9 simulations are run on one desktop at the same time it runs at approx $1.5x$ real time at model scale. The full scale time is then $\sqrt{(70)}$ times this - so approx $12.5x$ real time e.g. $3hrs$ full scale equivalent data can be run in 14.4 mins on one desktop. So $100hrs$ (the minimum requirement suggested by the WDRT studies (Coe et al. (2018)) for full long term analysis) can be run on one desktop in just $8hrs$. This illustrates the significant advantage of the WEC-Sim model being that it is extremely fast and easy to edit.

A breaking wave case was run through WEC-Sim and it appears the drag modification still captures the surge motions well in Fig.6.5. This implies that the slamming effects due to wave breaking on the surge excitation are not substantially different to those of large, steep, non-breaking waves. The figure also highlights the importance of using the relative velocity between the model and particle velocities for the additional drag term rather than using just the model velocity as is used for the standard Morison equation. This can be seen by the under prediction of the model, shown by the surge given by the red line, when velocity rather than relative velocity is used.

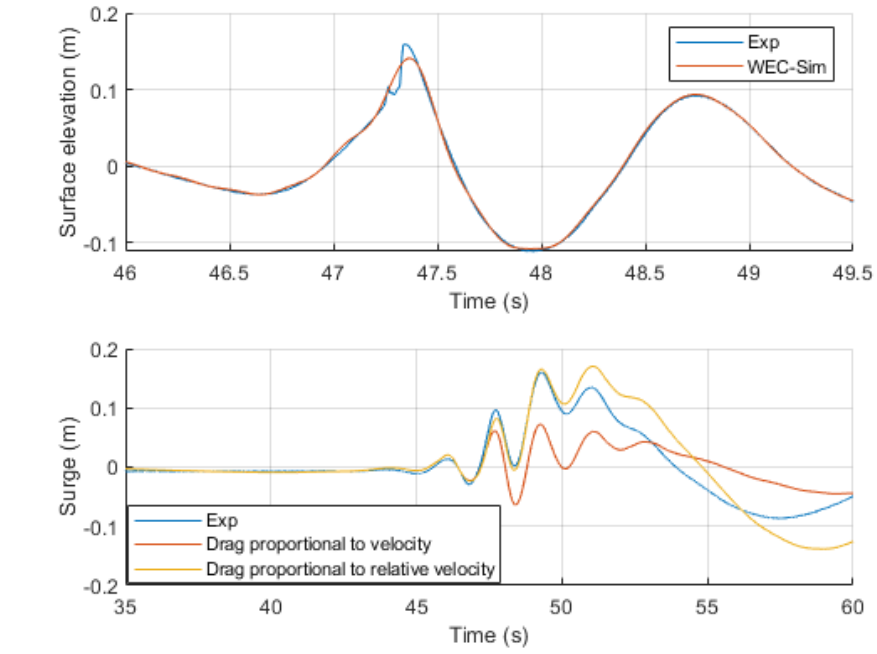

Figure 6.5: Comparison of the experimental and numerical wave and the drag modification formulation for a breaking wave case.

The extreme pitch response appears to be correlated with the z component of the orbital velocity Fig.6.6a) and so it is possible a similar additional drag term as introduced for surge could improve the model. Preliminary results are presented in Fig.6.6b) but the improvement is not as drastic as for surge. It is possible that a similar approach using the orbital velocity at the CoM and a point at the front and possibly back of the model, in order to better capture the pitching moment, could yield better results. How-

ever, to improve the accuracy of the pitch response in WEC-Sim it would be necessary to include the non-linear terms (Froude-Krylov) which would significantly increase the run time, further development of such an approach would be more appropriate in OpenFAST as it runs much faster with the QTF approach. It is therefore left for future work.

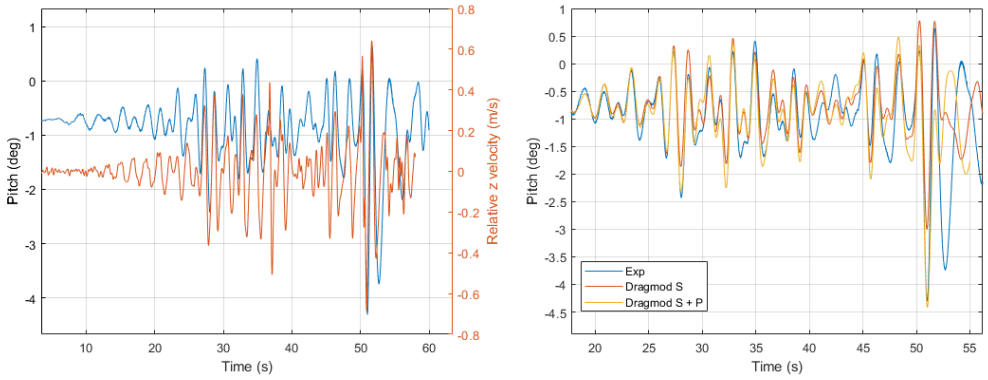

(a) z relative velocity *(b)* Pitch response

Figure 6.6: For a 50yr contour CRRW time series conditioned on the negative pitch response a) Relative velocity in z (red) compared to pitch (blue) b) Pitch comparison between the physical experiment, the WEC-Sim model with the surge drag term and the WEC-Sim model with surge and pitch drag terms.

6.2 Constrained focused waves

The effect of gamma and 'groupiness' of the CNW cases can be studied further by investigating the additional surge excitation of the modified WEC-Sim model. Fig.6.7 shows how the force in x provided by the additional drag term increases with increasing gamma for the 'groupiest' CNW cases.

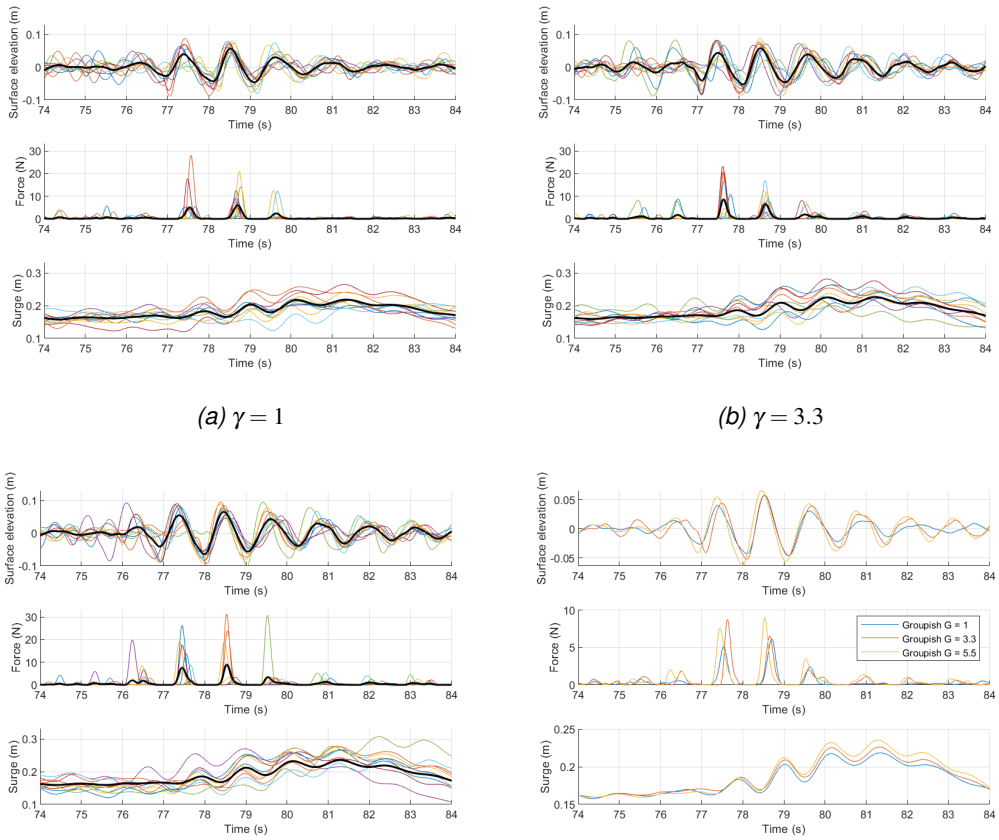

(a) $\gamma = 1$ *(b)* $\gamma = 3.3$

(c) $\gamma = 5.5$ *(d)* Mean comparison

Figure 6.7: Additional drag excitation force in x due to modified drag term, a comparison between the CNWG3 cases for the different gamma values.

6.3 REEF3D::FNPF

The deviations from linear theory of the amplitude distributions presented in section 5.0.1 demonstrates that non-linear wave development is important to the accurate reproduction of the largest crest heights. This, and the fact that increased gamma and wave 'groupiness' lead to increased extreme mooring responses suggests that making sure the wave input to the numerical model is true to non-linear wave theory may be essential to accurately modelling the extreme responses.

Oceanwave3D and REEF3D are two free, fully non-linear, potential flow based models which are capable of producing realistic non-linear wave time series (at least for low to moderate steepness sea states where breaking does not occur) by means of solving

the Laplace equation with boundary conditions at the free surface and at the bed. In this work REEF3D is utilised.

The model is based on potential flow meaning wave breaking is not captured and so a breaking filter is required to dissipate energy. Here the value of the filter has not been altered from the default 1.25 and the model parameters were kept as close as possible to the default values. The 2D numerical wave tank was setup to be $35m$ long consisting of 700 cells with a depth of $2.86m$ consisting of 15 cells. Vertical grid clustering is employed so that the separation of the grid points in z increases with water depth to concentrate computational effort close to the free surface. The generation and absorption zones consisted of single relaxation zones of length $6m$ and $10m$ respectively. A fixed time step of $0.01s$ was applied. For a summary of the key parameters used see table 6.1, for further details on the underlying equations governing the model, see appendix B.

Table 6.1: REEF3D model parameters

Parameter	Value
Time treatment	3rd order Runge-kutta
Spatial treatment	5th order WENO
Breaking wave algorithm	Filter based
breaking wave slope threshold	1.25
Vertical grid clustering	5
Stretching factor in z	1.5

The model was used here to generate time series using the same target surface elevations as those used in the physical experiments, including the spectral amplitude corrections. No calibrated breaking filter was applied initially to get a sense of the accuracy of the model for various sea states. The model mesh was also chosen so that the simulations would run at the equivalent of real time when all processors on a single desktop were utilised to run several simulations simultaneously. The model is not therefore as accurate as it could be and substantially less so than the results reported in Pakozdi et al. (2020). Nevertheless the basic model was able to produce results

more in line with those from the experiments compared to those using linear wave theory provided wave breaking was not significant (as was found in the Rated 2 sea state). A comparison of the surface elevation statistics at the target location $(17.3m)$ are given in table.6.2 and Fig.6.8 below. These detail skewness and kurtosis which characterise the nonlinearity of the wave time series. Skewness gives a measure of asymmetry with positive values indicating the wave crests are larger than the troughs and zero indicating equal size. Kurtosis gives a measure of the likelihood of extreme values with a larger value indicating more observations in the tail of the distribution.

Table 6.2: REEF3D surface elevation statistics for the uncalibrated model, BF = 1.25

Sea state	model	H_s error $(\%)$	Skewness	Kurtosis
50yr contour	R3D	7.43	0.212	3.273
	Exp	0.41	0.192	3.252
	Lin	−0.17	−0.004	3.055
Max hindcast	R3D	11.68	0.228	3.225
	Exp	−2.29	0.230	3.350
	Lin	−0.29	−0.011	3.048
Rated 2	R3D	12.18	0.2774	3.67
	Exp	−6.44	−0.0037	3.5815
	Lin	−4.08	−0.006	3.1056

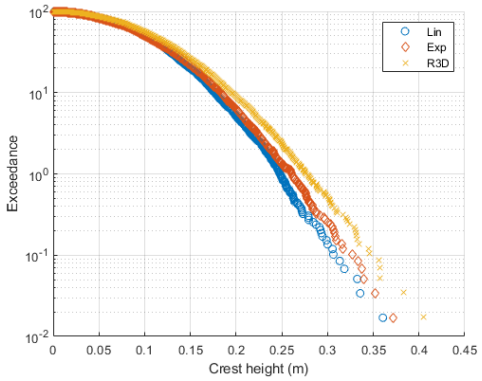

(a) 50yr contour crest heights

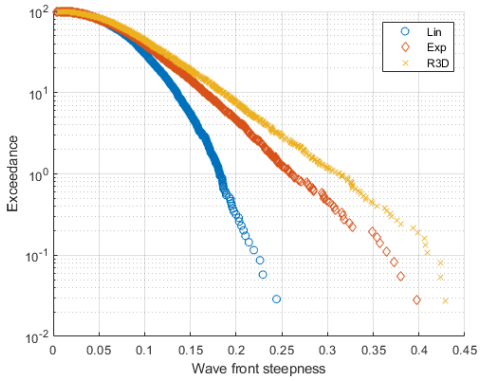

(b) 50yr contour wave front steepness

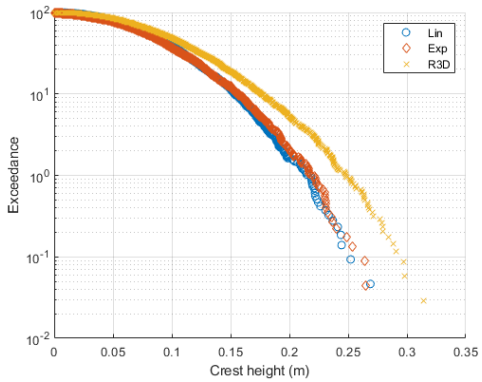

(c) Max hindcast crest heights

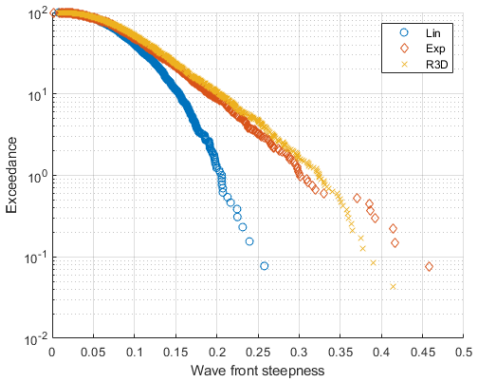

(d) Max hindcast wave front steepness

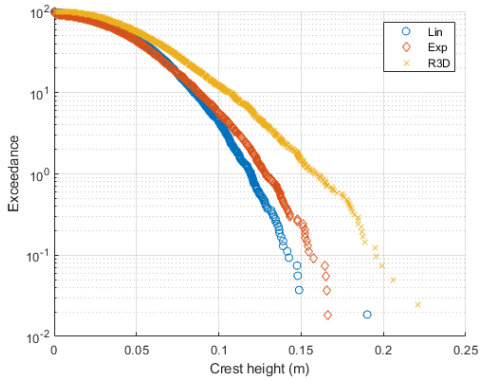

(e) Rated 2 crest heights

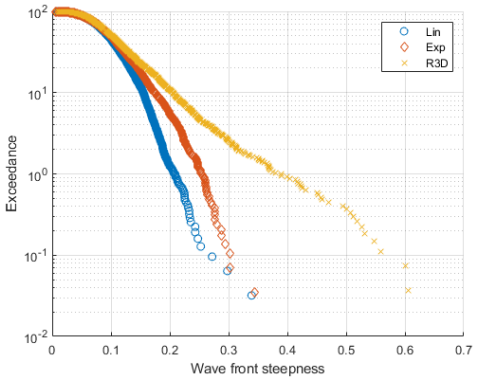

(f) Rated 2 wave front steepness

Figure 6.8: Exceedance plots comparing the crest height and wave front steepness peak distributions.

The REEF3D::FNPF model provides a means to save further lab time when following a constrained focused wave approach in physical experiments by calculating the focused

wave phase correction numerically. It may also be possible in future, with a suitably calibrated model, to produce the constrained focused wave profiles in REEF3D then use the wave surface elevation time series as the input to WEC-Sim or OpenFAST. Fig.6.9 compares the calibrated and uncalibrated NW in the 50yr contour sea state produced in REEF3D vs the experiments. The phase corrections are compared in Fig.6.9c), their similarity suggests that if a more accurate 'digital twin' of the tank were to be developed then the phase corrections calculated from REEF3D could be used in physical tank tests for sea sates of moderate steepness. This would save money on expensive physical tank time.

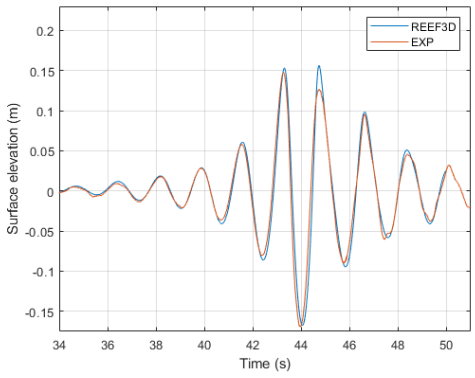

(a) Uncalibrated

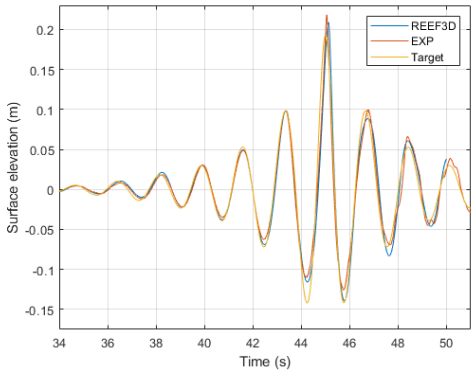

(b) Calibrated with phase correction

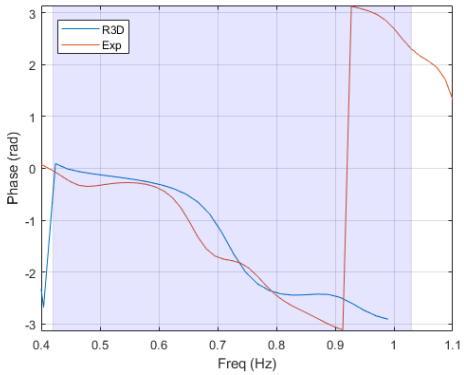

(c) Phase correction

Figure 6.9: a) Uncalibrated NW comparion b) Calibrated NW comparison c) Phase correction comparisons where the blue shading represents the approximate wave frequency range for the 50yr contour sea state.

6.4 Irregular wave results

Fig.6.10 and Fig.6.12 show the spectral density comparisons between the various model setups and the experiments and Fig.6.11 and Fig.6.13 the EVD CDFs. It can be seen in Fig.6.10 that the low frequency response close to the surge natural frequency which is amplified by the extra drag term is well modelled. However although the surge motions are well captured the front mooring load in the wave frequency range is under predicted. MoorDyn only applies the Morison equation in the absence of waves e.g. using the velocity of the line rather than the relative velocity between line and fluid, and so does not capture the wave loading on the excitation of the mooring. There is no under prediction for the back mooring lines, presumably as the line is not under so much tension and has limited transverse motion. The pitch response deviates from experiments most at the pitch natural frequency. The effect of using linear wave theory on the low frequency surge response and front mooring load can be seen along with the exclusion of the drag modification and the use of the uncalibrated REEF3D model. The results for the 50yr Vesilli and max hindcast sea states can be found in appendix C.

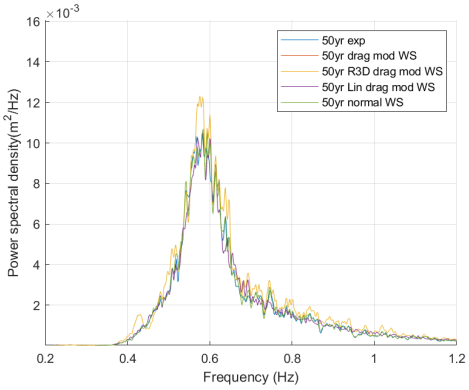

(a) Wave spectrum

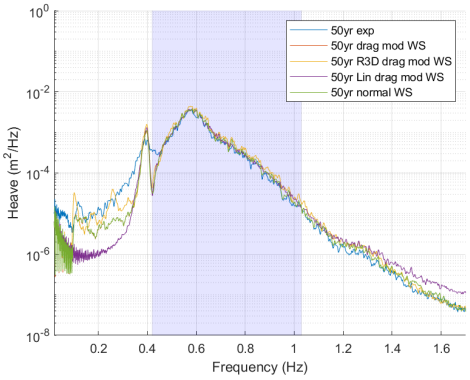

(b) Heave spectral density

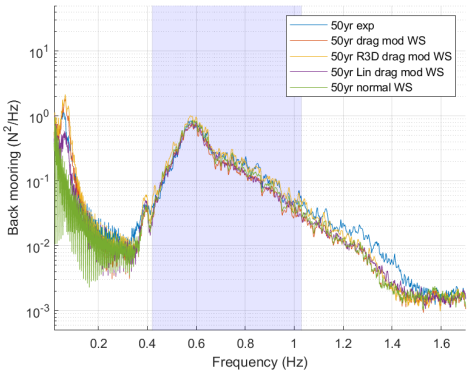

(c) Back mooring load spectral density

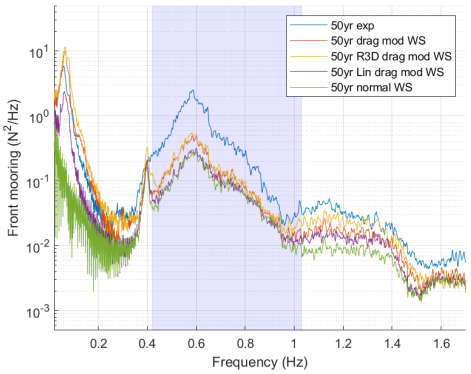

(d) Front mooring load spectral density

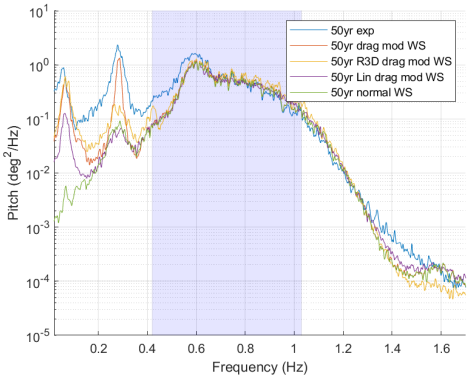

(e) Pitch spectral density

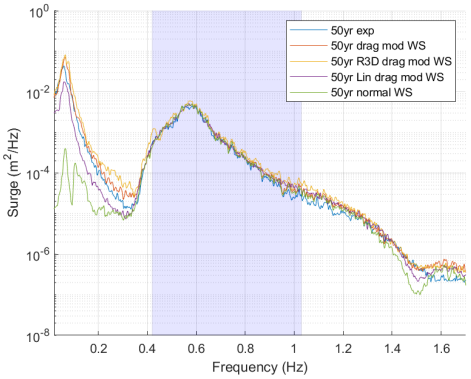

(f) Surge spectral density

Figure 6.10: Power spectral density for the device responses in the 50yr contour sea state. Comparisons between physical and numerical models. The approximate wave frequency region is indicated by the grey background shading.

It can be seen through the discrepancies between the normal and modified WEC-Sim

models in Fig.6.10 (b) and (e) that the pitch and heave responses deviate around the same lower frequency range. This supports the idea that applying a correction to the pitch and heave responses based on the z component of the orbital velocity could be a fruitful approach.

The discrepancy between the front mooring EVD CDFs from the different model configurations show the importance of the inclusion of non-linear wave development and the drag modification. The differences between the characteristic load predictions are presented later in table 6.3.

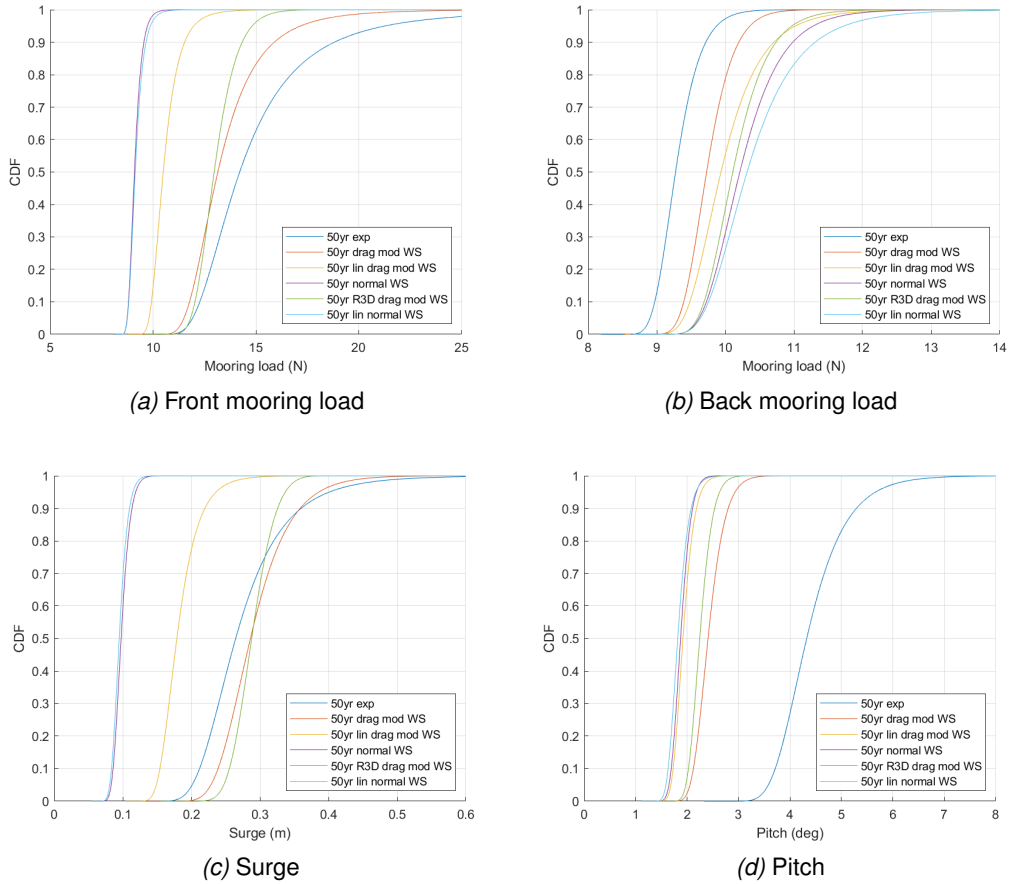

(a) Front mooring load

(b) Back mooring load

(c) Surge

(d) Pitch

Figure 6.11: EVD CDFs for the device responses in the 50 year contour sea state. Comparisons between physical and numerical models. The WEC-Sim model uses the surface elevation from the physical experiments except R3D which uses the time series from REEF3D and 'lin' which uses the target surface elevation according to linear wave theory.

The rated wind thrust generated in the experiments is uncertain due to the calibration of the thruster and the WEC-Sim model doesn't exactly produce the surge and pitch offsets from the recalibrated thruster. A thrust of $3.5N$ is used for the WEC-Sim model as it approximates the surge and pitch offsets, and the static mooring loads but these results should be taken as qualitative only. OpenFAST would presumably be a better choice for modelling with wind but WEC-Sim is used here as it is much quicker and easier to edit the code.

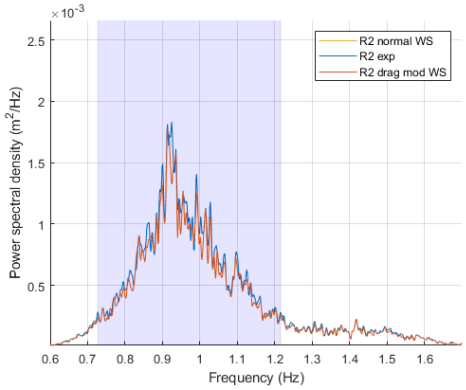

(a) Wave spectrum

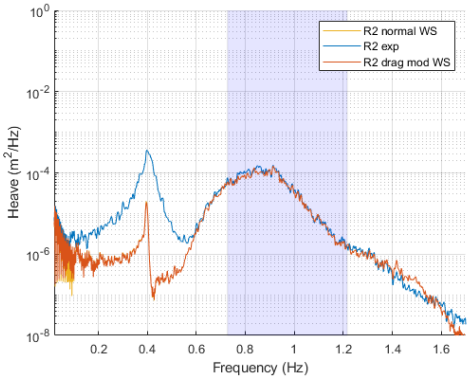

(b) Heave spectral density

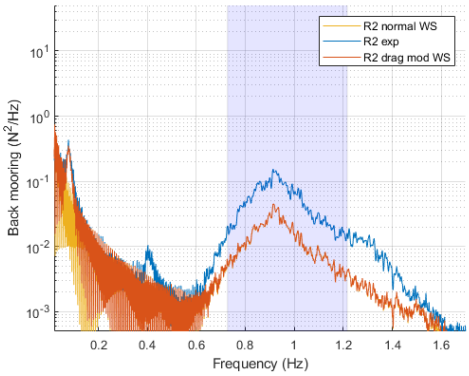

(c) Back mooring load spectral density

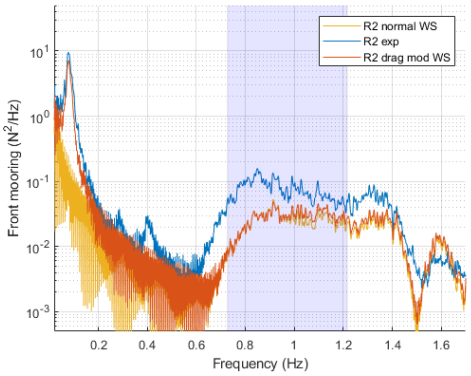

(d) Front mooring load spectral density

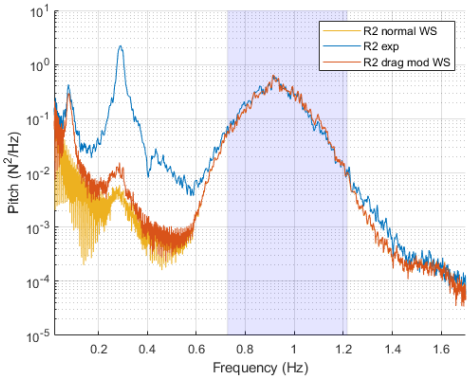

(e) Pitch spectral density

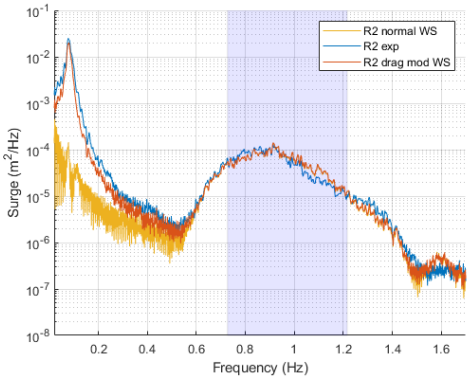

(f) Surge spectral density

Figure 6.12: Power spectral density for the device responses in the Rated 2 sea state. Comparisons between physical and numerical models. The approximate wave frequency region is indicated by the grey background shading.

The impact of using non-linear waves can be seen in the CDFs of the front mooring load and surge but it is of less importance than for the 50 year contour case. The under

prediction of the surge position is due to a reduced low frequency response which could either be due to the modified drag term needing a tuning to the steeper sea state or fluctuations in the thruster output. Fig.6.12 shows that in the Rated 2 sea state both the back and front mooring responses at wave frequency are under predicted.

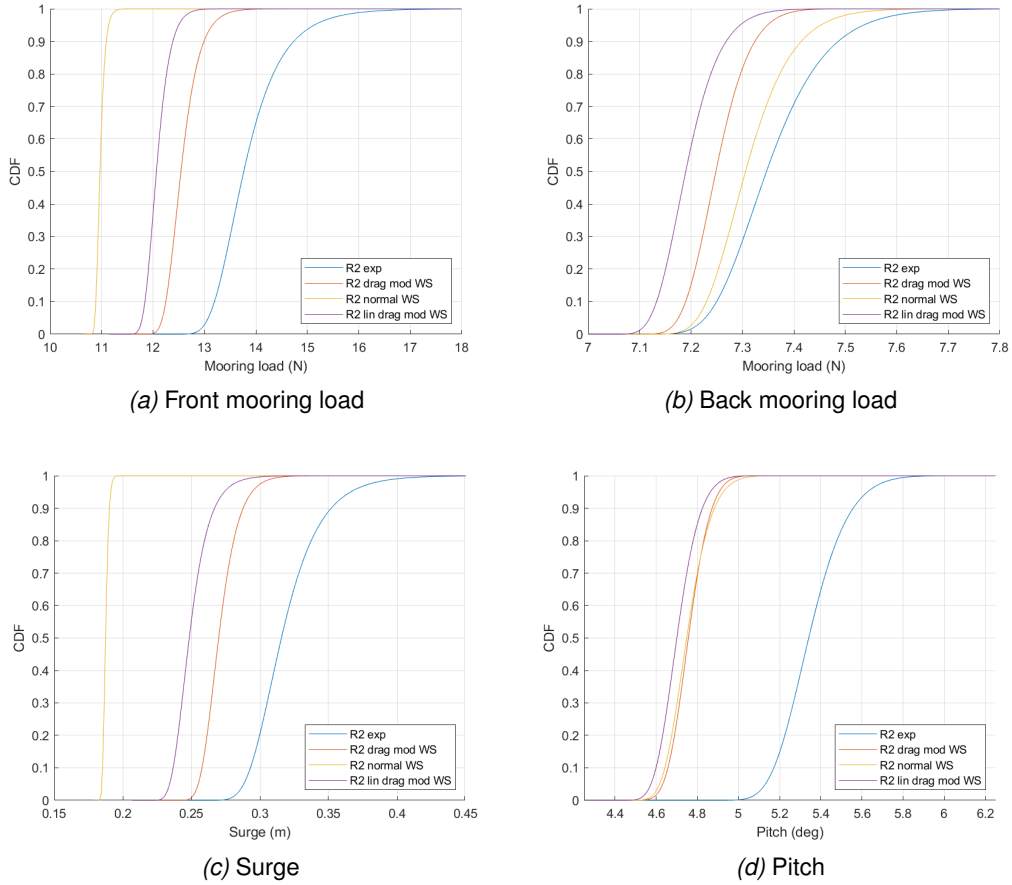

(a) Front mooring load

(b) Back mooring load

(c) Surge

(d) Pitch

Figure 6.13: EVD CDFs for the device responses in the Rated 2 sea state. Comparisons between physical and numerical models. The WEC-Sim model uses the surface elevation from the physical experiments except R3D which uses the time series from REEF3D and 'lin' which uses the target surface elevation according to linear wave theory.

The characteristic load predictions for the front mooring load, pitch and extreme surge position for the different methods and model arrangements are presented in table 6.3.

Table 6.3: Characteristic prediction comparisons for different model cases. FM = front mooring. mean of seeds / $95th$ percentile

Sea state	model	Surge (m)	FM (N)	Pitch (deg)
50yr contour	Exp	$0.258/0.401$	$13.44/21.28$	$4.3/5.7$
	Drag mod	$0.267/0.386$	$12.21/17.17$	$2.5/2.9$
	Lin drag mod	$0.171/0.236$	$10.43/11.98$	$1.9/2.3$
	Normal WS	$0.096/0.119$	$9.19/9.73$	$1.9/2.2$
	R3D drag mod	$0.269/0.337$	$12.41/14.82$	$2.2/2.6$
	Lin normal WS	$0.095/0.115$	$9.24/9.87$	$1.8/2.2$
Rated 2	Exp	$0.272/0.350$	$13.17/14.77$	$5.2/5.5$
	Drag mod	$0.254/0.294$	$12.23/13.16$	$4.7/4.9$
	Normal WS	$0.187/0.191$	$11.01/11.14$	$4.7/4.9$
	Lin drag mod	$0.241/0.274$	$11.96/12.50$	$4.7/4.9$

Comparing the percentage errors of the characteristic load predictions from the different WEC-Sim model configurations as shown in Fig.6.14 it is clear that there are only small differences in the predictions when the normal WEC-Sim model is used with different wave theories. However, for the 50 year contour case if the drag modification is implemented large differences between the predictions for wave theories emerge for the surge and front mooring responses. This is due to the larger steeper waves having larger orbital velocities and so increasing the surge excitation and viscous drift. This effect is much more prominent for the 50 year contour case than for Rated 2, partly due to the larger waves and orbital velocities but also likely due to the reduced importance of hydrodynamic loading relative to wind. Using linear wave theory appears to have much less of an impact on the characteristic load prediction in the Rated 2 case but the impact of the modified drag term is still significant.

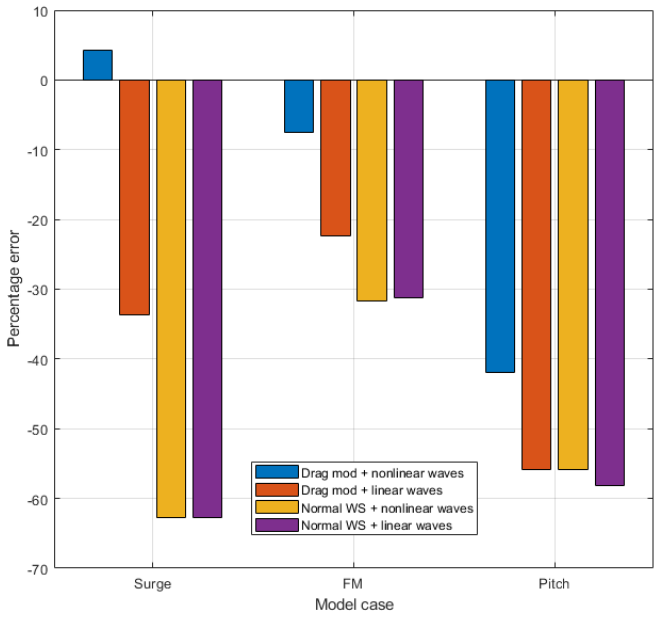

(a) 50 year contour

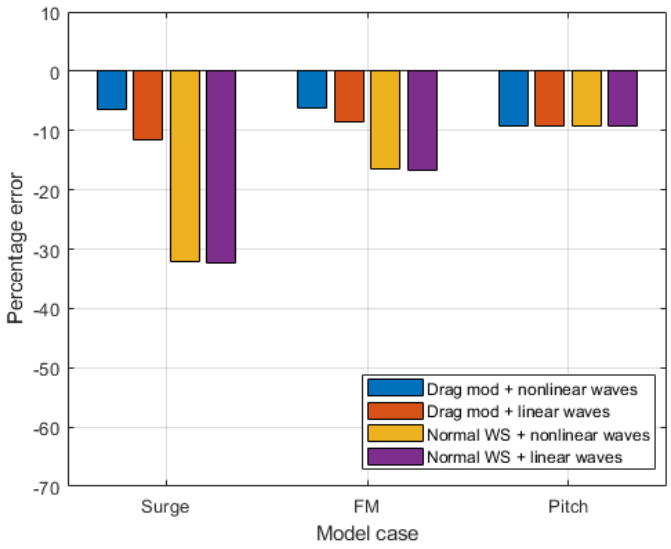

(b) Rated 2

Figure 6.14: Percentage error in the characteristic load predictions for the different WEC-Sim model configurations.

Johannesson et al. (2016) developed a methodology for uncertainty quantification to be used for probabilistic design of ORE devices. The method quantifies the relative

contributions of the sources of uncertainty by varying the parameters in the numerical model one at a time compared to a baseline model. However, the significant impact of varying the wave theory and drag modification in combination shown in Fig.6.14 demonstrate how applying a univariate approach for uncertainty quantification would not be appropriate in this instance as the assumption that the uncertainty can be assessed by varying one parameter at a time is not met. E.g. if the baseline numerical model used linear wave theory then the uncertainty contribution from the drag modification in the absence of realistic waves would be under estimated. It is therefore not applied here.

A full long term approach has not been carried out due to the discrepancies between the modelled and measured mooring loads and pitch responses. This will be undertaken at a later date when Moordyn version 2 is released and further work capturing the low frequency pitch response is completed. Although the full long term approach is considered the best method for predicting design loads it is questionable whether this holds true if the model doesn't capture the extremes. In such circumstances an experimental approach such as following the contour method may well be preferable. A caveat to this point is that if the turbulent wind loading dominates the response in the design sea then perhaps the shortcomings of the hydrodynamic model are less relevant.

6.5 Standard model analysis

Up to this point the response modelling has attempted to be as accurate as possible to the measurements from the physical experiments. It would also be interesting however to gauge how well the constrained focused waves (CRRWs and CG2s) do at estimating characteristic loads compared to the irregular wave method when using an unedited response model more in line with one used in industry which does not have the additional drag term for modelling viscous drift. The unedited WEC-Sim model is therefore run using waves produced from linear theory to investigate. The weak nonlinearities are included in the model as models typically used in industry such as Bladed

and OpenFAST apply QTFs, or at the very least mean drift forces, to capture these effects. Although in this instance they are not thought to significantly impact the low frequency surge motions as Fig.6.2 shows. WEC-Sim is used here for consistency. This analysis is considered sufficient in this instance as the QTFs don't significantly alter the results for the surge or front mooring as demonstrated by the similarity between the OpenFAST and WEC-Sim models in Fig.6.2.

Fig.6.15 shows how the constrained focused waves compare with the EVD for the 50 year contour sea state. They produce estimates larger than the irregular wave method for the mooring loads and at the higher percentiles of the EVD. The Back mooring loads are larger than the front for this model setup, this is a significant difference to the experiments and modified WEC-Sim model due to the significant under prediction of the low frequency surge response.

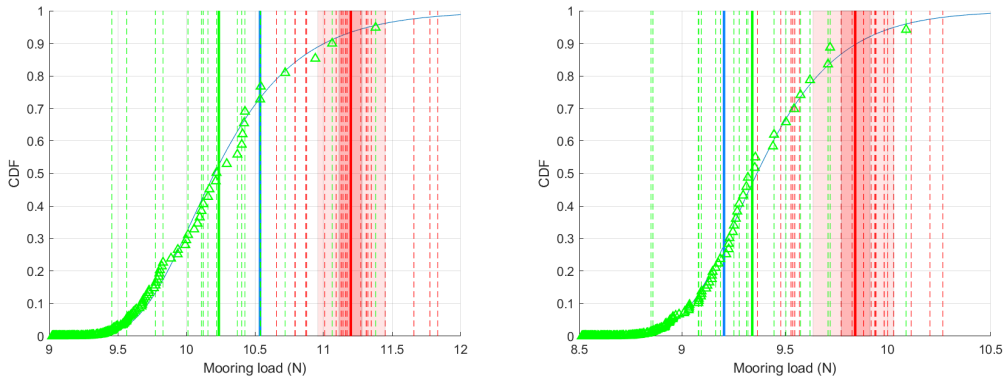

(a) Back mooring *(b)* Front mooring

Figure 6.15: Characteristic load estimates from linear target waves and WEC-Sim model with weak nonlinearities and without the additional drag term.

The characteristic load estimates for the pitch and nacelle acceleration shown in Fig.6.16 reach high percentiles in the EVD for the 50 year contour sea state. The same is true of the front mooring and pitch responses for the Rated 2 sea state in Fig.6.17. It is expected that, as the $99th$ percentile target is used according to linear assumptions, the closer the response model conforms to these assumptions the closer the characteristic load estimates will be to this value.

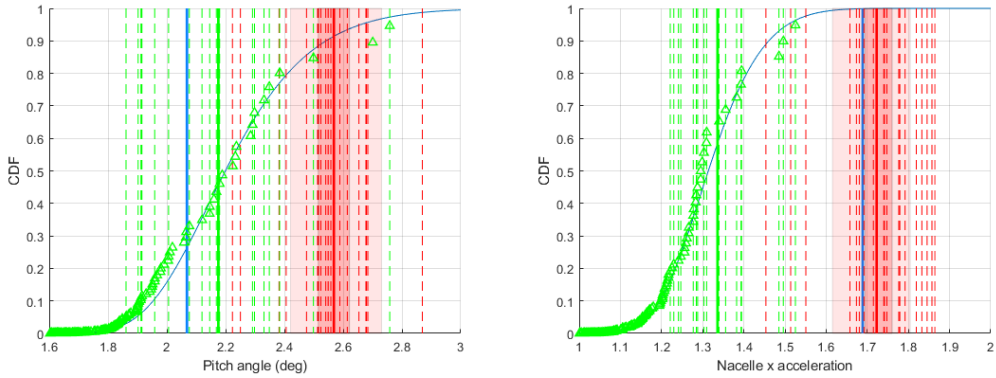

(a) Pitch *(b)* Nacelle x acceleration

Figure 6.16: Characteristic response estimates from linear target waves and WEC-Sim model with weak nonlinearities and without the additional drag term.

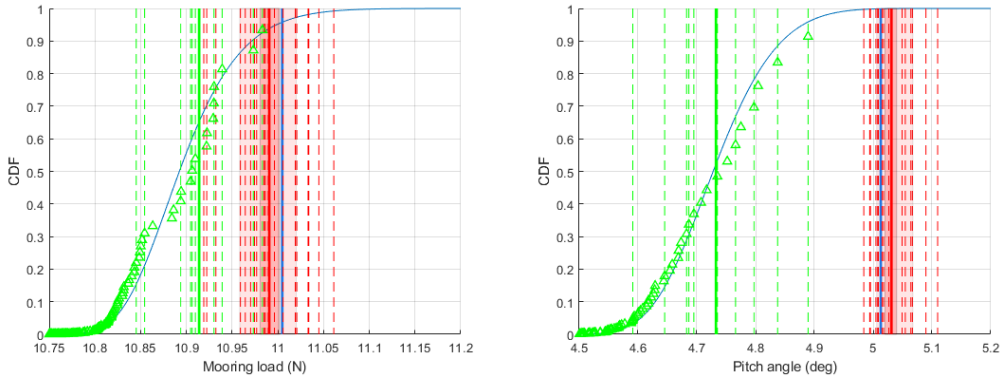

(a) Front mooring *(b)* Pitch

Figure 6.17: Characteristic estimates for the Rated 2 sea state from linear target waves and WEC-Sim model with weak nonlinearities and without the additional drag term.

6.6 Summary

A simple modified drag term was introduced which greatly improved the capture of the extreme surge and front mooring responses. The improved model accuracy due to this approach support the conclusions in Ma et al. (2020) and Robertson and Wang (2021) on the viscous drag effects. The pitch response was less straightforward to capture and is left for future work. The dynamic part of the mooring response was under predicted for the front mooring, most likely due to the fact that the current version of Moordyn,

used in WEC-Sim and OpenFAST, doesn't take into account the wave kinematics. A mooring model which does account for these dynamics, such as Orcaflex, is therefore likely to give more accurate results. WEC-Sim is due to be updated with Moordyn version 2 some time in 2023.

Even with the modified drag term, non-linear wave development and a high gamma were also found to be important for capturing the extreme responses in unidirectional waves. This is likely to still be true, but to a lesser extent, with increased directional spreading. To produce accurate results numerically therefore a nonlinear wave model is required.

A rough, uncalibrated, REEF3D:FNPF model for the wave basin was set up to run in real time and found to produce wave time series whose statistics were approximately in line with the physical experiments for moderate seas. However, it would need a further calibration effort to be used for steeper sea states such as the Rated 2 and Max hindcast cases. It can also be used to save lab time by calibrating the focused waves.

The edited WEC-Sim model was found to be a useful tool for understanding the extreme responses of the device. The unedited WEC-Sim model with linear wave theory was used to demonstrate how the characteristic predictions using the focused and constrained focused wave method were more conservative compared with the irregular waves than if using the experiments or more complex response models. This indicates that the method is very unlikely to give an under prediction if using standard industry tools which do not as yet capture all the more complex physics (drag and nonlinear wave development).

6.7 Questions and future work

The success of the modified drag term in modelling the low frequency surge raises the question of whether a similar drag modification could be used to improve the pitch response. The significant effect that the wave theory used as input to the numerical model has on the low frequency surge response highlights the importance of using

realistic inputs. An accurate surrogate model capturing the statistics of a realistic range of sea states, perhaps with small directional spreading to reduce unrealistic nonlinear wave amplification, should be developed to quickly produce realistic irregular wave inputs to numerical models. An accurate nonlinear wave model however would still be required to produce the focused and constrained focused waves in the absence of a physical wave tank.

Turbulent wind has an impact on low frequency surge motions and so the conclusions from this chapter should be reassessed in the presence of turbulent wind. This however would likely require a similar 'response conditioned focused wind' approach to be developed alongside the short design waves. The contour method assumes the response increases substantially with an increasing return period. During the rated sea states wind is dominating most responses and so a fairly large reduction in the return period contour (in terms of H_s T_p) could produce similar extreme responses with much higher probability of occurrence. This means taking the characteristic load at the mean or a percentile between $70-99$ may be an under prediction. On the other hand, there's a large safety factor and unidirectional waves from an unfavourable direction are used (DNV floating foundations DNV (2013) says if an unfavourable direction is assumed then no inflation factor need be used). In order to know whether the contour approach is appropriate an accurate but fast response model would need to be used to conduct a full long term analysis and compare to the contour method. This is left for future work as the issues with the response model and environmental characterisation discussed in this chapter are thought to restrict the validity of the analysis.

Chapter 7

Conclusions

Chapter summary

In this chapter the key findings of the thesis are summarised in relation to the stated aims and objectives. Future work and unresolved questions are also highlighted.

7.1 Summary

The key objectives of this thesis were to produce a constrained focused wave methodology to improve the efficiency of the design process in line with the existing design standards and assess the ability of existing, fast, mid-fidelity numerical models to model the extremes of floating ORE devices.

The Xmed buoy case study demonstrated the difficulties in design load prediction for dynamic ORE devices and the limits of existing fast numerical models and physical wave modelling. A WEC-Sim model was calibrated and validated and used to explore the applicability of constrained wave methods. Existing constrained wave approaches such as the CRRW and DLG methods for predicting the short term EVD of a response were shown to produce underestimates of the mooring response due to the condition of the nonlinear response being a small perturbation from the linear one being violated. Inflating the linear target waves to a much higher percentile was found to produce a CDF and characteristic response more in line with the prediction from the irregular waves following IEC design standards. This also raised questions about the suitability of the widely used approach of scaling focused waves to the most probable maximum when investigating extreme responses of devices generically. It is therefore recommended that when studying the extreme responses of floating ORE using fo-

cused waves that the target amplitude or response should be inflated to the region of the $80th$ - $99th$ percentile.

The Mocean experiments developed a quick approach to calibrating constrained focused waves and demonstrated the limitations of short design wave methods in steep sea states due to wave breaking, non-linear wave development and snatch loading. It is possible that using NewWaves scaled to the 99th percentile and taking the mean of the upper half of the largest responses could produce characteristic load predictions more in agreement with the irregular wave method when snatch loading occurs. The evidence from this single case however is weak and so more data from other cases would need to be assessed to check this. It is recommended that when running constrained focused waves in a physical or numerical wave tank that the calibration from a single focused wave, in the form of a single phase correction, be used to improve the accuracy of the generated wave in the shortest amount of time.

The FOWT experiments demonstrated the ability of constrained focused waves to produce design load predictions in line with post processing methods commonly used in the IEC standards. The addition of an extra term in the Morison equation in the WEC-Sim model to account for viscous drift was shown to significantly improve the capture of the low frequency surge motions required to model extreme mooring loads. However, the mooring model under predicts the loads, likely as a result of neglecting the wave kinematics. Constrained wave groups were introduced to model the extreme mooring loads in the physical experiments and are suggested for use as a generic design wave option when studying extremes due to viscous drift. The constrained wave approach developed in this thesis was shown to produce conservative results relative to the irregular wave method when the analysis was applied using a numerical model with a setup judged closest to that likely used in industry. Although such models are known to capture the low frequency device motions poorly and so lead to under predictions.

Whilst there is a large uncertainty in the environmental characterisation of each site studied in this work, when a suitable adjustment to the contour is made based on the

breaking limit, we can have most confidence in the regions of the return contour close to the steepness limit. This is encouraging as it is in this region where the design seas are likely to be found. However, it is also in this region where a small change in the H_s and T_p values will lead to the largest changes in return period and so potentially invalidate the contour approach. The validity of contour methods still require confirming therefore, and validated response models are needed for this purpose to run the simulations comprising the full long term method for comparison.

Based on the limitations observed in these experiments due to wave breaking and steepness, Fig.5.49 hlwas produced to try and specify some regions of applicability for the constrained wave method in physical experiments.

The developed constrained wave methodology consists of inflating the linear percentile which is scaled to in order to alleviate the shortcomings of neglecting history effects. In instances where nonlinear responses arise, the response conditioned focused waves will not necessarily produce extreme responses and so knowledge of the particular device and response will be required to understand the nature of the wave or wave sequence which should be used in it's place. Care should be taken when using short design wave approaches in the steeper sea states. The MLER profile scaled to the 99th percentile gave a design load prediction in line with the IEC post processing approach for pitch related responses, provided they are not affected by snatch loading. Constrained wave methods need to be employed to model extreme mooring loads where surge drift is considered important.

7.2 Future work

The improvement of fast mid-fidelity numerical models such as WEC-Sim and OpenFAST in accurately modelling the physics responsible for the extreme responses of devices in storm conditions is a necessary prerequisite to unlocking the advantages of full probabilistic design.

As shown in this thesis, producing fast, accurate nonlinear wave elevation time series

is essential to modelling some extreme responses accurately. Producing such time series using FNPF based models may be the answer when generating constrained focused waves. For the modelling of irregular waves however a surrogate model approach could lead to great time savings. Analytical second order wave models may or may not be appropriate, depending on how well realistically directionally spread storm conditions reflect the extreme statistics. The impact of directionally spread waves on the low frequency surge response of semi-sub FOWTs is an interesting area to investigate because as the extreme amplitudes reduce in directionally spread seas the magnitude of the response will be reduced. Furthermore, the extension of the CRRWs to directionaly spread seas to investigate responses which may be more extreme or relevant when subjected to loading from multiple directions would be of interest. The roll stability of a hinged raft for example would make a good case study. A comparison of the average of maxima approach employed in this thesis with the most probable maximum estimate assuming a Gumbel distribution should be made in future alongside the high percentile method.

The application of reponse conditioned methods to fixed structures, shallow water conditions and more complex cases involving sloshing of liquid hydrogen on floating vessels are some of the future applications relevent to offshore renewables. A potentially important effect which focused waves would be suitable to study would be the slamming loads on ORE devices. The development of a focused wave method for producing breaking waves would therefore be highly relevant.

The further study of snatch load events and how well the short design wave methods developed here can estimate characteristic mooring loads is necessary to draw meaningful conclusions. There are many different types of WEC and FOWT which have not been modeled in this thesis and so the application of the method to these is an essential step to drawing generalisable conclusions. It is possible that for less dynamic devices that the 99th percentile inflation would need to be relaxed. It would also be interesting to study the effect of using a fast running frequency domain model to estimate

the RAOs instead of haveing to run a long time domain simulation or experiment.

The characteristic prediction methodology outlined in this thesis shows promise under the right conditions, particularly for FOWTs. The extension of this methodology to include 'focused wind' time series and whether or not this produces significantly different estimates to just applying wave loading with constant wind is an important line of further enquiry.

Once the method has been extended to wind the applicability of the approach to FOWTs in operating conditions with turbulent wind and turbine control should be investigated. This is of particular interest as for some locations and response types it is likely to be the conditions at rated wind speed, where the thrust is at a maximum, which produce the extremes. The application of the method to cases where a WEC is in power production mode could also produce interesting results.

The application of the short design weave methods to dynamic power cables, tower base loads or floating tidal devices was not discussed in this thesis and would make for interesting investigations.

Appendix A

Slepian model

A.1 Slepian model process overview

A Slepian model process can be obtained by conditioning a Gaussian vector process $\mathbf{V}(\mathbf{t})$ on a set of vectors $\mathbf{Y}$. The model is breifly outlined here following Dietz (2005).

The model follows a linear regression of $\mathbf{V}(\mathbf{t})$ on $\mathbf{Y}$

$$[\mathbf{V}(t)|\mathbf{Y}] = \hat{\mathrm{E}}[\mathbf{V}(t)|\mathbf{Y}] + \Delta(t) \tag{A.1}$$

where $\hat{\mathrm{E}}[\mathbf{V}(t)|\mathbf{Y}]$ is the conditional mean vector function.

$$\hat{\mathrm{E}}[\mathbf{V}(t)|\mathbf{Y}] = \mathrm{E}[\mathbf{V}] + \mathrm{Cov}[\mathbf{V},\mathbf{Y}^{\mathrm{T}}]\mathrm{Cov}[\mathbf{Y},\mathbf{Y}^{\mathrm{T}}]^{-1}(\mathbf{Y}-\mathrm{E}[\mathbf{Y}]) \tag{A.2}$$

where $\mathrm{E}[\cdot]$ is the mean and $\mathrm{Cov}[\cdot]$ the covariance. $\Delta(t)$ is the residual vector process, which is a zero-mean Gaussian process, with the covariance matrix function given as

$$\begin{aligned}\mathrm{Cov}[\Delta(t_1),\Delta^{\mathrm{T}}(t_2)] = \mathrm{Cov}[\mathbf{V}(t_1),\mathbf{V}^{\mathrm{T}}(t_2)] - \\ \mathrm{Cov}[\mathbf{V}(t_1),\mathbf{Y}^{\mathrm{T}}(t_2)]\mathrm{Cov}[\mathbf{Y},\mathbf{Y}^{\mathrm{T}}]^{-1}\mathrm{Cov}[\mathbf{Y},\mathbf{V}^{\mathrm{T}}(t_2)]\end{aligned} \tag{A.3}$$

For a Gaussian process the covariance matrix of the residual process matches with the conditional covariance matrix, $\mathrm{Cov}[\Delta(t_1),\Delta^{\mathrm{T}}(t_2)] = \mathrm{Cov}[\mathbf{V}(t_1),\mathbf{V}^{\mathrm{T}}(t_2)|\mathbf{Y}]$.

Appendix B

REEF3D model

B.1 REEF3D::FNPF theory

The main aspects of the REEF3D nonlinear potential flow model are presented below following Wang et al. (2021c), where more detail, including on the discretisation and wave breaking formulation, can be found.

The governing equation for potential flow is the Laplace equation:

$$\frac{\partial^2 \phi}{\partial x^2} + \frac{\partial^2 \phi}{\partial y^2} + \frac{\partial^2 \phi}{\partial z^2} = 0 \tag{B.1}$$

The free surface conditions, that the surface particles remain at the free surface and the pressure there should be equal the atmospheric pressure, are given by:

$$\frac{\partial \eta}{\partial t} = -\frac{\partial \eta}{\partial x}\frac{\partial \widetilde{\phi}}{\partial x} - \frac{\partial \eta}{\partial y}\frac{\partial \widetilde{\phi}}{\partial y} + \widetilde{w}\left(1 + \left(\frac{\partial \eta}{\partial x}\right)^2 + \left(\frac{\partial \eta}{\partial y}\right)^2\right), \tag{B.2}$$

$$\frac{\partial \widetilde{\phi}}{\partial t} = -\frac{1}{2}\left(\left(\frac{\partial \widetilde{\phi}}{\partial x}\right)^2 + \left(\frac{\partial \widetilde{\phi}}{\partial y}\right)^2 - \widetilde{w}^2\left(1 + \left(\frac{\partial \eta}{\partial x}\right)^2 + \left(\frac{\partial \eta}{\partial y}\right)^2\right)\right) - g\eta \tag{B.3}$$

Where $\widetilde{\phi} = \phi(\mathbf{x}, \eta, t)$ is the velocity potential at the free surface η. $\widetilde{w}$ is the vertical velocity at the free surface.

At the sea bed the bottom boundary condition assuring the fluid particles can't pass through the bed is given by:

$$\frac{\partial \phi}{\partial z} + \frac{\partial h}{\partial x}\frac{\partial \phi}{\partial x} + \frac{\partial h}{\partial y}\frac{\partial \phi}{\partial y} = 0, \quad z = -h \tag{B.4}$$

Where h is the water depth.

A sigma coordinate system is used, the conversion of which from Cartesian is given by:

$$\sigma = \frac{z + h(\mathbf{x})}{\eta(\mathbf{x},t) + h(\mathbf{x})} \tag{B.5}$$

After this transformation the velocity potential is denoted by Φ and the above equations rewriten as:

$$\begin{array}{ll} \Phi = \widetilde{\phi} & ,\sigma = 1; \\ \frac{\partial^2\Phi}{\partial x^2} + \frac{\partial^2\Phi}{\partial y^2} + \left(\frac{\partial^2\sigma}{\partial x^2} + \frac{\partial^2\sigma}{\partial y^2}\right)\frac{\partial\Phi}{\partial\sigma} + 2\left(\frac{\partial\sigma}{\partial x}\frac{\partial}{\partial x}\left(\frac{\partial\Phi}{\partial\sigma}\right) + \right. & \\ \left.\frac{\partial\sigma}{\partial y}\frac{\partial}{\partial y}\left(\frac{\partial\Phi}{\partial\sigma}\right)\right) + \left(\left(\frac{\partial\sigma}{\partial x}\right)^2 + \left(\frac{\partial\sigma}{\partial y}\right)^2 + \left(\frac{\partial\sigma}{\partial z}\right)^2\right)\frac{\partial^2\Phi}{\partial\sigma^2} = 0 & ,0 < \sigma < 1; \\ \left(\frac{\partial\sigma}{\partial z} + \frac{\partial h}{\partial x}\frac{\partial\sigma}{\partial x} + \frac{\partial h}{\partial y}\frac{\partial\sigma}{\partial y}\right)\frac{\partial\Phi}{\partial\sigma} + \frac{\partial h}{\partial x}\frac{\partial\Phi}{\partial x} + \frac{\partial h}{\partial y}\frac{\partial\Phi}{\partial y} = 0 & ,\sigma = 0 \end{array} \tag{B.6}$$

Where $\sigma = 1$ corresponds to the free surface and 0 the sea bed. Particle velocities can be calculated from:

$$u(\mathbf{x},z) = \frac{\partial\Phi(\mathbf{x},z)}{\partial x} = \frac{\partial\Phi(\mathbf{x},\sigma)}{\partial x} + \frac{\partial\sigma}{\partial x}\frac{\partial\Phi(\mathbf{x},\sigma)}{\partial\sigma}, \tag{B.7}$$

$$v(\mathbf{x},z) = \frac{\partial\Phi(\mathbf{x},z)}{\partial y} = \frac{\partial\Phi(\mathbf{x},\sigma)}{\partial y} + \frac{\partial\sigma}{\partial y}\frac{\partial\Phi(\mathbf{x},\sigma)}{\partial\sigma}, \tag{B.8}$$

$$w(\mathbf{x},z) = \frac{\partial\Phi(\mathbf{x},z)}{\partial z} = \frac{\partial\sigma}{\partial z}\frac{\partial\Phi(\mathbf{x},\sigma)}{\partial\sigma} \tag{B.9}$$

Appendix C

FOWT Response spectra from the numerical models

C.1 50 year Vesilli sea state

The same trends are visible in Fig.C.1 as were in Fig.6.10. That is, the under prediction of the surge and front mooring responses of the WEC-Sim model. In this case however, the edited WEC-Sim model leads to an over prediction of the low frequency surge response, this is because it is a less steep sea state and the additional drag term was tuned to the steeper 50 year contour sea state.

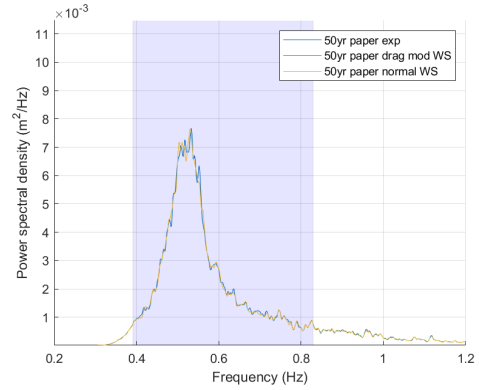

(a) Wave spectrum

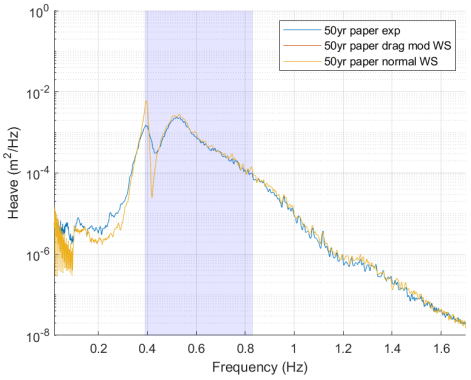

(b) Heave spectral density

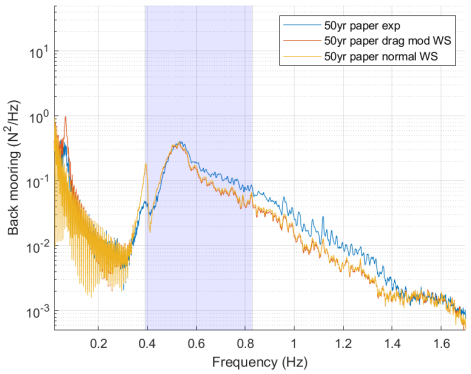

(c) Back mooring load spectral density

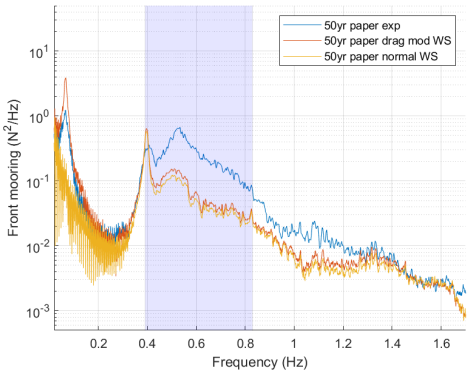

(d) Front mooring load spectral density

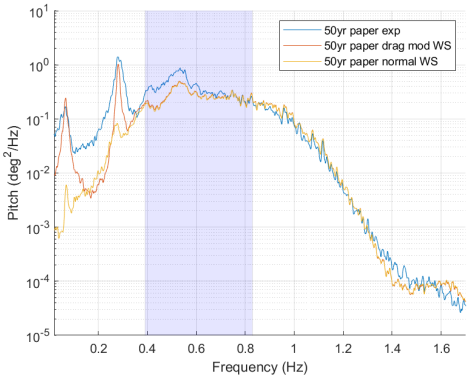

(e) Pitch spectral density

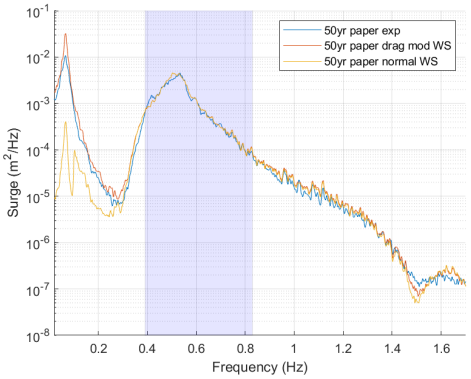

(f) Surge spectral density

Figure C.1: Power spectral density for the device responses in the 50yr Vesilli sea state. Comparisons between physical and numerical models. The approximate wave frequency region is indicated by the grey background shading.

C.2 Maxhindcast sea state

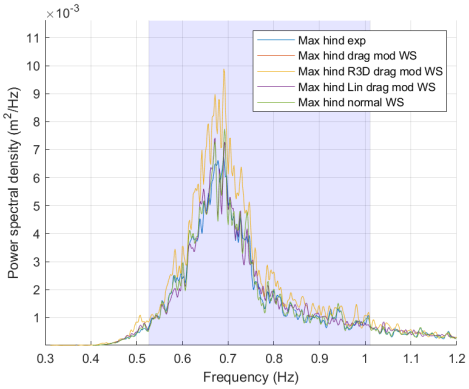

(a) Wave spectrum

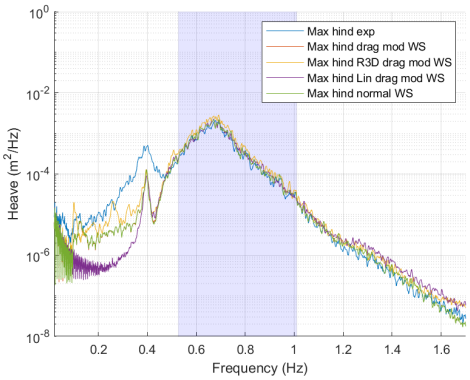

(b) Heave spectral density

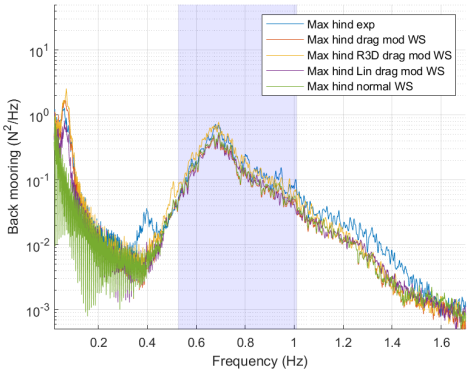

(c) Back mooring load spectral density

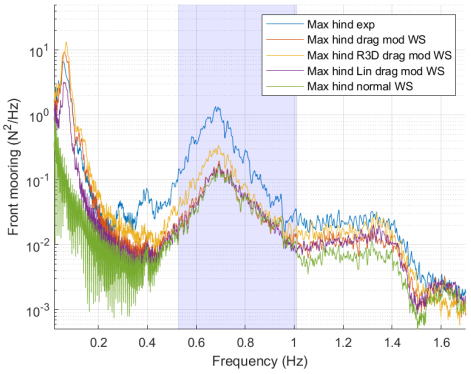

(d) Front mooring load spectral density

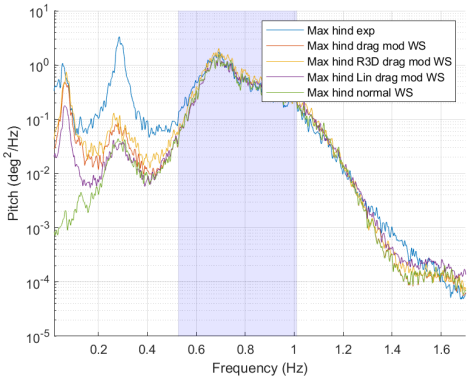

(e) Pitch spectral density

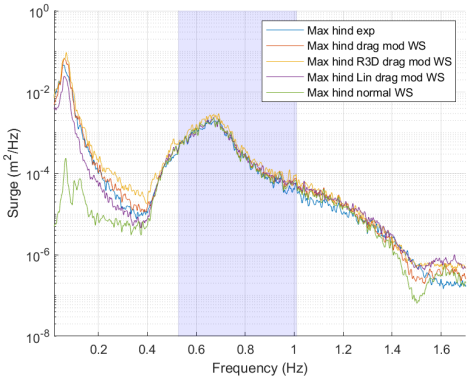

(f) Surge spectral density

Figure C.2: Power spectral density for the device responses in the Maxhindcast sea state. Comparisons between physical and numerical models. The approximate wave frequency region is indicated by the grey background shading.

The same trends are visible in Fig.C.2 as were in Fig.6.10. That is, the underprediction of the surge and front mooring responses of the WEC-Sim model.

List of references

Adegeest, L., 1998. Use of nonlinear sea-load simulations in the design of ships. Proceedings of PRADS'1998, Delft .

Airy, G.B., 1845. Tides and waves. B. Fellowes.

Alford, L.K., 2008. Estimating Extreme Responses Using a Non-Uniform Phase Distribution. Ph.D. thesis.

Alford, L.K., Maki, K.J., 2015. Generating large deterministic water waves for numerical simulation. Ann Arbor 1001, 48109.

Allen, C., Viscelli, A., Dagher, H., Goupee, A., Gaertner, E., Abbas, N., Hall, M., Barter, G., 2020. Definition of the UMaine VolturnUS-S Reference Platform Developed for the IEA Wind 15-Megawatt Offshore Reference Wind Turbine. Technical Report. National Renewable Energy Lab.(NREL), Golden, CO (United States).

Ambühl, S., Kramer, M., Sørensen, J.D., 2014. Reliability-based structural optimization of wave energy converters. Energies 7, 8178–8200.

ANSYS, i., 2024. Ansys simulation software. URL: https://www.ansys.com/. accessed on 2024-03-17.

Atcheson, M., Cruz, J., Martins, T., Johannesson, P., Svensson, P., 2019. Quantification of load uncertainties in the design process of a wec, in: Proceedings of the Thirteenth European Wave and Tidal Energy Conference.

Babarit, A., 2014. Nemoh, laboratory for research in hydrodynamics. Energy, Environment, and Atmosphere, http://lheea. ec-nantes. fr/doku. php/emo/nemoh/start .

Bachynski, E.E., Moan, T., 2014. Ringing loads on tension leg platform wind turbines. Ocean engineering 84, 237–248.

Bennett, S., Hudson, D., Temarel, P., 2012. A comparison of abnormal wave generation techniques for experimental modelling of abnormal wave–vessel interactions. Ocean engineering 51, 34–48.

Department for Business, Energy Industrial Strategy, U.g., 2022. british-energy-security-strategy. URL: https://www.gov.uk/government/publications/british-energy-security-strategy. accessed on 2022-08-01.

Caio, A., Davey, T., McNatt, J.C., 2021. Preliminary hydrodynamic assessment of mocean energy's blue star wec via fast-turnaround physical model testing, in: 14th European Wave and Tidal Energy Conference; under review, European Tidal and Wave Energy Conference.

Carbon Trust, A., 2012. Carbon Trust Foreword to UK Wave Resource Study. Technical Report. Tech. Rep. October.

Cassidy, M.J., 2011. Offshore foundation systems for resource recovery: Assessing the three-dimensional response of jack-up platforms. KSCE Journal of Civil Engineering 15, 623–634.

Christou, M., Ewans, K., 2014. Field measurements of rogue water waves. Journal of Physical Oceanography 44, 2317–2335.

Clark, C.E., DuPont, B., 2018. Reliability-based design optimization in offshore renewable energy systems. Renewable and Sustainable Energy Reviews 97, 390–400. URL: https://www.sciencedirect.com/science/article/pii/S1364032118306154, doi:https://doi.org/10.1016/j.rser.2018.08.030.

Coe, R., Michelen, C., Eckert-Gallup, A., Yu, Y.H., Rij, J.V., 2016a. WEC Design Response Toolbox v. 1.0. Technical Report. Sandia National Lab.(SNL-NM), Albuquerque, NM (United States).

Coe, R.G., Michelen, C., Eckert-Gallup, A., Sallaberry, C., 2018. Full long-term design response analysis of a wave energy converter. Renewable Energy 116, 356–366.

Coe, R.G., Michelen, C., Yu, Y.H., Rij, J.V., Eckert-Gallup, A.C., 2016b. WDRT: A toolbox for design-response analysis of wave energy converters. Technical Report. Sandia National Lab.(SNL-NM), Albuquerque, NM (United States).

Coe, R.G., Rosenberg, B.J., Quon, E.W., Chartrand, C.C., Yu, Y.H., Van Rij, J., Mundon, T.R., 2019. Cfd design-load analysis of a two-body wave energy converter. Journal of Ocean Engineering and Marine Energy 5, 99–117.

Coe, R.G., Yu, Y.H., Van Rij, J., 2017. A survey of wec reliability, survival and design practices. Energies 11, 4.

Coles, D., Angeloudis, A., Greaves, D., Hastie, G., Lewis, M., Mackie, L., McNaughton, J., Miles, J., Neill, S., Piggott, M., et al., 2021. A review of the uk and british channel islands practical tidal stream energy resource. Proceedings of the Royal Society A 477, 20210469.

Collins, K.M., Stripling, S., Simmonds, D.J., Greaves, D.M., 2018. Quantitative metrics for evaluation of wave fields in basins. Ocean Engineering 169, 300–314.

Commission, I.E., et al., 2015. Marine Energy: Wave, Tidal and Other Water Current Converters. Tidal Energy Resource Assessment and Characterization. International Electrotechnical Commission.

Cruz Atcheson Consulting Engineers, L., 2018. D1.1Advanced Wave-Structure Interaction Model –Theory and User Manual. Technical Report. Tech. Rep.

Cummins, W., Iiuhl, W., Uinm, A., 1962. The impulse response function and ship motions .

Davidson, J., Costello, R., 2020. Efficient nonlinear hydrodynamic models for wave energy converter design—a scoping study. Journal of Marine Science and Engineering 8, 35.

Davidson, J., Ringwood, J.V., 2017. Mathematical modelling of mooring systems for wave energy converters—a review. Energies 10, 666.

Dietz, J.S., 2005. Application of conditional waves as critical wave episodes for extreme loads on marine structures. Technical University of Denmark.

DNV, 2013. Design of floating wind turbine structures. Offshore Standard DNV-OS-J103 5, 116.

DNV, 2014. Environmental conditions and environmental loads. Høvik, Norway: DNV GL. Available at: https://rules. dnvgl. com/docs/pdf/DNV/codes/docs/2014-04/RP-C205. pdf. Accessed March 15, 2018.

DNV, 2015. Offshore standard dnvgl-os-e301 position mooring. Høvik, DNV GL AS.[Online] Available from: https://rules. dnvgl. com/docs/pdf/dnvgl/os/2015-07/DNVGLOS-E301. pdf [Accessed 5th February 2018] .

DNV, 2016. Loads and site conditions for wind turbines.

DNV, 2018. Dnvgl-st-0119: Floating wind turbine structures. DNV GL .

Doherty, K., Folley, M., Whittaker, T., Doherty, R., et al., 2011. Extreme value analysis of wave energy converters, in: The Twenty-first International Offshore and Polar Engineering Conference, International Society of Offshore and Polar Engineers.

Drago, M., Giovanetti, G., Pizzigalli, C., 2013. Assessment of significant wave height–peak period distribution considering the wave steepness limit, in: International Conference on Offshore Mechanics and Arctic Engineering, American Society of Mechanical Engineers. p. V005T06A015.

Drummen, I., Wu, M., Moan, T., 2009. Numerical and experimental investigations into the application of response conditioned waves for long-term nonlinear analyses. Marine Structures 22, 576–593.

Eckert, A., Martin, N., G. Coe, R., Seng, B., Stuart, Z., Morrell, Z., 2020. Development of a comparison framework for evaluating environmental contours of extreme sea states. Journal of Marine Science and Engineering 9, 16.

Edwards, S.J., Coe, R.G., 2019. The effect of environmental contour selection on expected wave energy converter response. Journal of Offshore Mechanics and Arctic Engineering 141.

EMEC, 2022. wave devices. URL: https://www.emec.org.uk/marine-energy/wave-devices/. accessed on 2021-08-01.

engie, 2022. offshore wind a key step towards the worlds first large scale floating wind projec. URL: https://www.engie.com/en/journalists/press-releases/offshore-wind-a-key-step-towards-the-world-s-first-large-scale-floating accessed on 2022-08-01.

Eskilsson, C., Palm, J., Johannesson, P., Paredes, G.M., 2022. Sensitivity analysis of extreme loads acting on a point-absorbing wave energy converter. International Marine Energy Journal 5, 91–101.

Fonseca, N., Pascoal, R., Marinho, J.o., Morais, T., 2008. Analysis of wave drift forces on a floating wave energy converter, in: International Conference on Offshore Mechanics and Arctic Engineering, pp. 831–839.

Gaertner, E., et al., 2020. Definition of the iea wind 15-megawatt offshore reference wind turbine tech. rep.

Gibson, R., 2020a. Extreme Environmental Loading of Fixed Offshore Structures: Extreme Loading Events, Part A. Technical Report. Health and Safety Executive.

Gibson, R., 2020b. Extreme Environmental Loading of Fixed Offshore Structures: Metocean Analysis Part A. Technical Report. Health and Safety Executive.

Gibson, R., 2020c. Extreme Environmental Loading of Fixed O˙shore Structures: Summary Report, Component 2. Technical Report. Health and Safety Executive.

Giorgi, G., 2018. Nonlinear hydrodynamic modelling of wave energy converters under controlled conditions. Ph.D. thesis. National University of Ireland, Maynooth (Ireland).

Göteman, M., Engström, J., Eriksson, M., Hann, M., Ransley, E., Greaves, D., Leijon, M., et al., 2015. Wave loads on a point-absorbing wave energy device in extreme waves, in: The Twenty-fifth International Ocean and Polar Engineering Conference, International Society of Offshore and Polar Engineers.

Greaves, D., Byrne, B., Chen, J., Scott, B., Brennan, F., Thies, P., Richards, L., Henderson, K., Mascall, R., White, D., Gilbert, J., Jeffrey, H., Zhao, X., Wilden, R., Stallard, T., 2023. Delivering Net Zero: the Role of Offshore Renewable Energy. Technical Report. Supergen ORE hub.

Gueydon, S., Judge, F., Lyden, E., O'Shea, M., Thiebaut, F., Boulluec, M.L., Caverne, J., Ohana, J., Bouscasse, B., Kim, S., et al., 2021. A heuristic approach for inter-facility comparison of results from round robin testing of a floating wind turbine in irregular waves. Journal of Marine Science and Engineering 9, 1030.

Hall, M., 2015. Moordyn user's guide. 2015.

Hann, M., Greaves, D., Raby, A., 2015. Snatch loading of a single taut moored floating wave energy converter due to focussed wave groups. Ocean Engineering 96, 258–271.

Hann, M., Greaves, D., Raby, A., Howey, B., 2018. Use of constrained focused waves to measure extreme loading of a taut moored floating wave energy converter. Ocean Engineering 148, 33–42.

Hansen, R.H., Kramer, M.M., Vidal, E., 2013. Discrete displacement hydraulic power take-off system for the wavestar wave energy converter. Energies 6, 4001–4044.

Haselsteiner, A.F., Frieling, M., Mackay, E., Sander, A., Thoben, K.D., 2022. Long-term extreme response of an offshore turbine: How accurate are contour-based estimates? Renewable Energy 181, 945–965.

Haver, S., Bruserud, K., Baarholm, G.S., Veritas, D.N., 2013. Environmental contour method: An approximate method for obtaining characteristic response extremes for design purposes, in: Proceedings of 13th International Workshop on Wave Hindcasting and Forecasting and 4th Coastal Hazard Symposium.

Hsu, W.T., Thiagarajan, K.P., Manuel, L., 2017. Extreme mooring tensions due to snap loads on a floating offshore wind turbine system. Marine Structures 55, 182–199.

Hunt-Raby, A.C., Borthwick, A.G., Stansby, P.K., Taylor, P.H., 2011. Experimental measurement of focused wave group and solitary wave overtopping. Journal of Hydraulic Research 49, 450–464.

IEAWindTask37, 2021. Iea-15-240-rwt. URL: https://github.com/IEAWindTask37/IEA-15-240-RWT. accessed on 2021-06-01.

IEC, 2014. IEC 61400-3-1, Wind turbines-Part 3-1: Design requirements for offshore wind turbines, Committee Draft. sl: IEC, 2014. Technical Report.

IEC, 2015. Iec ts 62600-10: Marine energy—wave, tidal and other water current converters.

IEC, 2016. 62600-2. 2016. marine energy-wave, tidal and other water current converters-part 2: design requirements for marine energy systems .

IEC, 2019. Iec 61400-3-2 wind energy generation systems-part 3-2: Design requirements for floating offshore wind turbines.

Jensen, J.J., 1996. Second-order wave kinematics conditional on a given wave crest. Applied Ocean Research 18, 119–128.

Jie, Y., Yan-ping, H., Yong-sheng, Z., Yan-lin, S., et al., 2020. Current effect on the hydrodynamic responses of spar type floating offshore wind turbine, in: The 30th International Ocean and Polar Engineering Conference, OnePetro.

Johannesson, P., Svensson, T., Santandrea, F., Ng, C., Jia, C., Buck, E., Shanks, A., 2016. Reliability guidance for marine energy converters. RiaSor: Stromness, Scotland .

Journe, J., Massie, W., 2001. Offshore hydromechanics. Delft University of Technology .

Journee, J., Massie, W., 2001. Wave forces on slender cylinders. Delft University of Technology: Delft, The Netherlands , 469–498.

Katsidoniotaki, E., 2021. Extreme wave conditions and the impact on wave energy converters. Ph.D. thesis. Acta Universitatis Upsaliensis.

Kim, D.H., 2012. Design Loads Generator: Estimation of Extreme Environmental Loadings for Ship and Offshore Applications. Ph.D. thesis.

Kim, D.H., Troesch, A.W., 2013. Statistical estimation of extreme roll responses in short crested irregular head seas, in: SNAME Maritime Convention, OnePetro.

Laporte Weywada, P., Cruz, J., Scriven, J., 2019. D1.2 Definition of Priority DLCs and Load Characterisation Report. Technical Report. K2Management.

Latheef, M., Swan, C., 2013. A laboratory study of wave crest statistics and the role of directional spreading. Proceedings of the Royal Society A: Mathematical, Physical and Engineering Sciences 469, 20120696.

Lawson, M., Yu, Y.H., Nelessen, A., Ruehl, K., Michelen, C., 2014a. Implementing nonlinear buoyancy and excitation forces in the wec-sim wave energy converter modeling tool, in: International Conference on Offshore Mechanics and Arctic Engineering, American Society of Mechanical Engineers. p. V09BT09A043.

Lawson, M., Yu, Y.H., Ruehl, K., Michelen, C., et al., 2014b. Development and demonstration of the wec-sim wave energy converter simulation tool .

Leimeister, M., Kolios, A., Collu, M., 2018. Critical review of floating support structures for offshore wind farm deployment, in: Journal of Physics: Conference Series, IOP Publishing. p. 012007.

Li, L., Cheng, Z., Yuan, Z., Gao, Y., 2018. Short-term extreme response and fatigue damage of an integrated offshore renewable energy system. Renewable Energy 126, 617–629.

Li, L., Gao, Z., Moan, T., 2013. Joint environmental data at five european offshore sites for design of combined wind and wave energy devices, in: International Conference on Offshore Mechanics and Arctic Engineering, American Society of Mechanical Engineers. p. V008T09A006.

Li, Q., Gao, Z., Moan, T., 2017. Modified environmental contour method to determine the long-term extreme responses of a semi-submersible wind turbine. Ocean Engineering 142, 563–576.

Ltd, O., 2024. Orcaflex manual. URL: https://www.orcina.com/webhelp/OrcaFlex/Default.htm. accessed on 2024-03-17.

Ma, S., Xu, D.k., Duan, W.y., Chen, J.k., Liao, K.p., Wang, H., 2020. The numerical study of viscous drag force influence on low-frequency surge motion of a semi-submersible in storm sea states. Ocean Engineering 213, 107511.

MacKay, D., 2008. Sustainable Energy-without the hot air. UIT cambridge.

Mahfouz, M., Salari, M., Hernández, S., Vigara, F., Molins, C., Trubat, P., Bredmose, H., Pegalar-Jurado, A., 2020. Public design and fast models of the two 15mw floater-turbine concepts.

Martin, A.E.G..N., 2016. Kernel density estimation (kde) with adaptive bandwidth se-

lection for environmental contours of extreme sea states. URL: https://www.osti.gov/servlets/purl/1394048. accessed on 2021-06-01.

Mei, X., Xiong, M., 2021. Effects of second-order hydrodynamics on the dynamic responses and fatigue damage of a 15 mw floating offshore wind turbine. Journal of Marine Science and Engineering 9, 1232.

Meng, L., He, Y.p., Zhao, Y.s., Yang, J., Yang, H., Han, Z.l., Yu, L., Mao, W.g., Du, W.k., 2020. Dynamic response of 6mw spar type floating offshore wind turbine by experiment and numerical analyses. China Ocean Engineering 34, 608–620.

Merigaud, A., Gilloteaux, J.C., Ringwood, J.V., 2012. A nonlinear extension for linear boundary element methods in wave energy device modelling, in: International Conference on Offshore Mechanics and Arctic Engineering, American Society of Mechanical Engineers. pp. 615–621.

Michelen, C., Coe, R., 2015. Comparison of methods for estimating short-term extreme response of wave energy converters, in: OCEANS 2015-MTS/IEEE Washington, IEEE. pp. 1–6.

Mirzadeh, J., Kimiaei, M., Cassidy, M.J., 2016. Performance of an example jack-up platform under directional random ocean waves. Applied Ocean Research 54, 87–100.

Mortimer, W.G., 2022. Physical modelling of wave group interactions with a vertical wall. Ph.D. thesis. University of Plymouth.

Musiedlak, P.H., Ransley, E.J., Greaves, D., Hann, M., Iglesias, G., Child, B., 2017. Investigation of model validity for numerical survivability testing of wecs .

Myrhaug, D., 2018. Some probabilistic properties of deep water wave steepness. Oceanologia 60, 187–192.

Norge, S., 2007. Norsok-n003: Actions and actions effects.

NORSOK, N., 2017. 003, 2017. NORSOK Standard N-003 .

NREL, 2021. Openfast documentation.

NREL, SNL, 2021. Modeling considerations. URL: https://openfast.readthedocs.io/en/main/source/user/hydrodyn/modeling_considerations.html. accessed on 2022-06-10.

NREL, SNL, 2022a. Wec-sim development roadmap. URL: https://github.com/WEC-Sim/WEC-Sim/projects/58. accessed on 2023-01-10.

NREL, SNL, 2022b. Wec-sim theory overview. URL: https://wec-sim.github.io/WEC-Sim/master/theory/theory.html. accessed on 2022-06-20.

Ochi, M., 1990. Applied probability and stochastic processes. New York: Wiley.

Ochi, M., 1998. Ocean waves. Cambridge, UK: Cambridge University Press.

Orszaghova, J., Rafiee, A., Wolgamot, H., Draper, S., Taylor, P., 2016. Experimental study of extreme responses of a point absorber wave energy converter, in: Proceedings of the 20th Australasian Fluid Mechanics Conference, Perth, Australia, pp. 1–8.

Pacheco, A., Gorbeña, E., Sequeira, C., Jerez, S., 2017. An evaluation of offshore wind power production by floatable systems: A case study from sw portugal. Energy 131, 239–250.

Pakozdi, C., Fouques, S., Thys, M., Kamath, A., Wang, W., Dadmarzi, F.H., Bachynski, E., Bihs, H., 2020. Validation of numerical wave tank simulations using reef3d with jonswap spectra in intermediate water depth, in: International Conference on Offshore Mechanics and Arctic Engineering, American Society of Mechanical Engineers. p. V001T01A012.

Palm, J., Eskilsson, C., Bergdahl, L., 2016. Mooring cable simulations with snap load capturing for wave energy applications, in: Proceedings of the 2nd International Conference on Renewable Energies Offshore, Lisbon, Portugal, pp. 24–28.

Pastoor, L.W., 2002. On the assessment of nonlinear ship motions and loads. Ph. D. Thesis, Delft Univ. of Tech. .

Pierella, F., Lindberg, O., Bredmose, H., Bingham, H.B., Read, R.W., Engsig-Karup, A.P., 2021. The derisk database: Extreme design waves for offshore wind turbines. Marine Structures 80, 103046.

Quon, E., Platt, A., Yu, Y.H., Lawson, M., 2016. Application of the most likely extreme response method for wave energy converters, in: ASME 2016 35th International Conference on Ocean, Offshore and Arctic Engineering, American Society of Mechanical Engineers Digital Collection.

Rafiee, A., Wolgamot, H., Draper, S., Orszaghova, J., Fiévez, J., Sawyer, T., 2016. Identifying the design wave group for the extreme response of a point absorber wave energy converter, in: Proceedings of the Asian Wave and Tidal Energy Conference (AWTEC), Singapore.

Rainey, P., Camp, T., 2007. Constrained non-linear waves for offshore wind turbine design, in: Journal of Physics: Conference Series, IOP Publishing. p. 012067.

Ransley, E., 2015. Focused wave interaction with a floating structure (incl. heave decay tests). URL: https://www.ccp-wsi.ac.uk/catalogue/test_cases/test_case_002#description. accessed on 2024-03-27.

Ransley, E., Yan, S., Brown, S., Hann, M., Graham, D., Windt, C., Schmitt, P., Davidson, J., Ringwood, J., Musiedlak, P.H., et al., 2020. A blind comparative study of focused wave interactions with floating structures (ccp-wsi blind test series 3). International Journal of Offshore and Polar Engineering 30, 1–10.

Rendon, E.A., Manuel, L., 2014. Long-term loads for a monopile-supported offshore wind turbine. Wind Energy 17, 209–223.

van Rij, J.A., Yu, Y.H., Tom, N.M., 2019. Validation of simulated wave energy converter

responses to focused waves for CCP-WSI blind test series 2. Technical Report. National Renewable Energy Lab.(NREL), Golden, CO (United States).

Robertson, A., Wang, L., 2021. Oc6 phase ib: Floating wind component experiment for difference-frequency hydrodynamic load validation. Energies 14, 6417.

Robertson, A.N., Bachynski, E.E., Gueydon, S., Wendt, F., Schünemann, P., Jonkman, J., 2018. Assessment of experimental uncertainty for a floating wind semisubmersible under hydrodynamic loading, in: International Conference on Offshore Mechanics and Arctic Engineering, American Society of Mechanical Engineers. p. V010T09A076.

Robertson, A.N., Gueydon, S., Bachynski, E., Wang, L., Jonkman, J., Alarcón, D., Amet, E., Beardsell, A., Bonnet, P., Boudet, B., et al., 2020. Oc6 phase i: Investigating the underprediction of low-frequency hydrodynamic loads and responses of a floating wind turbine, in: Journal of Physics: Conference Series, IOP Publishing. p. 032033.

Robertson, A.N., Wendt, F., Jonkman, J.M., Popko, W., Dagher, H., Gueydon, S., Qvist, J., Vittori, F., Azcona, J., Uzunoglu, E., et al., 2017. Oc5 project phase ii: validation of global loads of the deepcwind floating semisubmersible wind turbine. Energy Procedia 137, 38–57.

Rosenberg, B.J., Mundon, T.R., Coe, R.G., Quon, E.W., Chartrand, C.C., Yu, Y.H., Van Rij, J.A., 2019. Development of WEC design loads: A comparison of numerical and experimental approaches. Technical Report. National Renewable Energy Lab.(NREL), Golden, CO (United States).

Ross, E., Astrup, O.C., Bitner-Gregersen, E., Bunn, N., Feld, G., Gouldby, B., Huseby, A., Liu, Y., Randell, D., Vanem, E., et al., 2020. On environmental contours for marine and coastal design. Ocean Engineering 195, 106194.

Saeed Far, S., Abd. Wahab, A.K., 2016. Evaluation of peaks-over-threshold method. Ocean Science Discussions 2016, 1–25.

Santo, H., Taylor, P., Carpintero Moreno, E., Stansby, P., Eatock Taylor, R., Sun, L., Zang, J., 2017. Extreme motion and response statistics for survival of the three-float wave energy converter m4 in intermediate water depth. Journal of Fluid Mechanics 813.

Saranyasoontorn, K., 2006. A simulation-based procedure for* reliability analysis of wind turbines. The University of Texas at Austin.

Schmittner, C., Kosleck, S., Hennig, J., 2009. A phase-amplitude iteration scheme for the optimization of deterministic wave sequences, in: International Conference on Offshore Mechanics and Arctic Engineering, pp. 653–660.

Serio, M., Onorato, M., Osborne, A.R., Janssen, P., et al., 2005. On the computation of the benjamin-feir index. Nuovo Cimento-Societa Italiana di Fisica Sezione C 28, 893.

Seyffert, H., 2018. Extreme design events due to combined, non-Gaussian loading. Ph.D. thesis.

Seyffert, H.C., Kim, D.H., Troesch, A.W., 2016. Rare wave groups. Ocean Engineering 122, 241–252.

Sirigu, S.A., Bonfanti, M., Begovic, E., Bertorello, C., Dafnakis, P., Giorgi, G., Bracco, G., Mattiazzo, G., 2020. Experimental investigation of the mooring system of a wave energy converter in operating and extreme wave conditions. Journal of Marine Science and Engineering 8, 180.

Sirnivas, S., Yu, Y.H., Hall, M., Bosma, B., 2016. Coupled mooring analyses for the wec-sim wave energy converter design tool, in: International Conference on Offshore Mechanics and Arctic Engineering, American Society of Mechanical Engineers. p. V006T09A023.

Suja-Thauvin, L., Krokstad, J.R., Bachynski, E.E., 2018. Critical assessment of non-

linear hydrodynamic load models for a fully flexible monopile offshore wind turbine. Ocean Engineering 164, 87–104.

Sutherland, J., Peet, A., Soulsby, R., 2004. Evaluating the performance of morphological models. Coastal engineering 51, 917–939.

Swan, C., 2018. Extreme Environmental Loading of Fixed Offshore Structures: Current Code Requirements. Technical Report. Health and Safety Executive.

Swan, C., 2020. Extreme Environmental Loading of Fixed Offshore Structures: Metocean Research. Technical Report. Health and Safety Executive.

Tang, T., Xu, W., Barratt, D., Bingham, H.B., Li, Y., Taylor, P., Van Den Bremer, T., Adcock, T., 2021. Spatial evolution of the kurtosis of steep unidirectional random waves. Journal of Fluid Mechanics 908.

Taylor, P.H., Jonathan, P., Harland, L.A., 1997. Time domain simulation of jack-up dynamics with the extremes of a gaussian process .

Tromans, P.S., Anaturk, A.R., Hagemeijer, P., et al., 1991. A new model for the kinematics of large ocean waves-application as a design wave, in: The first international offshore and polar engineering conference, International Society of Offshore and Polar Engineers.

University of Maine, 2022. Volturnus. URL: https://composites.umaine.edu/volturnus/. accessed on 2022-08-01.

Van Rij, J., Yu, Y.H., Coe, R.G., 2018. Design load analysis for wave energy converters, in: International Conference on Offshore Mechanics and Arctic Engineering, American Society of Mechanical Engineers. p. V010T09A031.

Van Rij, J., Yu, Y.H., Guo, Y., Coe, R.G., 2019a. A wave energy converter design load case study. Journal of Marine Science and Engineering 7, 250.

Van Rij, J., Yu, Y.H., McCall, A., Coe, R.G., 2019b. Extreme load computational fluid dynamics analysis and verification for a multibody wave energy converter, in: International Conference on Offshore Mechanics and Arctic Engineering, American Society of Mechanical Engineers. p. V010T09A042.

Vigara, F., Cerdan, L., Duran, R., Munoz, S., Lynch, M., Doole, S., 2019a. Corewind d1.2: Design load basis.

Vigara, F., Cerdán, L., Durán, R., Muñoz, S., Lynch, M., Doole, S., et al., 2019b. Corewind d1. 2: Design load basis.

Viselli, A.M., Forristall, G.Z., Pearce, B.R., Dagher, H.J., 2015. Estimation of extreme wave and wind design parameters for offshore wind turbines in the gulf of maine using a pot method. Ocean Engineering 104, 649–658.

Vyzikas, T., Stagonas, D., Buldakov, E., Greaves, D., 2018. The evolution of free and bound waves during dispersive focusing in a numerical and physical flume. Coastal Engineering 132, 95–109.

Wamit, i., 2024. The state of the art in wave interaction analysis. URL: https://www.wamit.com/. accessed on 2024-03-17.

Wang, L., Robertson, A., Jonkman, J., Yu, Y.H., Koop, A., Nadal, A.B., Li, H., Bachynski-Polić, E., Pinguet, R., Shi, W., et al., 2021a. Oc6 phase ib: Validation of the cfd predictions of difference-frequency wave excitation on a fowt semisubmersible. Ocean Engineering 241, 110026.

Wang, S., Larsen, T.J., Bredmose, H., 2021b. Ultimate load analysis of a 10 mw offshore monopile wind turbine incorporating fully nonlinear irregular wave kinematics. Marine Structures 76, 102922.

Wang, W., Pákozdi, C., Kamath, A., Bihs, H., 2021c. A fully nonlinear potential flow wave modelling procedure for simulations of offshore sea states with various wave breaking scenarios. Applied Ocean Research 117, 102898.

Wheeler, J., 1970. Method for calculating forces produced by irregular waves. Journal of petroleum technology 22, 359–367.

Winterstein, S.R., Ude, T.C., Cornell, C.A., Bjerager, P., Haver, S., 1993. Environmental parameters for extreme response: Inverse form with omission factors, in: Proc. 6th Int. Conf. on Structural Safety and Reliability, Innsbruck, Austria.

Yu, Y.H., Van Rij, J., Coe, R., Lawson, M., 2015. Preliminary wave energy converters extreme load analysis, in: ASME 2015 34th International Conference on Ocean, Offshore and Arctic Engineering, American Society of Mechanical Engineers Digital Collection.